

INFLUENCE OF AGING ON PROLIFERATION, PLURIPOTENCY, IMMUNOGENIC PROFILES FROM BONE MARROW MESENCHYMAL STEM CELLS

Autor: Juan Antonio Fafián Labora

Tese de doutoramento UDC / 2016

Directora e tutora: María del Carmen Arufe Gonda

Departamento de Medicina



UNIVERSIDADE DA CORUÑA

Dra. M^a del Carmen Arufe Gonda, PDI no Dpto. de Medicina da Facultade de Ciencias da Saude da Universidade da Coruña.

CERTIFICA:

Que a presente memoria de tesis titulada: “INFLUENCIA DO ENVELLECIMENTO NOS PERFIS DE PROLIFERACIÓN, PLURIPOTENCIA E POTENCIAL INMUNOXÉNICO DAS CÉLULAS NAIS MESEQUIMAS DE MEDULA OSEA” presentada por D. Juan Antonio Fafián Labora para optar o grado de Doutor, foi realizada baixo a miña dirección no Dpto. de Medicina da Facultade de Ciencias de Saude da Universidade da Coruña e cumpre tódolos requisitos de orixinalidade e rigor científico necesarios para a súa defensa.

Asdo. M^a del Carmen Arufe Gonda

En A Coruña, 1 de Setembro de 2016

Yo, Juan Antonio Fafián Labora, estudiante de doctorado de Ciencias de la Salud RD 99/2011, deposito mi tesis doctoral titulada INFLUENCE OF AGING ON PROLIFERATION, PLURIPOTENCY AND IMMUNOGENIC PROFILES OF BONE MARROW MESENCHYMAL STEM CELLS

A Coruña, 22 de Septiembre de 2016



Asdo. Don. Juan Antonio Fafián Labora
Estudiante de Doctorado Ciencias de la Salud

ABSTRACT

ABSTRACT

Mesenchymal stem cells (MSCs) are highly relevant for regeneration of mesoderm tissues such as bone and cartilage. The promising role of MSCs in cell-based therapies and tissue engineering appears to be limited due to a decline of their regenerative potential with increasing donor age. In this research we have studied and treated to understand how aging influences in proliferation and pluripotency capacities from these cells and also into their immunogenic potential.

Six age groups from bone marrow mesenchymal stem cells of Wistar rats were studied (newborn, infant, young, pre-pubertal, pubertal and adult). Quantitative proteomic assay was performance by iTRAQ-8-plex and the proteins statistically significant modulated were grouped in pluripotency, proliferative and metabolism processes. Proliferation makers, CD117 and Ki67 were measure by flow cytometry assay. Real time polymerase chain reaction analysis of pluripotency markers Rex1, Oct4, Sox2 and Nanog were done. Biological differentiation was realized using specific mediums for 14 days to induce osteogenesis, adipogenesis and chondrogenesis and differentiated cells were analysed using histochemical techniques. Enzymatic analysis of several enzymes as L-lactate dehydrogenase and glucose-6-phosphate isomerase were done to validate iTRAQ data. To deeply study these differences we have analyzed by Next Generation Sequencing six age groups from bone marrow mesenchymal stem cells. A total of 9628 genes presented differences of expression among age groups and those genes were grouped into metabolic pathways. We focused our research in young, pre-pubertal and adult groups which presented the highest amount of genes differentially expressed related with inflammation mediated by chemokine and cytokine signalling pathway when compared with newborn group which was used as a control. Afterwards, extracellular vesicles from those groups were isolated and characterized by nanoparticle tracking analysis and flow cytometry and several micro-RNAs were checked by qRT-PCR because of their relationship with the pathway of interest. Since miR-21-5p was statistically significant highest in extracellular vesicles from mesenchymal stem cells of pre-pubertal group, we realized a functional experiment inhibiting it expression and investigating the modulation of Toll-Like Receptor 4 and their link to damage-associated molecular patterns.

Aging affects proliferation, pluripotency and immunogenic profiles of bone marrow mesenchymal stem cells. Also its affects production, content of pro-inflammatory miRs and affectivity of bone marrow mesenchymal stem cell-derived extracellular vesicles. These findings are important to the understanding about influence of the aging on mesenchymal stem cells and to advance in the development EV-based therapies.

RESUMEN

Las células madre mesenquimales (CMMs) tiene una gran relevancia en la regeneración de tejidos mesenquimales como hueso y cartílago. El prometedor papel de las CMMs en terapia celular e ingeniería tisular parece estar limitado debido a la pérdida de potencial de regeneración con el incremento de la edad del donante. En esta investigación hemos tratado de entender como el envejecimiento influye en la capacidad de proliferación y pluripotencia en estas células y también en su potencial inmunogénico.

CMMs de médula ósea procedentes de ratas *Wistar* de seis estadios de edad (neonato, infantil, juvenil, pre-pubertal, pubertal e adulto) fueron usadas en este estudio. Se llevo a cabo un ensayo proteómico cuantitativo usando iTRAQ 8-plex y las proteínas estadísticamente moduladas fueron agrupadas en tres procesos: pluripotencia, proliferación y metabolismo energético. Se midieron mediante citometría de flujo los marcadores de proliferación CD117 y Ki67. El análisis de los marcadores de pluripotencia Rex1, Oct4, Sox2 y Nanog usando reacción en cadena de la polimerasa a tiempo real. Evaluación biológica mediante diferenciaciones dirigidas usando medios específicos de osteogénesis, adipogénesis y condrogenénesis durante 14 días, las células diferenciadas fueron analizadas usando técnicas histoquímicas. También se realizaron ensayos enzimáticos de varias enzimas como L-lactato deshidrogenasa y glucosa-6-fosfato isomerasa para validar los datos obtenidos del iTRAQ. Para profundizar en el estudio de las diferencias obtenidas a nivel proteómico hemos analizado el transcriptoma de los seis grupos de edad de CMMs de médula ósea usando *Next Generation Sequencing*. Un total de 9628 genes se encontraron modulados significativamente entre los grupos de edad y estos fueron agrupados en rutas metabólicas. Encontramos en los grupos juvenil, pre-pubertal y adulto una gran cantidad de genes diferencialmente expresados relacionados con inflamación mediada por la ruta de señalización de quimiocinas y citoquinas comparados con el grupo control. Además, las vesículas extracelulares de estos grupos de edad fueron aisladas y caracterizadas usando el análisis de tráfico de nanopartículas y citometría de flujo y la expresión de varios micro-ARNs relacionados con la ruta de interés, se evaluaron por qPCR-RT. El miR-21-5p fue estadísticamente significativamente alto en vesículas extracelular de CMMs del grupo pre-pubertal, mediante experimentos funcionales inhibiendo su expresión, investigamos la modulación del receptor tipo Toll 4 y los patrones moleculares asociados al daño.

El envejecimiento afecta al perfil de proliferación, pluripotencia e inmunogénico de CMMs de médula ósea, También afecta la producción, contenido de micro-ARNs pro-inflamatorios y la efectividad de las vesículas extracelulares procedentes de células madre mesenquimales de médula ósea. Estos descubrimientos son importantes para entender la influencia del envejecimiento en las células madre mesenquimales y el avance en el desarrollo de terapias basadas en vesículas extracelulares de las mismas.

RESUMO

As células nai mesenquimais (CNMs) teñen unha gran relevancia na rexeneración de tecidos mesenquimais coma óso e cartilaxe. O prometedor papel das CNMs en terapia celular e inxenería tisular parece estar limitado debido a perda do potencial de rexeneración co incremento da idade do doante. Nesta investigación tratamos de entender coma o envellecemento inflúe na capacidade de proliferación e pluripotencia e no potencial inmunoxénica destas células.

CNMs de medula ósea procedentes de ratas *Wistar* de seis estadios de idade (neonato, infantil, xuvenil, pre-púbere, púbere e adulto) foron empregadas neste estudo. Levouse a cabo un ensaio proteómico cuantitativo empregando iTRAQ 8-plex e as proteínas estadisticamente moduladas agrupáronse en tres procesos: pluripotencia, proliferación e metabolismo enerxético. Medíronse empregando citometría de fluxo os marcadores de proliferación CD117 e Ki67. A análise dos marcadores de pluripotencia Rex1, Oct4, Sox2 e Nanog empregando a reacción en cadea da polimerasa a tempo real. A avaliación biolóxica mediante diferenciacións dirixidas empregando medios específicos de osteoxénesis, adipoxénesis e condroxénesis durante 14 días, as células diferenciadas foron avaliadas empregando técnicas histoquímicas. Tamén leváronse a cabo ensaios enzimáticos de varias enzimas coma L-lactato deshidroxenasa e glicosa-6-fosfato isomerasa para validar os datos obtidos do iTRAQ. Para profundizar no estudo das diferenzas obtidas a nivel proteómico analizouse o transcriptoma dos seis grupos de idade das CNMs empregando *Next Generation Sequencing*. Un total de 9628 xenes atopáronse modulados significativamente entre os grupos de idades e estes foron agrupados en rutas metabólicas. Atopamos nos grupos xuvenil, pre-púbere e adulto una gran cantidade de xenes diferencialmente expresados relacionados coa inflamación mediada pola ruta de sinalización de quimiocinas e citoquinas comparadas co grupo control. Ademais, as vesículas extracelulares dos grupos de idade foron aisladas e caracterizadas empregando a análise de tráfico de nanopartículas e citometría de fluxo e a avaliación da expresión de varios micro-ARNs relacionados coa ruta de interese mediante qPCR-RT. O miR-21-5p foi estadisticamente significativamente alto nas vesículas extracelulares de CNMs do grupo pre-púbere, mediante experimentos funcionais, inhibindo a súa expresión, investigamos a modulación do receptor tipo Toll 4 e os patrones moleculares asociados ao dano.

O envellecemento afecta ao perfil de proliferación, pluripotencia e inmunoxénica das CNMs de medula ósea. Tamén afecta a produción, contido de micro-ARNs pro-inflamatorios e a efectividade das vesículas extracelulares procedentes de CNMs de medula ósea. Estes descubrimentos son importantes para entender a influencia do envellecemento nas CNMs e o avance no desenvolvemento de terapias baseadas nas vesículas extracelulares das mesmas.

TABLE OF CONTENTS

TABLE OF CONTENTS

1. INTRODUCTION	1
1.1 Mesenchymal stem cells	3
1.1.1 Definition	3
1.1.2 Sources for mesenchymal stem cells	3
1.1.3 Properties of mesenchymal stem cells supporting therapeutic application	4
1.1.3.1 Differentiation	4
1.1.3.2 Paracrine effects and immunomodulation	5
1.1.3.3 Homing mechanism	5
1.1.4 Applications in clinical use	6
1.2 Aging	7
1.2.1 Definition	7
1.2.2 The hallmarks of aging	7
1.2.2.1 Genomic instability	8
1.2.2.2 Telomere attrition	9
1.2.2.3 Epigenetic alterations	9
1.2.2.4 Loss of proteostasis	9
1.2.2.5 Deregulated nutrient-sensing	9
1.2.2.6 Mitochondrial dysfunction	9
1.2.2.7 Cellular senescence	10
1.2.2.8 Stem cell exhaustion	10
1.2.2.9 Altered intercellular communication	10
1.2.3 Mechanisms of aging on mesenchymal stem cells	10
1.3 Extracellular vesicles	12
1.3.1 Definition	12
1.3.2 Types of extracellular vesicles	13
1.3.3 Composition of Extracellular Vesicles	14
1.3.3.1 Protein and protein-associated of EVs	14
1.3.3.2 RNA composition	15
1.3.3.3 DNA contain	15
1.3.3.4 Lipid composition	15
1.3.4 Formation and sorting EVs	16
1.3.4.1 Exosomes biogenesis	16
1.3.4.2 Microvesicles biogenesis	17
1.3.5 EVs uptake	17
1.3.5.1 Endocytosis	17
1.3.5.2 Cell surface membrane fusion	18
1.3.5.3 Cell specific EV uptake	18
1.3.6 Application in clinical use	19
1.4 miRNAs	19
1.4.1 Definition	19
1.4.2 Biogenesis of miRNAs	19
1.4.3 miRNAs in EVs	20
1.4.4 Role in biological process	20

2. HIPOTHESIS AND AIMS	25
3. MATERIAL AND METHODS	27
3.1 Isolation and culture of rBM-MSCs	29
3.2 Characterization of rBM-MSCs by flow cytometry	29
3.3 Proliferation analysis by flow cytometry	30
3.4 Reactive oxygen species analysis by flow cytometry	30
3.5 Cell cycle analysis	30
3.6 Pro-inflammatory phenotype analysis	31
3.6.1 Determination expression of CD200 by flow cytometry	31
3.6.2 Activation TLR4 in rBM-MSCs	31
3.7 Characterization MSC-derived EVs by flow cytometry	31
3.8 Proliferation assay	31
3.9 Cytotoxicity assay	32
3.10 Biological characterization	32
3.10.1 Adipogenic differentiation	32
3.10.2 Chondrogenic differentiation	32
3.10.3 Osteogenic differentiation	33
3.11 Histochemical analysis	33
3.12 Densitometry analysis	34
3.13 Total RNA and miRNAs isolation	34
3.14 Determination of RNA integrity	34
3.15 Real time quantitative polymerase chain reaction (qRT-PCR) analysis	34
3.16 miRNAs analysis	35
3.17 Protein extraction and preparation procedures	35
3.18 Silver-staining of proteins in polyacrylamide gels	36
3.19 iTRAQ®-8plex labelling. Amine-Modifying Labelling Reagents for Multiplexed Relative and Absolute Protein Quantification	36
3.20 Relative quantification by two dimensional-liquid chromatography coupled offline to matrix-associated laser desorption ionization time of flight (2D-LC-MALDI-TOF/TOF) analysis	37
3.21 Immunoblot analysis	38
3.22 Enzymatic analysis	38
3.23 Next Generation Sequencing using RNA sequencing technique	39
3.24 Isolation rBM-MSC-derived EVs	40
3.25 Quantification of protein in rBM-MSC-derived EVs	40
3.26 Characterization of rBM-MSC-derived EVs by size	40
3.26.1 Nanoparticle Tracking Analysis (NTA)	40
3.26.2 Electronic microscopy	40
3.27 miRNA transitory transfections	41
3.28 <i>In vitro</i> model using rBM-MSC-derived EVs	41
3.29 Fluorescence microscopy	41
3.30 Bioinformatics analysis	41
3.31 Statistics analysis	42

4	RESULTS	43
4.1	Characterization of rBM MSCs	47
4.2	Study of proliferation of rBM-MSCs at different ages	47
4.3	Evaluation of biological capacity of rBM-MSCs at different ages	49
4.4	Evaluation of pluripotency markers in rBM-MSCs at different ages	51
4.5	Analysis of proteome in rBM-MSCs at different ages	51
4.6	Mitochondrial function in rBM-MSCs in different age groups	56
4.7	Glucolytic metabolism of rBM-MSCs at different ages	58
4.8	mTOR pathway in rBM-MSCs at different ages	60
4.9	Relationship of mTOR pathway with proliferation markers (CD117 and Ki67) in rBM-MSCs from adult group	61
4.10	Transcriptome analysis using Next Generation Sequencing (NGS) of rBM-MSCs	67
4.11	Analysis of pro-inflammatory potential in rBM-MSCs at different ages	72
4.12	Characterization of rBM-MSC-derived EVs	74
4.13	Detection of miRs relationship with Toll-like receptor in rBM-MSC-derived EVs at different ages	77
4.14	miR-21-5p as regulator on pro-inflammatory and differentiation capacities of TLR4 in rBM-MSCs from pre-pubertal group	79
4.15	Variation on rBM-MSC-derived EVs characteristic during aging	85
5	DISCUSSION	93
6	CONCLUSIONS	103
7	REFERENCES	107
8	SUPPLEMENTS	123
9	PUBLICATIONS	143
10	CURRICULUM VITAE	

LIST OF FIGURES

Figure 1.1. Definition of mesenchymal stem cells	3
Figure 1.2. Several sources from MSCs	4
Figure 1.3. Properties of MSCs	6
Figure 1.4. Number and percentage of MSC-based clinical trials classified by disease type	7
Figure 1.5. The Hallmarks of aging	8
Figure 1.6. Extrinsic and intrinsic influences on stem cell aging	11
Figure 1.7. Phenotype characterization of senescence MSCs	12
Figure 1.8. Different types of EVs	14
Figure 1.9. Protein composition of EVs	15
Figure 1.10. Formation and sorting EVs	17
Figure 1.11. Origin of EVs	18
Figure 1.12. Process miRNAs biogenesis	20
Figure 3.1. Workflow of iTRAQ-8plex	37
Figure 3.2. Workflow of RNA-sequencing	39
Figure 4.1. Characterization by flow cytometry	47
Figure 4.2. Proliferation profile from rBM-MSCs at different age	48
Figure 4.3. Evaluation of biological capacity of rBM-MSCs at different ages	50
Figure 4.4. Pluripotency profile from rBM-MSCs at different ages	51
Figure 4.5. Statistical analysis of iTRAQ-8plex	52
Figure 4.6. iTRAQ of modulated proteins in rBM-MSCs	53
Figure 4.7. Validation iTRAQ analysis	55
Figure 4.8. Mitochondrial function in rBM-MSCs at different ages	57
Figure 4.9. Glucolitic metabolism profile from rBM-MSCs at several ages	59
Figure 4.10. mTOR pathway profile from rBM-MSCs at different ages	60
Figure 4.11. Inhibition of proliferation markers (CD117 and Ki67) in rBM-MSCs from adult group	62
Figure 4.12. PI3K/Akt pathway in rBM-MSCs from adult group treated with 5 μ M or 10 μ M IM and 0.1 ng/ml or 1 ng/ml JK184	63

Figure 4.13. Level of p70S6k and AMPK α in rBM-MSCs from adult group treated with 5 μ M or 10 μ M IM and 0.1 ng/ml or 1 ng/ml JK184	64
Figure 4.14. mTOR pathway in rBM-MSCs from adult group treated with 5 μ M or 10 μ M IM and 0.1 ng/ml or 1 ng/ml JK184	65
Figure 4.15. mTOR pathway in rBM-MSCs from adult group treated with 5 μ M or 10 μ M IM and 0.1 ng/ml or 1 ng/ml JK184	66
Figure 4.16. Proliferation markers (Ki67 and CD117) in rBM-MSCs from old group treated with 10 nM rapamycin	67
Figure 4.17. Next Generation Sequencing study	68
Figure 4.18. Metabolic pathways with statistically significant changes among rBM-MSCs Part I	70
Figure 4.19. Metabolic pathways with statistically significant changes among rBM-MSCs Part II	71
Figure 4.20. Pro-inflammatory phenotype of rBM-MSCs at several ages	73
Figure 4.21. Characterization of MSC-derived EVs	75
Figure 4.22. NTA study of MSC-derived EVs at several ages	76
Figure 4.23. Pro-inflammatory profile of micro-RNAs contained in MSC-derived EVs with age	78
Figure 4.24. Effect of miR-21-5p on DAMPs and Nanog in mesenchymal stem cells from pre-pubertal group	80
Figure 4.25. Effect of miR-21-5p on senescence and pro-inflammatory phenotype in rBM-MSCs from pre-pubertal group	82
Figure 4.26. Effect of miR-21-5p on PI3K/Akt in rBM-MSCs from pre-pubertal group	83
Figure 4.27. Effect of miR-21-5p on immune response in rBM-MSCs from pre-pubertal group	84
Figure 4.28. Observation our <i>in vitro</i> model using fluorescence microscopy	86
Figure 4.29. Nanog, Oct4 and Vinculin expression at genetic level in our <i>in vitro</i> model	88
Figure 4.30. Analysis of isoforms of Lamin A using western-blot in our <i>in vitro</i> model	90

Figure 4.31. Analysis of isoforms of Lamin A using western-blot in
Our *in vitro* model

LIST OF TABLES

Table 1.1. Different types of EVs	13
Table 8.1. List of antibodies to flow cytometry	125
Table 8.2. List of antibodies to western-blot	126
Table 8.3. Specific primers of different rat genes for qRT-PCR	127
Table 8.4. Specific primers of miRNAs for qRT-PCR	127
Table 8.5. List of buffer to silver-staining	128
Table 8.6. List of modulated proteins ($P < 0.05$) in rBM-MSCs at different ages classified according to their principal biological process using iTRAQ-8plex	129

ABBREVIATIONS AND ACRONYMS

µg	Micrograme
µl	Mililiter
µl/min	Microliter per minute
µl/ml	Microliter per milliliter
µM	Micromolar
µm	Micrometer
11-β-HSD1	11-βeta-hydroxysteroid dehydrogenase type 1
2D-LC-MALDI-TOF/TOF	Two dimensional-liquid chromatography coupled offline to matrix-associated laser desorption ionization-time of flight
53BP1	Octomer-binding transcription factor 4
60S RP L10	60S Ribosomal protein L10
60S RP L23	60S Ribosomal protein L23
60S RP L24	60S Ribosomal protein L24
60S RP L4	60S Ribosomal protein L4
60S RP L6	60S Ribosomal protein L6
60S RP L7	60S Ribosomal protein L7
60S RP L9	60S Ribosomal protein L9
6PGDH	6-phosphogluconate dehydrogenase, decarboxylating
A	Adult
Å	Angström
A.U	Arbitrary units
A/P	Adult vs pubertal
aBM-MSCs	Bone marrow-mesenchymal stem cells from adult group
AcN	Acetonitrile
AD	Adipogenic medium
aEVs	Mesenchymal stem cell-derived extracellular vesicles from adult group
AMPK	Adenosine monophosphate kinase
AMPKα	Adenosine monophosphate kinase alpha
aMSCs	Mesenchymal stem cells from adult group
AP-1	Activator protein-1
Ar	Alizarin red
ATP	Adenosine triphosphate
bFGF	Basis fibroblast growth factor
BM-MSCs	Bone marrow-mesenchymal stem cells
BMP-2	Bone morphogenetic protein-2
bp	bases pairs
BSA	Bovine serum albumin
C18-silice	Column18-silice
Ca²⁺	Calcium ion
CD105	Endoglobin
CD117	Mast/stem cell growth factor receptor
CD11b	Integrin alpha M
CD14	Cluster of differentiation 14 or monocyte differentiation antigen CD14
CD200	Cluster of differentiation 200 or OX-2 membrane glycoprotein
CD29	Integrin beta 1
CD34	Hematopoietic progenitor cell antigen cluster of differentiation 34

CD45	Protein tyrosine phosphatase, receptor type C
CD63	Lysosome-associated membrane glycoprotein 3
CD73	5'-Nucleotidase
CD79α	Immunoglobulin associated alpha
CD81	Target of the antiproliferative antibody 1
CD82	Metastasis suppressor Kangai-1
CD9	Motility-related protein
CD90	Thy-1 cell surface antigen
cDNA	Complementary DNA
CH	Chondrogenic medium
CID	Collision-induced dissociation
cm²	Square centimeter
CM-CSF	Granulocyte-macrophage colony-stimulating factor
CMMs	Células madre mesenquimales
CNMs	Células nai mesenquimais
CO₂	Carbon dioxide
Conf	Confidence
d	Day(s)
DAMPs	Damage-associated molecular pattern
DAPI	4',6-diamidino-2-phenylindole
DDR	DNA Damage Response
Dicer-TRBP	Endoribonuclease Dicer-TAR RNA binding protein or helicase with RNase motif-TAR RNA binding protein
Dil	3-3'-diethylthiacarbocyanineiodide
DNA	Deoxyribonucleic acid
DROSHA RNase III	Ribonuclease III enzyme
dsDNA	Double-stranded DNA
ECM	Extracellular matrix
EDTA	Ethylenediaminetetraacetic acid
ESCRT	Endosomal sorting complex required for transport
ESCRT-0	Endosomal sorting complex required for transport-0
ESCRT-3	Endosomal sorting complex required for transport-3
ESCRT-I	Endosomal sorting complex required for transport-I
ESCRT-II	Endosomal sorting complex required for transport-II
ESCRT-III	Endosomal sorting complex required for transport-III
<i>et al.</i>	<i>et les autres personnes</i>
EV	Extracellular vesicle
EVs	Extracellular vesicles
FBS	Fetal bovine serum
FDR	False discovery rate
FPKM	Fragments per kilo base of exons per million
G₀	Gap 0/Resting
G₁	Gap 1
G₂	Gap 2 phase
G6PDH	Glucose-6-phosphate-1-dehydrogenase
GO	Gene ontology

GTPase Rab11	Small GTPase rab11
GTPase Rab7	Small GTPase rab7
GVHD	Graft-versus-host disease
GβI	Gbetal
h	hour(s)
H1.5	Histone variant 1.5
H2B	Histone variant 2B
H₂DCF-DA	2',7'-dichlorodihydrofluorescein diacetate
H4	Histone variant H4
HDCF-DA	2',7'-dichlorofluorescein diacetate
hESCs	Human embryonic stem cells
HGF	Hepatocyte growth factor precursor
HMGB1	High motility box 1
hMSCs	Human mesenchymal stem cells
HPLC	High-performer liquid chromatography
HPRT	Hypoxanthine-guanine phosphoribosyltransferase
HRP	Horseradish peroxidase
hsa	<i>Homo sapiens</i>
HSPs	Heat shock proteins
I	Infant
I/N	Infant vs newborn
ID	Identification
IDO	Indoleamine 2,3-dioxygenase 1
IFN	Type 1 interferon
IGFBP3	Insulin-like growth factor-binding protein 3
IGFBP4	Insulin-like growth factor-binding protein 4
IGFBP7	Insulin-like growth factor-binding protein 7
IIS	Insulin/insulin-like growth factor signaling
IL-1	Interleukin-1
IL-6	Interleukin-6
IL-8	Interleukin-8
ILV	Intraluminal vesicle
ILVs	Intraluminal vesicles
IM	Imatinib mesylate Cyclin-dependent kinase inhibitor 2A, multiple tumor suppressor 1 <i>loci</i>
<i>INK4/ARF loci</i>	
iNOS	Nitric oxide synthase
iPSCs	Induced pluripotent stem cells
ISCT	International Society for Cellular Therapy
ISEV	International Society for Extracellular Vesicles
iTRAQ	Isobaric tag for relative and absolute quantitation
iTRAQ-8plex	Isobaric tag for relative and absolute quantitation-eightplex
IU/ml	International units per milliliter
kDa	Kilodalton(s)
KO	Knockout
KRAS	Kirsten rat sarcoma viral oncogene homolog
kV	Kilovoltie(s)

LC-MALDI-TOF/TOF	Liquid chromatography coupled offline to matrix-associated laser desorption ionization-time of flight
LDH	Lactate dehydrogenase
LPS	Lipopolysaccharides
M	Molar
M	Mitosis
MALDI-TOF/TOF	Matrix-assisted laser desorption/ionization
MCP-1	Monocyte chemoattractant protein-1
mg/ml	Miligramme per militer
MgCl₂	Magnesium chloride
MHC	Major histocompatibility complex
micro-ARNs	Micro-ácidos ribonucleicos
microRNA	Micro-RNA
microRNAs	Micro-RNAs
min	Minute(s)
miR	Micro-RNA
miRNA	Micro-RNA
miRNAs	Micro-RNAs
miRs	Micro-RNAs
MM	Modified Masson´s
mM	Milimolar
mm²	Square milimeter
mRNA	MessengerRNA
MSC-EV	Mesenchymal stem cell-extracellular vesicle
MSC-EVs	Mesenchymal stem cell-extracellular vesicles
MSCs	Mesenchymal stem cells
mtDNA	Mitochondrial DNA
mTOR	Mammalian target of rapamycin
mTORC1	Mammalian target of rapamycin complex 1
mTORC2	Mammalian target of rapamycin complex 2
MVB	Microvesicular body
MVBs	Microvesicular bodies
N	Newborn
NAD(P)H	Nicotinamide adenine dinucleotide (phosphate) reductase
NADP	Nicotinamide adenine dinucleotide phosphate
Nanog	Homeobox protein NANOG
nanoHPLC	Nano-high-performer liquid chromatography
ND	Nodocazole
NF-κB	Nuclear factor kappa-light-chain-enhancer of activated B cells
ng/ml	Nanogramme per militer
NGF	Nerve growth factor
NGS	Next Generation Sequencing
nm	Nanometer
nM	Nanomolar
nt	Nucleotide
NTA	Nanoparticle tracking analysis
° C	° Celsius

Oct4	Octomer-binding transcription factor 4
Or	Oil red
OS	Osteogenic medium
P	Pubertal
P/PP	Pubertal vs pre-pubertal
P0	Passage zero
p53/p21	Tumor antigen p53/cyclin-dependent kinase inhibitor 1A
P70s6k	Ribosomal protein S6 kinase beta-1
p-Akt	Phospho-Akt
PBS	Phosphate-buffered saline
PDDF	Presence of characteristic enlarged
PDGF	Platelet-derived growth factor receptor A
PDIA1	Protein disulfide-isomerase A1
PGE2	Prostaglandin E2
PI	Propidium iodide
PI3K/Akt	Phosphatidylinositol-3-kinase/Akt
p-Mtor	Phospho-mTOR
PP	Pre-pubertal
PP/Y	Pre-pubertal vs young
pri-miRNAs	Long miRNA precursors
PRKD1	Protein kinase D1
qRT-PCR	Real time quantitative polymerase chain reaction
Raptor	Regulatory-associated protein of mTOR
Rb/p16	Retinoblastoma protein/cyclin-dependent kinase inhibitor 2A
rBM-MSCs	Rat bone marrow-mesenchymal stem cells
Rex1	Zinc finger protein 42 homolog
rhTGF-β3	Recombinant human transforming growth factor-βeta 3
Rictor	Rapamycin-insensitive companion of mTOR
RIN	RNA integrity
RISC	RNA-induced silencing complex
RNA	Ribonucleic acid
RNA Pol II	RNA Polymerase II
RNAi	RNAinhibitor
RNAs	Ribonucleic acids
Rnase A	Ribonuclease A
RNA-seq	RNA-sequencing
rno	<i>Rattus norvegicus</i>
RNU6	RNA, U6 small nuclear 1
ROCKi	Rho-associated protein kinase inhibitor
ROS	Reactive oxygen species
rpm	Revolutions per minute
rrTNFα	Recombinant rat tumor necrosis factor alpha
RT	Retrotranscription
s	Second(s)
S	Synthesis
S100	S100 calcium-binding protein

S100A4	S100 calcium-binding protein A4
S100A6	S100 calcium-binding protein A6
Saf O	Safranine O
SASP	Senescence-associated Secretory Phenotype
SA-β-gal	Senescence-associated β-galactosidase
SDS-PAGE	SDS polyacrylamide gel
Sec1/Munc-18	Protein transport protein SEC1/ Mammalian uncoordinated-18
Ser2448	Serine2448
Ser/thr	Serine/threonine
SIPS	Stress-induced premature senescence (Soluble <i>N</i> -ethylmaleimide sensitive fusion proteins Attachment Protein) Receptors
SNAREs	
SOD-2	Superoxide dismutase-2
Sox2	(Sex determining region Y)-box 2
SPRY229	SPRY domain-containing SOCS box protein 3
St.Clara	Saint Clara
St.Louis	Saint Louis
T	Temperature
T cells	Tregs cells
TAB2	TGF-βeta activated kinase 1/MAP3K7 Binding Protein 2
TAK1	TGF-βeta activated kinase 1
TBS	Tris buffered saline
TBST	Standard buffer tris buffered saline with 0.1% (v/v) Tween® 20
TCEP	Tris-(2-carboxyethyl) phosphine
TEAB	Tryethylammonium bicarbonate
TFA	Trifluoroacetic acid
TGF-β	Transforming Growth Factor-beta
TGF-β1	Transforming growth factor-beta1
TIMP-2	TIMP metalloproteinase inhibitor-2
TLR	Toll-like receptor
TLR4	Toll-like receptor type 4
TMRM	Tetramethylrhodamine methyl ester
TNF	Tumour necrosis factor
TSAP6	Tumour suppressor-activated pathway 6
Tsg101	Tumor susceptibility gene 101 protein
V	Voltie(s)
v/v	Volume/volume
VEGF	Vascular endothelial growth factor
w/v	Weight/volume
Wnt	Wingless-type MMTV integration site family
Wnt5a	Wnt family member type 5A
xg	G-force or relative centrifugal forces
Y	Young
Y/I	Young vs infant
yBM-MSCs	Bone marrow-mesenchymal stem cells from young group Mesenchymal stem cell-derived extracellular vesicles from young group
yEVs	

yMSCs	Mesenchymal stem cells from young group
Y-RNA	Small non-coding RNA
α-ciano	Alpha-ciano
β-actin	beta-actin
γH2AX	Histone variant gamma H2AX
Δratio	Differential of ratio
$\Delta\Delta$Ct	Delta(delta(threshold cycles))

1. INTRODUCTION

1.1 Mesenchymal stem cells

1.1.1 Definition

Mesenchymal stem cells (MSCs) are multipotent fibroblast-like cells that can be found in almost all tissues and they can differentiate into bone¹, cartilage², muscle³, tendon, ligament⁴, fat⁵, and a variety of other connectives tissues^{6,7}. MSCs were first reported in 1968 by Friedenstein *et al.*⁸ when human bone marrow cells were cultured in plastic dishes colonies of adhered fibroblastoid cells proliferative.

MSCs are adult stem cells which have a great self-renewal capacity, is the process by which a stem cell divides asymmetrically or symmetrically to propagate one or two daughter stem cells with similar development potential as the mother cells⁹ while maintaining pluripotency, namely the capacity to self-maintained in undifferentiated state¹⁰ (**Figure 1.1**).

The International Society for Cellular Therapy (ISCT) suggested the following criteria for the identification of MSCs¹¹:

- Adherence to plastic.
- Differentiation into chondrocytes, osteoblasts and adipocytes under standard *in vitro* differentiating conditions.
- Expression of surface markers CD105, CD73, CD29 and CD90, in the absence of CD45, CD34, CD14, CD11b, CD79 α .

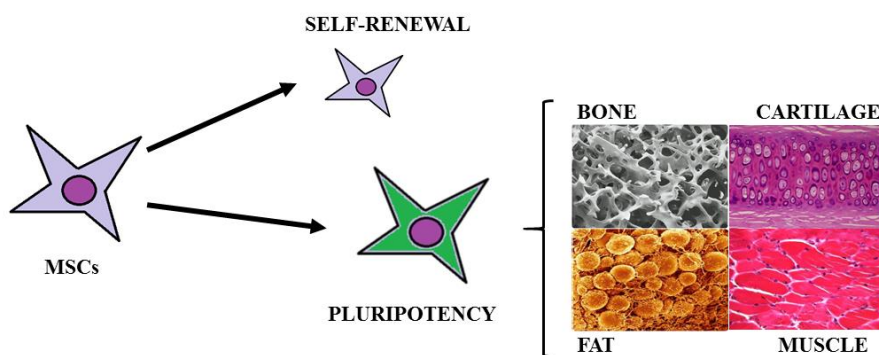


Figure 1.1. Definition of mesenchymal stem cells.

1.1.2 Sources for mesenchymal stem cells

MSCs have been isolated from many different adult tissues, including bone marrow¹², adipose tissue¹³, synovial membrane¹⁴, connectives tissues of dermis¹⁵, skeletal muscle¹⁶, peripheral blood¹⁷, liver¹⁸, lung¹⁹ and blood vessels²⁰ and from rather “young sources” such as amniotic fluid²¹, amniotic membrane²², umbilical cord blood²³, umbilical cord stroma²⁴, or placenta²⁵. In the last years the number of tissues with a potential for tissue engineering has increased^{6,26} (**Figure1.2**).

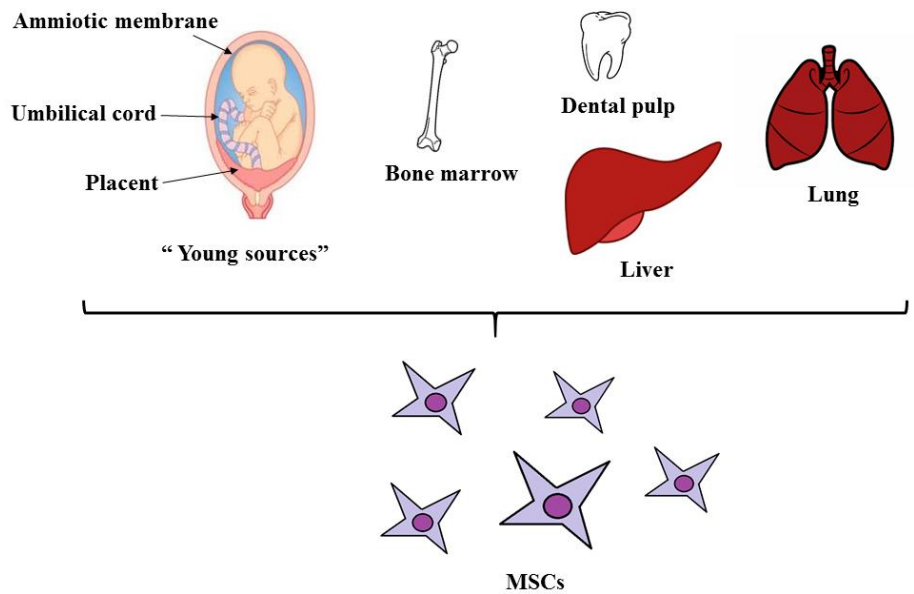


Figure 1.2. Several sources from MSCs.

Therefore, there are more studies about differences at cellular and molecular levels such as, cell morphology, surface markers²⁷, differentiation²⁸, proliferation^{27,1}, transcriptomic²⁹ and proteomic³⁰ analyses among MSCs from several tissue sources.

1.1.3 Properties of mesenchymal stem cells supporting therapeutic application

To date, the clinical use of stem cells presents some disadvantages because stem cells from certain sources, such as somatic nuclear transfer, embryo destruction, or even induced pluripotent stem cells (iPSCs) obtained by reprogramming have raised deep ethical issues depending on the country work^{31,32}. Besides, they could produce neoplastic disorders and immunologic rejection when they are injected in *in vivo* models³². For these reasons, MSCs are a good alternative because they don't produce immunologic disorders due to their autologous origin and there are not ethical issues about their clinical use³¹. Additionally MSCs possess the following properties:

1.1.3.1 Differentiation

MSCs can differentiate both *in vivo* and *in vitro*, into various mesenchymal cells and exhibit remarkable plasticity given their ability to trans-differentiate, or undergo an abrupt alteration in phenotype, thereby giving rise to cells possessing the characteristics of different lineages^{33,34}.

1.1.3.2 Paracrine effects and immunomodulation

It is the capacity of MSCs to secrete a wide variety of cytokines, chemokines, and growth factors.

Several studies based on examination of MSCs secretome *in vivo* and the strategies to modulate the secretion of molecules of MSCs have identified high levels of proteins involved in immune response such as interleukin-6 (IL-6), IL-8, monocyte chemoattractant protein (MCP-1), and transforming growth factor- β (TGF- β); extracellular matrix remodelers like TIMP metalloproteinase inhibitor 2 (TIMP-2), fibronectin, periostin, collagen, decorin, metalloproteinase inhibitors; growth factors and their regulators such as vascular endothelial growth factor (VEGF), granulocyte-macrophage colony-stimulating factor (GM-CSF), bone morphogenetic protein 2 (BMP-2), basis fibroblast growth factor (bFGF), and insulin-like growth factor-binding protein 3 (IGFBP3), IGFBP4, IGFBP7³⁵.

Also, MSCs can modulate immune response system and they were effective for treatment of various immune response disorders in both human and animal models³⁶⁻³⁸. However, the underlying mechanism of that modulation is not fully understood. The most accredited theory points to the important cell-to-cell contact and/or the release of soluble immunosuppressive factors. They interacted with a broad range of immune cells and displayed an ability to suppress the excessive response of T and B cells, dendritic cells, macrophages and natural killer cells^{39,38}. Besides, MSCs can also induce regulatory T cells (Tregs) and maintain the capability of Tregs to suppress self-reactive T-effector responses⁴⁰ (**Figure 1.3**).

In the last years, it was proposed that MSCs interact with their environments both by negatively regulating the immune response in the case of major inflammation and by stimulating the immune response system by releasing pro-inflammatory molecules if the level of inflammatory cytokines is low⁴¹.

1.1.3.3 Homing mechanism

The homing mechanism of MSCs lies in their ability to reach damaged tissue in response to a correct combination of signalling molecules from the injured tissue and corresponding receptors. Homing-related molecules in general can be up-regulated by inflammatory cytokines such as tumour necrosis factor (TNF) and IL-1⁴², suggesting that different inflammation states might promote distinct MSC engraftment and therapeutic efficiencies⁴³ (**Figure 1.3**).

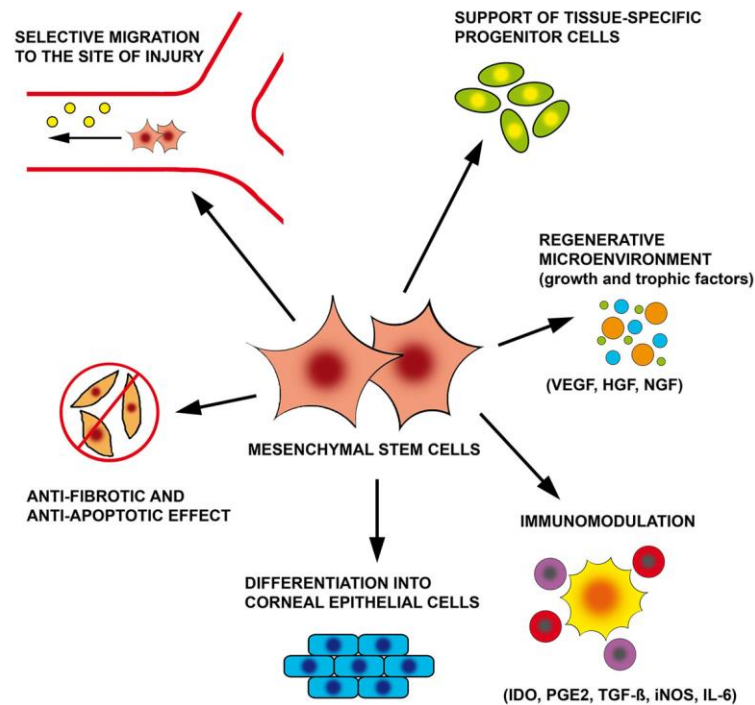


Figure 1.3. Properties of MSCs. From <http://www.iem.cas.cz/research/departments/transplantation-immunology.html> at June 30, 2016.

1.1.4 Applications in clinical use

MSCs have emerged as a novel strategy to therapeutic application of the US National Institute of Health 493 MSC-based clinical trial have been reported as of June 15, 2015; most were performed to evaluate the biomedical potential of MSCs in treating haematological diseases including Graft-versus-host disease (GVHD), diabetes, inflammatory diseases, and disease in the liver, kidneys, and lungs, as well as cardiovascular, bone and cartilage, neurological (**Figure 1.4**). MSCs have the ability to differentiate into several mesenchymal lineages²⁷ and contribute to the replacement of the damaged tissue, but rather act as trophic mediators, promoting tissue repair by production and release of soluble factors that inhibit inflammation, reduce fibrosis, and induce angiogenesis⁴⁴ among other functions.

Phases of investigation of 493 MSC-based clinical trials and the most representative treated pathologies are shown in the **figure 1.4** According to these data, most clinical trials occurred in an early phase (phase I, I/II, or II), demonstrating that more investigation about the therapeutic effectiveness of MSCs is required.

Several studies indicate that donor heterogeneity, *ex vivo* expansion, immunogenicity, and cryopreservation can be considered the Achilles'-heel of MSC-base therapies. Therefore, it is necessary that researchers and clinical discoveries will address the mechanisms influencing their therapeutic use.

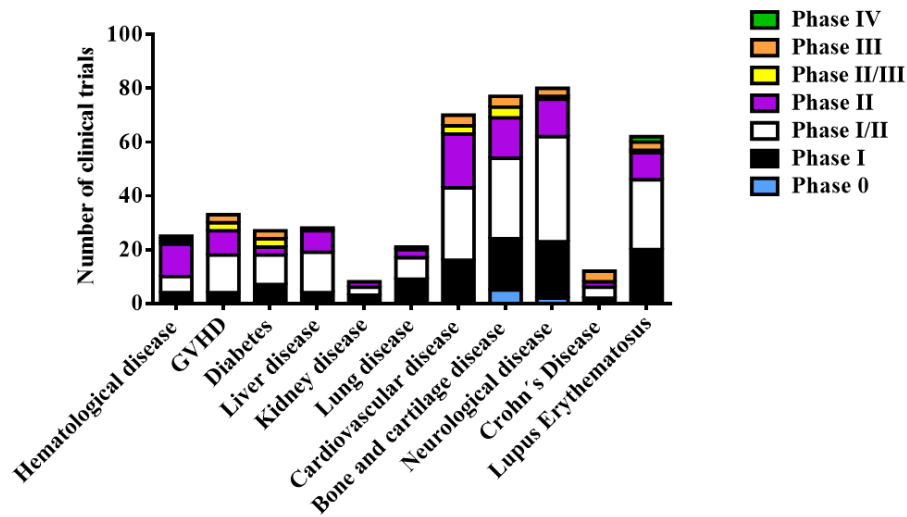


Figure 1.4. Number and percentage of MSC-based clinical trials classified by disease type. Data from www.clinicaltrial.gov at June 30, 2015.

1.2 Aging

1.2.1 Definition

Aging is the decline in the homeostasis and regenerative capacity of all tissues and organs and it is the greatest risk factor for the development of chronic diseases which comprise the majority of global disease burden and are the most common causes of mortality. Mammalian aging can be delayed with genetic, dietary, and pharmacological approaches. Given that the elderly population is dramatically increasing. (<http://www.healthmetricsandevaluation.org/data-visualizations> at July 9, 2016).

Actually, in the world the number of people aged 65 or older will outnumber children under age 5. Driven by falling fertility rates and increasing in life expectancy, population aging will continue, even accelerate. The number of people aged 65 or older are projected to grow from an estimated 1.5 billion in 2050, with most of the increase in developing countries⁴⁵. Actually, there is an urgent need to extend healthspan.

1.2.2 The hallmarks of aging

Defining the causes of aging is a difficult work because it is impeded by the complexity of the phenotype coupled with the costs and duration of longevity studies but in recent years, progress has accelerated, bringing geroscience to the forefront.

Firstly, genetic and environmental interventions and pathways that regulate longevity were studied in yeast (particularly the budding yeast, *Saccharomyces cerevisiae*)^{46,47} and invertebrate model organisms, such as *Caenorhabditis elegans*^{47,48}. Conserved molecular pathways impacting aging have been identified, such as insulin/ insulin-like growth factor signalling (IIS). Secondly, mammalian studies have generated a more detailed understanding of age-associated pathologic changes. Additionally, studies about effects of environmental interventions on the lifespan have been performed. Those studies have revealed key genes and pathways for cellular ageing such as IIS and the mammalian target of rapamycin (mTOR) which are implicated in mediating the effects of dietary restriction^{49,50}.

In the last years, López-Otín *et al.*⁵¹ have identified and categorized the cellular and molecular hallmarks of aging. These hallmarks are not independent factors driving aging; rather, they were highly intertwined processes, and understanding the interplay among them is critical (**Figure 1.5**).

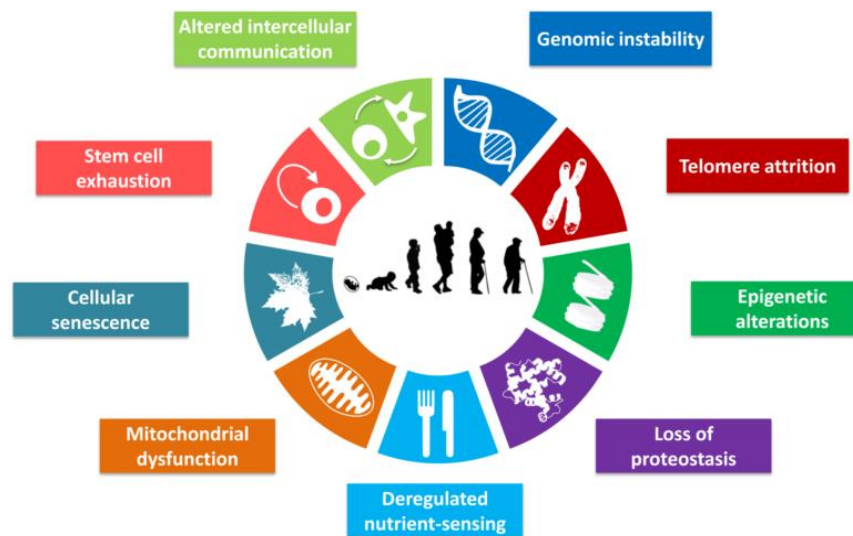


Figure 1.5. The Hallmarks of aging. From López-Otín *et al.*⁵¹.

1.2.2.1 Genomic instability

The accumulation of genetic damage throughout life is the most studied cause of aging⁵². In this hallmark are included several areas of aging research such as mechanisms for the maintaining the appropriate length and functionality of telomeres^{53,54} and for ensuring the integrity of mitochondrial DNA (mtDNA)⁵⁵, as well as defects in the nuclear architecture known as laminopathies which causes premature aging syndromes⁵⁶.

1.2.2.2 Telomere attrition

Telomere attrition is associated with aging in mammal models because pathological telomerase dysfunction accelerates aging in mice and humans⁵⁷, while experimental stimulation of telomerase can delay aging in mice⁵⁸.

1.2.2.3 Epigenetic alterations

This hallmark contains a variety of epigenetic alterations affecting lifespan of cells and tissues such as DNA methylations patterns⁵⁹, post-translational modification of histones^{60,61} and chromatin remodelling^{62,63}. The important goals of this hallmark are biomarker development between chronological age and biologic aging, link age-related environment inputs to epigenetic signatures and test small molecules that regulate enzymes controlling epigenetic events^{48,64,65}.

1.2.2.4 Loss of proteostasis

Proteostasis involves mechanisms for the stabilization of correctly folded proteins, most prominently the heat-shock family of proteins, and mechanisms for the degradation of proteins by the proteasome or the lysosome^{66,67}. Many studies have demonstrated that proteostasis is altered with aging⁶⁶, also chronic expression of unfolded, misfolded or aggregated proteins contribute to the development of some age-related pathologies, such as Alzheimer's disease, Parkinson's disease and cataracts⁶⁸.

Some important studies to advance this hallmark through identification of proteostasis pathways that are overwhelming in specific chronic disease states, examination crosstalk between proteostasis machineries and understand non-cell-autonomous signalling and activation of proteostasis pathways.

1.2.2.5 Deregulated nutrient-sensing

There are several conserved pathways related to deregulated nutrient-sensing such as IIS pathways, which is related to metabolism of glucose in the cells⁶⁹, mTOR pathway which is also involved in anabolism metabolism and aging^{50,70} and AMPK and sirtuins, acting in the opposite direction to IIS and mTOR⁷¹.

This hallmark have important focus as determination role of signal transduction pathways linked to metabolism in the aging process and pharmacological manipulation that mimics a state of limited nutrient availability like rapamycin⁷².

1.2.2.6 Mitochondrial dysfunction

This detrimental process has been long associated with aging because the efficacy of the respiratory chain tends to diminish with increasing age, thus increasing electron leakage and reducing ATP generation⁷³. But. there are less clear different aspects for example, knowledge about bridge continuum from physiological to molecular stresses, differentiation between toxic stress and hormesis, is the mechanism to response to harmless doses of toxins and other stressors. It could

constitute to one of the mechanisms that allows stressed cells to avoid senescence and death⁷⁴.

1.2.2.7 Cellular senescence

It is a stable arrest of the cell cycle coupled to stereotyped phenotypic changes⁷⁵. This phenomenon was described by Hayflick⁷⁶. To date, it is known that the senescence observed by Hayflick *et al.*⁷⁶ is caused by telomere shortening, but there are other aging-associated stimuli that trigger senescence independently of telomeric process^{77,78}. The most famous non-telomeric DNA damage is de-repression of *INK4/ARF locus*⁷⁵. The controversy of cell senescence as a beneficial compensation on aging and cancer or deleterious and accelerate aging.

1.2.2.8 Stem cell exhaustion

The most obvious characteristic of aging is the decline in the regenerative potential of tissues. For example, hematopoiesis declines with age, resulting in a decreasing production of adaptive immune cells, a process termed immunosenescence⁷⁹.

The important goals in this hallmark are:

- To determine whether declining adult stem cell function drives to aging and chronic disease.
- To examine how aging and associated diseases impair adult stem cell function.
- To define how macromolecular damage accumulates in aging adult stem cells pools.

1.2.2.9 Altered intercellular communication

A prominent aging-associated alteration in intercellular communication is “Inflammaging”, which may result from multiples causes such as the accumulation of pro-inflammatory tissue damage, the failure of an ever more dysfunctional immune system to effectively clear pathogens and dysfunctional host cells, the propensity of senescent cells to secrete pro-inflammatory cytokines through activation of the NF-κB transcription factor, chemokines and extracellular matrix (ECM) remodelling proteases, is named the senescence-associated secretory phenotype (SASP)^{80,81}.

Also, there are other processes related to cellular communication which induce senescence in neighbouring cells via gap junction-mediated cell-cell contacts and processes involving ROS⁸².

1.2.3 Mechanisms of aging on mesenchymal stem cells

Aging is associated with a marked decline in functionalities of adult stem cells, namely tissue homeostasis, repair and regeneration⁸³.

The combination of cell-intrinsic changes leads to decline in cellular function, which in turn contributes to tissue dysfunction and organism aging (**Figure 1.6**). The intrinsic changes are:

- Genomic changes: include accumulation measurable genomic lesions, including single- and double-strand DNA breaks, chromosomal translocations, telomere shortening⁸⁴.
- Epigenetic changes: include DNA methylation and post-translation modification of histones, are dynamically maintained by a balance among chromatin-remodeling complexes and, thus, reversible⁸⁵ and altered expression of cofactors of histones⁸⁶.
- Proteomic changes: maintenance of the intracellular proteome requires timely removal of improperly folded or damaged proteins that can otherwise impede normal cellular function⁶⁶. The machineries and cellular processes, which maintain protein homeostasis are autophagosomes, chaperones, lysosomes and the ubiquitin-proteasome system⁶⁸.

Also the extrinsic influences, such as inflammatory cytokines and Wnt activators influence in the aging process of the tissue and organism. The niche is profoundly influenced by the systemic milieu and dynamically changing to regulate stem cell function, a feature that is especially relevant with regard to the process aging⁸⁷ (**Figure 1.6**).

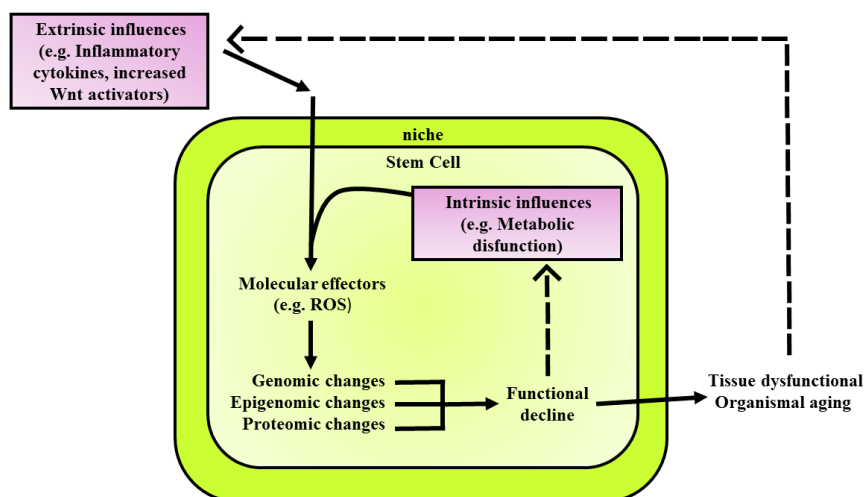


Figure 1.6. Extrinsic and intrinsic influences on stem cell aging. Adapted from Liu *et al.*⁸⁸.

MSCs have been reported to be highly resistant to apoptosis induced by different genotoxic insults and preferentially respond to injury with activation of stress-induced premature senescence (SIPS), which had been widely studied in MSCs, particularly for its clinical implications⁸⁹. Also, it was demonstrated that the senescence activation pathway in MSCs is independent of the tissue source^{89–92}.

Senescent MSCs activate p53/p21 and Rb/p16 pathways to block the cell cycle and sustain growth arrest but they continue to be metabolically active⁹³. The cells in a senescent state are characterized by a large, flat morphology, display changes in gene expression, typically exhibit a senescence-associated β -galactosidase (SA- β -gal), for persistent DNA damage response (DDR) activation, as highlighted by the presence of characteristic enlarged (PDDF), containing γ H2AX and 53BP1 *foci*⁹⁴ and SASP^{81,91} (Figure 1.7).

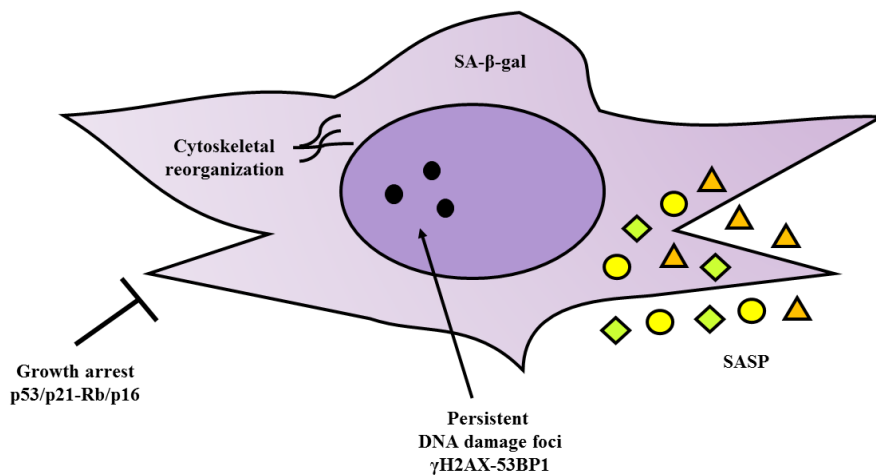


Figure 1.7. Phenotype characterization of senescence MSCs. Adapted from Turinetto V *et al.*⁹⁵

Senescence impacts on migratory ability^{96,97}, differentiation potential⁹⁸, immunomodulation ability⁹⁷, loss of proliferation capacity and tumour progression⁹².

1.3 Extracellular vesicles

1.3.1 Definition

Extracellular vesicles (EVs) are membrane-contained vesicles released in an evolutionally conserved manner by cells ranging from organisms such as prokaryotes.

During the past decades, EVs have been recognized as potent vehicles of intercellular communication in different model systems with respect to other cell-to-cell communication strategies, such as quorum sensing, juxtacrine signalling, autocrine signalling, paracrine signalling, endocrine signalling and direct cell-to-cell communication (desmosomes, adherents and gap junctions).

1.3.2 Types of extracellular vesicles

EVs can be isolated from all types of body fluids including blood, urine, bronchoalveolar lavage fluid, breast milk, amniotic fluid, synovial fluid, pleural effusions and ascites⁹⁹ and from several cell types¹⁰⁰⁻¹⁰⁴.

The term EVs comprise a highly heterogeneous and dynamic group of nanoparticles. Therefore, International Society of Extracellular Vesicles (www.isev.org)¹⁰⁵ have promoted the collaboration work since 2011 by the members to unify the nomenclature and the methodologies of EVs by the contents, size, membrane composition, cellular source, state and environmental conditions.

Actually, three main subgroups of EVs have defined depend on size, sucrose gradient and origin (**Table 1.1 and Figure 1.8**).

Vesicle	Size (Diameter)/nm	Sucrose gradient/ g.ml ⁻¹	Origin
Exosomes	40-100	1.13-1.19	Luminal budding into MVBs Release by fusion of MVB with cell membrane
Microvesicles Microparticles Ectosomes	50-1000	1.04-1.07	Outward budding of cell membrane
Apoptotic bodies	1-5000	1.16 and 1.28	Outward blebbing of apoptotic cell membrane

Table 1.1 Different types of EVs. Adapted from Rani *et al.*¹⁰⁶.

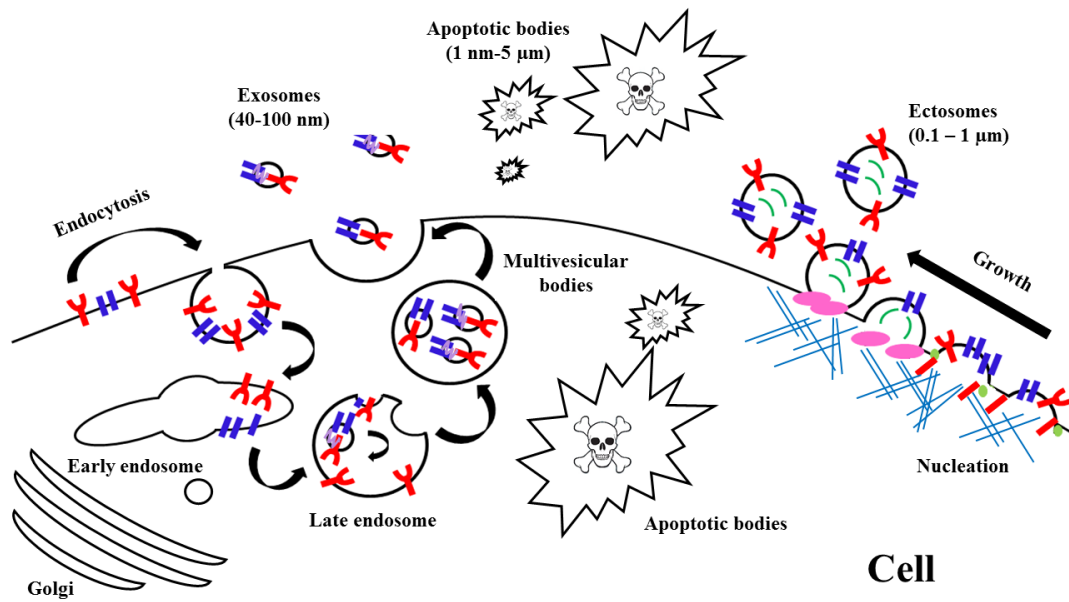


Figure 1.8. Different types of EVs. Adapted from Cocucci *et al.*¹⁰⁷

1.3.3 Composition of Extracellular Vesicles

Public on-line databases that catalogue EV-associated components, are available. These include Vesiclepedia (www.microvesicles.org/)¹⁰⁸, EVpedia (www.evpedia.info)¹⁰⁹ and ExoCarta (www.exocarta.org)¹¹⁰.

1.3.3.1 Protein and protein-associated of EVs

Proteomic studies of EVs released by primary cell cultures, cell lines, tissue cultures or isolated from biofluids have yielded extensive number of protein abundance in different types of EVs. In general, EVs are highly abundant in cytoskeletal, cytosolic, heat shock, plasma membrane proteins and proteins involved in vesicle trafficking.

Also there are some studies where it have identifying some markers of EV sub-populations that are often used as markers, such as tetraspanins (CD9, CD63, CD81 and CD82) which are considered marker of exosomes, 14-3-3 protein, major histocompatibility complex (MHC) molecules and heat shock proteins (HSPs), Tsg101 and the Endosomal Sorting Complex Required for Transport (ESCRT-3) binding protein a Alix which are considered marker of exosomes¹¹¹⁻¹¹³ (Figure 1.9).

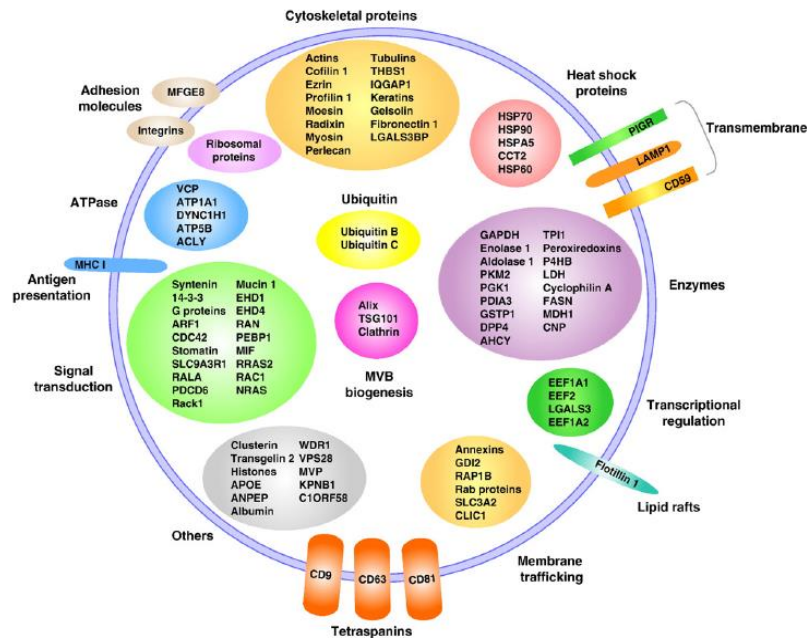


Figure 1.9. Protein composition of EVs. From Mathivanan *et al.*¹¹⁴.

Several studies reported about changes in the glycosylation patterns of EVs^{115–118}, protein signature of different EVs which may be involved in biogenesis, sorting^{119,120}, uptake¹¹⁰ and EV-associated cytokines^{121,122} (Figure 1.9).

1.3.3.2 RNA composition

EVs contain intact mRNA¹²³, mRNA fragments¹²⁴, long non-coding RNA^{125,126}, miRNA^{127,128}, piwi-interacting RNA¹²⁵, ribosomal RNA¹²⁵ and fragments of tRNA, vault- and Y-RNA^{129,130}. It occurred an increased of studies about activity of RNA in EVs because they are more enriched in EVs with respect to parental cells¹⁰¹. EVs contained RNAs are involved in cell differentiation^{131–133}, proliferation^{132,134}, immune regulation¹³⁵, modulation stress¹³⁴ condition and other^{117,136–138}.

1.3.3.3 DNA contain

The study of the DNA contained in EVs represents a relatively new approach to the field. Oncogenic DNA was found in apoptotic bodies¹³⁹. Also, mitochondrial DNA (mtDNA), single-stranded DNA, double-stranded DNA (dsDNA) and oncogene amplifications have been detected in EVs^{140,141}.

1.3.3.4 Lipid composition

EVs are generally enriched in sphingomyelin, cholesterol and glycosphingolipids similar to raft domain¹⁴². Some studies reported that the specific lipid that confers the stability of EVs may be used to improve liposomal drug delivery systems^{143,144}, sorting, biogenesis^{142,145}.

1.3.4 Formation and sorting EVs

1.3.4.1 Exosome biogenesis

The membrane of late endosomes invaginates and forms small vesicles that are pinched off into the endosomal space. These are the intraluminal vesicles (ILVs) and the whole is the MVE. Notice that the internal face of an ILV membrane corresponds to the cytoplasmic face of the endosome limiting membrane, and the content of the ILV is originated from the cytosol prior to ILV formation. A set of MVEs fuse their limiting membranes to the plasma membrane and the ILVs with their cargo into the extracellular space¹⁴⁶.

Formation of ILVs in the late endosome involves the endosomal sorting complex required for transport (ESCRT) proteins. ESCRT proteins are components of four ESCRT complexes, ESCRT-0, ESCRT-I, ESCRT-II, and ESCRT-III. Each of these complexes is sequentially and transiently recruited to the forming MVE until a vesicle is fully shaped and released as an ILV into the endosomal space^{146,147} (**Figure 1.10**).

However, increasing evidences about the key role of some lipids such as ceramide in ILV formation, independently of ESCRT complexes¹⁴⁶.

As mentioned above, a set of MVE fuses with the plasma membrane while other MVEs follow a degradative route and fuse with lysosomes (**Figure 1.10**).

Some studies identified the existence of different populations of MVEs:

- MVEs rich in GTPase Rab7 and ILVs containing phosphatidylinositol-3-phosphate and ubiquitinated proteins are sorted to lysosomes¹⁴⁸.
- MVEs rich in GTPase Rab11 and ILVs with high amounts ceramide are sorted for exosome secretion^{149,150}.

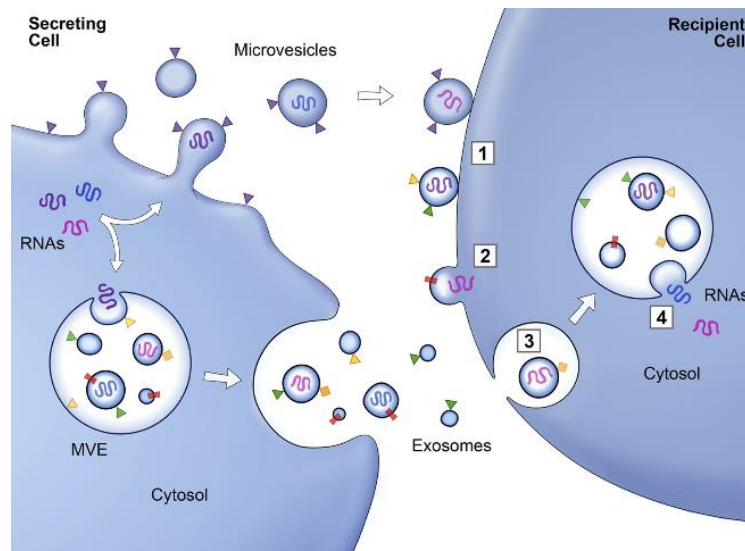


Figure 1.10. Formation and sorting EVs. Membrane-associated (triangles) and transmembrane proteins (rectangles) and RNAs (curved symbols) are selectively incorporated into the ILV of MVEs or into MVs budding from the plasma membrane. MVEs fuse with the plasma membrane to release exosomes into the extracellular milieu. MVs and exosomes may dock at the plasma membrane of a target cell (1). Bound vesicles may either fuse directly with the plasma membrane (2) or be endocytosed (3). Endocytosed vesicles may then fuse with the delimiting membrane of an endocytic compartment (4). Both pathways result in the delivery of proteins and RNA into the membrane or cytosol of the target cell. Fusion and endocytosis are only represented for exosomal vesicles, but plasma membrane-derived MVs may have similar fates. From Raposo *et al.*¹⁵¹.

MSC releases EVs differently depending on the external stimulation, such as hypoxia and inflammatory¹⁵². Tumour suppressor-activated pathway 6 (TSAP6) is found regulate EV formation¹⁵³ and this pathway is regulated by p53 thereby enhancing EV production^{154,155}.

1.3.4.2 Microvesicles biogenesis

Microvesicles result from outward budding and fusion of the plasma membrane. Membrane budding initiated by the activity of aminophospholipid translocase, responsible for placing phosphatidylserine to the outer membrane. ADP-ribosylation factor 6 plays an important role in enabling MV budding^{156,157} and contractile protein myosin light chain kinase 2 in release of MVs¹⁵⁷⁻¹⁵⁹ (**Figure 1.11**).

1.3.5 EVs uptake

1.3.5.1 Endocytosis

It is the most evidence process of internalization because EVs are usually taken up into endosomal compartment via endocytosis. It was identified inside cells from as early as 15 minutes after initial introduction^{160,161}. By using a range of inhibitor to block specific pathways and other experimental techniques such as

RNA inhibitor (RNAi) to knockdown certain genes the role of the endocytosis processes responsible for EV uptake and they found several subtypes of endocytosis, such as clathrin-mediated endocytosis^{117,162,163}, caveolin-dependent endocytosis^{162,164–167}, macropinocytosis¹⁶⁸, phagocytosis^{168,169} and involvement lipid raft¹⁷⁰ (Figure 1.11).

1.3.5.2 Cell surface membrane fusion

It is via direct fusion between the EV membrane with cell plasma membrane¹⁷¹. Several proteins participate in this process including SNAREs, Rab proteins and Sec1/Munc-18 related proteins^{150,172,173}.

1.3.5.3 Cell specific EV uptake

Results from some studies show that fluorescently labelled EVs can be taken up by virtually every cell type tested^{174,175}, whereas other suggest that vesicular uptake is a highly specific process which can only occur if cell and EV share the right combination of ligand and receptor.

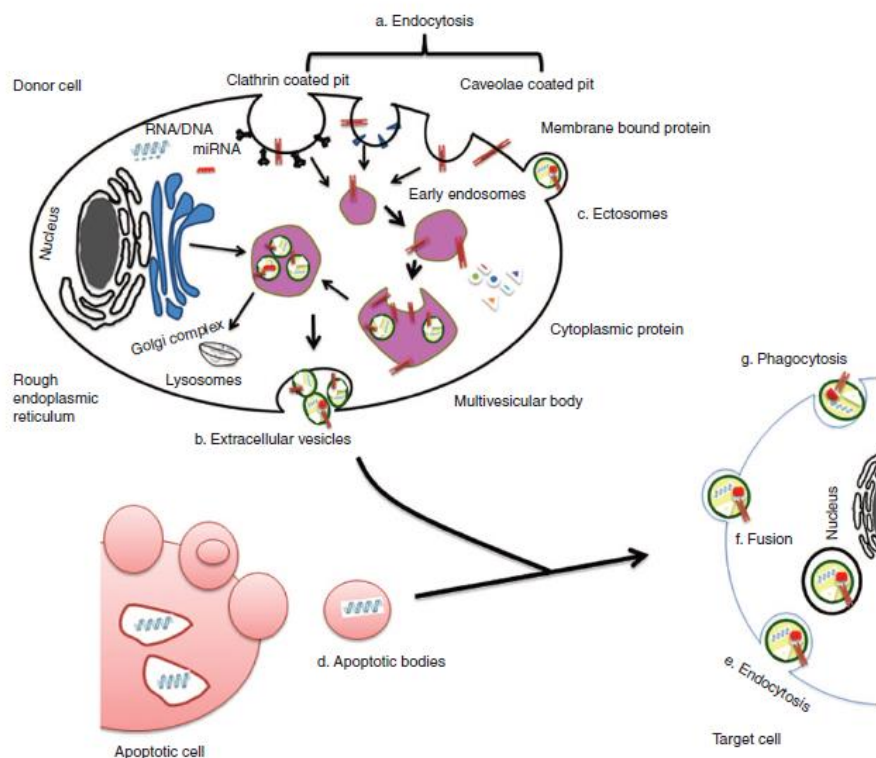


Figure 1.11. Origin of EVs. It is generally via (a) endocytosis or inward budding of plasma membrane that consist of lipid rafts and is mediated by clathrin-dependent or caveolae-dependent pathway, This gives rise to (b) early endosomes leading to the formation of numerous ILVs within a membrane maturing to MVBs. Finally MVBs fuse with plasma membrane releasing ILVs as exosomes. (c) Ectosomes are vesicles shed from the cell surface and (d) apoptotic bodies are also known as apobodies and are released by cells undergoing apoptosis. EVs are internalized by the target cells through several pathways including (e) endocytosis, (f) fusion, and (g) phagocytosis. From Rani *et al.*¹⁰⁶.

1.3.6 Applications in clinical use

Recent animal model-based studies suggest that EVs have significant potential as a novel alternative to whole cell therapies^{106,176} and they were used to discovery biomarkers of diseases^{177,178}.

Compared to MSC, EVs may have a superior safety profile and can be safely stored without losing function¹⁰⁶ but it is necessary to advance to clinical use of MSC-EVs for common human diseases because there are unresolved questions, such as definition, standardisation, cost-effective production, optimal dosing and, most importantly, safety.

There are more studies about therapeutic effects of MSC-derived EVs in cardiovascular disease¹⁷⁹, acute kidney injury¹³⁵, liver disease¹⁸⁰, lung diseases¹⁸¹, cutaneous wound healing¹⁸², Alzheimer's disease¹⁸³ and drug delivery^{143,184}.

1.4 miRNAs

1.4.1 Definition

miRNAs are small, noncoding RNAs, 19-24 nucleotides in length, which regulate gene expression post transcriptionally¹⁸⁵.

1.4.2 Biogenesis of miRNAs

miRNA biogenesis pathway starts in the nucleus¹⁸⁶. Firstly, they are transcribed by RNA polymerase II (RNA Pol II) as an approximately 70-nucleotide (nt) long stem-loop primary structure named primary-miRNA transcripts, pri-miRNAs (long miRNA precursors), which are processed by DROSHA RNase III enzyme into precursors to generate pre-miRNAs structure¹⁸⁵.

Finally, the two strands of the duplex are separated from each other by the Dicer-TRBP complex. Next, the RNA-induced silencing complex (RISC), which also consists of the Argonaute protein and the target mRNA, is complementary bound by specific miRNAs. Consequently, the target mRNAs translation is repressed resulting in translational silencing or induction of mRNA degradation by RNases¹⁸⁷ (**Figure 1.12**).

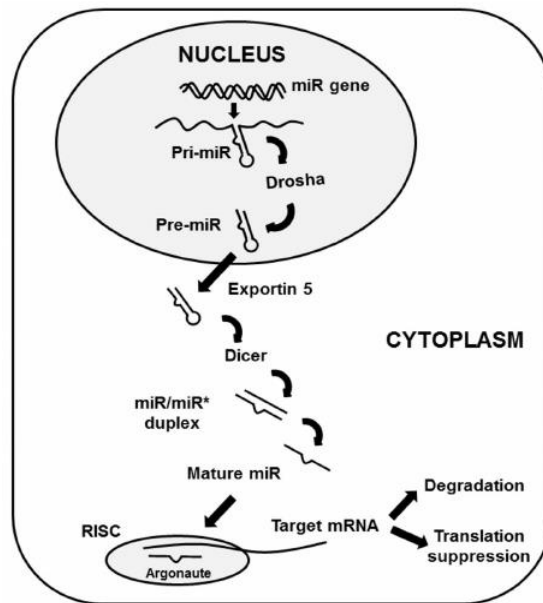


Figure 1.12. Process miRNAs biogenesis. From Jin Jung *et al.*¹⁸⁸

1.4.3 miRNAs in EVs

Secretion of miRNAs in EVs is a novel form of the intercellular communication. However, the mechanisms governing miRNA and miRNA-binding protein secretion into EVs remain largely unknown. Recently, mutant KRAS shown to regulate the content of RNA-binding protein in EVs^{189,190}.

1.4.4 Role in biological process

miRNAs have crucial regulatory roles in development of hematopoietic lineage, maturation, and differentiation of B,T lymphocytes¹⁹¹ and MSCs¹⁹², proliferation of neutrophils, monocytes^{193,194} and MSCs¹⁹⁵, secretion of type 1 interferon (IFN) and inflammatory cytokine/chemokine¹⁹³, and effectiveness of immune system response^{196,194}, immunosenescence¹⁹⁷, inflammaging¹⁹⁸, cancer¹⁹⁹ and other²⁰⁰. In the last years, miRs have been suggested possible therapeutic approaches for age-related life-threatening diseases^{201,202}.

2. HYPHOTESIS AND AIMS

Mesenchymal stem cells have self-renewal capacity and multiple differentiation potentials, and *a priori*, could play important roles in regenerative medicine but the promising role of MSCs in cell-based therapies and tissue engineering appears to be limited due to a decline of their regenerative potential with increasing donor age. For that, we proposed the following aims to understand whether aging affects the properties of MSCs:

1. Determination of proliferation profile of rat bone marrow mesenchymal stem cells at different ages.
2. Determination of pluripotency profile of rat bone marrow mesenchymal stem cells at different ages.
3. Proteome and transcriptome descriptive study of rat bone marrow mesenchymal stem cells at different ages.
4. Pro-inflammatory phenotype of rat bone marrow mesenchymal stem cells at different ages.
5. Characterization of rat bone marrow mesenchymal stem cell-derived extracellular vesicles at different ages.
6. Evaluation of relationship between miRNAs and Toll like receptor 4 pathway in rat bone marrow mesenchymal stem cell-derived extracellular vesicles at different ages.
7. Effect of miR-21-5p on pro-inflammatory and pluripotent capabilities from Toll-like receptor 4 in rat bone marrow mesenchymal stem cells.
8. Influence of rat bone marrow mesenchymal stem cells-derived extracellular vesicles on their self-renewal using an *in vitro* model.

3. MATERIAL AND METHODS

3.1 Isolation and culture of rBM-MSCs

The animals were euthanized with Fluorane (Izasa, A Coruña, Spain) and sacrificed by cervical dislocation method. Femurs were dissected from male Wistar rats (Animal Service, Complejo Hospitalario Universitario de A Coruña, Spain) at different ages: newborn (0 days old), infant (7 days old), young (14 days old), pre-pubertal (35-38 days old), pubertal (45 days old) and adult (+2 months old). All methods were carried out in “accordance” with the approved guidelines of the Spanish law (32/2007). All experimental protocols were approved by The Animal Ethical Committee of Galicia. The protocol used by Karaoz *et al.*¹² was followed in this work. Briefly, the end of the bones were cut away and a 21-gauge needle that was inserted into shaft of the bone marrow was extruded by flushing with 5 ml D-Hank’s solution supplemented with 100 IU/ml penicillin-100 mg/ml streptomycin (all from Life Technologies, Madrid, Spain). Marrow plug suspension was dispersed by pipetting, successively filtered through 70- μ m mesh nylon filter (BD Biosciences, Bedford, United States) and centrifuged at 2000 xg for 10 minutes. Supernatant containing thrombocytes and erythrocytes was discarded, and the cell pellet was re-suspended in the RPMI supplemented with 10% (v/v) fetal bovine serum (FBS), 1% (v/v) penicillin, 1% (v/v) streptomycin (all from Life Technologies, Madrid, Spain). The cells from four rats were seeded into 100 cm² dish plate (Corning Inc., New York, United States) and incubated at 37°C with humidified atmosphere 5% CO₂. rBM-MSCs were isolated on the basis of their ability to adhere to culture plates. On the third day, red blood cells and other non-adherent cells were removed by the pre-plating technique and fresh medium was added to allow further growth. The adherent cells grown to 70% confluence were defined passage zero (P0) cells. After 5 min of centrifugation, 1×10^6 rBM-MSCs were seeded on two 100 cm² dish plates (Corning Inc., New York, United States) in RPMI supplemented with 10% (v/v) FBS, 1% (v/v) penicillin and 1% (v/v) streptomycin (all from Life Technologies, Madrid, Spain). The culture medium was added and replaced every 3 or 4 days for 2 weeks. rBM-MSCs have been expanded for 2 passages to use in the following techniques.

3.2 Characterization of rBM-MSCs by flow cytometry

To characterize the populations of rBM-MSCs from chronologically different animals, their rBM-MSCs were washed twice in phosphate-buffered saline (PBS) (MP Biomedicals, Illkrich, France), then pre-blocked with 2% (v/v) rat serum (Life Technologies, Madrid, Spain) in PBS (MP Biomedicals, Illkrich, France). The following direct antibodies were used at different dilutions and wavelength detection windows (**Table 8.1**) to check mesenchymal and hematopoietic markers of the different populations of rBM-MSCs from chronologically different animals.

2×10^5 cells were analyzed by FACS Aria flow cytometer (BD Science, Madrid, Spain). FACS data was generated by DIVA software (BD Science, Madrid, Spain).

3.3 Proliferation analysis by flow cytometry

rBM-MSCs from adult cultured with medium RPMI supplemented with 10% (v/v) FBS, 1% (v/v) penicillin, 1% (v/v) streptomycin (all from Life Technologies, Madrid, Spain) with 10 nM rapamycin (Sigma-Aldrich, St.Louis, United States) for 2 days. After incubation with the drug, the cells were washed with PBS (MP Biomedicals, Illkrich, France), then fixed in 4% (w/v) (Sigma-Aldrich, St.Louis, United States) for 10 min. After the fixation, the cells were washed twice in phosphate-buffered saline (PBS) (MP Biomedicals, Illkrich, France), then pre-blocked with 2% (v/v) rat serum (Life Technologies, Madrid, Spain) in PBS (MP Biomedicals, Illkrich, France).

The following direct antibodies against CD117 and Ki67 were used at different dilutions and wavelength detection windows (**Table 8.1**) to check proliferation profile of the different populations of rBM-MSCs from chronological different animals. The stained cells were washed twice with PBS (MP Biomedicals, Illkrich, France) and 2×10^5 cells were analyzed by FACS Aria flow cytometer (BD Science, Madrid, Spain). FACS data was generated by DIVA software (BD Science, Madrid, Spain).

3.4 Reactive oxygen species analysis by flow cytometry

Intracellular reactive oxygen species (ROS) accumulation was measured using 2',7'-dichlorodihydrofluorescein diacetate (H₂DCF-DA) (Thermo Fisher, Waltham, United States). Upon oxidation by ROS, the non-fluorescent H₂DCF-DA is converted to the highly fluorescent 2',7'-dichlorofluorescein diacetate (HDCF-DA)²⁰³. MitoSOX™ Red mitochondrial superoxide indicator *for live-cell imaging* (Life Technologies, Madrid, Spain) was used to determine mitochondrial ROS, including superoxide dismutase activity²⁰⁴. Tetramethylrhodamine methyl ester (TMRM) (Life Technologies, Madrid, Spain), a permanent dye that accumulates in active mitochondria with intact potential²⁰⁵, was used to detect functional mitochondria in the rBM-MSCs at different ages following functional mitochondrial staining protocol from commercial.

3.5 Cell cycle analysis

Cell cycle analysis of rBM-MSCs from adult cultured with medium RPMI supplemented with 10% (v/v) FBS, 1% (v/v) penicillin, 1% (v/v) streptomycin (all from Life Technologies, Madrid, Spain) with different concentrations of imatinib mesylate (5 μM and 10 μM) or JK184 (0.1 ng/ml and 1 ng/ml) (all from Sigma-Aldrich, St.Louis, United States) for 2 days. After incubation with the drug, the cells were washed with PBS (MP Biomedicals, Illkrich, France), then fixed in 70% (v/v) ethanol (Panreac, Darmstadt, Germany). Posteriorly, the cells were incubated with 1 mg/ml RNase A (Sigma-Aldrich, St.Louis, United States) and 100 μg/ml propidium iodide (PI) (Sigma-Aldrich, St.Louis, United States). The cells cultured in RPMI 0% for 48 h were used such positive control

and the cells cultured in RPMI supplemented with 10% FBS (v/v), 1% (v/v) penicillin, 1% (v/v) streptomycin and 1.5 mg/ml methyl-(5-[2-thienylcarbonyl]-1-H-benzimidazol-2-YL) carbamate (Nodocazole) (all from Sigma-Aldrich, St.Louis, United States) overnight.

2×10^5 cells were analyzed by FACS Aria flow cytometer (BD Science, Madrid, Spain). FACS data was generated by DIVA software (BD Science, Madrid, Spain).

3.6 Pro-inflammatory phenotype analysis

3.6.1 Determination expression of CD200 by flow cytometry

rBM-MSCs at different ages were cultured with RPMI supplemented with 10% (v/v) FBS, 1% (v/v) penicillin and 1% (v/v) streptomycin (all from Life Technologies, Madrid, Spain) and 1 ng/ml recombinant rat tumor necrosis factor- α (rrTNF α) (Immunotools, Gladiolenweg, Germany) for 2 days. After that, cells were washed with Hank's balanced salt solution (HBSS) (Life Thecnologies, Madrid, Spain) and they were stained with anti-CD200 (**Table 8.1**). The stained cells were washed twice with PBS (MP Biomedicals, Illkrich, France) and 2×10^5 cells were analyzed by FACS Aria flow cytometer (BD Science, Madrid, Spain). FACS data was generated by DIVA software (BD Science, Madrid, Spain).

3.6.2 Activation TLR4 in rBM-MSCs

rBM-MSCs at different ages were cultured with RPMI supplemented with 10% (v/v) FBS, 1% (v/v) penicillin and 1% (v/v) streptomycin (all from Life Technologies, Madrid, Spain) and 10 ng/ml lipopolysaccharides (LPS) (Sigma-Aldrich, St. Louis, United States) for 4 hours.

3.7 Characterization MSC-derived EVs by flow cytometry

MSC-derived EVs were stained with 10 μ M 3-3-Diethylthiadicyanobenzocyanineiodide (DiI) (all from Sigma-Aldrich, St.Louis, United States). MSC-EVs were incubated using anti-CD63 Dynabeads (Thermo Fisher, Waltham, United States) overnight at 4°C and they were detected by FACs (Becton Dickinson, Mountain View, United States). MSC-derived EVs with dynabeads were washed twice with PBS (MP Biomedicals, Illkrich, France) and 2×10^5 cells were analyzed by flow cytometry. Anti-CD63 Dynabeads (Thermo Fisher, Waltham, United States) alone were used as negative control.

3.8 Proliferation assay

Different numbers of cells (0, 1000, 2000, 4000, 8000 and 16000 cells), were plated for triplicate at 96-well plates (Corning Inc., New York, United States) and allowed to adhere

for 8 h to calculate the proliferation curve. The number of cells was calculated using CellTiter 96[®] Aqueous Non-Radiative Cell Proliferation Assay (Promega, Madison, United States) following manufacturer's instructions. 4000 cells were plated for each cell line in triplicate at 96-well plates (Corning Inc., New York, United States), and the total number of cells was calculated at different points (0, 1, 2, 5 and 6 days).

3.9 Cytotoxicity assay

Cell Counting Kit-8 (Dojindo Molecular Technologies, Rockville, United States) was used to check cytotoxicity in our cell cultures when they were supplemented with imatinib mesylate or JK184. Briefly 5000 cells/well were cultured with RPMI supplemented with 10% (v/v) FBS, 1% (v/v) penicillin, 1% (v/v) streptomycin (all from Life Technologies, Madrid, Spain) and imatinib mesylate (5 μ M and 10 μ M) or JK184 (0.1 ng/ml and 1 ng/ml) (all from Sigma-Aldrich, St. Louis, United States) at 96-well plate (Corning Inc., New York, United States) at 37°C, 5% CO₂ for 2 days. After the incubation with 10 μ l of CCK-8 solution in each well for 2 h, the absorbance was measured at 450 nm using a SUNRISE spectrophotometer (TECAN, Mannedorf, Switzerland). It was used as negative control cells cultured with RPMI supplemented with 10% (v/v) FBS, 1% (v/v) penicillin, 1% (v/v) streptomycin (all from Life Technologies, Madrid, Spain) for 2 days.

3.10 Biological characterization

rBM-MSCs from different ages were cultured with RPMI supplemented with 10% (v/v) FBS, 1% (v/v) penicillin, 1% (v/v) streptomycin (all from Life Technologies, Madrid, Spain) in cell culture chambers (Millipore, Billeica, United States) until reaching 80% confluency.

3.10.1 Adipogenic differentiation

Cells at 80% confluency were incubated with RPMI supplemented with 1 μ M dexamethasone, 10 μ g/ml insulin, 0.5 mM of 3-isobutyl-1-methylxantine (all from Sigma-Aldrich, St. Louis, United States). After 2 days, cells were incubated with RPMI supplemented with 10% (v/v) FBS (all from Life Technologies, Madrid, Spain) and 5 μ g/ml insulin (Sigma-Aldrich, St. Louis, United States). This medium was replaced every 3 days for 14 days.

3.10.2 Chondrogenic differentiation

rBM-MSCs from different ages were cultured with RPMI supplemented with 15% (v/v) knockout (KO) serum, 1% (v/v) penicillin, 1% (v/v) streptomycin (all from Life Technologies, Madrid, Spain), 10 μ l/ml ascorbic acid (Sigma-Aldrich, St. Louis, United States), 10 μ M dexasomehasone (Sigma-Aldrich, St. Louis, United States), 1 ng/ml recombinant human transforming growth factor-beta 3

(rhTGF- β_3) (ProsSpec-Tany TechnoGene Ltd., Ness Ziona, Israel), 10^{-7} M retinoic acid (Sigma-Aldrich, St.Louis, United States), 6 μ l/ml transferrine (Sigma-Aldrich, St.Louis, United States) in chambers (Millipore, Billeica, United States) for 14 days. The medium was replaced every 3 days.

3.10.3 Osteogenic differentiation

rBM-MSCs from different ages were cultured in chamber (Millipore, Billeica, United States) with osteogenic commercial medium (Lonza, A Coruña, Spain) for 14 days. The medium was replaced every 3 days.

3.11 Histochemical analysis

All the cell cultures were fixed with 4 % (w/v) paraformaldehyde (Sigma-Aldrich, St.Louis, United States) for 10 min. After the fixation, cells were washed with PBS (MP Biomedicals, Illkrich, France) and they were incubated with 60% (w/w) isopropyl alcohol (PANREAC, Barcelona, Spain).

Adipogenic cultures were stained with 0.5% (w/v) oil red O (Sigma-Aldrich, St.Louis, United States) solution for 20 min to check lipid drops formation in cells differentiated towards adipocyte-like cells. After that, cells were washed with 1% (v/v) isopropyl alcohol (PANREAC, Barcelona, Spain) and distilled water (LABESFAL, Santiago de Besteiros, Portugal).

After the fixation, osteogenic cultures were washed with PBS (MP Biomedicals, Illkrich, France). After they were stained with 2% (v/v) alizarin red aqueous solution at pH 4.2 (Sigma-Aldrich, St.Louis, United States) to check alkaline deposits in cell differentiated towards osteocyte-like cells. Then the slides were air dried and mounted with glicerol mounting medium (Dako, Glostrup, Denmark).

Chondrogenic cultures were fixed with 4% (w/v) paraformaldehyde (Sigma-Aldrich, St.Louis, United States) for 10 min. Then cells were washed with PBS (MP Biomedicals, Illkrich, France) and they were stained with safranin O (Sigma-Aldrich, St.Louis, United States) for 30 min to evaluate the distribution of proteoglycan in the extracellular matrix generated by cells differentiated towards chondrocyte-like cells.

Also chondrogenic cultures were washed with PBS (MP Biomedicals, Illkrich, France) at pH 7.4. Then they were incubated with 5% (w/v) ferric ammonium sulfate (MERCK, Darmstadt, Germany) for 30 min. After, they were washed twice with distilled water (LABESFAL, Santiago de Besteiros, Portugal). Cells were incubated with weigert's hematoxylin (1% (w/v) ferric hematoxylin (Sigma-Aldrich, St.Louis, United States) in absolute alcohol (PANREAC, Barcelona, Spain) for 10 min. Later, they were washed twice with distilled water (LABESFAL, Santiago de Besteiros, Portugal) and the cells were incubated with picric acid saturated in ethanol at 96% (v/v) (all from Sigma-Aldrich, St. Louis, United States) for 6 min and then they were washed five times with distilled water (LABESFAL, Santiago de Besteiros, Portugal). The cells were stained with Ponceau-fuchsin (Masson) (MERCK, Darmstadt, Germany) for 8 min. After, cells were

washed twice with 1% (w/v) phosphomolybdic acid (MERCK, Darmstadt, Germany) and they were incubated with aniline blue (MERCK, Darmstadt, Germany). Finally, the cells were washed twice with distilled water (LABESFAL, Santiago de Besteiros, Portugal) and the slides were mounted with glicerol mounting medium (Dako, Glostrup, Denmark).

3.12 Densitometry analysis

AnalySIS Image Processing (Soft Imaging system GmbH V.5.0, Olympus, Münster, Germany) was used to perform a densitometry quantification of the staining obtained by histochemistry analysis. Three 200 mm² fields in size from each staining: safranin O; oil red; modified Masson's and alizarin red were quantized using arbitrary units provided by the computer program. Values were expressed as percentage of positive stain for each tintion. All values were referenced with respect to values obtained from cells cultured with the control medium (RPMI supplemented with 5% (v/v) KO serum, 1% (v/v) penicillin and 1% (v/v) streptomycin (all from Life Technologies, Madrid, Spain).

3.13 Total RNA and miRNAs isolation

Total RNA, including miRNAs and other RNAs, were isolated using TRIzol[®] Reagent (Invitrogen, Carlsbad, United States) according to manufacturer's instructions.

3.14 Determination of RNA integrity

The quality of 1 µl of each RNA sample from rBM-MSCs at different ages was assessed using Agilent Bioanalyzer 2100 (Agilent, St.Clara, United States) to determine the RNA integrity score (RIN) with the Nanochip Agilent 6000 (Agilent, St.Clara, United States) according to manufacturer's instructions. Samples with a RIN score > 7 were retained and converted to cDNA by SureSelect Strand Specific RNA library (Agilent, St.Clara, United States).

3.15 Real time quantitative polymerase chain reaction (qRT-PCR) analysis

RNA was transformed to complementary DNA (cDNA) using NZY First-Strand cDNA synthesis kit (NZYTECH, Lisboa, Portugal) according to manufacturer's instructions. cDNA was amplified using specific primers for different rat genes (**Table 8.3**). The design of primers was carried out using the software Primer3: WWW primer tool (<http://biotools.umassmed.edu/bioapps/primer3>).

qRT-PCR was carried out using LightCycler 480 Instrument Roche Applied Science using Light Cycler 4800 SYBR Green I Master kit (Roche, Basilea, Switzerland). The amplification program consisted on initial denaturation of 92°C for 2 min followed by 40 cycles at 92°C for 15 s, annealing at 55-62°C, depending on the gene, for 30 s and extension at 72°C for 15 s. qRT-PCR were done in triplicate, with each set of assays repeated three times. For control experiments no reverse transcriptase was used.

3.16 miRNAs analysis

cDNA was generated with QuantiMir RT Kit (System Biosciences, Palo Alto, United States) according to the manufacturer's instructions. The Product from retrotranscription reaction was amplified using specific primers for miRNAs (**Table 8.4**) and the universal QuantiMir reverse primer (System Biosciences, Palo Alto, United States). The amplification program consisted on initial denaturation at 50°C for 2 min followed by a cycle at 95°C for 10 min and 50 cycles of annealing at 95°C for 15 s and extension at 60°C for 1 min. qRT-PCR analyses were done in triplicate, with each set of assays repeated three times. Also, for miRNA detection, cDNA of hsa-miR-21-5p was generated using 10 ng of total RNA using TaqMan-sepecific retrotranscription primers and TaqMan microRNA reverse transcription kit (Applied Biosystems, California, United States) according to manufacturer's instructions. Thereafter, qRT-PCR was performed using predesigned assays for hsa-miR-21-5p and RNU6 (Applied Biosystems, California, United States). qRT-PCR reactions were carried out as follows: 50°C for 2 min, 95°C for 10 min, followed by 40 cycles at 95°C for 15 s and 60°C for 1 min.

To minimize the effects of unequal quantities of starting RNA and to eliminate potential sources of inconsistency, relative expression levels of each gene was normalized to hypoxanthine guanine phosphoribosyl transferase (HPRT), miR-16 or RNU6 using the $2^{-\Delta\Delta C_t}$ method²⁰⁶. For control experiments no reverse transcriptase was used.

3.17 Protein extraction and preparation procedures

Cell monolayers were grown until a 70% confluency at 6-wells culture plates (Corning, New York, United States). They were washed three times with PBS (MP Biomedicals, Illkrich, France) and harvested using a scraper with sodium dodecyl sulphate (SDS) lysis buffer (20% (v/v) glycerol, 500 mM Tris-HCl, pH 6.8, 10% (w/v) SDS and 10% protease inhibitor cocktail (all from Sigma-Aldrich, St.Louis, United States). These samples were incubated at 100°C for 10 min followed by two consecutive cycles of vortexing and sonication. After that, samples were centrifuged at 4 °C for 10 min at 11000 *xg*. Proteins were quantified (total protein A280) using a NanodropTM 1000 instrument (Thermo Scientific, Waltham, United States). Protein extracts were aliquoted and stored at -80°C until further analysis.

3.18 Silver-staining of proteins in polyacrylamide gels

To check the protein integrity and to correct putative differences in proteins quantification, proteins were separated according to their molecular weight using SDS PolyAcrylamide Gel Electrophoresis (SDS-PAGE), 10% (w/v) bis-acrylamide (Sigma-Aldrich, St.Louis, United States). 2 µg of total protein from rBM-MSCs from different ages were loaded into a SDS-PAGE gels. Previous, samples were treated with 1% (v/v) loading buffer after incubation at 100°C for 10 min. Gels were run at 80-120 V for 120 min in electrophoresis units (Bio-Rad, California, United States). Gels were fixed for 30 min. And washed twice with distilled water (Grifolds, Barcelona, Spain) for 10 min. Gels were sensed with sensitizer buffer for 1 min followed by two washes with distilled water (Grifolds, Barcelona, Spain), 1 min each one. Then, they were incubated for 1 hour with a silver stain followed by one rinse using distilled water (Grifolds, Barcelona, Spain). The silver stain was revealed with a revealing buffer for 5 minutes and the reaction was stopped using stop buffer (All reagents were described in **Table 8.5**)²⁰⁷. Densitometry analysis of the band intensities was performed using ImageQuant 5.2 software (GE Healthcare, Little Chalfont, United Kingdom).

3.19 iTRAQ[®]-8plex labelling. Amine-Modifying Labelling Reagents for Multiplexed Relative and Absolute Protein Quantification

Firstly, 100 µg proteins from rBM-MSCs at different ages were precipitated using acetone according to manufacturer's instructions (PIERCE, Rockford, United States). Then, proteins were denatured with 2% (v/v) SDS in 1 M tryethylammonium bicarbonate (TEAB) (AB Sciex, Foster City, United States). Then samples were reduced for 1 h at 60°C using 50 mM tris-(2-carboxyethyl) phosphine (TCEP) (AB Sciex, Foster City, United States) and cysteine-blocked with 84 mM iodoacetamide (all from Sigma-Aldrich, St.Louis, United States) at room temperature in dark for 30 min. Proteins were digested with spectrometry grade trypsin Gold Mass (Promega, Madison, United States) at a concentration of 1:50 trypsin/protein for 16 h at 37°C. Each peptide solution was labelled for 1.5 h at room temperature using iTRAQ[®] reagent (AB Sciex, Foster City, United States) as follows: newborn: 119 and 121 as a control; infant: 114; young: 116; pre-pubertal: 118; pubertal: 115 and adult: 117. The reaction was stopped by adding deionized water (Grifols, Barcelona, Spain) and labelled samples were combined. The mixture was desalted using home-made stage-tips²⁰⁸ (**Figure 3.1**).

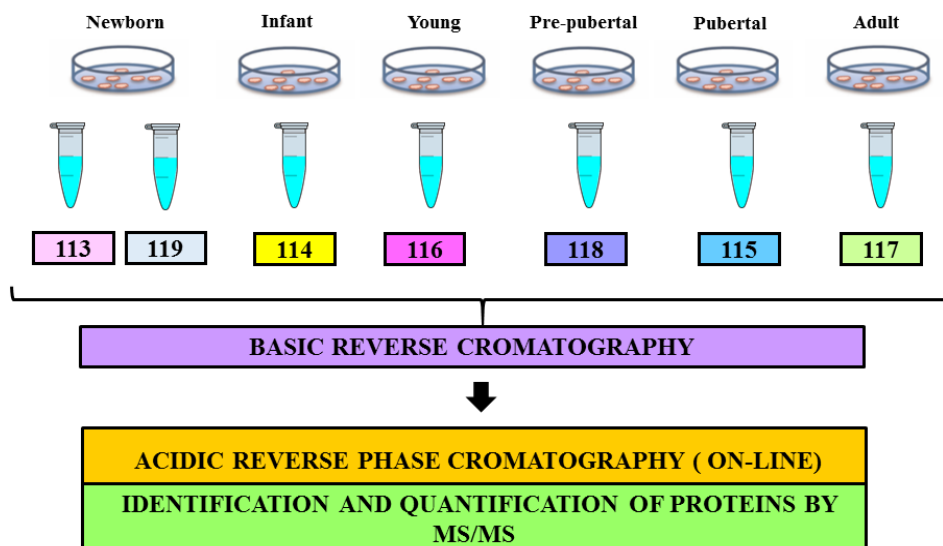


Figure 3.1. Workflow of iTRAQ-8plex.

3.20 Relative quantification by two dimensional-liquid chromatography coupled offline to matrix-associated laser desorption ionization-time of flight (2D-LC-MALDI-TOF/TOF) analysis

In a first step, the desalted peptides were fractionated by basic reverse phase extraction at 1400 High-performer liquid chromatography (HPLC) system (Agilent, St.Clara, United States). The extraction was done in a nanoHPLC system (Tempo, AB Sciex, Framingham, United States) into a C18 silica-based column (New Objective, Woburn, United States) with an internal diameter of 300 Å. The injection volume was 5 µl, and peptides were eluted during a 90 min-gradient with a constant flow rate of 0.35 µl/min. Eluting peptides were automatically mixed with 4 mg/ml α -ciano in 70% (v/v) acetonitrile (AcN) (Sigma-Aldrich, St.Louis, United States), 0.1% trifluoroacetic acid (TFA) (LabScan, Bangkok, Thailand) and deposited on a MALDI LC-plate using SunCollect MALDI spotter (SunChrom, Friedrichsdorf, Germany). The chromatograms, composed by 350 spots, each one comprising a 15 s deposition, were analyzed in a 4800 MALDI-TOF/TOF platform (AB Sciex, Framingham, United States). 4000 series Explorer v.4.2 software was used to generate the spectra and peak list. After manual deposition of mass calibrate, plate model and default calibration of the MALDI plate were done with a laser voltage of 34000 kV and 1500 shots/spectrum. Automated precursor selection was done using a Job-wide interpretation method (up to 12 precursors/fraction, Signal to Noise loxer threshold= 50) excluding trypsin autolytic peptides and other background ions, with a laser voltage of 4200 and 2000 shots/spectrum. Collision-induced dissociation (CID) energy range: medium. LC-MALDI-TOF/TOF data were analyzed using ProteinPilot 4.0 software (AB Sciex, Framingham, United States). Protein Pilot Search parameters were as follows: sample type: iTRAQ 8-plex; cys-alkylation: iodoacetamide; digestion: trypsin;

identification (ID) focus: biological modifications; database: last SwissProt release 2013_12 of 11-Dec-2013 of UniprotKB/TreEMBL contains 48701576 sequence entries, comprising 15448487119 amino acids; species filtering: none; Search effort: Thorough ID and detection protein threshold unused ProtScore (Conf) > 1.3 (95.0%). Scoring model was defined using the Paragon algorithm. In the case of the high complexity samples, False Discovery Rate-FDR- was estimated in less than 1% by doing the searching in parallel against a decoy database using “PSPEP on” mode.

3.21 Immunoblot analysis

Immunoblot analysis was performed with 40 µg of total protein extracted from rBM- MSCs. Firstly, proteins were separated according to their molecular weight using SDS-PAGE, the percentage (w/v) bis-acrylamide (Sigma-Aldrich, St.Louis, United States) of resolving gels were determined by the size of protein. The transference was performed as a semi-dry transfer way using transfer buffer with 20% (v/v) methanol (Panreac, Barcelona, Spain) for small proteins (<100 kDa) or 10% (v/v) methanol (Panreac, Barcelona, Spain) for large ones (>100 kDa). After that, the membrane of nitrocellulose was blocked using blocking buffer consisting of 5% (w/v) bovine serum albumin (BSA) for phospho-proteins and 5% (w/v) milk (all from Sigma-Aldrich, St.Louis, United States). The incubation was performed for other proteins, for 1 h in agitation at room temperature. Membranes were probed with antibodies diluted in blocking buffer at 4°C overnight. The following day, membranes were washed three times for 5 min with standard buffer tris buffered saline with 0.1% (v/v) Tween[®] 20 (TBST). Then, HRP-conjugated secondary antibodies diluted in blocking buffer were incubated for 1 h at room temperature. Next, membranes were washed three times in standard buffer TBST for 5 min with agitation and twice using tris buffered saline (TBS) for 5 min in agitation. Amersham[™] ECL[™] Western Blotting Analysis System (GE Healthcare, Little Chalfont, United Kingdom) was used to visualize proteins. Adequate concentration for each antibody was determined empirically. Blots were digitized using the LAS 3000 image analyser (GE Healthcare, Little Chalfont, United Kingdom). Densitometry analysis of the band intensities was performed using ImageQuant 5.2 software (GE Healthcare, Little Chalfont, United Kingdom). (All reagents were described in **Table 7.2**).

3.22 Enzymatic analysis

5×10^5 cells from each group of different age were used for the assessment of enzyme activities. Cells were homogenized with buffer lysis (250 mM sucrose, 50 mM HEPES, 0.5 mM ethylenediaminetetraacetic acid (EDTA) (all from Sigma-Aldrich, St.Louis, United States) and one tablet cOmplete[™] protease inhibitor cocktail (Roche, Mannheim, Germany)). Enzymes activities were determined using a SUNRISE spectrophotometer (TECAN, Mannedorf, Switzerland). Reactions rates were determined by the increase or

decrease in absorbance of NAD(P)H (Sigma-Aldrich, St.Louis, United States) at 340 nm at 37°C.

Lactate dehydrogenase (LDH) (EC 1.1.1.27) was determined in rBM-MSCs using 50 mM Trizma base at pH 7.4, 0.15 mM NADH and 5 mM sodium pyruvate (omitted for control) (all from Sigma-Aldrich, St.Louis, United States). Glucose-6-phosphate-1-dehydrogenase (G6PDH) (EC 1.1.1.49) and 6-phosphogluconate dehydrogenase, decarboxylating (6PGDH) (EC 1.1.1.343) was determined in rBM-MSCs using 78 mM Trizma base, 5 mM MgCl₂ at pH 7.4, 0.1 mM NADP, 0.5 mM D-Glucose-6-phosphate disodium salt hydrate and 6-phosphogluconic acid trisodium salt (omitted for control) (all Sigma-Aldrich, St.Louis, United States).

3.23 Next Generation Sequencing (NGS) using RNA sequencing technique

The study was designed to screen the complete transcriptome per age group of Wistar rats, covering coding, intronic and splicing regions of complete genes from Wistar rat. Sample preparation was carried out as recommended by Agilent SureSelect Strand-Specific RNA Library Prep (Agilent, St.Clara, United States) for Illumina multiplex sequencing method²⁰⁹. 1 µg of total RNA per sample was used. Fragmented DNA was end-repaired and the sequencing data was generated on Hiseq 1500 (Illumina, San Diego, United States) on a rapid mode flowcell (Illumina, San Diego, United States). All samples were sequencing twice (**Figure 3.2**) and they were prepared in duplicate.

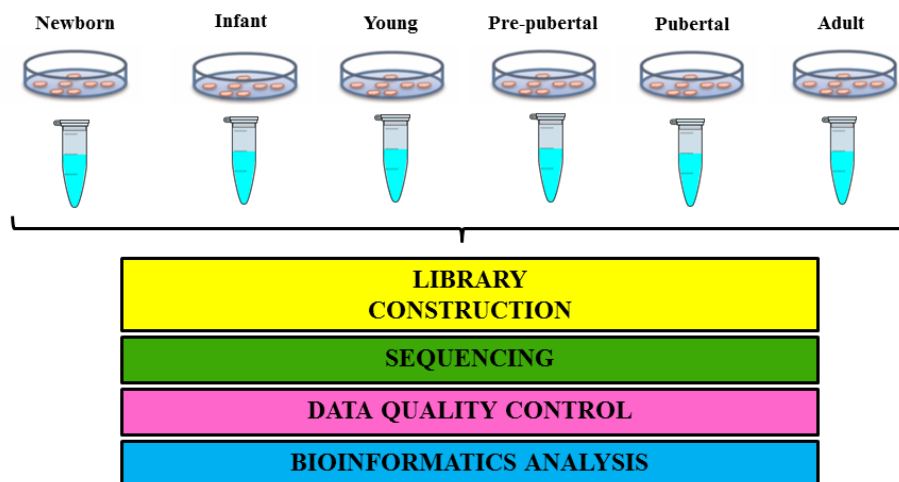


Figure 3.2. Workflow of RNA-sequencing.

3.24 Isolation rBM-MSC-derived EVs

rBM-MSCs from newborn (0 days), young (14 days), pre-pubertal (35-38 days) and adult (+2 months) were cultured with RPMI 1640 Medium with GlutaMAX™ supplement and 10% FBS-free exosomes (all from Thermo Fisher Scientific, Massachusetts, United States), 100 IU/ml penicillin-100 mg/ml streptomycin (all from Life Technologies, Madrid, Spain). Firstly, cells were cultured until 80% confluence and supernatants were collected each 48 h. Supernatants were centrifuged at 252 *xg* for 10 min at 4°C and filtered using 0.22 µm sterilized filter (GE Healthcare Life Sciences, Little Chalfont, United Kingdom) to eliminate debris. Supernatants were transferred into ultracentrifugation tubes (Beckman Coulter, Mississauga, Canada) and they were ultra-centrifuged at 100000 *xg* for 2 h at 4°C in an Optimal-90K ultracentrifuge with 60 Ti rotor (Beckman Coulter, Mississauga, Canada). Supernatant containing exosomes-free media were removed and the pellets were re-suspended in 200 µl PBS (MP Biomedicals, Illkrich, France).

3.25 Quantification of protein in rBM-MSC-derived EVs

Proteins from rBM-MSC-derived EVs content were measured with a Micro-BCA kit (Thermo Scientific, Rockford, United States) according to manufacturer's instructions.

3.26 Characterization of rBM-MSC-derived EVs by size

3.26.1 Nanoparticle Tracking Analysis (NTA)

MSC-derived EVs size distribution was estimated by the Brownian motion of the particles in NanoSight LM12 using Nanoparticle Tracking Analysis 2.3 software (Nanosight Ltd, Amesbury, United Kingdom). MSC-derived EVs were diluted in PBS (MP Biomedicals, Illkrich, France), until a suitable concentration for analysis was reached. Particle concentration was evaluated for the particles between 30–150 nm in diameter.

3.26.2 Electron microscopy

MSC-derived EVs were concentrated using Vivaspin concentrators (Sartorius, Gottingen, Germany). MSC-derived EVs were taken up in small volumes of deionized water, which were placed on nickel grids and allowed to dry for 45 min at 37°C. The grids with MSC-derived EVs were fixed with 4% (w/v) paraformaldehyde (Sigma-Aldrich, St.Louis, United States) for 10 min and then washed by transferring them onto several drops of deionized water (Grisfold, Barcelona, Spain). Excess fluid was removed and the grids were allowed to dry before examination on a JEOL JEM1400 Transmission Electron Microscope (JEOL Ltd, Tokyo, Japan).

3.27 miRNA transitory transfections

rBM-MSCs from pre-pubertal group with 80 % of confluence were incubated with 40 nM hsa-miR-21-5p miRVana™ miRNA inhibitor or 40 nM control negative miRVana™ (all from Applied Biosystem, Madrid, Spain) following manufacturer's instructions.

3.28 *In vitro* Model using rBM-MSC-derived EVs

2.5×10^5 rBM-MSCs from old individuals were cultured at 6 well-plate (Corning Inc, New York, United States) for 8 hours and 2×10^7 MSC-derived EVs from young individuals were added to these well-plate and vice versa. At different times (2, 3 and 6 days) were collected the cells and RNA and protein isolations from the cells were performed.

3.29 Fluorescence microscopy

2.5×10^5 rBM-MSCs from old individuals were cultured in slides (Sigma-Aldrich, St.Louis, United States) which were pre-treated with poli-D-lysine (Sigma-Aldrich, St.Louis, United States) at 6-well-plate (Corning Inc, New York, United States) for 8 h (this time was named 1 day). 2×10^7 MSC-derived EVs from young individuals were marked with 10 μ M DiI (3-3'-diethylthiacarbocyanineiodide) which was added in each well and vice versa and it was added PBS (MP Biomedicals, Illkrich, France) in control. At different times (2, 3 and 6 days), the cells were washed three times with PBS (MP Biomedicals, Illkrich, France) and fixed with 4% (w/v) paraformaldehyde (Sigma-Aldrich, St.Louis, United States) for 10 min and slides were mounted using ProLong® Gold Antifade Mountant with DAPI (4',6-diamidino-2-phenylindole) (Thermo Fisher Scientific, California, United States). Slides were observed with microscopy Olympus BX61 using digital chamber DP71 (Olympus, Tokyo, Japan) with software DP Controller and DP Manager.

3.30 Bioinformatics analysis

Biological functional analysis of different modulated proteins detected by iTRAQ quantification, were categorized according to their function, biological process and cellular component using the database of functional protein association networks String 9.0²¹⁰ (string-db.org). Proteins with statistically significant changes were identified by filtering according to these criteria: 1) they had to be present in two biological replicates; 2) changes between groups had to be statistically significant ($P < 0.05$); and 3) fold change had to be greater than 1.2 and lower than 0.8 (**Figure 8.1**). This approach selected 201 differentially expressed proteins for further analysis.

The identification of markers from extracellular vesicles in proteomic analysis was done using EVs databases: Vesiclepedia (www.microvesicles.org/)¹⁰⁸, EVpedia (www.evpedia.info)¹⁰⁹ and ExoCarta (www.exocarta.org)¹¹⁰.

An average of 25 million paired-end 100 bases pairs (bp) reads was obtained per sample in transcriptome analysis. The raw RNA-sequencing reads for each sample were aligned to the reference rat genome browser (rn6assembly) using Bowtie2 (bowtie-bio.sourceforge.net/index.shtml/) and Tophat2 (<http://tophat.cbcb.umd.edu/>). After alignment, raw sequence read depths was converted to estimate transcript abundance measures as fragments per kilo base of exons per million (FPKM) values cufflinks (<http://cufflinks.cbcb.umd.edu/>) differentially expressed genes and transcripts were calculate with Cuttdiff and fold change had to be greater than 1.23 and lower than 0.78. Each group was compared with previous age group. Identified genes with statistically significant changes ($P < 0.05$) were categorized according to their function, biological process and cellular component using the R/Bioconductor package RamiGO (<http://bioconductor.org/packages/release/bioc/html/RamiGO.html>)²¹¹.

MicroRNA.org (<http://www.microrna.org>) was a resource of microRNA target predictions and expression profiles used in this work. Target predictions were based on a development of the miRanda algorithm²¹² and TargetScan²¹³.

3.31 Statistics analysis

All experiments were performed in triplicate and one representative is shown. Non-parametric statistical analyses were performed by Mann-Whitney-U and Kruskal-Wallis tests using GraphPad Prism6 (GraphPad Software, La Jolla, United States). Each group was compared with previous age group. A P -value less than 0.05 or 0.01 was considered statistically significant. All the results were presented as standard error of the mean.

iTRAQ and RNA-sequencing were performed in duplicated. Proteomic results were normalized with ProteinPilot software 4.5 based on ParagonTM Algorithim 4.5.0. Differentially expressed genes and transcripts from RNA-seq were calculated with Cuttdiff analysis using CummeRbund software (<http://compbio.mit.edu/cummerbund/>).

4. RESULTS

4.1 Characterization of rBM-MSCs

Characterization of rBM-MSCs at different ages by flow cytometry revealed that no statistical differences exist between groups in respect to the levels of mesenchymal and hematopoietic markers used. CD34 and CD45 positive cells were less than 1% and CD29 positive cells were $30\pm 5\%$ and CD90 positive cells were $75\pm 5\%$ in all groups studied (Figure 4.1).

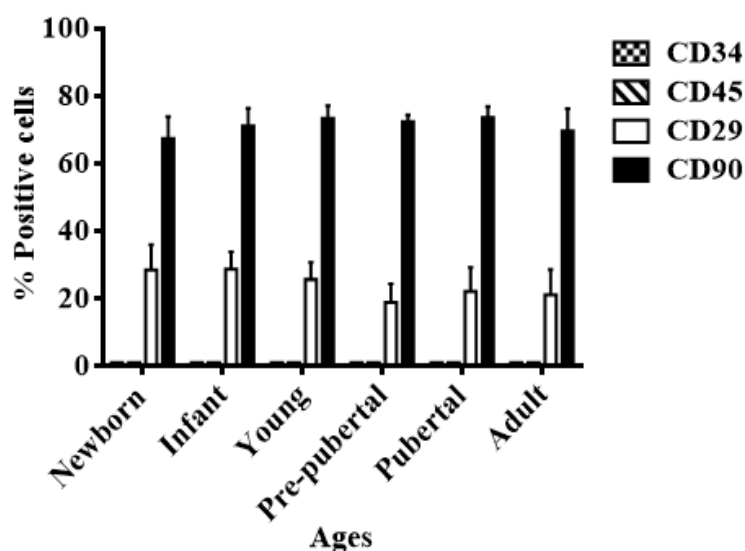
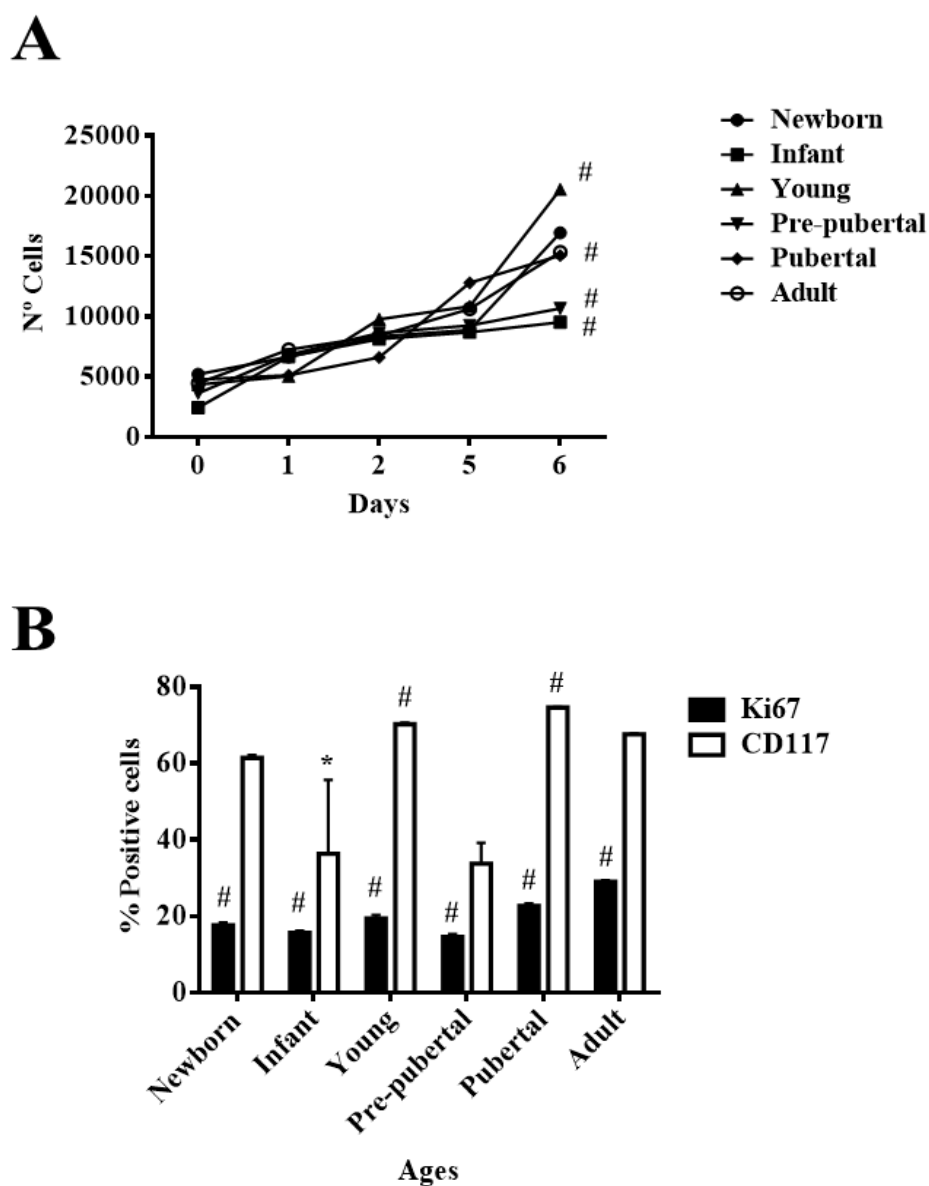


Figure 4.1. Characterization by flow cytometry. Percentage of cells positives for MSCs markers (CD29 and CD90) and for hematopoietic markers (CD34 and CD45). One representative experiment is shown.

4.2 Study of proliferation of rBM-MSCs at different ages

Flow cytometry assays to detect CD117 and Ki67 positive cells indicated that MSCs from pubertal and young groups had the statistical significant ($P < 0.05$) higher CD117 positive cells of MSCs (74.6 ± 0.07 and 71.9 ± 3.10 respectively) when compared with to other groups studied, newborn: 61.5 ± 0.37 ; adult: 61.1 ± 6.35 ; infant: 60.5 ± 1.58 and pre-pubertal: 35.2 ± 2.14 . On the other hand, pre-pubertal and infant groups had the statistical significant ($P < 0.05$) lower Ki67 positive cells percentage (14.65 ± 0.41 and 15.63 ± 0.24 respectively) than the rest of the groups studied, newborn: 18.0 ± 0.55 ; young: 19.3 ± 0.43 ; pubertal: 22.9 ± 0.40 ; adult: 29.0 ± 0.16 (Figure 4.2A).

Proliferation assays results indicated that MSCs from young ($21.0 \times 10^3 \pm 200$), newborn ($17.0 \times 10^3 \pm 100$), adult ($16.0 \times 10^3 \pm 100$) and pubertal ($15.0 \times 10^3 \pm 300$) groups had a statistically significant higher ($P < 0.05$) proliferation capacity compared to pre-pubertal ($10.0 \times 10^3 \pm 500$) and infant ($9.00 \times 10^3 \pm 500$) groups (Figure 4.2B).



4.3 Evaluation of biological capacity of rBM-MSCs at different ages

Differentiation capacity of the groups studied was tested through direct mesoderm induction using specific culture medium. It was observed that pre-pubertal group presented statistically significant ($P<0.05$) highest stain for safranin O, modified Masson's and oil red by histochemistry analysis followed by pubertal with respect to other groups. Infant group presented the highest staining, statistically significant ($P<0.05$) for alizarin red with respect to other groups and the adult group presented the lowest statistically significant ($P<0.05$) differentiation potential with respect to other groups (**Figure 4.3**).

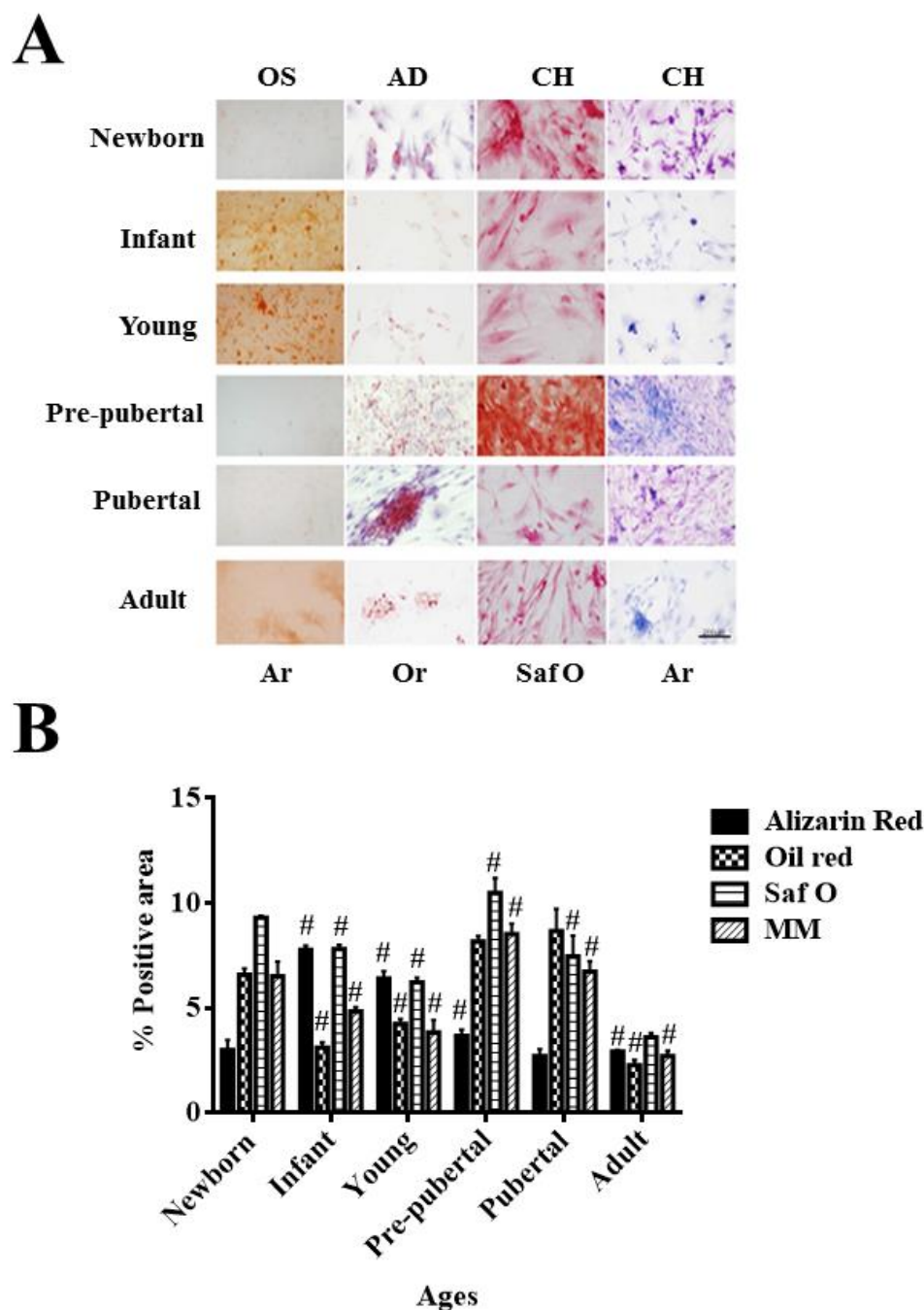


Figure 4.3. Evaluation of the biological capacity of rBM-MSCs at different ages. (A) Representative images of rBM-MSCs of studied age groups after 14 days with specific differentiation medium. Specific medium is indicated on the top; OS= osteogenic medium; AD= adipogenic medium; CH= chondrogenic medium. Stain is indicated at the bottom; Ar= alizarin red; Or= oil red; Saf.O= safranin O and MM= Modified Masson's stain. Straight size is 200 μ M. **(B)** Densitometry study of rBM-MSCs at different ages after 14 days with specific differentiation medium after histochemical techniques. AnalySIS Image Processing computer was used to quantify the signal of different stain obtained. One representative experiment is shown. # P <0.05 compared with previous age group and * P <0.01 compared with previous age group, were considered statistically significant using Mann-Whitney-U and Kruskal-Wallis tests.

4.4 Evaluation of pluripotency markers in rBM-MSCs at different ages

Nanog, Oct4, Rex1 and Sox2 gene expression were tested by qRT-PCR analysis to check the pluripotency potential of the studied groups. The results show the statistically significant ($P<0.05$) highest expression of Nanog in the young group when compared to other groups. In contrast, Nanog decreased in a statistically significant ($P<0.05$) way in the pre-pubertal group in respect to the other groups (**Figure 4.4**).

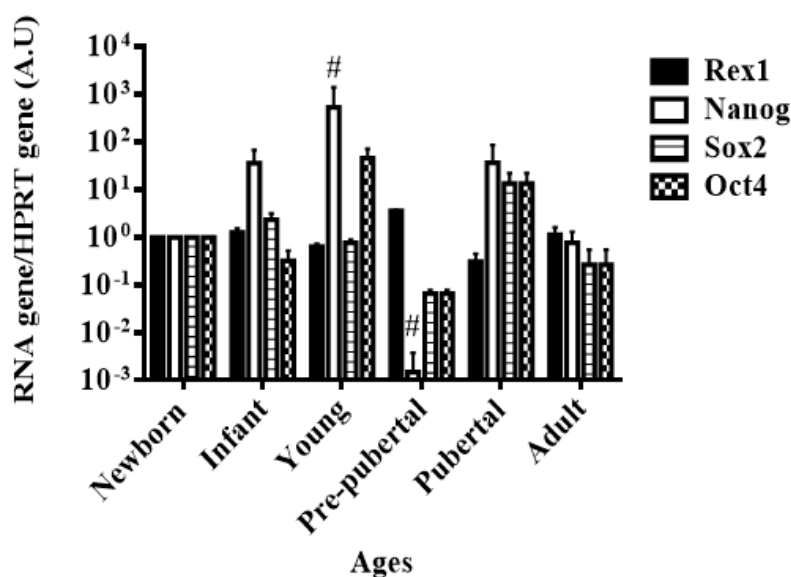


Figure 4.4. Pluripotency profile from rBM-MSCs at different ages. Histogram represents gene expression of pluripotency markers, Rex1, Nanog, Sox2 and Oct4. Real-time reverse transcriptase PCR (qRT-PCR) analysis normalized by expression of HPRT gene used as housekeeping. One representative experiment is shown. # $P<0.05$ compared with previous age group was considered statistically significant using Mann-Whitney-U and Kruskal-Wallis tests. A.U= arbitrary units.

4.5 Analysis of proteome in rBM-MSCs at different ages

All proteins from BM-MSCs of rat Wistar at different ages studied were compared among them. In summary, each group was composed of a pool from 6 animals and 2 different iTRAQ experiments were performed. To generate the quantitative proteome using iTRAQ labelling, first the labelling was determined efficiency, which exceeded 99%. Next, the cut-off for significant fold-change was determined based on biological replicates of two iTRAQ experiments which were chosen based on the following criteria: containing more than 3 unique peptides (>95%) and P value <0.05 for the 114/119 reporters ions. Accordingly, 90% of the commonly observed proteins in the biological replicates fell within 25% of the respective experimental variation (**Figure 4.5**). The fold-

change thresholds of >1.20 or <0.80 was set to identify true differences among expression of reporter ions.

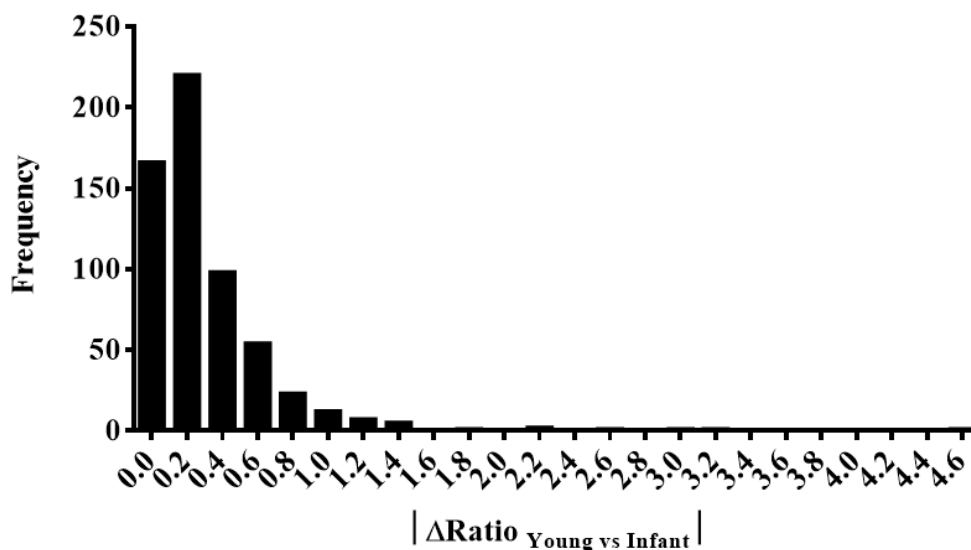


Figure 4.5. Statistic analysis of iTRAQ-8plex.

The results obtained in the iTRAQ analysis indicated that 1072 proteins were identified, 201 of them statistically significant modulated among groups (**Figure 4.6A** and **Table 8.6**). These proteins have been grouped by three biological processes attending String 9.0 software; those groups were proliferation (60 proteins), pluripotency (86 protein) and energy metabolism (55 proteins) (**Figure 4.6B** and **Table 8.6**). Significant activated pathways obtained by comparing modulated proteins detected by iTRAQ analysis employing functional annotations according to the String 9.0 software and classified in three biological process for better comprehension were shown in **Figure 4.6B**.

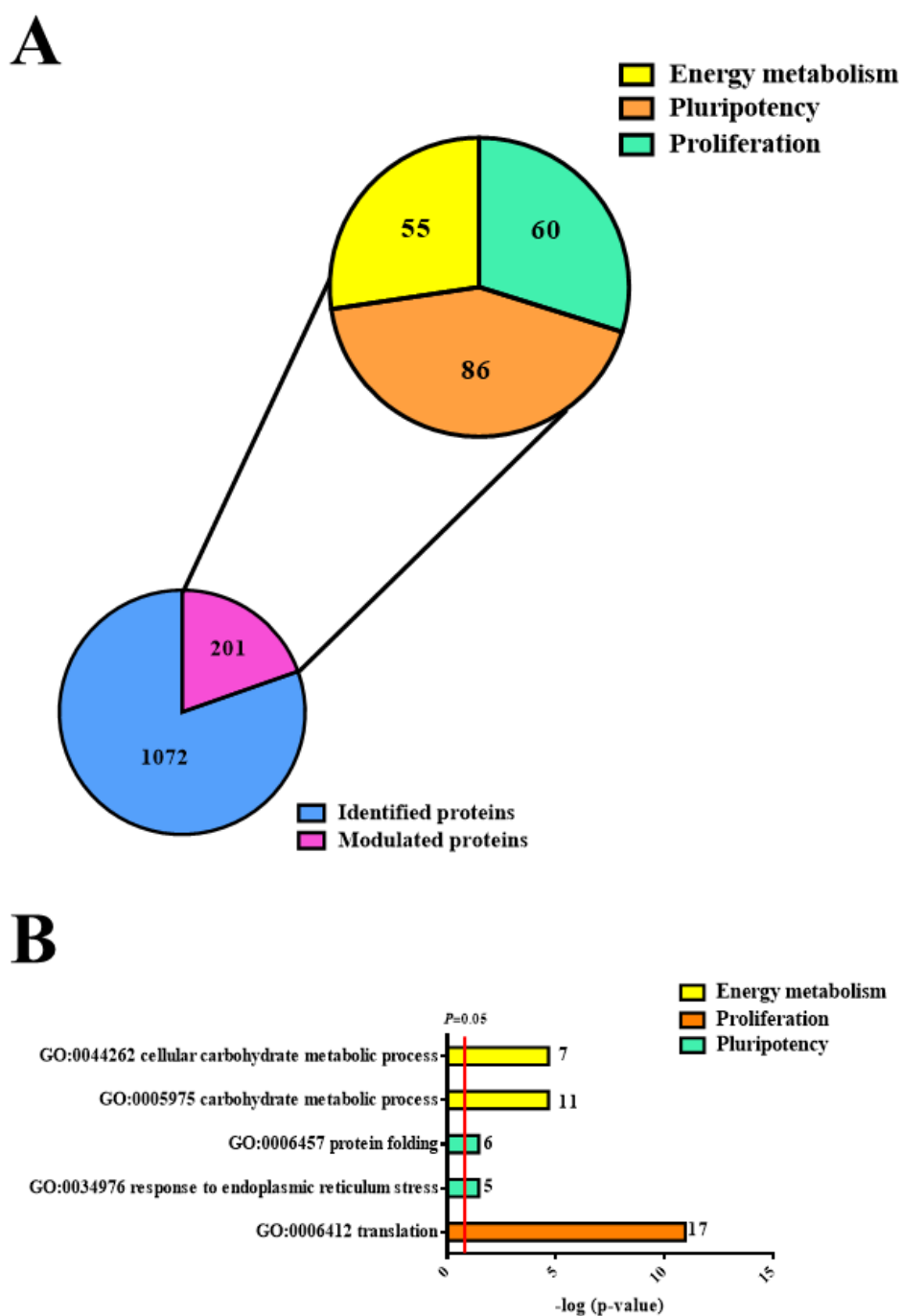
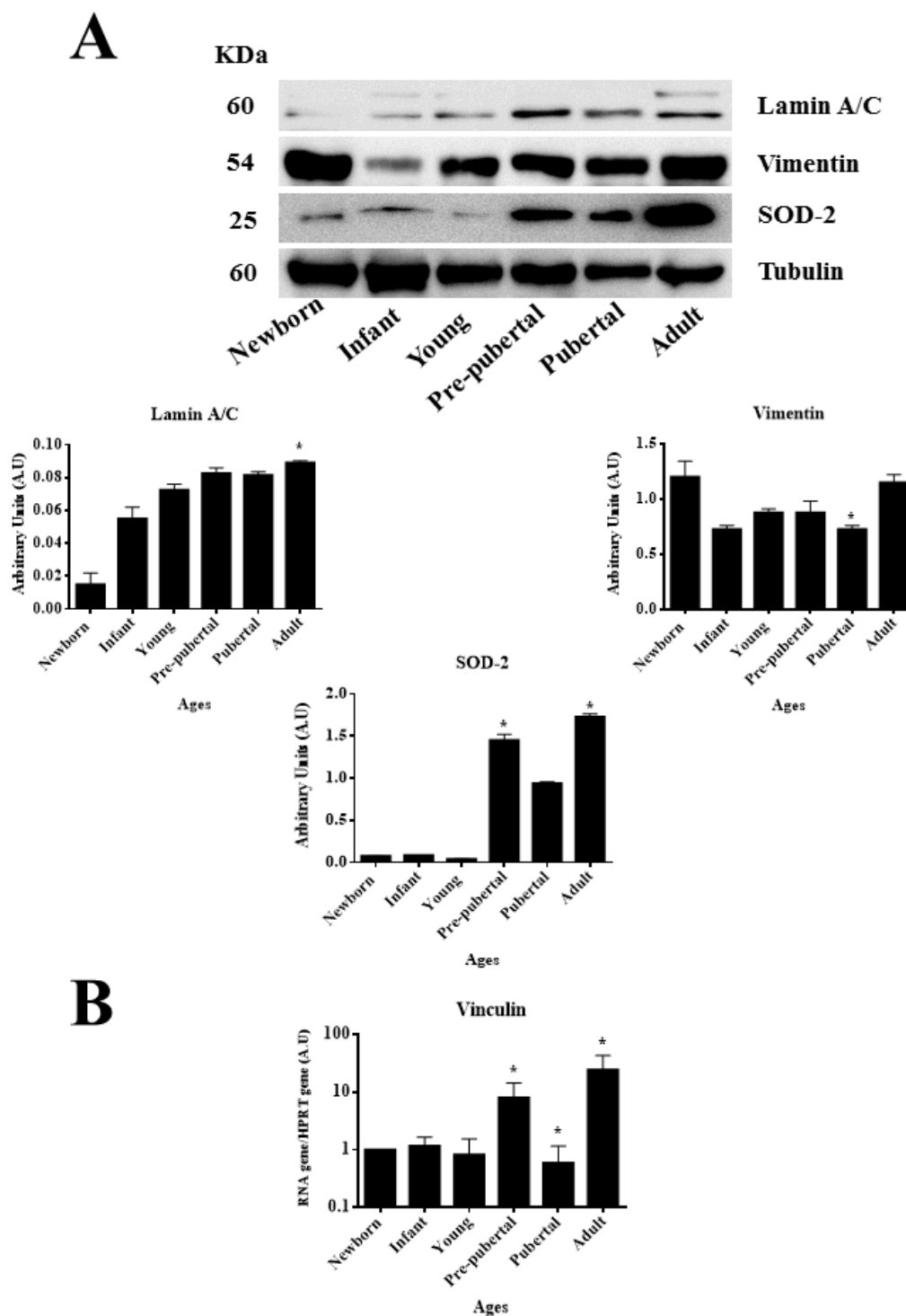


Figure 4.6. iTRAQ of modulated proteins in rBM-MSCs. (A) Summary of protein identification and relative quantification. **(B)** Significantly modulated biological processes after String 9.0 analysis of the modulated proteins. GO=gene ontology.

Several proteins found in our analysis associated with proliferation were 60S ribosomal proteins with different sedimentation speed such as, 60S RP L4,60S RP L6, 60S RP L7,60S RP L9,60S RP L10, 60S RP L23 and 60S RP L24; also vinculin which gene expression was validated using qRT-PCR analysis (**Figure 4.7B**), all of them were statistically significant ($P<0.05$) higher in newborn and adult groups when compared to the other groups. Superoxide dismutase-2 (SOD-2) and Lamin A were increased with increasing age similar as it occurred in iTRAQ analysis; all of them were validated by western blot (**Figure 4.7A**). Proteins found in our iTRAQ analysis were associated with proliferation like histones H1.5; H2B and H4 also protein disulfide-isomerase A1 (PDIA1) which were statistically significant ($P<0.05$) high regulated in infant and pubertal group with respect to other groups (**Table 8.6**).



4.6 Mitochondrial function in rBM-MSCs in different age groups

MitoSOXTM and total ROS were analyzed by flow cytometry to study in depth the age-related increase of SOD-2 detected previously by quantitative proteomic (**Table 8.6**), infant and pre-pubertal groups were statistically significant ($P<0.01$ and $P<0.05$, respectively) with lower percentage positive cell levels (11.1 ± 4.15 and 32.0 ± 1.25 , respectively) for MitoSOXTM. Beside, the pre-pubertal group was statistically significant ($P<0.01$) lower for DCFH when compared to other groups (**Figures 4.8A** and **4.8B**). The permanent dye TMRM analysis indicated a decrease in functional mitochondria which was statistically significant ($P<0.01$) in infant and adult groups with 53.5 ± 3.01 and 27.43 ± 2.74 positive cells respect to newborn and pubertal groups respectively (**Figure 4.8C**).

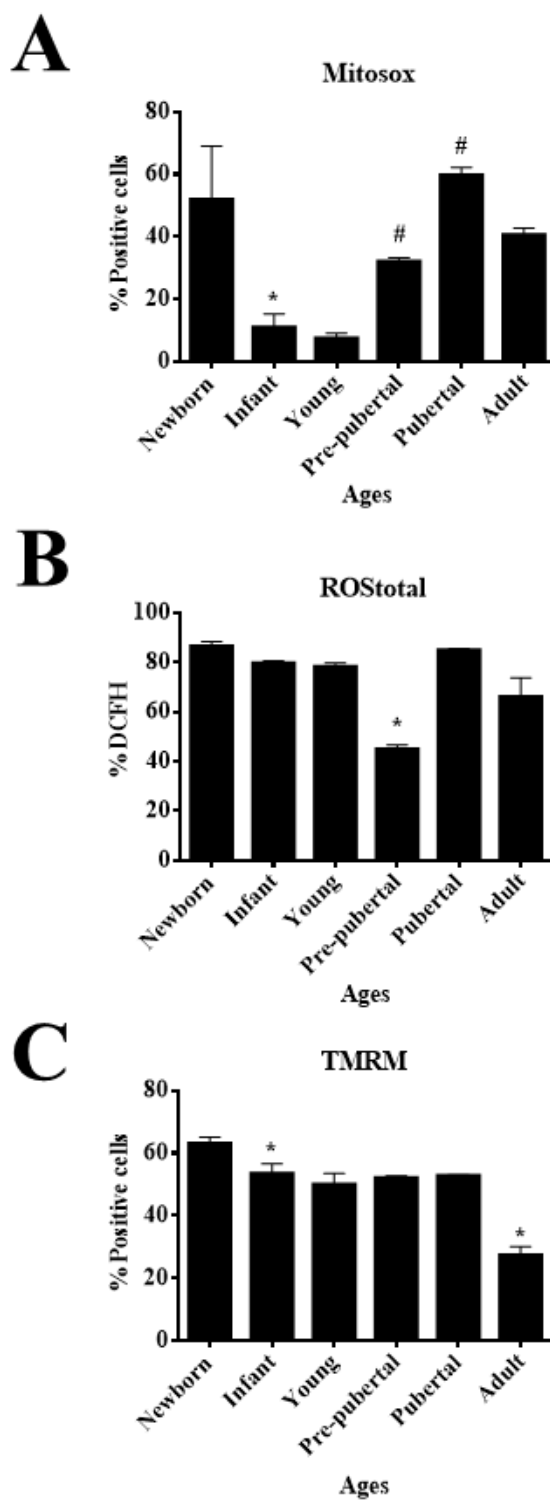


Figure 4.8. Mitochondrial function in rBM-MSCs at different ages. (A) Mitosox signal measured by flow cytometry to check mitochondrial ROS. (B) DCFH signal measured by flow cytometry to check intracellular ROS. (C) TMRM dye accumulated in active mitochondria with intact potentials. One representative experiment is shown. # $P < 0.05$ compared with previous age group and * $P < 0.01$ compared with previous age group, were considered statistically significant using Mann-Whitney-U and Kruskal-Wallis tests.

4.7 Glucolitic metabolism of rBM-MSCs at different ages

Proteins found in our proteomic study associated with energy metabolism were lactate dehydrogenase (LDH), glucos-6-phosphate dehydrogenase (G6PDH) and 6-phosphogluconate dehydrogenase (6PGDH), which were validated through analysis of their activity by enzymatic assays. LDH activity was increased in young group when compared to infant and newborn groups, levels decreased in pre-pubertal group in a statistically significant way ($P<0.05$) and finally its activity increased in pubertal and adult groups (**Figure 4.9A**), G6PDH and 6PGDH were statistically significant increased ($P<0.05$) in pubertal and adult groups when compared to the other groups (**Figure 4.9B**).

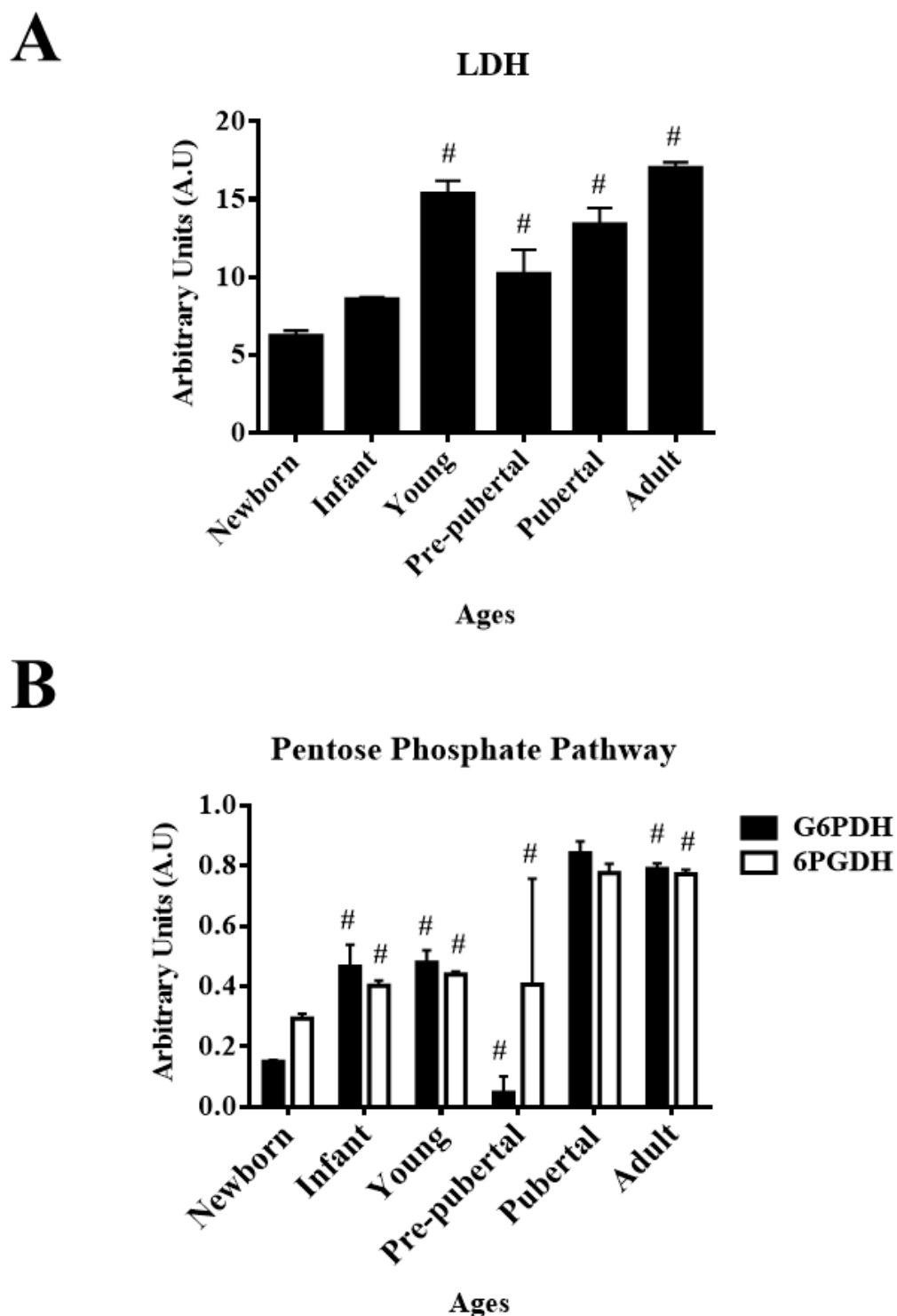


Figure 4.9. Glucolytic metabolism profile from rBM-MSCs at several ages. (A) Lactate-dehydrogenase (LDH) activity measured by spectrophotometer analysis. **(B)** Pentose phosphate pathway activity measured by spectrometer analysis. G6PDH= glucose-6-phosphate-1-dehydrogenase; 6PGDH= 6-phosphogluconate-dehydrogenase. One representative experiment is shown. # $P < 0.05$ compared with previous age group, was considered statistically significant using Mann-Whitney-U and Kruskal-Wallis tests.

4.8 mTOR pathway in rBM-MSCs at different ages

It was evaluated mTOR pathway which is key of energy metabolism and proliferation processes in rBM-MSCs at different ages. Immunoblot analysis indicated that mTOR and Raptor were statistically significant ($P<0.05$) lower in pre-pubertal and pubertal groups in compared to the other groups. Adult group presented the statistically significant ($P<0.01$) most increased level of mTOR and Raptor (**Figure 4.10**).

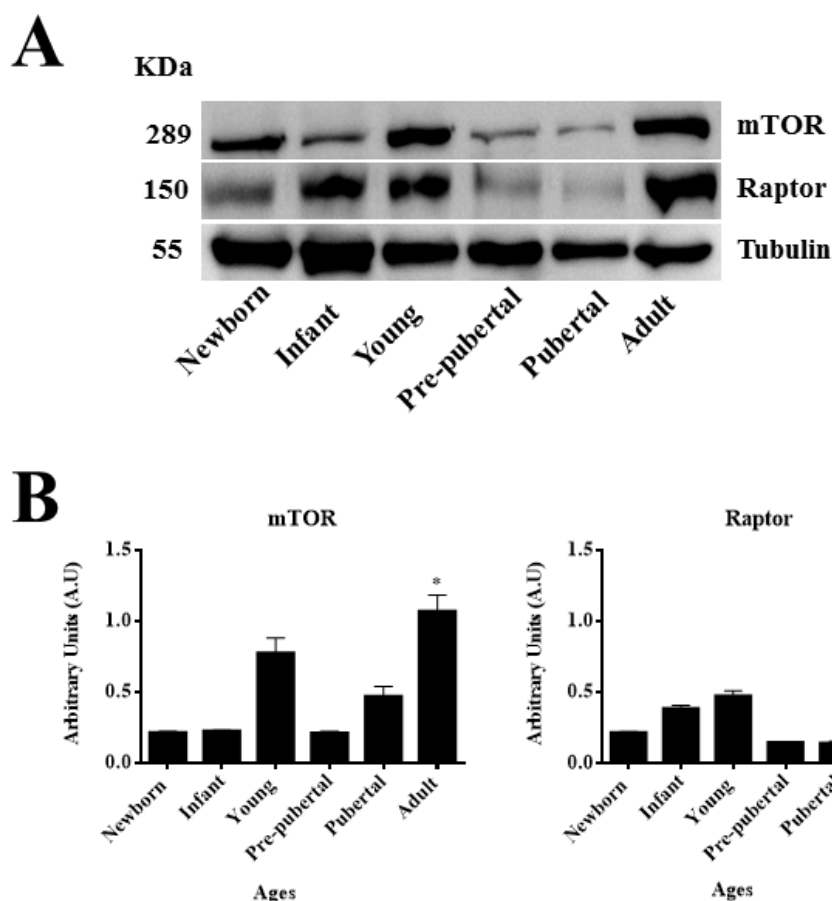


Figure 4.10. mTOR pathway profile from rBM-MSCs at different ages. (A) Western-blot of mTOR and Raptor and tubulin was used as housekeeping. **(B)** Densitometry analysis of western-blot of mTOR and Raptor normalized against to tubulin using Image Quant 5.2. One representative experiment is shown. * $P<0.01$ compared with previous age group was considered statistically significant using Mann-Whitney-U and Kruskal-Wallis tests.

4.9 Relationship of mTOR pathway with proliferation markers (CD117 and Ki67) in rBM-MSCs from adult group

rBM-MSCs from adult group were treated with different concentrations of imatinib mesylate (IM) (5 μ M and 10 μ M) or JK184 (0.1 ng/ml and 1 ng/ml), which inhibit CD117 and Ki67 respectively, for 2 days. Viability assay indicates that the used concentrations of IM and JK184 did not affect the cells in culture (**Figure 4.11A**). JK184 promoted a statistically significant ($P < 0.01$) decrease in the expression of Ki67 at 1 ng/ml dose in culture (**Figure 4.11B**). Also, we observed the inhibition capacity on proliferation of these drugs over the cells and we obtained cells arrested in G₂/M phase when they were treated with IM (5 μ M and 10 μ M) or JK184 (0.1 ng/ml and 1 ng/ml). The same results were found when rBM-MSCs were treated with 1 mg/ml nodocazole used as positive control (**Figure 4.11C**).

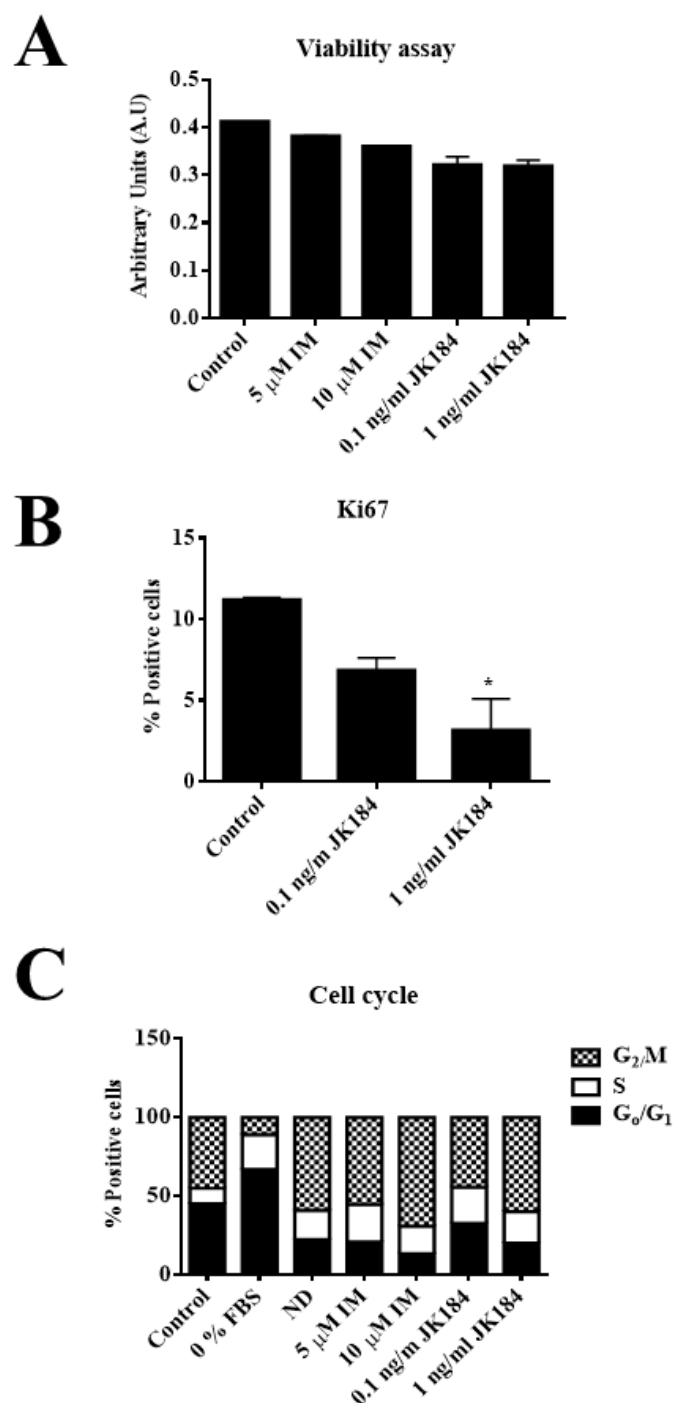


Figure 4.11. Inhibition of proliferation markers (CD117 and Ki67) in rBM-MSCs from adult group. (A) Viability assay of rBM-MSCs from adult group incubated with 5 μ M or 10 μ M of IM and 0.1 ng/ml or 1 ng/ml of JK184 in the culture medium. **(B)** Flow cytometry of Ki67 from rBM-MSCs from adult group incubated with 0.1 ng/ml or 1 ng/ml of JK184. **(C)** Analysis of cell cycle by flow cytometry of rBM-MSCs from adult group incubated with 5 μ M or 10 μ M of IM and 0.1 ng/ml or 1 ng/ml of JK184 in the culture medium. One representative experiment is shown. * P <0.01 compared with control, was considered statistically significant using Mann-Whitney-U and Kruskal-Wallis tests. IM= imatinib mesylate; control= rBM-MSCs incubated with growth medium without drug.

mTOR, p-Akt/Akt, AMPK α and p70S6K decreased statistically significant ($P<0.01$ and $P<0.05$) in adult group when the cells were incubated with IM or JK184 (Figure 4.12, 4.13 and 4.14A).

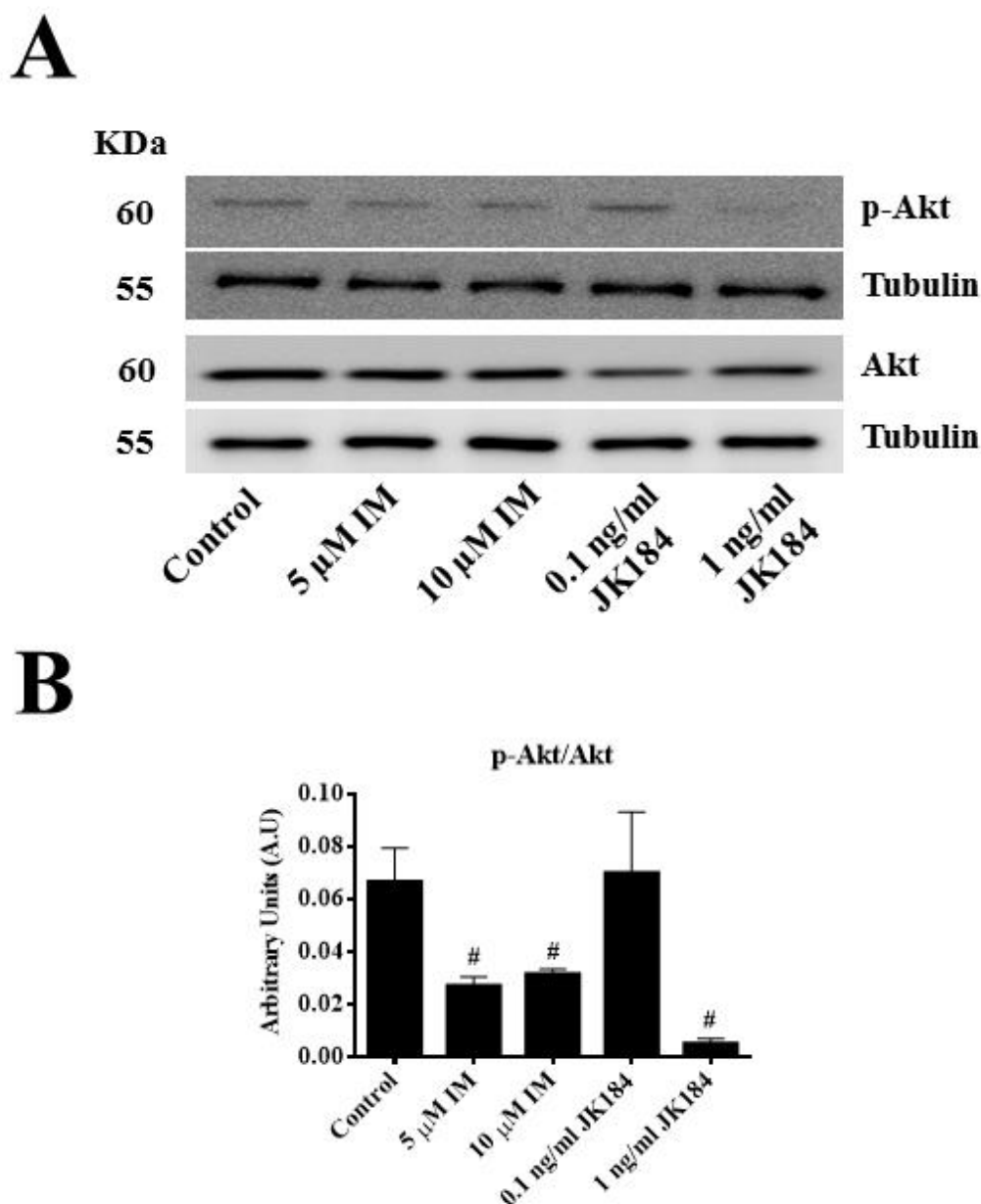


Figure 4.12. PI3K/Akt pathway in rBM-MSCs from adult group treated with 5 μ M or 10 μ M IM and 0.1 ng/ml or 1 ng/ml JK184. (A) Western-blot of p-Akt, Akt and tubulin used as housekeeping. **(B)** Densitometry analysis of western-blot of p-Akt and Akt normalized against to tubulin using Image Quant 5.2. One representative experiment is shown. [#] $P<0.05$ compared with control, was considered statistically significant using Mann-Whitney-U and Kruskal-Wallis tests. IM= imatinib mesylate; control= rBM-MSCs incubated with growth medium without drug.

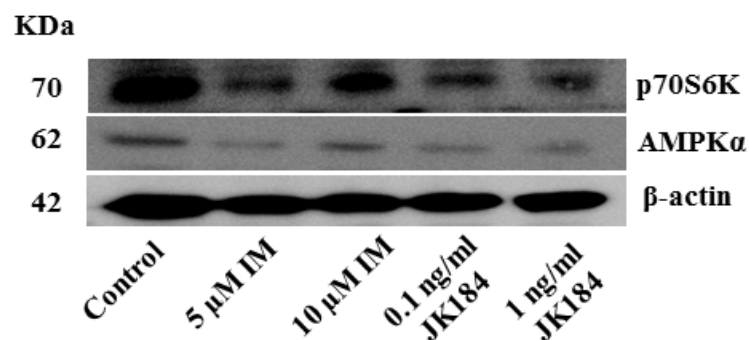
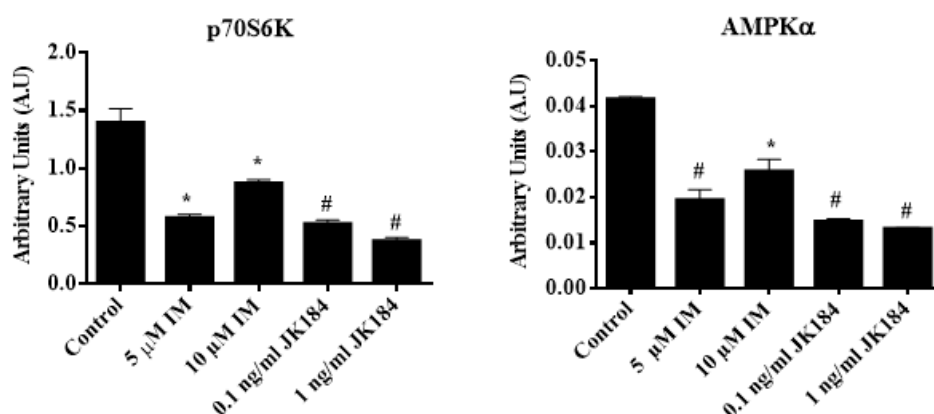
A**B**

Figure 4.13. Level of p70S6k and AMPK α in rBM-MSCs from adult group treated with 5 μ M or 10 μ M IM and 0.1 ng/ml or 1 ng/ml JK184. (A) Western-blot of p70S6K, AMPK α and β -actin used as housekeeping. (B) Densitometry analysis of western-blot of p70S6K and AMPK α normalized against to β -actin using Image Quant 5.2. One representative experiment is shown. * P <0.01 compared with control, were considered statistically significant and # P <0.05 compared with control using Mann-Whitney-U and Kruskal-Wallis tests. IM= imatinib mesylate; control= rBM-MSCs incubated with growth medium without drug.

Also, p-mTOR, rictor, raptor and G β 1 were statistically significant (P <0.01) decreased with respect to control (**Figure 4.14B** and **Figure 4.15**) in adult group when the cells were incubated with JK184.

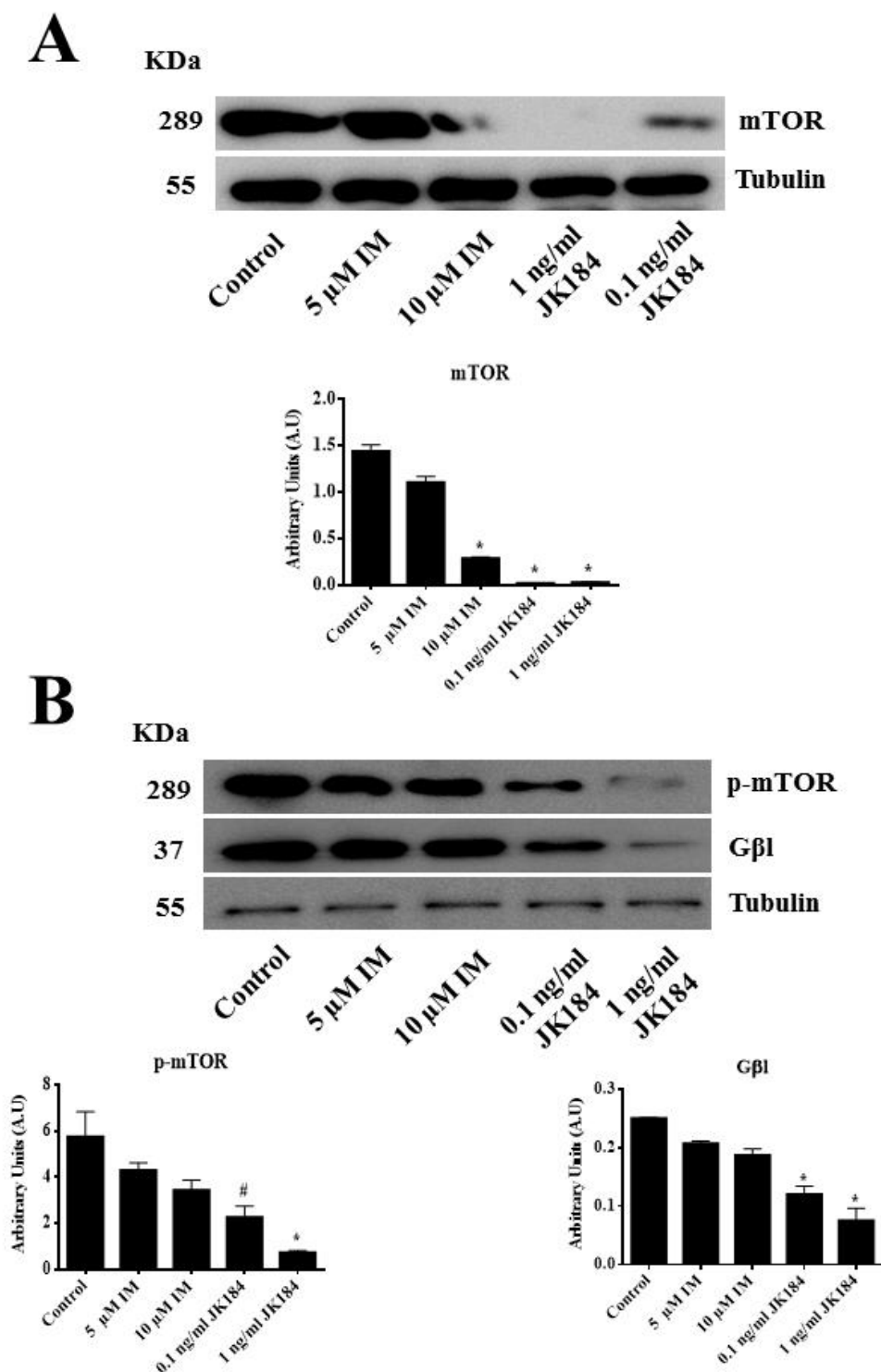


Figure 4.14. mTOR pathway in rBM-MSCs from adult group treated with 5 μ M or 10 μ M IM and 0.1 ng/ml or 1 ng/ml JK184. **(A)** Western-blot mTOR and tubulin used as housekeeping and densitometry analysis of western-blot of mTOR normalized against to tubulin using Image Quant 5.2. **(B)** Western-blot p-mTOR, G β 1 and tubulin used as housekeeping and densitometry analysis of western-blot of p-mTOR, G β 1 normalized with respect to tubulin using Image Quant 5.2. One representative experiment is shown. * P <0.01 compared with control, were considered statistically significant and # P <0.05 compared with control using Mann-Whitney-U tests and Kruskal-Wallis. IM= imatinib mesylate; control=rBM-MSCs incubated with growth medium without drug.

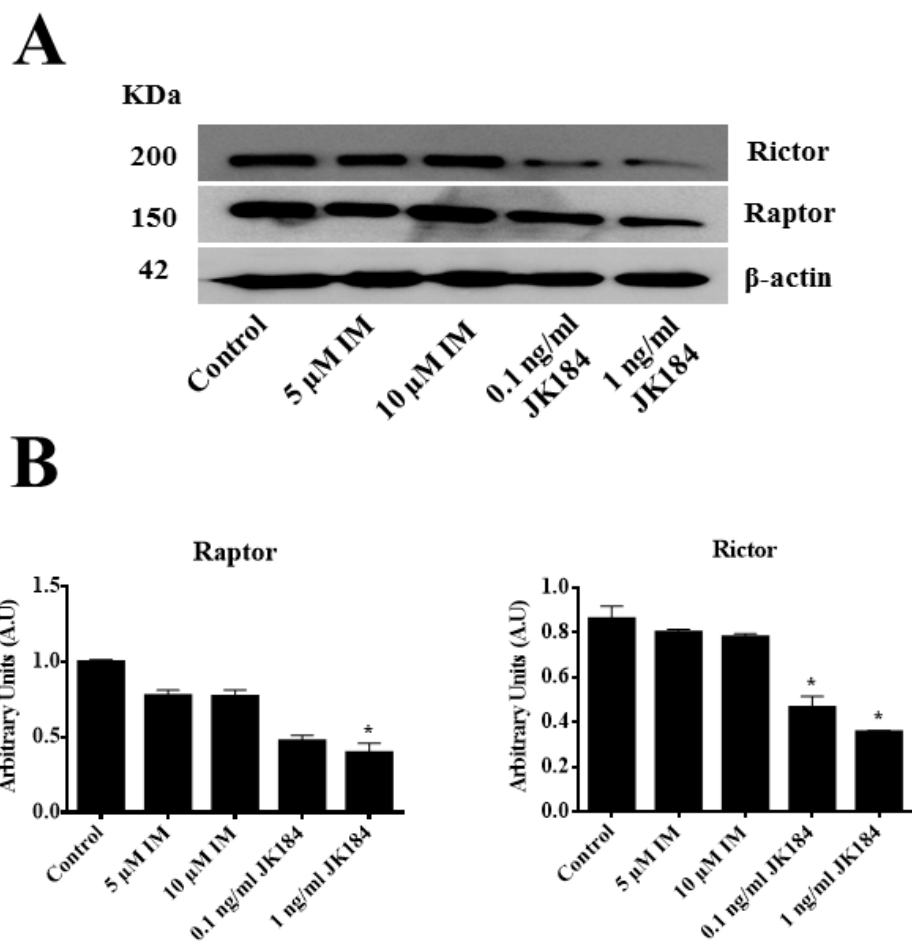


Figure 4.15. mTOR pathway in rBM-MSCs from adult group treated with 5 μ M or 10 μ M IM and 0.1 ng/ml or 1 ng/ml JK184. (A) Western-blot of rictor, raptor and β -actin used as housekeeping. **(B)** Densitometry analysis of western-blot of rictor and raptor normalized with respect to β -actin using Image Quant 5.2. One representative experiment is shown. * P <0.01 compared with control and # P <0.05 compared with control, were considered statistically significant using Mann-Whitney-U and Kruskal-Wallis tests. IM= imatinib mesylate; control= rBM-MSCs incubated with growth medium without drug.

Also, cells that were treated with 10 nM rapamycin to inhibit mTOR pathway presented lower levels of CD117 and Ki67 (4.57 ± 2.95 and 7.60 ± 2.94 respectively) than control (Figure 4.16).

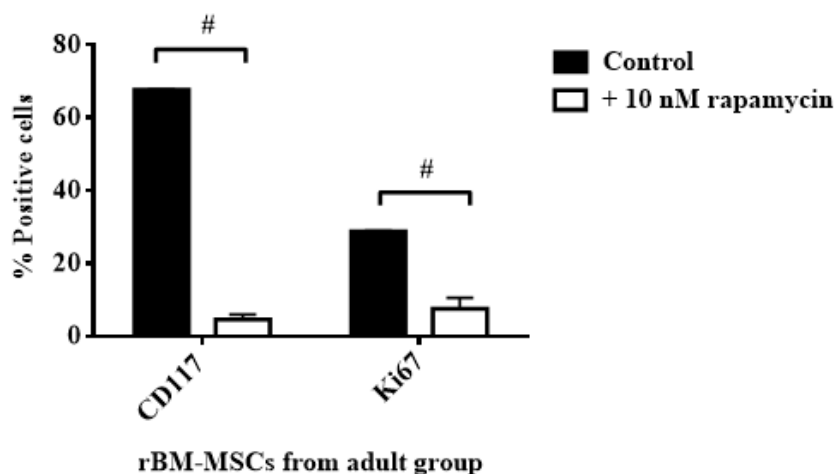
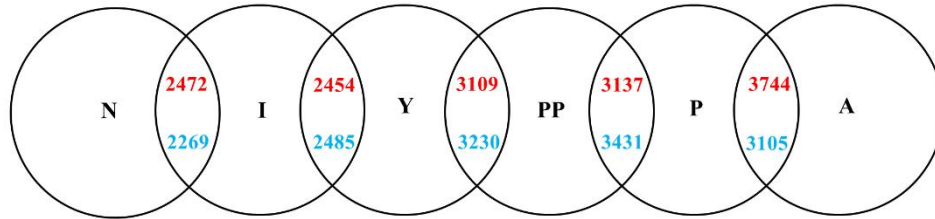


Figure 4.16. Proliferation markers (Ki67 and CD117) in rBM-MSCs from old group treated with 10 nM rapamycin. One representative experiment is shown. # $P < 0.05$ compared with control, was considered statistically significant using Mann-Whitney-U tests and Kruskal-Wallis. Control= rBM-MSCs incubated with growth medium without drug.

4.10 Transcriptome analysis using Next Generation Sequencing (NGS) of rBM-MSCs

NGS analysis indicated that a total of 9628 genes presented differences of expression among groups of age as shown in Figure 4.17. Genes were divided into up-regulated in red and down-regulated in blue between age groups chronologically continuous. The results indicated that 4741 genes modified their expression between newborn and infant groups; 4939 genes modified their expression between infant and young groups; 6339 genes modified their expression between young and pre-pubertal groups; 6568 genes modified their expression between pre-pubertal and pubertal groups and 6849 genes modified their expression between pubertal and adult groups.

A



B

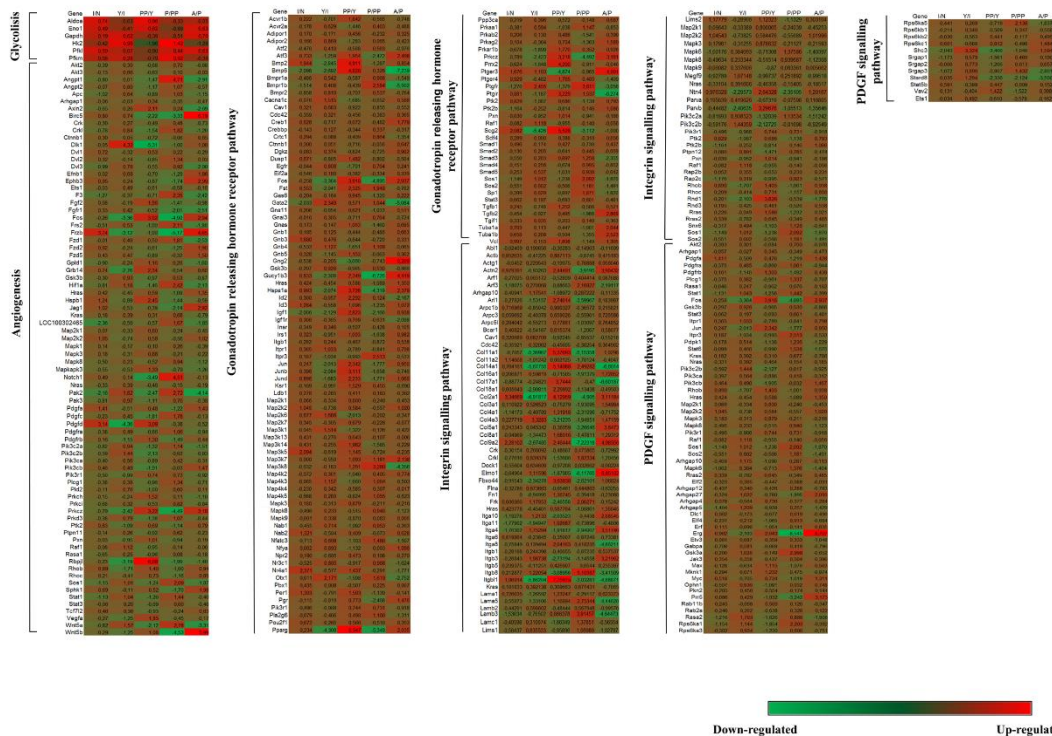


Figure 4.17. Next Generation Sequencing study. (A) Modified expression genes among rBM-MSCs obtained in the RNA-sequencing. N= newborn; I= infant; Y= young; PP= pre-pubertal; P= pubertal; A=adult, blue genes= down-regulated; red genes= up-regulated. (B) Hierarchical clustering of modulated genes among rBM-MSCs age groups into pathways common in all of them. N=newborn; I=infant; Y= young; PP= pre-pubertal; P= pubertal; A= adult; I/N= infant vs newborn; Y/I= young vs infant; PP/Y= pre-pubertal vs young; P/PP= pubertal vs pre-pubertal; A/P= adult vs pubertal

Hierarchical clustering of genes involved into five common pathways between six groups studied the R/Bioconductor package RamiGO was shown in the **Figure 4.17B**. In detail, it was done a study assigning genes to metabolism pathways where genes modulated between newborn and infant groups were grouped at eight metabolism pathways. However genes modulated from infant until adult groups were grouped between 12 and 15 metabolism pathways. Genes involved into hormonal changes, as gonadotropin releasing hormone pathway (PO6664), were increasing their number of from infant age group until adult group (76, 89, 116, 112 and 121 genes respectively). Genes involved in programmed death as apoptotic signalling pathway (PO00006) were observed modulated among young, pre-pubertal and adult groups (46, 57 and 66 respectively). Genes involved into inflammation mediated by chemokine and cytokine signalling pathway (PO00031) were modulated in infant, young and pubertal groups (78,82 and 103 genes respectively) (**Figure 4.18** and **4.19**).

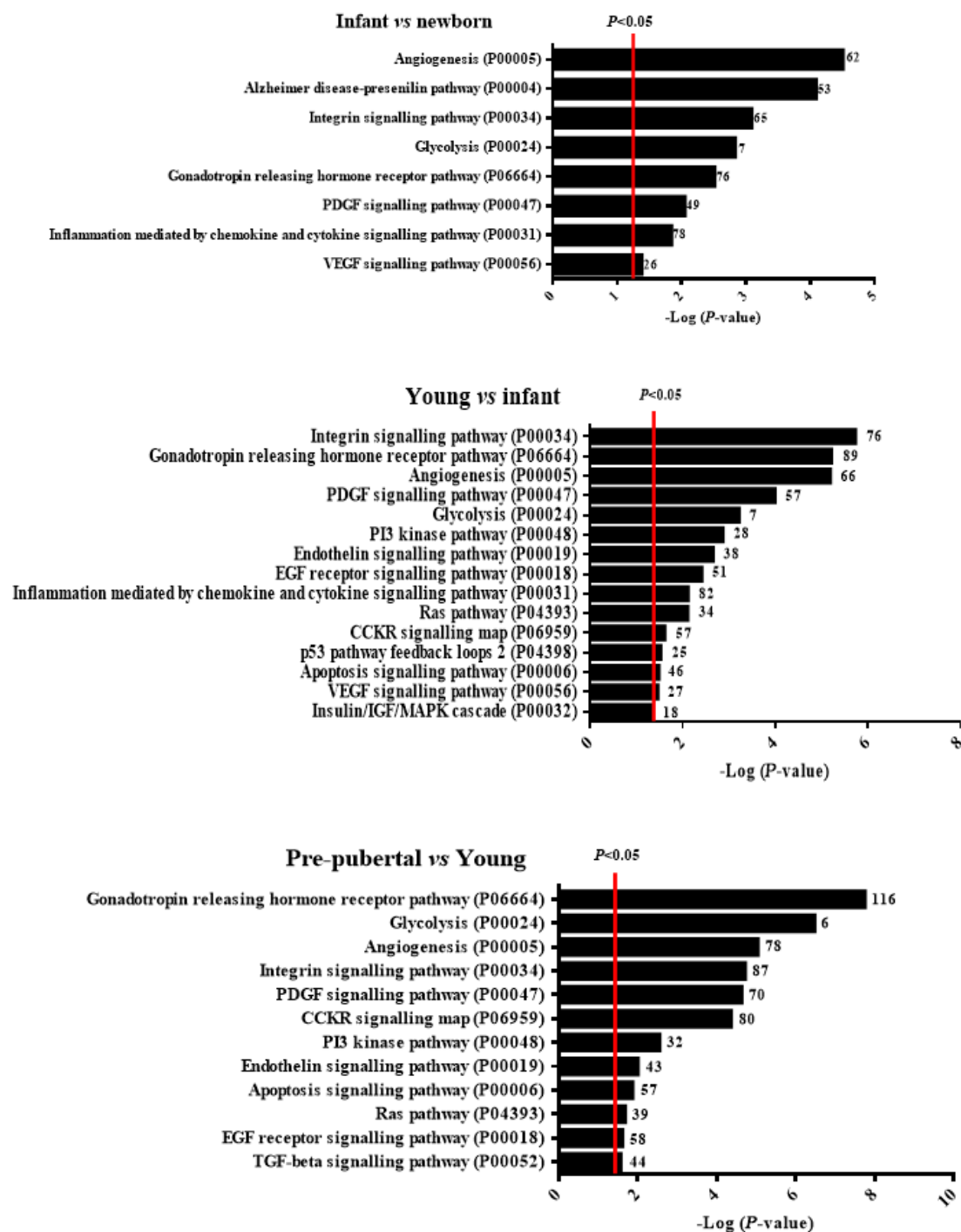


Figure 4.18. Metabolic pathways with statistically significant changes among rBM-MSCs Part I. Modulated genes were categorized according to their function, biological process and cellular component using RamiGO. The small number on the right of each bar indicated the modulated genes involved in each pathway. GO= gene ontology.

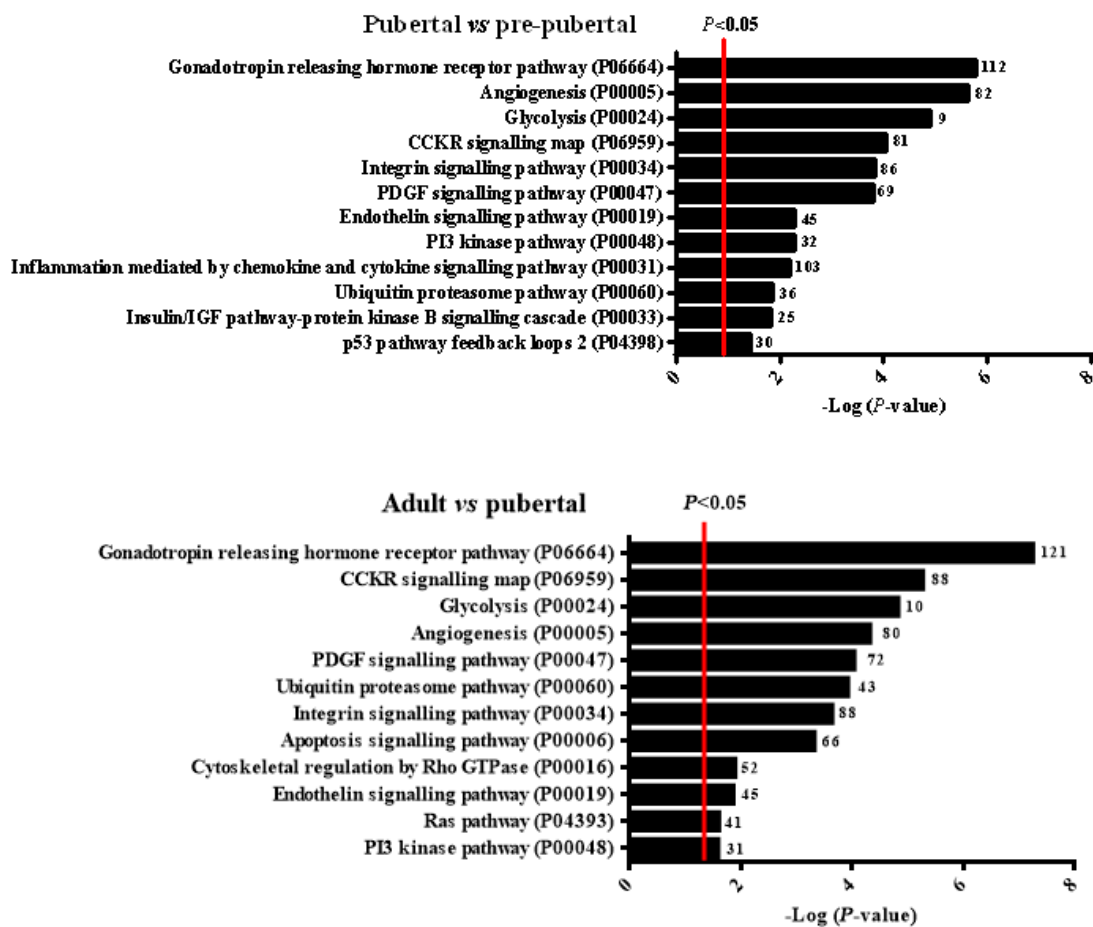


Figure 4.19. Metabolic pathways with statistically significant changes among rBM-MSCs Part II. Modulated genes were categorized according to their function, biological process and cellular component using RamiGO. The small number on the right of each bar indicates the modulated genes involved in each pathway. GO= gene ontology.

4.11 Analysis of pro-inflammatory potential in rBM-MSCs at different ages

rBM-MSCs from different ages were treated with 10 ng/ml rrTNF α for 2 days to activate immunogenic response and it was checked CD200 by flow cytometry. It was obtained high percentage of positive cells ($13.5\pm 3.11\%$) statistically significant ($P<0.05$) in pre-pubertal group when compared to other groups and the lowest expression statistically significant ($P<0.05$) in adult group (1.80 ± 1.11) (**Figure 4.20A**).

Also, TLR4 protein concentration was checked by western blot after 4 hours with 10 ng/ml LPS treatment to activate TLR4 pathway (**Figure 4.20B**). It was observed an increase of TLR4 with increasing age of the cells that were treated with LPS.

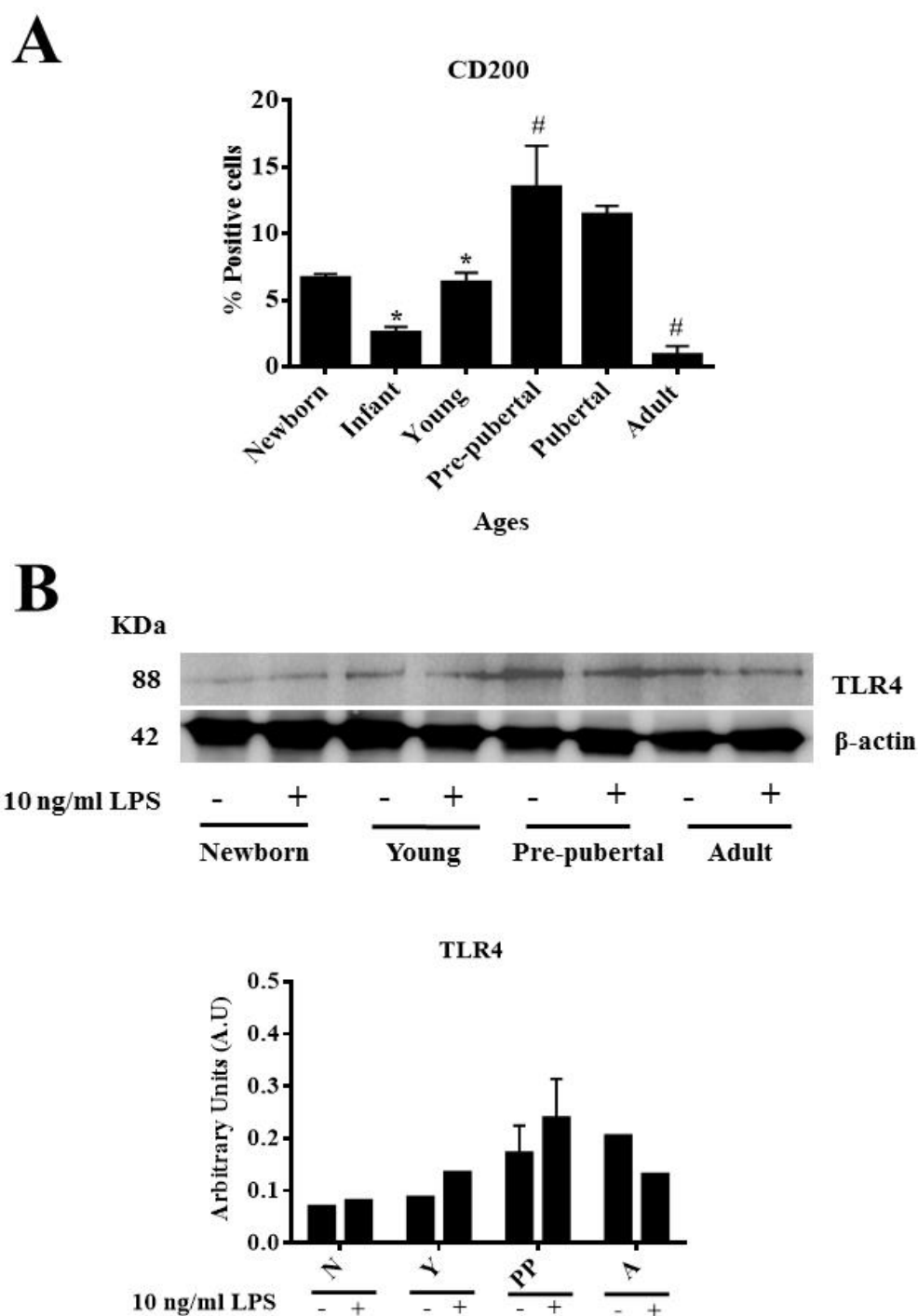
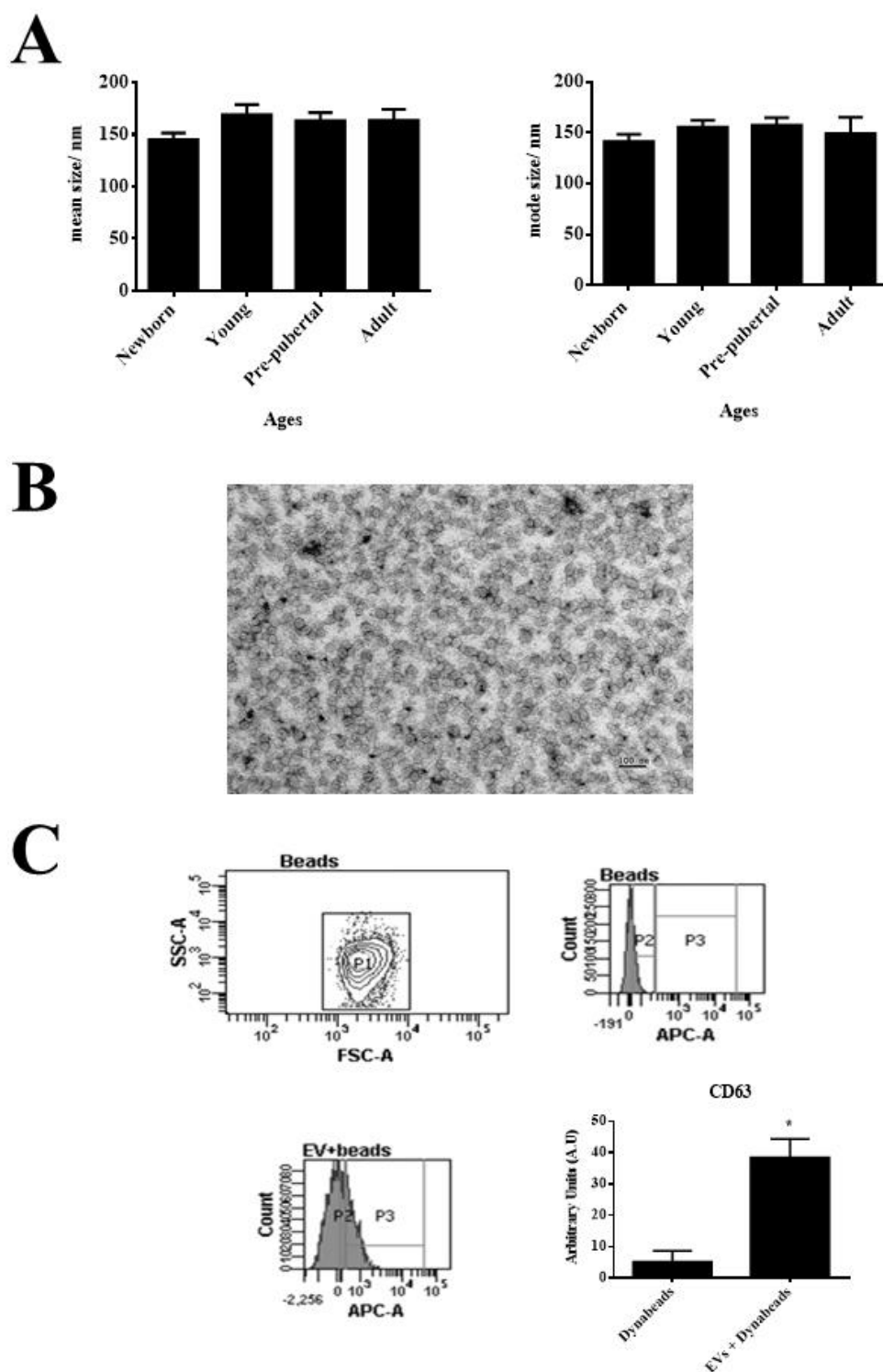


Figure 4.20. Pro-inflammatory phenotype of rBM-MSCs at several ages. (A) Percentage of positive cells for CD200 treated with 10 ng/ml rTNF α . **(B)** Western-blot analysis of TLR4. β -actin was used as housekeeping and densitometry analysis of TLR4 normalized with respect to β -actin of rBM-MSCs treated with 10 ng/ml LPS. The molecular weight of each protein is shown in the left. At the bottom the the group's source of rBM-MSCs used. N= Newborn; Y= Young; PP= pre-pubertal; A= adult; -= without 10 ng/ml LPS; += with 10 ng/ml LPS. One representative experiment is shown. # P <0.05 compared with previous age group, * P <0.01 compared with previous age group were considered statistically significant using Mann-Whitney-U and Kruskal-Wallis tests.

4.12 Characterization of rBM-MSC-derived EVs

Nanoparticle tracking analysis (NTA) was made to verify the extracellular vesicles (EV) nature obtained after the ultracentrifugation at 100,000 xg . The size of extracellular vesicles were 160 ± 18 nm as exosomes and there weren't significant differences among groups (**Figure 4.21A**). rBM-MSC- derived EVs were visualized by electronic microscopy as small vesicles, typically 40-80 nm in diameter (**Figure 4.21B**). Flow cytometry analysis of exosomes attached to anti-CD63 beads revealed that they were positive for the tetraspanins CD63, which is a membrane protein from exosomes (**Figure 4.21C**).



The ratio protein per particle and production of MSC derived EVs by NTA revealed that ratio protein/particle decreased with increasing donor age (**Figure 4.22B**), however with respect production rBM-MSC-derived EVs increased with age ($26\pm 1\%$) (**Figures 4.22A** and **4.22B**).

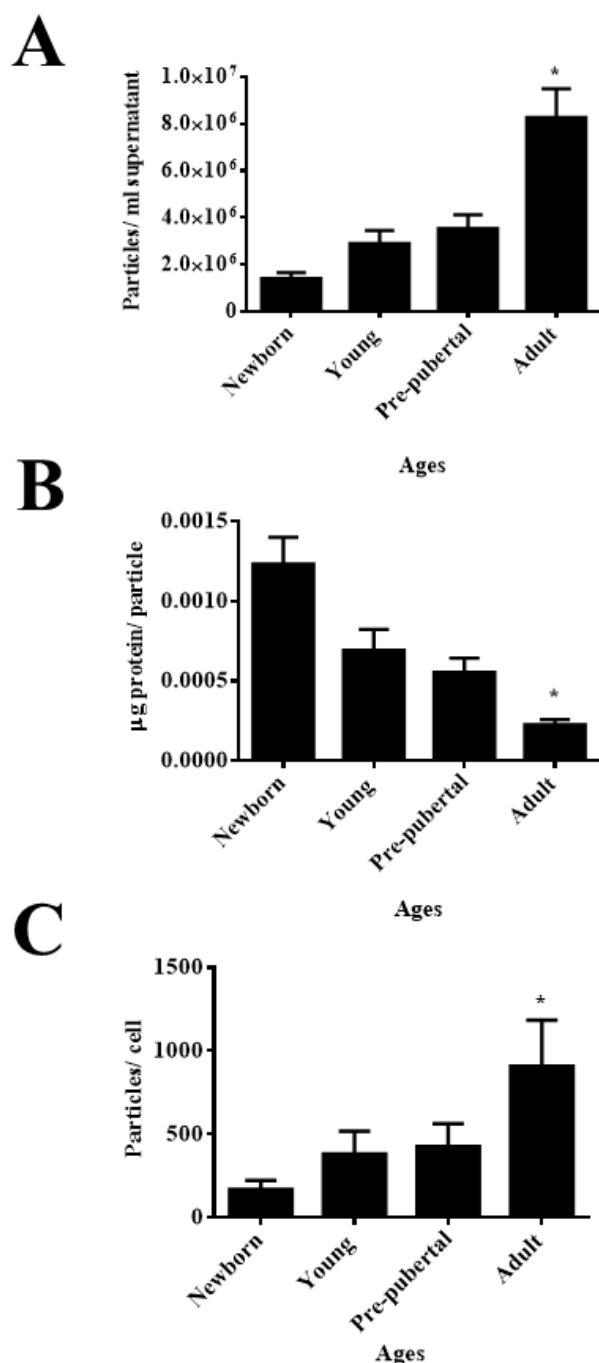


Figure 4.22. NTA study of MSC-derived EVs at several ages. (A) Number of particles per ml supernatant from rBM-MSCs at several ages. **(B)** Protein concentration per particle at different ages. **(C)** Particles per cell at several ages. One representative experiment is shown. # $P < 0.05$ compared with previous age group and * $P < 0.01$ compared with previous age group, were considered statistically significant using Mann-Whitney-U and Kruskal-Wallis tests.

4.13 Detection of miRs relationship with Toll-like receptor 4 in rBM-MSC-derived EVs at different ages

qRT-PCR analysis of miRs associated with Toll like receptor 4: miR-146a; miR-155; miR-132; miR-21-5p and miR-335, determined that miR-146a, miR-155 and miR-132 decreased their expression 93 ± 3 % with the increase donor age (**Figures 4.23A, 4.23B and 4.23C**). However, the adult group presented the highest expression of miR-335 ($P<0.05$) (**Figure 4.23D**) and miR-21-5p increased its expression in pre-pubertal group when compared to other groups ($P<0.05$) (**Figure 4.23E**).

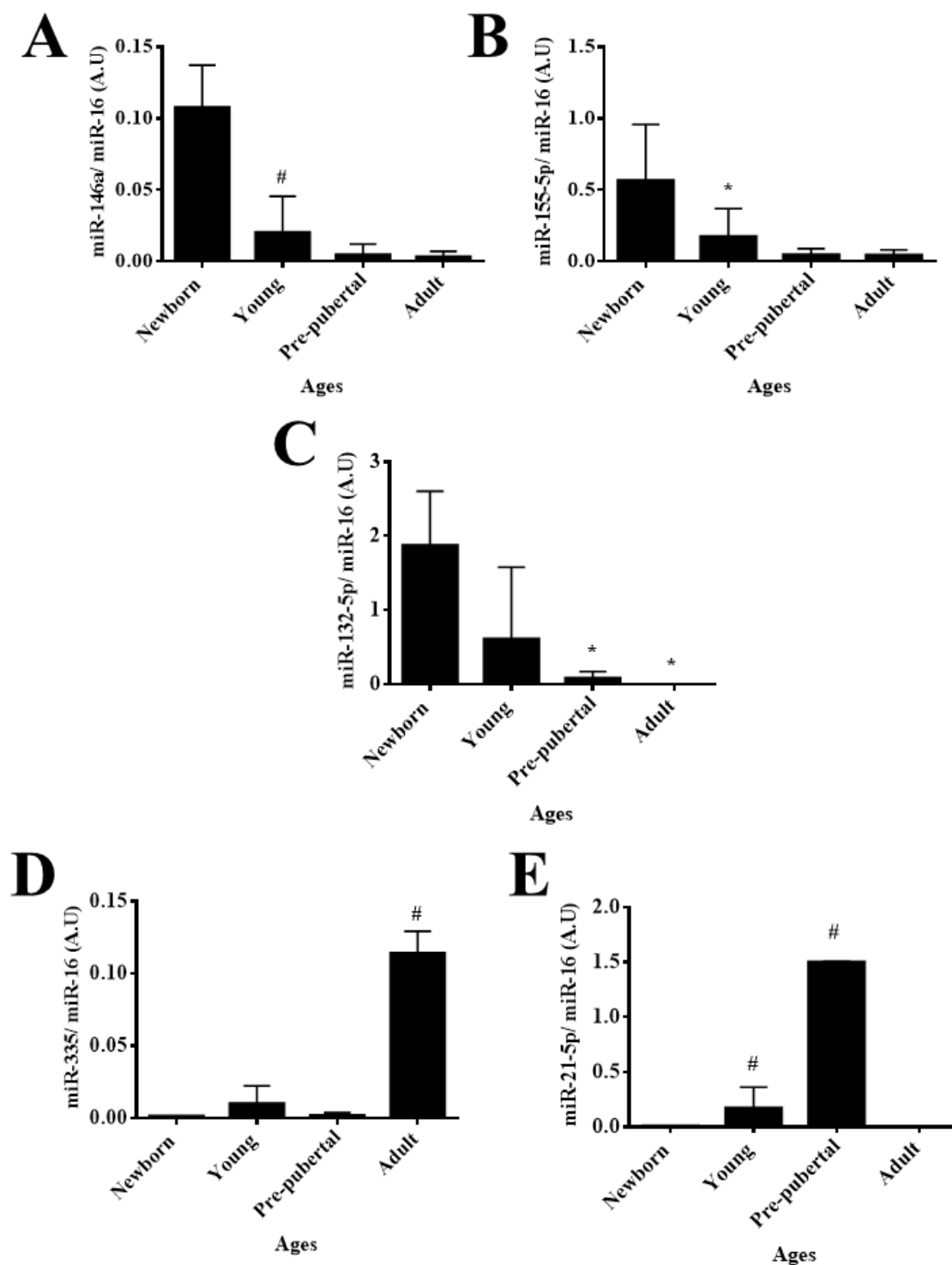


Figure 4.23. Pro-inflammatory profile of micro-RNAs contained in MSC-derived EVs with age. (A) miR-146a expression using qRT-PCR analysis normalized by expression miR-16 used as housekeeping. (B) miR-155-5p expression using qRT-PCR analysis normalized by expression miR-16 used as housekeeping. (C) miR-132-5p expression using qRT-PCR analysis normalized by expression miR-16 used as housekeeping. (D) miR-335 expression using qRT-PCR analysis normalized by expression miR-16 used as housekeeping. (E) miR-21-5p expression using qRT-PCR analysis normalized by expression miR-16 used as housekeeping. One representative experiment is shown. # $P < 0.05$ compared with previous age group, * $P < 0.01$ compared with previous age group were considered statistically significant using Mann-Whitney-U and Kruskal-Wallis tests. A.U.= arbitrary units.

4.14 miR-21-5p as regulator on pro-inflammatory and differentiation capacities of TLR4 in rBM-MSCs from pre-pubertal group

rBM-MSCs from pre-pubertal group were transiently transfected with miRvana miR-21-5p and its expression was checked by qRT-PCR (**Figure 4.24A**), the transfected cells expressed levels of miR-21-5p statistically significant lower ($P<0.05$) than the same cells transfected with mimic miRNA used as control. qRT-PCR analysis of damage-associated molecular pattern (DAMPs) associated with TLR4 indicated that miR-21-5p inhibition produced a statistically significant decrease ($P<0.05$) of S100A4, S100A6 and HMGB1 with respect to rBM-MSCs control (**Figure 4.24B**). Also, it was checked Nanog gene expression at mRNA level and it was statistically significant higher ($P<0.05$) in cells transfected with miRvana miR-21-5p with respect to control (**Figure 4.24C**).

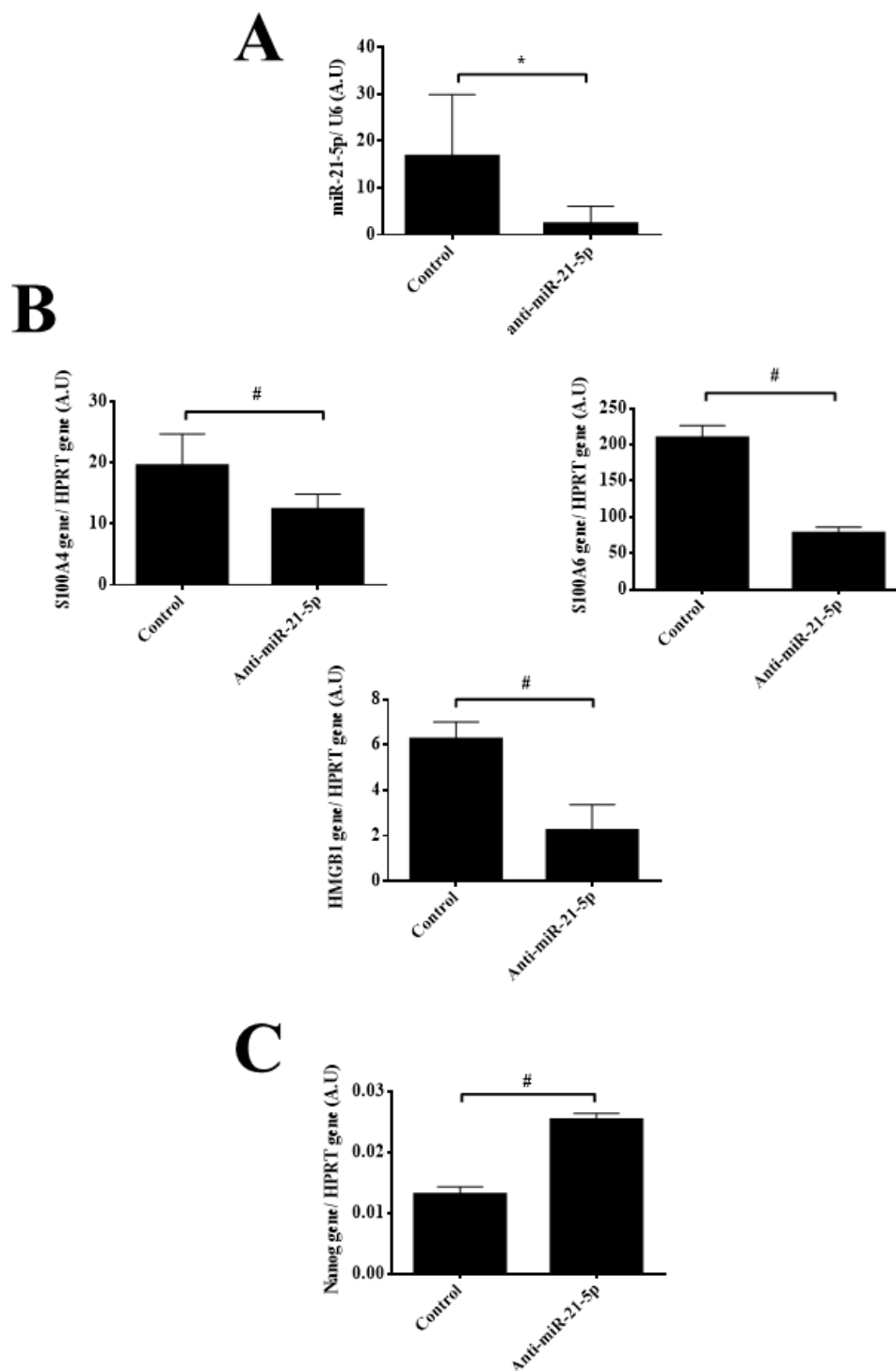


Figure 4.24. Effect of miR-21-5p on DAMPs and Nanog in mesenchymal stem cells from pre-pubertal group. (A) miR-21-5p expression using qRT-PCR analysis normalized by expression U6 used as housekeeping. (B) S100A4, S100A6 and HMGB1 using qRT-PCR analysis normalized by expression HPRT used as housekeeping. (C) Nanog gene expression using qRT-PCR analysis normalized by expression HPRT used as housekeeping. One representative experiment is shown. # $P < 0.05$ compared with control, was considered statistically significant using Mann-Whitney-U and Kruskal-Wallis tests. A.U= arbitrary units; Control= without inhibition miR-21-5p; anti-miR-21-5p= with inhibition miR-21-5p.

Western blot analysis of rBM-MSCs from pre-pubertal group where miR-21-5p was inhibited revealed that lamin A/C, mTOR, HMGB1, TLR4 and p-Akt were statistically significant ($P<0.05$) down-regulated in the inhibited cells with respect to control cells (**Figures 4.25** and **4.26**). On the other way Wnt5a and Akt were over-expressed statistically significant ($P<0.05$) when compared to control cells (**Figures 4.25** and **4.26**).

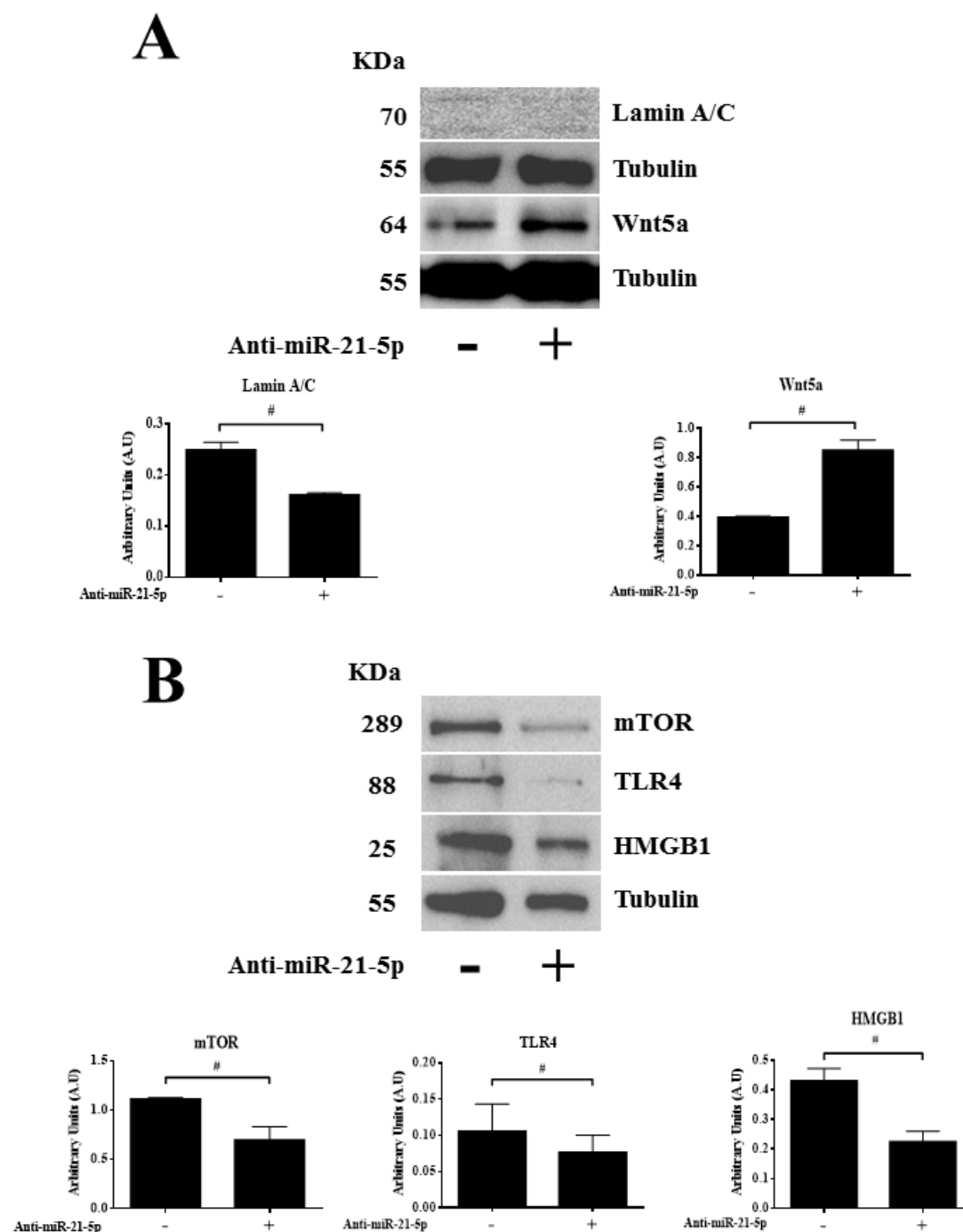


Figure 4.25. Effect of miR-21-5p on senescence and pro-inflammatory phenotype in rBM-MSCs from pre-pubertal group. (A) Western blot analysis of LMNA/C and Wnt5a in pre-pubertal rBM-MSCs from pre-pubertal group with or without inhibition of miR-21-5p and their densitometry analysis normalized with respect to tubulin using Image Quant 5.2. **(B)** Western blot analysis of TLR4, mTOR and HMGB1 in rBM-MSCs from pre-pubertal group with or without inhibition of miR-2-5p and their densitometry analysis normalized with respect to tubulin using Image Quant 5.2. The molecular weight of each protein is shown in the left. One representative experiment is shown. # $P < 0.05$ compared with control, was considered statistically significant using Mann-Withney-U and Kruskal-Wallis tests. - = without inhibition miR-21-5p; + = with inhibition miR-21-5p.

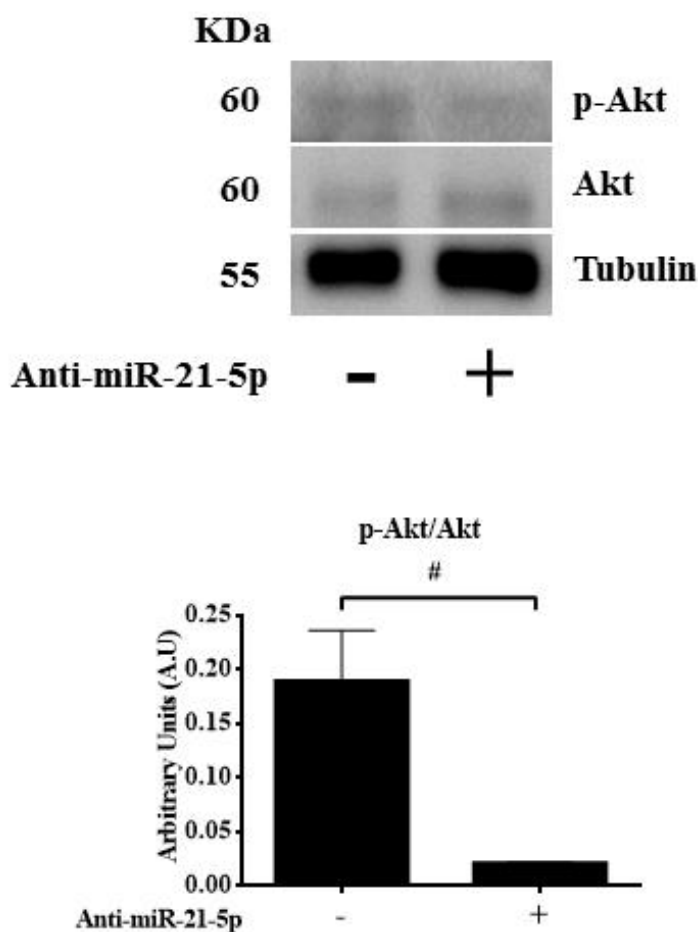


Figure 4.26. Effect of miR-21-5p on PI3K/Akt in rBM-MSCs from pre-pubertal group. Western blot analysis of p-Akt and Akt in pre-pubertal rBM-MSCs group with or without inhibition of miR-21 and their densitometry analysis normalized with respect to tubulin using Image Quant 5.2. The molecular weight of each protein is shown in the left. One representative experiment is shown. # $P < 0.05$ compared with control was considered statistically significant using Mann-Whitney-U and Kruskal-Wallis tests. -= without inhibition miR-21-5p; += with inhibition miR-21-5p.

Also, rBM-MSCs from pre-pubertal where miR-21-5p were inhibited when treated with 10 ng/ml LPS for 4 hours, and it was observed an increased expression statistically significant ($P < 0.05$) at proteomic level of TLR4 and ratio pAkt/Akt in comparison with rBM-MSCs which presented miR-21-5p inhibited without the treatment of LPS (**Figure 4.27**).

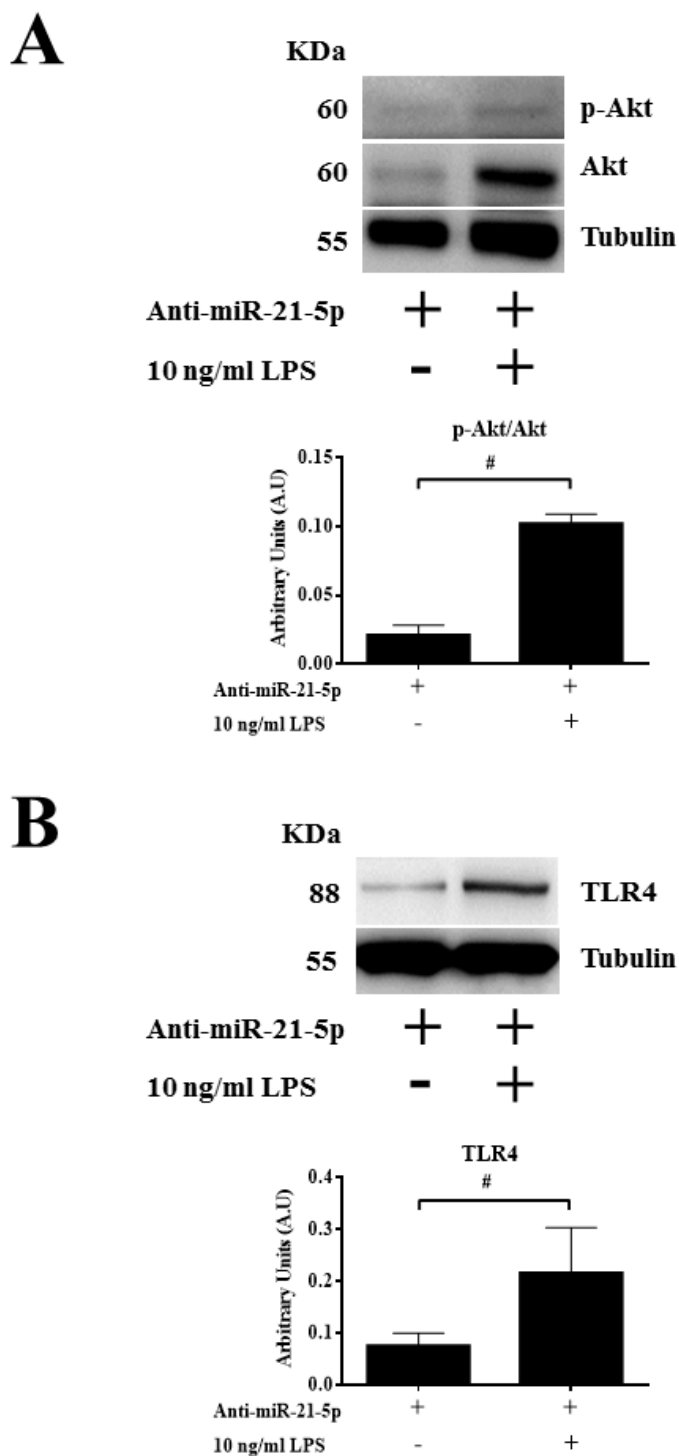


Figure 4.27. Effect of miR-21-5p on immune response in rBM-MSCs from pre-pubertal group. (A) Western blot analysis of p-Akt and Akt pathway and in pre-pubertal MSCs group miR-21-5p inhibited with or without LPS treatment and their densitometry analysis normalized with respect to tubulin using Image Quant 5.2. **(B)** Western-blot analysis of TLR4 in pre-pubertal MSCs group miR-21-5p inhibited with or without LPS treatment and their densitometry analysis normalized with respect to tubulin using Image Quant 5.2. The molecular weight of each protein is shown in the left. One representative experiment is shown. # $P < 0.05$ compared with cells without treatment of 10 ng/ml LPS, was considered statistically significant using Mann-Whitney-U and Kruskal-Wallis tests. - = without; + = with.

4.15 Variation on rBM-MSC-derived EVs characteristic during aging

Using fluorescence microscopy, it was observed internalizing of MSC-derived EVs from adult group (aEVs) in rBM-MSCs from young group (yMSCs) at 2 days and increase of EVs inside of rBM-MSCs along the time (**Figure 4.28**), the similar profile it was observed in aMSCs co-cultured with yEVs (**Figure 4.28**). Additionally, some MSC-derived EVs labelled with DiI were observed in the perinuclear region (**Figure 4.28**).

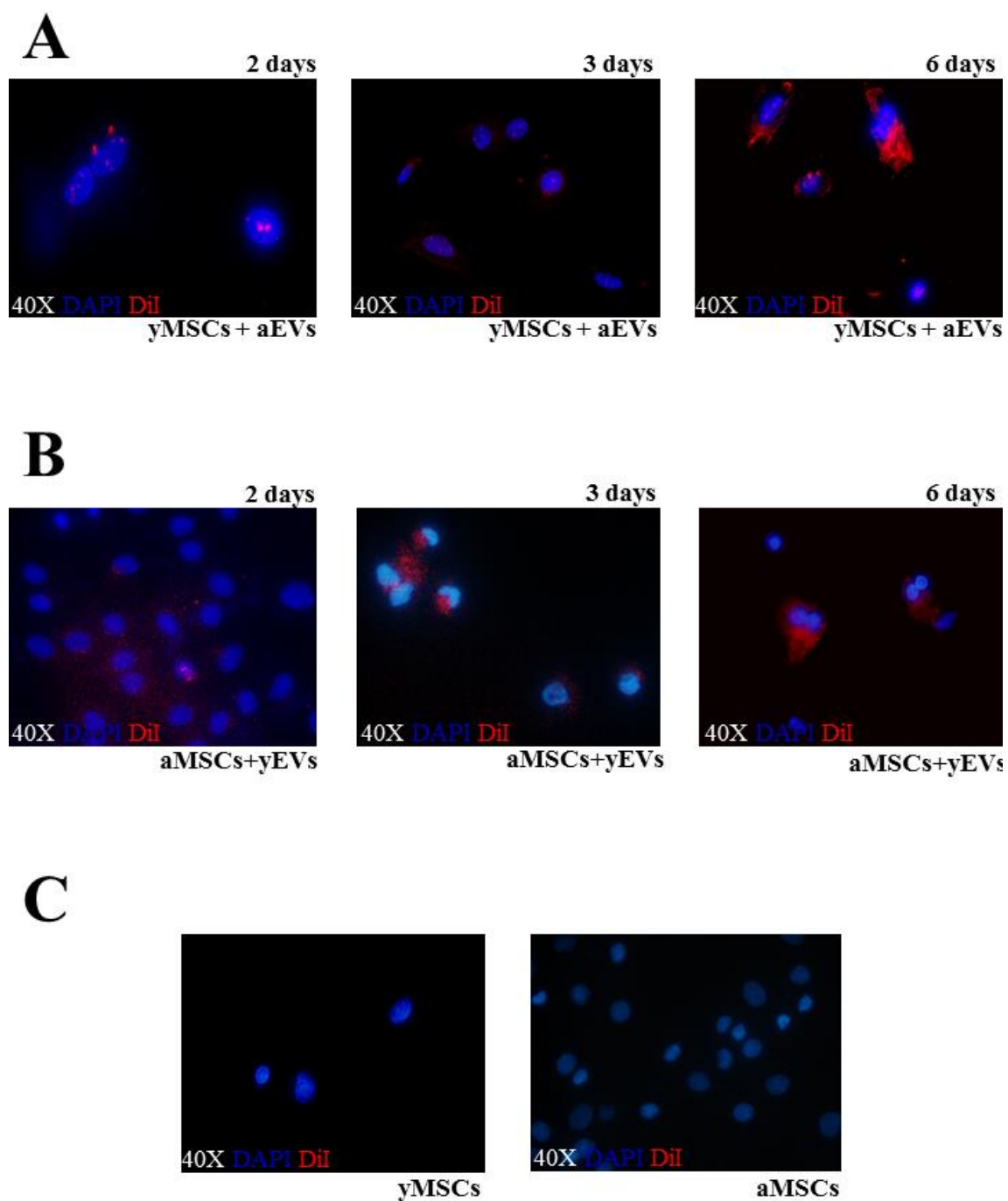


Figure 4.28. Observation of our *in vitro* model using fluorescence microscopy. Images of fluorescence microscopy (40X) of nucleus of MSCs were stained with DAPI and EV-derived MSCs were stained with DiI. **(A)** yMSCs cultured with aEVs at 2, 3 and 6 days. **(B)** aMSCs cultured with yEVs at 2, 3 and 6 days. **(C)** Control yMSCs and aMSCs without EVs. One representative experiment is shown. aMSCs= MSCs from adult group; yMSCs= MSCs from young group; aEVs= MSC-derived EVs from young group; yEVs= EV-derived MSCs from young group.

Expression of Nanog, a pluripotency marker, was statistically significant decreased ($P<0.05$) in yMSCs with aEVs in comparison with yMSCs without aEVs used as control at 2 days. Instead aMSCs with yEVs presented increased expression ($P<0.05$) with respect to control at 6 days (**Figure 4.29A**) and it was observed an increased expression of Oct4 gene in aMSCs with yEVs with respect to the control after 3 days. However, Oct4 expression in yMSCs with aEVs had a lower statistically significance ($P<0.05$) after 3 days than the control (**Figure 4.29B**).

Vinculin presented a statistically significant ($P<0.05$) increased expression at 2 days in yBM-MSCs with aEVs with respect to the control (**Figure 4.29C**). aMSCs with yEVs present a statistically significant ($P<0.05$) decreased expression with respect to controls at 6 days (**Figure 4.29C**).

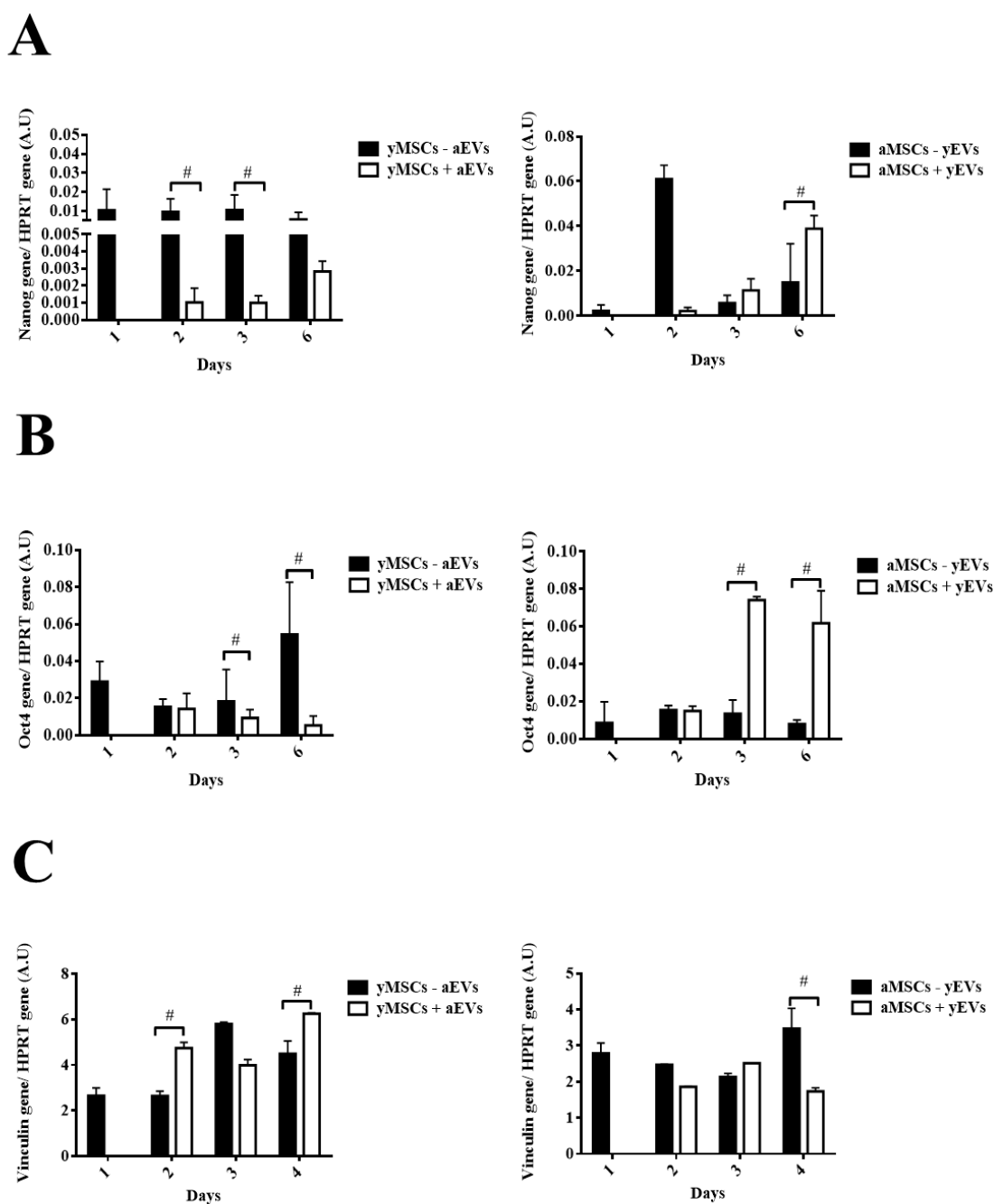


Figure 4.29. Nanog, Oct4 and Vinculin expression at genetic level in our *in vitro* model. (A) Histograms represent gene expression of Nanog normalized by HPRT expression gene used as housekeeping in MSCs with or without EVs. (B) Histograms represent gene expression of Oct4 normalized by HPRT gene used as housekeeping in MSCs with or without EVs. (C) Histograms represent gene expression of Vinculin normalized by HPRT gene used as housekeeping in MSCs with or without EVs. One representative experiment is shown. # $P < 0.05$ compared with control was considered statistically significant using Mann-Whitney-U and Kruskal-Wallis tests. Control= MSCs cultured with growth medium without EVs; aMSCs= MSCs from adult group; yMSCs= MSCs from young group; aEVs= EVs from adult group; yEVs= MSC-derived EVs from young group.

Also, yMSCs with aEVs showed statistically significant ($P<0.01$) higher expression with respect to the control (**Figure 4.30**) and aMSCs with yEVs presented a statistically significant ($P<0.01$) decreased in expression of three isoforms of Lamin A/C with respect to control at 6 days (**Figure 4.31**).

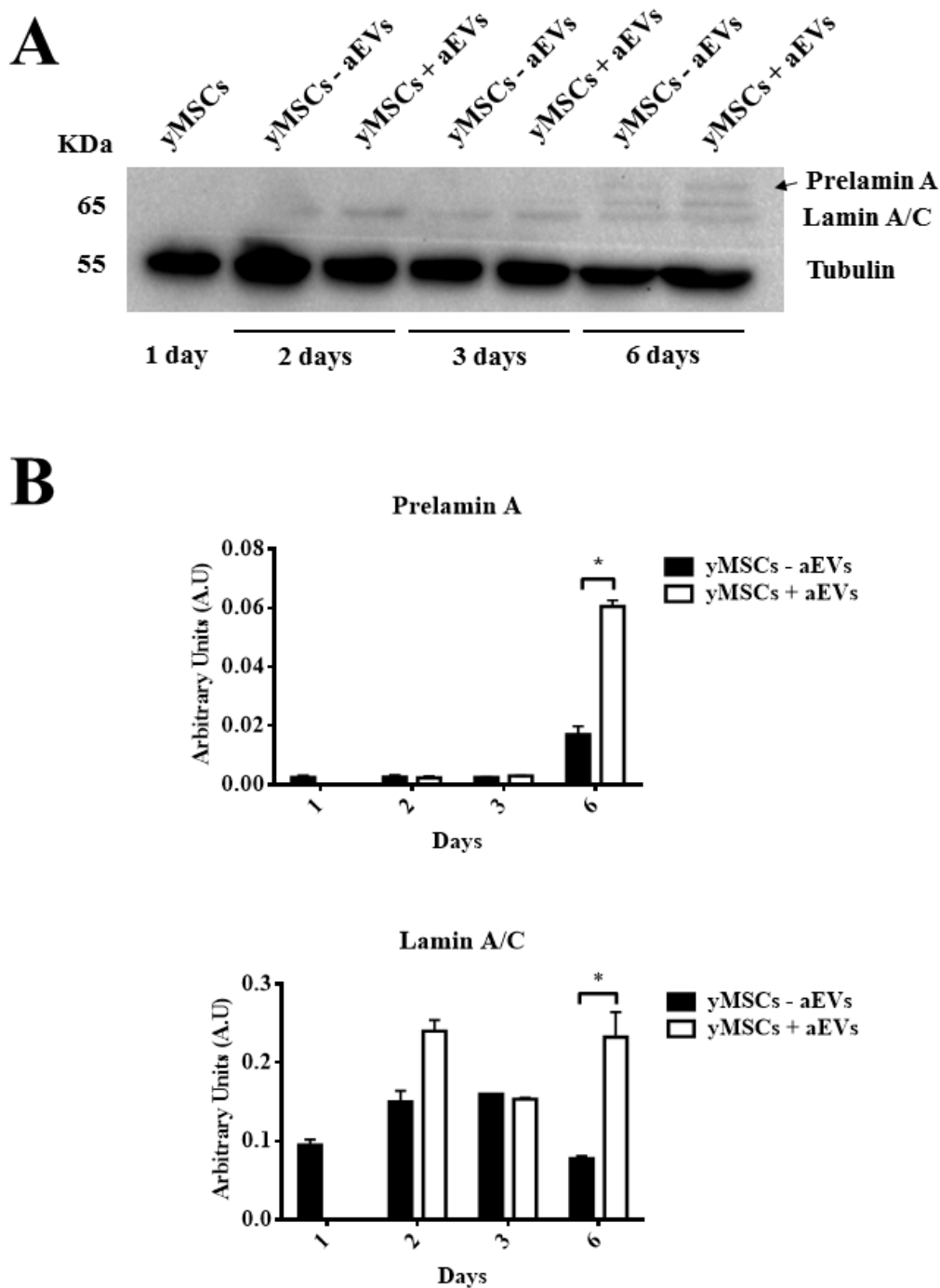


Figure 4.30. Analysis of isoforms of Lamin A using western-blot in our *in vitro* model. (A) Western-blot analysis of prelamina A, Lamin A/C yMSCs with or without aEVs at different times (1, 2, 3 and 6 days). **(B)** Densitometry analysis of three isoforms of Lamin A normalized with respect to tubulin using Image Quant 5.2. The molecular weight of each protein is shown in the left. One representative experiment is shown. * $P < 0.01$ compared with control was considered statistically significant using Mann-Whitney-U and Kruskal-Wallis tests. Control= MSCs cultured with growth medium without yMSCs= MSCs from young group; aEVs= MSC-derived EVs from adult group.

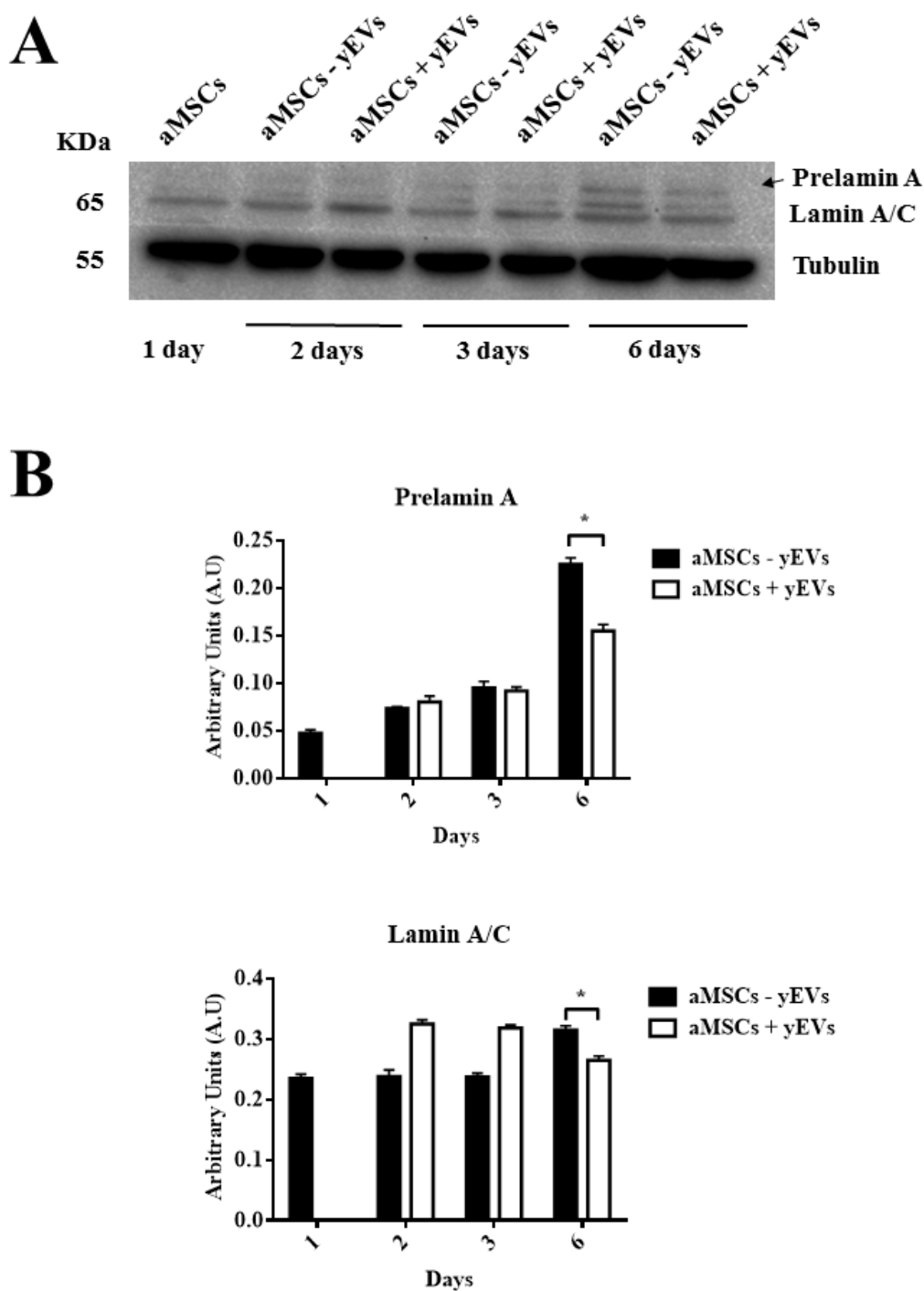


Figure 4.31. Analysis of isoforms of Lamin A using western blot in our *in vitro* model. (A) Western blot analysis of prelamin A, Lamin A/C aMSCs with or without yEVs at different times (1, 2, 3 and 6 days). **(B)** Densitometry analysis of three isoforms of Lamin A normalized with respect to tubulin using Image Quant 5.2. The molecular weight of each protein is shown in the left. One representative experiment is shown. * $P < 0.01$ compared with control was considered statistically significant using Mann-Whitney-U and Kruskal-Wallis tests aMSCs= MSCs from adult group; yEVs= MSC-derived EVs from young group.

5. DISCUSSION

It is well known that long-term *in vitro* culture alters the morphology, susceptibility to senescence and mitochondrial function of the cells. Thus, independently from donor age, *in vitro* aging of MSCs seems to result in complete loss of their progenitor characteristics²¹⁴. Accordingly, functional analysis demonstrated altered mitochondrial morphology, decreased antioxidant capacities and elevated ROS levels in long-term cultivated cells independently of the aged of the donor²¹⁵.

Our study is focused to know how aging could be influencing some kind of changes in the properties of rBM-MSCs using a direct comparison among chronological aged MSCs both at cellular and molecular levels to advance in the knowledge of MSCs and their clinical use.

BM-MSCs from Wistar rats at six different ages (newborn, infant, young, pre-pubertal, pubertal and adult) were used in this study, following the Sengupta's review to establish the aging groups, verifying the phase in days of the animals²¹⁶.

rBM-MSCs from different aging groups were characterized by flow cytometry. We didn't observe statistical significant differences among the mesenchymal and hematopoietic markers into the different rBM-MSCs aging groups studied (**Figure 4.1**). These results were coincident with results published by Jin *et al.*²⁸ indicating that rBM-MSCs have similar markers but were not as abundant as published by Harting *et al.*²¹⁷. These cells were able to adhere to the plastic culture plate which is an intrinsic characteristic of mesenchymal stem cells.

One of the aims of our study was to establish the differences into proliferation processes relating them to the chronological donor age. Our results indicated that chronological age is directly influencing the expression of proliferation marker Ki67²¹⁸ because the lowest levels of Ki67 corresponded with less cells present in proliferation assays in infant and pre-pubertal groups. On the other hand high levels of CD117, a self-renewal marker in MSCs as indicated by Blazquez-Martinez *et al.*¹³ were corresponding to higher cell in proliferation assays of young and adult groups respect to the other groups (**Figure 4.2**).

All of the groups were able to differentiate towards several mesoderm lineages (**Figure 4.3**) and together with the expression of pluripotency markers by qRT-PCR (**Figure 4.4**) indicated these MSCs keep their pluripotency capacity.

iTRAQ analysis is an adequate technique to study complex samples like we have used in this work²¹⁹. Our results by iTRAQ analysis allowed the identification of 1072 proteins, 201 of them were statistically significant modulated among the groups (**Figure 4.6** and **Table 8.6**). Our study represented a step further from a previous iTRAQ-based study²²⁰ where 156 differentially expressed proteins were detected.

60 modulated proteins found in our iTRAQ analysis were involved in proliferation as 60S ribosomal proteins with different sedimentation speed like 60S RP L10, 60S RP L9, 60S RP L23, 60S RP L24, 60S RP L4, 60S RP L6 and 60S RP L7, which were over-expressed in young group when compared to other groups. That could explain the highest expression of proliferation markers CD117 and Ki67 by flow cytometry (**Figure 4.2**) in this group. Maulik *et al.*²²¹ also found over expression of these proteins relationship with proliferation process. Our results indicated that expression of vinculin gene (**Figure 4.7B**) was very low in newborn and young, actually the most proliferative groups (**Figure 4.2**). On the contrary, pre-pubertal group presented high vinculin gene expression coincidentally

with less proliferative potential. Toma-Jonik *et al.*²²² published recently that great mobilization and proliferation potential related with vinculin in melanoma cells and at the same time Piltti *et al.*²²³ published that Rho kinase inhibitor (ROCKi) treatment increased the cellular proliferation in human foreskin fibroblast cells. It is known that significantly less Vinculin-associated focal adhesions were present in ROCKi-treated cells²²⁴. 11- β -hydroxysteroid dehydrogenase type 1 (11- β -HSD1), an enzyme which generates glucorticoids in cells, was found in our iTRAQ analysis significantly increased in pre-pubertal group. This fact could explain the decrease proliferation potential and increased capacity of differentiation in pre-pubertal group. All this is agreement with Bujalska *et al.*²²⁵ who published that 11- β -HSD1 activity in uncommitted adipose stromal cells may facility proliferation rather than differentiation. Transforming growth factor β 1 (TGF- β 1) induces senescence in BM-MSCs via an increased production of mitochondrial ROS and the production of ROS intracellular is associated with a decreased potential of mitochondrial membranes, DNA damage and cellular senescence^{226,227}. This fact could explain that the statistically significant ($P < 0.05$) decrease of total ROS in the pre-pubertal group because TGF- β 1 was found statistically significantly ($P < 0.05$) lower with respect to other groups in the iTRAQ analysis (**Figure 4.8B** and **Table 8.6**).

86 modulated proteins found in our iTRAQ analysis were involved in the pluripotency process. Terme *et al.*²²⁸ showed that pluripotent cells had decreased level of H1.0 and increased levels of H1.1, H1.3 and H1.5 when they were compared with differentiated cells. Differentiation of embryonic stem cells is accompanied by a global reduction of panacetylation of histones H3 and H4 suggesting that histone acetylation plays an important role the maintenance of embryonic stem cells pluripotency²²⁹. Our results indicated that H4 was statistically significant decreased in the adult group. It could point towards their lowest pluripotency with respect to the other groups. Results published by Bermeo *et al.*²³⁰ indicated that MSCs over-expressing Lamin A had higher osteogenic and lower adipogenic differentiation potential. Their studies demonstrated that Lamin A/C played a significant role in differentiation towards both osteoblast and adipocyte lines by regulating some of the elements of Wnt/ β -catenin signalling during early MSCs differentiation. We also found high levels of Lamin A/C by western-blot analysis in rBM-MSCs from adult group which we could link to the lowest adipogenic potential with the statistically significant ($P < 0.05$) lowest levels of oil red staining during its directed differentiation (**Figures 4.3** and **4.7A**). We considered the role of Lamin A, a senescence marker, and its relationship with the increase of ROS, which is associated with an increase of thioredoxin. We found increased Lamin A and SOD-2 (**Figure 4.7A**), producing a oxidative damage, in adult group which could indicate the influence of age²³¹ on impairment of MSCs functions in a similar way that results published by Stolzing *et al.*²³².

The decision to exit pluripotency and undergo differentiation is of singular importance for pluripotent cells, including MSCs. The molecular mechanisms for these decisions to differentiate, as well as reversing those during induced pluripotency have focused largely on transcriptomic controls. Easley *et al.*²³³ explored the role of translational control for the maintenance of pluripotency and the decisions to differentiate. ATP-citrate synthase is profoundly linked to the pentose phosphate route and its inhibition has been recently

linked to a decrease in the proliferation rate²³⁴. Also it has been reported by Pattapa *et al.*²³⁵ that MSCs resided under hypoxic conditions, which were associated with the inherent metabolism of the cells. However, MSCs under normoxia growth conditions derived a significant proportion of ATP from oxidative phosphorylation in addition to glycolysis. From the list of modulated proteins, 55 of them are involved in the energy metabolism process. We observed increase of LDH from adult group (**Figure 4.9A**), it could be explained by the fact that this group presented an increase in glycolysis. Pre-pubertal group showed decrease of LDH and decreased in glycolysis. All these results could be explained through pentose phosphate pathways because of we found a significant decrease G6PDH in the pre-pubertal group and a significant increase in the adult group (**Figure 4.9B**). mTOR is a Ser/Thr protein kinase that functions as an ATP and amino acid sensor to balance nutrient availability and cell growth²³⁶. mTOR regulates cellular senescence and drives bioenergetic infrastructure²³⁷, also it restrains proliferation potential of stem cells mediating their self-renewal loss, which is an effect that can be suppressed by mTOR-inhibitors, such as rapamycin, antagonizing senescence²³⁸. mTOR plays an important role in the regulation of hematopoietic stem cell self-renewal *in vitro* and inhibition of mTOR hyperactivation with rapamycin may represent a novel approach to promote *ex vivo* expansion and their long-term hematopoietic reconstitution of hematopoietic stem cells²³⁹. Our results from mTOR family by western blot analysis indicated that mTOR (**Figure 4.10**) was statistically significant increased in adult group when compared to other groups studied. It could be due BM-MSCs from the adult group were more senescence than BM-MSCs from young group. We corroborated that date checking expression of Lamin A/C in all groups. We observed that adult group had the highest expression of Lamin A (**Figure 4.7A**) together with less dye accumulation of TMRM (**Figure 4.8C**).

We found correlation between inhibition of mTOR and decrease of CD117 and Ki67 which are proliferation markers in the literature^{240,241} and we wonder if this relationship between the mTOR pathway on proliferation was present when the proliferation markers were inhibited by specific reagents. IM decreases CD117 expression in gastrointestinal stromal tumors²⁴² and JK184, a compound designed to antagonize Hh signalling, reduces expression of CD31, Ki67 and VEGF in tumour tissues²⁴³, respectively (**Figure 4.11B**). We also found these drugs arrested cells in transition from G2 phase to M phase in the cell cycle (**Figure 4.11C**).

We modified mTOR pathway through modification of proliferation markers for first time. We used two inhibitors of proliferation IM or JK184 at two physiological doses which did not affect the cell viability (**Figure 4.11A**). The expression of mTORC1 complex was modified (**Figures 4.12, 4.13, 4.14 and 4.15**) with both treatments. mTORC1 complex has been linked with cell growth⁵⁰, proliferation²⁴⁴, survival²⁴⁵, protein translation²³³ and other cellular metabolic processes²⁴⁶. Additionally, we confirmed the relationship between mTORC1 and proliferation markers when BM-MSCs from adult group were treated with rapamycin, an inhibitor of the mTOR signalling pathway, with potent immunosuppressive properties^{247,248}. The adult group presented a decrease of proliferation markers expression by flow cytometry (**Figure 4.16**). Our results were coincident with Gu Z *et al.* who reported that rapamycin decelerated senescence of BM-

MSCs from systemic lupus erythematosus patients by inhibiting excessive cellular growth caused by the mTOR pathway⁷². This discovery helped to advance the knowledge of the mTOR pathway in aging used in pharmacological approaches to treat human pathologies linked to mTOR deregulation.

We decided to study in depth the influence of aging on mesenchymal stem cells and we carried out a transcriptome analysis using RNA-sequencing which is an adequate technique to study complex samples such as we have used in our study²⁴⁹. Our results by RNA-seq analysis allowed the identification of 9628 genes that were statistically significant modulated among groups (**Figure 4.17A**). This analysis represented a step further from a previous iTRAQ-based study²⁵⁰. We used the R/Bioconductor package RamiGO which is an R interface for AmiGO that enables visualization of Gene Ontology (GO) trees²¹¹. RamiGO provides easy customization of annotation, highlighting of specific GO terms, using of terms by *P*-value. We showed RamiGO functionalities in a genome-wide gene set analysis of genes differently expressed comparing BM-MSCs from six chronologically different groups (**Figure 4.17B**). But, we focused on genes involved into inflammation mediated by chemokine and cytokine signalling pathways (PO00031), which were modulated in infant, young and pubertal groups (**Figures 4.18 and 4.19**). Within this pathway until 250 markers of extracellular vesicles were found using bioinformatics platforms: Vesiclepedia (www.microvesicles.org/)¹⁰⁸, EVpedia (www.evpedia.info)¹⁰⁹ and ExoCarta (www.exocarta.org)¹¹⁰, which are relevant software resources to extracellular vesicles research, also based on our iTRAQ results (**Table 8.6**). Micro-RNAs involved into extracellular vesicles and their relationship with inflammation mediated by chemokine and cytokine signalling pathways were obtained by open-source software for target predictions miRanda and TargetScan which are available at <http://www.microrna.org>²¹² and <http://www.targetscan.org>²¹³ respectively. Thus, we studied the influence of aging on the profile of micro-RNAs pro-inflammatory containing in MSC-derived EVs to advance in comprehension of immunosuppressive capacity of MSCs to use as future safe therapeutic approaches.

MSC-derived EVs present advantages over cell-based therapy as it eliminates the safety concerns associated with injection of MSC in patients and particularly useful for enhancing recovery from various diseases like as graft-versus-host disease^{12,101}. Hence it is necessary to advance our knowledge on the chronological age of MSC-derived EVs to maximize clinical utility. Firstly, we isolated MSC-derived EVs using the protocol of ultracentrifugation by Del Fattore *et al.*²⁵¹. Then they were characterized by size by NTA, which calculates the size of the total concentration of the vesicles in solution²⁵². Also, we followed the technique used by Gercel-Taylor *et al.*²⁵³ who reported their optimized method to measure the size distribution of cell-derived vesicles comparable to other instrumentation analysis. Additionally, we found an increase in the production of MSC-derived EVs from adult group when compared to other groups (**Figure 4.22**). This could be explained by the deregulation in intracellular and extracellular calcium level. Calcium balance plays a role in plasma membrane fusion events by small GTPase Rab11 and the citron kinase¹⁹. We found statistically significant high levels of calcium/calmodulin-dependent protein kinase type II, caldesmon, calponin-1, calumenin and calreticulin in adult group with respect to the other ages in iTRAQ analysis (**Table 8.6**) will be

corroborating this hypothesis. Our EVs had a similar diameter size as reported by Vallabhaneni *et al.*²⁵⁴ (**Figure 4.21A**). We confirmed that at least 30% from EVs were exosomes because they were CD63 positive (**Figure 4.21C**) as indicated by the International Society for Extracellular Vesicles (ISEV)¹⁰⁵.

Age-related changes of immune system functions are complex phenomena incompletely understood. The acquired immune system shows a functional decline in ability to respond to new pathogens during aging, whereas serum levels of inflammatory cytokines are increased with age⁵¹. “Inflammaging” is a prominent aging-associated alteration in intercellular communication and one of the major driving diseases associated with age. We observed CD200 levels in our age groups because Pietila *et al.*²⁵⁵ proposed CD200 is a good immunosuppressive marker in hMSCs, it is involved in the capacity of MSCs mediated immune behaviour of THP-1 macrophage-like cells. We found a decrease of CD200 in the adult group (**Figure 4.20A**) with respect to other groups, which could be explained by the loss of immunosuppressive capacity similar to results obtained by Kilpinen L *et al.*²¹⁵. who have published that aging affects immunological functions due the altered membrane glycerophospholipid composition

We checked TLR4, a receptor recognizing “danger” signals and its activation leads to cellular and systemic responses that regulate innate and adaptive immune cells²⁵⁶, therefore it is associated in pro-inflammatory signature of MSCs²⁵⁷. We found high levels of TLR4 in the pre-pubertal group (**Figure 4.20B**).

DAMPs are involved in regulation of proliferation²⁵⁸, differentiation, apoptosis²⁵⁸, Ca²⁺ homeostasis, energy metabolism, inflammation and migration²⁵⁹, and HMBG1 protein described as a DNA-binding protein that stabilizes nucleosomes and facilitates transcription and enhanced expression of pro-inflammatory cytokines²⁶⁰ (**Figure 4.20B** and **Table 8.6**). Pre-pubertal group showed a decreased capacity of self-renewal besides an increased expression of DAMPs²⁶¹ at protein level such as S100 proteins (S100A4, S100A6) (**Table 8.6**). All of these could be explained due to the deregulated in gonadotropin realising hormone pathway and inflammation mediated by chemokine and cytokine signalling pathways obtained by transcriptome analysis (**Figures 4.18** and **4.19**). There is a controversy on the role of TLR4 in pro-inflammatory and differentiation capacities⁹ in MSCs and this study thereby provides helpful tools for regenerative medicine. We checked miRs associated with TLR4 contained in MSC-derived EVs. miR-146a, known as one of key TLR-induced miRNAs, inhibits the TLR-signalling pathway by targeting IRAK1 kinase and TRAF6 ligase. miR-132 which is a target of IL1R associated kinase IRAK 4, regulator of production inflammatory cytokines²³. miR-155 which is induced via TLR in macrophages and dendritic cells and exerts profound effect on the activity of immune cells²⁴⁻²⁶. Xu *et al.*²⁶² reported that miR-155 regulates the immunosuppressive capacity of MSCs by TAK1-binding protein 2 (TAB2). In our study we observed a decrease of these miRs contained in EVs with increasing age groups (**Figures 4.23A**, **4.23B** and **4.23C**) and it could be associated with the decrease of MSC-derived EVs immunologically activity and loss of capacity to activate the immune system through the induction of anti-inflammatory cytokines and T cells. Additionally, MSC-derived EVs from adult group contained the highest level of miR-335 (**Figure 4.23D**). It could be associated with cellular senescence and the loss of therapeutic capacity because

it was linked to reduced capacity to activate protein kinase D1 (PRKD1) which in turn reduces the activity of AP-1 transcription factor^{263,264} *in vitro* aging corresponding with chronological *in vivo* aging. miR-21-5p regulates negatively LPS-induced lipid accumulation and inflammatory response in macrophages by the TLR4-NF- κ B pathway²⁶⁵ which is involved in human mesenchymal stem cells during differentiation by regulating SPRY229. We found the highest level of miR-21-5p in MSC-derived EVs from pre-pubertal group and the lowest level in adult group (**Figure 4.23E**) hence it could be a target to understand role of TLR4 in differentiation of pro-inflammatory capacity aging-dependending. To understand in depth the role of aging on TLR4 we studied AKT/mTOR and non-canonical pathways on pre-pubertal group. TLR4 regulates proliferation and osteogenic differentiation through Wnt3a and Wnt5a signaling²⁶⁶ while its activation into MSCs from umbilical cord increased this differentiation to a certain extent²⁶⁷. Gharibi *et al.*²⁶⁸ published that the chemically inhibition of the Akt/mTOR pathway affected TLR4. Our results indicated that TLR4 trend to increase with age and the treatment with LPS did not affect (**Figure 4.20B**) their immunological response within 4 hours. So we focused on Wnt5a protein which, through TLR4, is induced by inflammatory mediators, like LPS, in several stem cells types and regulated by cytokine and chemokine production^{269,270}. The inhibition of miR-21-5p resulted in the overexpression of Wnt5a accompanied by a decrease of Lamin A/C, a senescence marker²³¹ (**Figure 4.25A**). It looks like a decrease of miR-21 increased the self-renewal and pluripotent capacities in the pre-pubertal group, as demonstrated by the high expression of Nanog (**Figure 4.24C**). The inhibition of miR-21-5p affected also Akt/mTOR pathway because mTOR and pAkt were downregulated (**Figures 4.25B** and **4.26**). The immunological response of pre-pubertal BM-MSCs group was not statistically significant modulated (**Figure 4.27**). These data might suggest that miR-21-5p could be a regulator of TLR4 signalling without affecting the immune response. All results provide an insight into mechanisms involved in BM-MSC aging and suggest possible interventions on micro-RNAs to maintain quiescence and function of MSCs and their derived extracellular vesicles a priori to *in vivo* transplantation or pharmacological agents in disease.

There are many studies about the mechanisms of EVs uptake in target cells such as clathrin-mediated endocytosis^{117,162,163}, caveolin-dependent endocytosis¹⁶⁵⁻¹⁶⁷, macropinocytosis^{100,271}, phagocytosis¹⁶⁰, involvement of lipid rafts^{174,272} and cell surface membrane fusion^{273,171}. Furthermore, we demonstrated the internalization of MSC-derived EVs, labelled with DiI, was independent of the individual's age by fluorescence microscopy (**Figure 4.28**). These results were similar to other studies using other cellular types such as dendritic cells²⁷⁴ melanoma cells¹⁷¹. Moreover, we studied the influence of aging through MSC-derived EVs in self-renewal capacity of BM-MSCs. Therefore, we performed genetic studies to evaluate the expressions of pluripotency markers such as Nanog and Oct4, which are important transcription factors to control expression of multiples genes associated with pluripotency pathways of MSCs. Their expression is reduced *in vitro* culture under normoxia²⁷⁵ as a result an inactivation of these genes which reduce proliferation and pluripotency capacities²⁷⁶.

It is known epigenetic mechanisms for placing global chromatin dynamics are central to tracking pluripotency and lineage progression of hESCs and the deacetylation histone is necessary to expression of Oct4 and Nanog in hESCs²⁷⁷. We observed in our model that expression of these pluripotency markers changed when we cultured cells at medium with MSC-derived EVs. Adult group increased expression of Nanog and Oct4 when they were cultured at medium with yEVs by contrast, young group co-cultured with aEVs decreased expression of these transcription factors (**Figures 4.29A** and **4.29B**). In this way, we confirmed that EVs influenced the self-renewal capacity of MSCs at genetic levels. Additionally, we studied vinculin expression (**Figure 4.29C**) which is involved in proliferation through contractility and cellular adhesion²⁷⁸ and Lamin A/C (**Figures 4.30** and **4.31**). Additionally, we observed the greatest effectivity of aEVs in comparison with yEVs because of the changes at proteomic and genetic levels observed as soon as 2 days (**Figures 4.29**, **4.30** and **4.31**). All these results suggest that aEVs could contained “age-promoting” factors term used by Randon *et al.*²⁷⁹, which may be responsible for the age-associated decline of stem cells functionality. All of this provides an important key to the understanding of the aging process and the development of EV-based therapies^{254,280}.

6. CONCLUSIONS

1. Aging was affecting on the proliferation profile of bone marrow mesenchymal stem cells. Bone marrow mesenchymal stem cells from young group (14 days) had the most proliferative capacity. Conversely, the pre-pubertal (35-38 days) group was the less proliferative. Besides, mTORC1 complex modulated proliferation markers (CD117 and Ki67) in bone marrow mesenchymal stem cells from the oldest group.
2. Aging was affecting on the pluripotent profile of bone marrow mesenchymal stem cells because they had different expression of pluripotency marker (Nanog). Bone marrow mesenchymal stem cells from young group (14 days) are the most pluripotent and the oldest group have less capacity.
3. Proteomic analysis revealed 201 statistically significant modulated proteins among groups. Functional clustering revealed alterations in pathways related to proliferation, pluripotency and energy metabolism. NGS study found out 9628 genes statistically modulated among age groups and they are involved with glycolysis, gonadotropin realising hormone pathway, integrin signalling pathway, PDGF pathway and inflammation mediated by chemokine and cytokine signalling.
4. Aging influences on the pro-inflammatory phenotype of bone marrow mesenchymal stem cells, through the expression of pro-inflammatory markers such as CD200 and TLR4.
5. Bone marrow mesenchymal stem cells produced extracellular vesicles with different content of miRs inside them and their production age-dependent.
6. The miRNAs contained in EVs change in an age-dependent manner and these changes influence and determinate the therapeutic potential of the EVs through modulation of the innate immune response.
7. miR-21-5p was a regulator on pro-inflammatory and pluripotent capacities from TL4 signalling pathway through pAkt/Akt in bone marrow mesenchymal stem cells from pre-pubertal group (35-38 days).
8. Bone marrow mesenchymal stem cell-derived extracellular vesicles and their self-renewal was influenced by age, as revealed by changes in the expression of self-renewal markers such as Nanog, Oct4, Vinculin and Lamin A/C.

7. REFERENCES

8. REFERENCES

1. Tawonsawatruk, T., Spadaccino, A., Murray, I. R., Peault, B. & Simpson, H. A. H. R. W. S. Growth kinetics of rat mesenchymal stem cells from 3 potential sources: bone marrow, periosteum and adipose tissue. *J. Med. Assoc. Thai.* **95 Suppl 1**, 189–197 (2012).
2. Yeh, H. Y. *et al.* Neocartilage formation from mesenchymal stem cells grown in type II collagen-hyaluronan composite scaffolds. *Differentiation* **86**, 171–183 (2013).
3. Park, S. *et al.* Myogenic differentiation potential of human tonsil-derived mesenchymal stem cells and their potential for use to promote skeletal muscle regeneration. *Int. J. Mol. Med.* **37**, 1209–1220 (2016).
4. Liang, M.-S., Koobatian, M., Lei, P., Swartz, D. D. & Andreadis, S. T. Differential and synergistic effects of mechanical stimulation and growth factor presentation on vascular wall function. *Biomaterials* **34**, 7281–91 (2013).
5. Contador, D. *et al.* Dexamethasone and rosiglitazone are sufficient and necessary for producing functional adipocytes from mesenchymal stem cells. *Exp. Biol. Med. (Maywood)*. **240**, 1235–46 (2015).
6. Ullah, I. *et al.* In vitro comparative analysis of human dental stem cells from a single donor and its neuronal differentiation potential evaluated by electrophysiology. *Life Sci.* **154**, 39–51 (2016).
7. Kil, K., Choi, M. Y. & Ho Park, K. In Vitro Differentiation of Human Wharton's Jelly-Derived Mesenchymal Stem Cells into Auditory Hair Cells and Neurons. *J. Int. Adv. Otol.* **12**, 37–42 (2016).
8. Stromal cells responsible for transferring the microenvironment of the hemopoietic tissues. *Transplantation* **17**, 331–340 (1974).
9. Wang, K. *et al.* Redox homeostasis: the linchpin in stem cell self-renewal and differentiation. *Cell Death Dis.* **4**, e537 (2013).
10. Jiang, Y. *et al.* Pluripotency of mesenchymal stem cells derived from adult marrow. *Nature* **418**, 41–49 (2002).
11. Dominici, M. *et al.* Minimal criteria for defining multipotent mesenchymal stromal cells. The International Society for Cellular Therapy position statement. *Cytotherapy* **8**, 315–7 (2006).
12. Karaoz, E. *et al.* Characterization of mesenchymal stem cells from rat bone marrow: Ultrastructural properties, differentiation potential and immunophenotypic markers. *Histochem. Cell Biol.* **132**, 533–546 (2009).
13. Blazquez-Martinez, A. *et al.* C-Kit identifies a subpopulation of mesenchymal stem cells in adipose tissue with higher telomerase expression and differentiation potential. *Differentiation* **87**, 147–160 (2014).
14. Bari, C. De, Dell'Accio, F., Tylzanowski, P. & Luyten, F. P. Multipotent mesenchymal stem cells from adult human synovial membrane. *Arthritis Rheum.* **44**, 1928–1942 (2001).
15. Manini, I. *et al.* Multi-potent progenitors in freshly isolated and cultured human mesenchymal stem cells: A comparison between adipose and dermal tissue. *Cell Tissue Res.* **344**, 85–95 (2011).
16. Almeida, M. & O'Brien, C. A. Basic Biology of Skeletal Aging: Role of Stress Response Pathways. *Journals Gerontol. Ser. A Biol. Sci. Med. Sci.* **68**, 1197–1208 (2013).
17. Trivanović, D. *et al.* Mesenchymal stem cells isolated from peripheral blood and umbilical cord Wharton's jelly. *Srp. Arh. Celok. Lek.* **141**, 178–186 (2013).
18. D'souza, N. *et al.* Mesenchymal stem/stromal cells as a delivery platform in cell and gene therapies. *BMC Med.* **13**, 186 (2015).
19. Gong, X. *et al.* Isolation and characterization of lung resident mesenchymal stem cells capable of differentiating into alveolar epithelial type II cells. *Cell Biol. Int.* **38**, 405–411 (2014).
20. Pacini, S. & Petrini, I. Are MSCs angiogenic cells? New insights on human nestin-positive bone marrow-derived multipotent cells. *Cell Dev. Biol.* **2**, 1–11 (2014).
21. Pappa, K. I. & Anagnou, N. P. Novel sources of fetal stem cells: where do they

- fit on the developmental continuum? *Regen. Med.* **4**, 423–433 (2009).
22. Díaz-Prado, S. *et al.* Human amniotic membrane as an alternative source of stem cells for regenerative medicine. *Differentiation* **81**, 162–171 (2011).
 23. Secco, M. *et al.* Multipotent stem cells from umbilical cord: cord is richer than blood! *Stem Cells* **26**, 146–150 (2008).
 24. Fernández-Pernas, P. *et al.* 3, 3',5-Triiodo-L-Thyronine Increases In Vitro Chondrogenesis of Mesenchymal Stem Cells from Human Umbilical Cord Stroma Through SRC2. *J. Cell. Biochem.* (2016). doi:10.1002/jcb.25515
 25. Pelekanos, R. A. *et al.* Isolation and Expansion of Mesenchymal Stem/Stromal Cells Derived from Human Placenta Tissue. *J. Vis. Exp.* 1–13 (2016). doi:10.3791/54204
 26. Rossignoli, F. *et al.* Isolation, Characterization, and Transduction of Endometrial Decidual Tissue Multipotent Mesenchymal Stromal / Stem Cells from Menstrual Blood. **2013**, (2013).
 27. Jin, H. *et al.* Comparative Analysis of Human Mesenchymal Stem Cells from Bone Marrow, Adipose Tissue, and Umbilical Cord Blood as Sources of Cell Therapy. *Int. J. Mol. Sci.* **14**, 17986–18001 (2013).
 28. Jeon, Y.-J., Kim, J., Cho, J. H., Chung, H.-M. & Chae, J.-I. Comparative Analysis of Human Mesenchymal Stem Cells Derived from Bone Marrow, Placenta and Adipose Tissue as Sources of Cell Therapy. *J. Cell. Biochem.* n/a--n/a (2015). doi:10.1002/jcb.25395
 29. Elahi, K. C. *et al.* Human mesenchymal stromal cells from different sources diverge in their expression of cell surface proteins and display distinct differentiation patterns. *Stem Cells Int.* **2016**, (2016).
 30. Li, G. *et al.* Comparative proteomic analysis of mesenchymal stem cells derived from human bone marrow, umbilical cord, and placenta: implication in the migration. *Proteomics* **9**, 20–30 (2009).
 31. de Miguel-Beriain, I. The ethics of stem cells revisited. *Adv. Drug Deliv. Rev.* **82**, 176–180 (2015).
 32. Jung, Y., Bauer, G. & Nolte, J. A. Concise review: Induced pluripotent stem cell-derived mesenchymal stem cells: Progress toward safe clinical products. *Stem Cells* **30**, 42–47 (2012).
 33. Chao, K. C., Chao, K. F., Fu, Y. S. & Liu, S. H. Islet-like clusters derived from mesenchymal stem cells in Wharton's jelly of the human umbilical cord for transplantation to control type 1 diabetes. *PLoS One* **3**, (2008).
 34. Chen, L.-B., Jiang, X.-B. & Yang, L. Differentiation of rat marrow mesenchymal stem cells into pancreatic islet beta-cells. *World J. Gastroenterol.* **10**, 3016–3020 (2004).
 35. Xin, H. *et al.* Exosome-mediated transfer of miR-133b from multipotent mesenchymal stromal cells to neural cells contributes to neurite outgrowth. *Stem Cells* **30**, 1556–1564 (2012).
 36. Tanaka, Y. Human mesenchymal stem cells as a tool for joint repair in rheumatoid arthritis. *Clin. Exp. Rheumatol.* **33**, 58–62 (2015).
 37. Chen, F. H. & Tuan, R. S. Mesenchymal stem cells in arthritic diseases. *Arthritis Res. Ther.* **10**, 223 (2008).
 38. Gonzalez, M. A., Gonzalez-Rey, E., Rico, L., Buscher, D. & Delgado, M. Treatment of experimental arthritis by inducing immune tolerance with human adipose-derived mesenchymal stem cells. *Arthritis Rheum.* **60**, 1006–1019 (2009).
 39. Ghannam, S., Pène, J., Torcy-Moquet, G., Jorgensen, C. & Yssel, H. Mesenchymal stem cells inhibit human Th17 cell differentiation and function and induce a T regulatory cell phenotype. *J. Immunol.* **185**, 302–312 (2010).
 40. Tasso, R. *et al.* Mesenchymal stem cells induce functionally active T-regulatory lymphocytes in a paracrine fashion and ameliorate experimental autoimmune uveitis. *Investig. Ophthalmol. Vis. Sci.* **53**, 786–793 (2012).
 41. Ren, J. *et al.* Global transcriptome analysis of human bone marrow stromal cells (BMSC) reveals proliferative, mobile and interactive cells that produce abundant extracellular matrix proteins,

- some of which may affect BMSC potency. *Cytotherapy* **13**, 661–674 (2011).
42. Naaldijk, Y. *et al.* Migrational changes of mesenchymal stem cells in response to cytokines, growth factors, hypoxia, and aging. *Exp. Cell Res.* **338**, 97–104 (2015).
 43. Sohni, A. & Verfaillie, C. M. Mesenchymal stem cells migration homing and tracking. *Stem Cells Int.* **2013**, 14–16 (2013).
 44. Chou, H.-C., Li, Y.-T. & Chen, C.-M. Human mesenchymal stem cells attenuate experimental bronchopulmonary dysplasia induced by perinatal inflammation and hyperoxia. *Am. J. Transl. Res.* **8**, 342–53 (2016).
 45. Nations, U. *World Population Ageing 2013. World Population Aging* (2013). at <<http://www.un.org/en/development/desa/population/publications/pdf/ageing/WorldPopulationAgeing2013.pdf>>
 46. Kenyon, C. J. The genetics of ageing. *Nature* **464**, 504–512 (2010).
 47. Kennedy, B. K. The genetics of ageing: Insight from genome-wide approaches in invertebrate model organisms. *J. Intern. Med.* **263**, 142–152 (2008).
 48. Boulias, K. & Horvitz, H. R. The *C. elegans* MicroRNA mir-71 acts in neurons to promote germline-mediated longevity through regulation of DAF-16/FOXO. *Cell Metab.* **15**, 439–450 (2012).
 49. Kapahi, P. *et al.* With TOR less is more: a key role for the conserved nutrient sensing TOR pathway in aging. *Cell Metab.* **11**, 453–465 (2011).
 50. Laplante, M. & Sabatini, D. M. MTOR signaling in growth control and disease. *Cell* **149**, 274–293 (2012).
 51. López-otín, C., Blasco, M. a, Partridge, L. & Serrano, M. Europe PMC Funders Group The Hallmarks of Aging. **153**, 1194–1217 (2013).
 52. Moskalev, A. A. *et al.* The role of DNA damage and repair in aging through the prism of Koch-like criteria. *Ageing Res. Rev.* **12**, 661–684 (2013).
 53. Sethe, S., Scutt, A. & Stolzing, A. Aging of mesenchymal stem cells. *Ageing Res. Rev.* **5**, 91–116 (2006).
 54. Blackburn, E. H., Greider, C. W. & Szostak, J. W. Telomeres and telomerase: the path from maize, Tetrahymena and yeast to human cancer and aging. *Nat. Med.* **12**, 1133–1138 (2006).
 55. Kazak, L., Reyes, A. & Holt, I. J. Minimizing the damage: repair pathways keep mitochondrial DNA intact. *Nat. Rev. Mol. Cell Biol.* **13**, 726–726 (2012).
 56. Worman, H. J. Nuclear lamins and laminopathies. *J. Pathol.* **226**, 316–325 (2012).
 57. Martinez, P. & Blasco, M. A. Role of shelterin in cancer and aging. *Ageing Cell* **9**, 653–666 (2010).
 58. Jaskelioff, M. *et al.* Telomerase reactivation reverses tissue degeneration in aged telomerase deficient mice. *Nature* **469**, 102–106 (2011).
 59. Maegawa, S. *et al.* Widespread and tissue specific age-related DNA methylation changes in mice. 332–340 (2010). doi:10.1101/gr.096826.109.332
 60. Han, S. & Brunet, A. Histone methylation makes its mark on longevity. *Trends Cell Biol.* **22**, 42–49 (2012).
 61. Fraga, M. F. & Esteller, M. Epigenetics and aging: the targets and the marks. *Trends Genet.* **23**, 413–418 (2007).
 62. Pegoraro, G. *et al.* Aging-related chromatin defects via loss of the NURD complex. *Cell* **11**, 1261–1267 (2010).
 63. Pollina, E. a & Brunet, a. Epigenetic regulation of aging stem cells. *Oncogene* **30**, 3105–3126 (2011).
 64. Toledano, H. *et al.* The let-7–Imp axis regulates ageing of the *Drosophila* testis stem-cell niche. **485**, 605–610 (2016).
 65. Ugalde, A. P., Español, Y. & López-Otín, C. Micromanaging aging with miRNAs: New messages from the nuclear envelope. *Nucleus* **2**, 549–555 (2011).
 66. Koga, H., Kaushik, S. & Cuervo, a M. Protein Homeostasis and Aging: the importance of exquisite quality control. *Ageing Res. Rev.* **10**, 205–215 (2012).
 67. Mizushima, N., Levine, B., Cuervo, A.

- M. & Klionsky, D. J. Autophagy fights disease through cellular self-digestion. *Nature* **451**, 1069–1075 (2008).
68. Powers, E. T., Morimoto, R. I., Dillin, A., Kelly, J. W. & Balch, W. E. Biological and chemical approaches to diseases of proteostasis deficiency. *Annu. Rev. Biochem.* **78**, 959–991 (2009).
69. Barzilai, N., Huffman, D. M., Muzumdar, R. H. & Bartke, A. The critical role of metabolic pathways in aging. *Diabetes* **61**, 1315–1322 (2012).
70. Blagosklonny, M. V. Answering the ultimate question ‘What is the proximal cause of aging?’ *Aging (Albany. NY)*. **4**, 861–877 (2012).
71. Houtkooper, R. H., Williams, R. W. & Auwerx, J. Metabolic Networks of Longevity. *Cell* **142**, 9–14 (2010).
72. Gu, Z. *et al.* Rapamycin reverses the senescent phenotype and improves immunoregulation of mesenchymal stem cells from MRL/lpr mice and systemic lupus erythematosus patients through inhibition of the mTOR signaling pathway. *Aging (Albany. NY)*. **8**, 1–13 (2016).
73. Osorio, F. G. *et al.* Loss of the proteostasis factor AIRAPL causes myeloid transformation by deregulating IGF-1 signaling. *Nat. Med.* (2015). doi:10.1038/nm.4013
74. Martins, I., Galluzzi, L. & Kroemer, G. Hormesis, cell death and aging. *Aging (Albany. NY)*. **3**, 821–828 (2011).
75. Collado, M., Blasco, M. A. & Serrano, M. Cellular Senescence in Cancer and Aging. *Cell* **130**, 223–233 (2007).
76. Hayflick, L. & Moorhead, P. S. the Serial Cultivation of Human Diploid Cell Strains. *Exp. Cell Res.* **1**, 585–621 (1961).
77. Shin, D. M., Kucia, M. & Ratajczak, M. Z. Nuclear and chromatin reorganization during cell senescence and aging - A mini-review. *Gerontology* **57**, 76–84 (2010).
78. Raz, V. *et al.* The nuclear lamina promotes telomere aggregation and centromere peripheral localization during senescence of human mesenchymal stem cells. *J. Cell Sci.* **121**, 4018–4028 (2008).
79. Shaw, A. C., Goldstein, D. R. & Montgomery, R. R. Age-dependent dysregulation of innate immunity. *Nat. Rev. Immunol.* **13**, 875–87 (2013).
80. Xu, M. *et al.* JAK inhibition alleviates the cellular senescence-associated secretory phenotype and frailty in old age. *Proc. Natl. Acad. Sci. U. S. A.* **112**, E6301–E6310 (2015).
81. Olivieri, F. *et al.* DNA damage response (DDR) and senescence: shuttled inflamma-miRNAs on the stage of inflamm-aging. *Oncotarget* **6**, 35509–35521 (2015).
82. Nelson, G. *et al.* A senescent cell bystander effect: Senescence-induced senescence. *Aging Cell* **11**, 345–349 (2012).
83. Kirkwood, T. B. L. Understanding the odd science of aging. *Cell* **120**, 437–447 (2005).
84. Harbo, M., Koelvræ, S., Serakinci, N. & Bendix, L. Telomere dynamics in human mesenchymal stem cells after exposure to acute oxidative stress. *DNA Repair (Amst)*. **11**, 774–779 (2012).
85. Goldberg, A. D., Allis, C. D. & Bernstein, E. Epigenetics: A Landscape Takes Shape. *Cell* **128**, 635–638 (2007).
86. Chambers, S. M. *et al.* Aging hematopoietic stem cells decline in function and exhibit epigenetic dysregulation. *PLoS Biol.* **5**, 1750–1762 (2007).
87. Gopinath, S. D. & Rando, T. A. Stem Cell Review Series: Aging of the skeletal muscle stem cell niche. *Aging Cell* **7**, 590–598 (2008).
88. Liu, L. & Rando, T. A. Manifestations and mechanisms of stem cell aging. *J. Cell Biol.* **193**, 257–266 (2011).
89. Alekseenko, L. L. *et al.* Sublethal heat shock induces premature senescence rather than apoptosis in human mesenchymal stem cells. *Cell Stress Chaperones* 355–366 (2013). doi:10.1007/s12192-013-0463-6
90. Seifrtova, M. *et al.* Mitoxantrone Ability To Induce Premature Senescence. 255–265 (2013).

91. Minieri, V. *et al.* Persistent DNA damage-induced premature senescence alters the functional features of human bone marrow mesenchymal stem cells. *J. Cell. Mol. Med.* **19**, 734–743 (2015).
92. Skolekova, S. *et al.* Cisplatin-induced mesenchymal stromal cells-mediated mechanism contributing to decreased antitumor effect in breast cancer cells. *Cell Commun. Signal.* **14**, 4 (2016).
93. Prendergast, Á. M., Cruet-Hennequart, S., Shaw, G., Barry, F. P. & Carty, M. P. Activation of DNA damage response pathways in human mesenchymal stem cells exposed to cisplatin or γ -irradiation. *Cell Cycle* **10**, 3768–3777 (2011).
94. Rodier, F. *et al.* DNA-SCARS: distinct nuclear structures that sustain damage-induced senescence growth arrest and inflammatory cytokine secretion. *J. Cell Sci.* **124**, 68–81 (2011).
95. Turinetto, V., Vitale, E. & Giachino, C. Senescence in Human Mesenchymal Stem Cells: Functional Changes and Implications in Stem Cell-Based Therapy. *Int. J. Mol. Sci.* **17**, 1164 (2016).
96. Liang, X., Ding, Y., Zhang, Y., Tse, H. F. & Lian, Q. Paracrine mechanisms of Mesenchymal Stem cell-based therapy: Current status and perspectives. *Cell Transplant.* **23**, 1–32 (2013).
97. Sepúlveda, J. C. *et al.* Cell senescence abrogates the therapeutic potential of human mesenchymal stem cells in the lethal endotoxemia model. *Stem Cells* **32**, 1865–77 (2014).
98. Kuang, W. *et al.* Functional and Molecular Changes of MSCs in Aging. *Curr. Stem Cell Res. Ther.* (2015). doi:10.2174/1574888X10666150211162933
99. Keller, S., Sanderson, M. P., Stoeck, A. & Altevogt, P. Exosomes: From biogenesis and secretion to biological function. *Immunol. Lett.* **107**, 102–108 (2006).
100. Christianson, H. C., Svensson, K. J., van Kuppevelt, T. H., Li, J.-P. & Belting, M. Cancer cell exosomes depend on cell-surface heparan sulfate proteoglycans for their internalization and functional activity. *Proc. Natl. Acad. Sci. U. S. A.* **110**, 17380–5 (2013).
101. Baglio, S. R. *et al.* Human bone marrow and adipose-mesenchymal stem cells secrete exosomes enriched in distinctive miRNA and tRNA species. *Stem Cell Res. Ther.* **6**, 127 (2015).
102. Xiao, H. *et al.* Mast cell exosomes promote lung adenocarcinoma cell proliferation – role of KIT-stem cell factor signaling. *Cell Commun. Signal.* **12**, 64 (2014).
103. Kang, D., Oh, S., Ahn, S.-M., Lee, B.-H. & Moon, M. H. Proteomic analysis of exosomes from human neural stem cells by flow field-flow fractionation and nanoflow liquid chromatography-tandem mass spectrometry. *J. Proteome Res.* **7**, 3475–3480 (2008).
104. Fader, C. M. & Colombo, M. I. Multivesicular bodies and autophagy in erythrocyte maturation. *Autophagy* **2**, 122–125 (2006).
105. Gould, S. J. & Raposo, G. As we wait: coping with an imperfect nomenclature for extracellular vesicles. *J. Extracell. vesicles* **2**, 3–5 (2013).
106. Rani, S., Ryan, A. E., Griffin, M. D. & Ritter, T. Mesenchymal Stem Cell-derived Extracellular Vesicles: Toward Cell-free Therapeutic Applications. *Mol. Ther.* **23**, 812–823 (2015).
107. Cocucci, E. & Meldolesi, J. Ectosomes and exosomes: Shedding the confusion between extracellular vesicles. *Trends Cell Biol.* **25**, 364–372 (2015).
108. Kalra, H. *et al.* Vesiclepedia: A Compendium for Extracellular Vesicles with Continuous Community Annotation. *PLoS Biol.* **10**, 8–12 (2012).
109. Kim, D. K. *et al.* EVpedia: A community web portal for extracellular vesicles research. *Bioinformatics* **31**, 933–939 (2015).
110. Simpson, R. J., Kalra, H. & Mathivanan, S. ExoCarta as a resource for exosomal research. *J. Extracell. Vesicles* **1**, 1–6 (2012).
111. Jørgensen, M. *et al.* Extracellular Vesicle (EV) Array: microarray capturing of exosomes and other extracellular vesicles for multiplexed phenotyping. *J. Extracell. vesicles* **2**, 1–9 (2013).
112. Pols, M. S. & Klumperman, J. Trafficking and function of the

- tetraspanin CD63. *Exp. Cell Res.* **315**, 1584–1592 (2009).
113. Haqqani, A. S. *et al.* Method for isolation and molecular characterization of extracellular microvesicles released from brain endothelial cells. *Fluids Barriers CNS* **10**, 4 (2013).
 114. Mathivanan, S., Ji, H. & Simpson, R. J. Exosomes: Extracellular organelles important in intercellular communication. *J. Proteomics* **73**, 1907–1920 (2010).
 115. Liang, Y. *et al.* Complex N-linked glycans serve as a determinant for exosome/microvesicle cargo recruitment. *J. Biol. Chem.* **289**, 32526–32537 (2014).
 116. Menck, K. *et al.* Tumor-derived microvesicles mediate human breast cancer invasion through differentially glycosylated EMMPRIN. *J. Mol. Cell Biol.* **7**, 143–153 (2015).
 117. Escrivente, C., Keller, S., Altevogt, P. & Costa, J. Interaction and uptake of exosomes by ovarian cancer cells. *BMC Cancer* **11**, 108 (2011).
 118. Batista, B. S., Eng, W. S., Pilobello, K. T., Hendricks-Muñoz, K. D. & Mahal, L. K. Identification of a conserved glycan signature for microvesicles. *J. Proteome Res.* **10**, 4624–4633 (2011).
 119. Manuscript, A. & Syndromes, G. P. NIH Public Access. **48**, 1–6 (2010).
 120. Kralj-Iglič, V. & Veranič, P. Chapter 5 Curvature-Induced Sorting of Bilayer Membrane Constituents and Formation of Membrane Rafts. *Advances in Planar Lipid Bilayers and Liposomes* **5**, 129–149 (2006).
 121. Kandere-Grzybowska, K. *et al.* IL-1 induces vesicular secretion of IL-6 without degranulation from human mast cells. *J. Immunol.* **171**, 4830–4836 (2003).
 122. Chen, T., Guo, J., Yang, M., Zhu, X. & Cao, X. Chemokine-Containing Exosomes Are Released from Heat-Stressed Tumor Cells via Lipid Raft-Dependent Pathway and Act as Efficient Tumor Vaccine. *J. Immunol.* **186**, 2219–2228 (2011).
 123. Baj-Krzyworzeka, M. *et al.* Tumour-derived microvesicles carry several surface determinants and mRNA of tumour cells and transfer some of these determinants to monocytes. *Cancer Immunol. Immunother.* **55**, 808–818 (2006).
 124. Batagov, A. O. & Kurochkin, I. V. Exosomes secreted by human cells transport largely mRNA fragments that are enriched in the 3'-untranslated regions. *Biol. Direct* **8**, 12 (2013).
 125. Huang, X. *et al.* Characterization of human plasma-derived exosomal RNAs by deep sequencing. *BMC Genomics* **14**, 319 (2013).
 126. Kogure, T., Yan, I. K., Lin, W.-L. & Patel, T. Extracellular Vesicle-Mediated Transfer of a Novel Long Noncoding RNA TUC339: A Mechanism of Intercellular Signaling in Human Hepatocellular Cancer. *Genes Cancer* **4**, 261–72 (2013).
 127. Pigati, L. *et al.* Selective release of MicroRNA species from normal and malignant mammary epithelial cells. *PLoS One* **5**, (2010).
 128. Mittelbrunn, M. *et al.* Unidirectional transfer of microRNA-loaded exosomes from T cells to antigen-presenting cells. *Nat. Commun.* **2**, 282 (2011).
 129. Bellingham, S. A., Coleman, B. M. & Hill, A. F. Small RNA deep sequencing reveals a distinct miRNA signature released in exosomes from prion-infected neuronal cells. *Nucleic Acids Res.* **40**, 10937–10949 (2012).
 130. Nolte'T Hoen, E. N. M. *et al.* Deep sequencing of RNA from immune cell-derived vesicles uncovers the selective incorporation of small non-coding RNA biotypes with potential regulatory functions. *Nucleic Acids Res.* **40**, 9272–9285 (2012).
 131. Deregibus, M. C. *et al.* angiogenic program in endothelial cells by a horizontal transfer of mRNA Endothelial progenitor cell – derived microvesicles activate an angiogenic program in endothelial cells by a horizontal transfer of mRNA. **110**, 2440–2448 (2012).
 132. Aswad, H., Jalabert, A. & Rome, S. Depleting extracellular vesicles from fetal bovine serum alters proliferation and differentiation of skeletal muscle cells in vitro. *BMC Biotechnol.* **16**, 32

- (2016).
133. Oliveira, M. C. *et al.* Milk extracellular vesicles accelerate osteoblastogenesis but impair bone matrix formation. *J. Nutr. Biochem.* **30**, 74–84 (2016).
 134. Eldh, M. *et al.* Exosomes Communicate Protective Messages during Oxidative Stress; Possible Role of Exosomal Shuttle RNA. *PLoS One* **5**, 1–8 (2010).
 135. Bruno, S. *et al.* Mesenchymal Stem Cell-Derived Microvesicles Protect Against Acute Tubular Injury. *J Am Soc Nephrol* **20**, 1053–1067 (2009).
 136. Arntz, O. J. *et al.* Oral administration of bovine milk derived extracellular vesicles attenuates arthritis in two mouse models. *Mol. Nutr. Food Res.* **59**, 1701–1712 (2015).
 137. Pieters, B. C. H. *et al.* Commercial cow milk contains physically stable extracellular vesicles expressing immunoregulatory TGF- β 1. *PLoS One* **10**, 1–14 (2015).
 138. Ekström, K. *et al.* Characterization of mRNA and microRNA in human mast cell-derived exosomes and their transfer to other mast cells and blood CD34 progenitor cells. *J. Extracell. Vesicles* **1**, 1–12 (2012).
 139. Holmgren, L. *et al.* Horizontal transfer of DNA by the uptake of apoptotic bodies. *Blood* **93**, 3956–3963 (1999).
 140. Balaj, L. *et al.* Tumour microvesicles contain retrotransposon elements and amplified oncogene sequences. *Nat Commun* **1**, 180 (2011).
 141. Lee, T. H. *et al.* Oncogenic ras-driven cancer cell vesiculation leads to emission of double-stranded DNA capable of interacting with target cells. *Biochem. Biophys. Res. Commun.* **451**, 295–301 (2014).
 142. Record, M., Carayon, K., Poirot, M. & Silvente-Poirot, S. Exosomes as new vesicular lipid transporters involved in cell-cell communication and various pathophysiological processes. *Biochim. Biophys. Acta - Mol. Cell Biol. Lipids* **1841**, 108–120 (2014).
 143. Kooijmans, S. A. A., Vader, P., van Dommelen, S. M., van Solinge, W. W. & Schiffelers, R. M. Exosome mimetics: A novel class of drug delivery systems. *Int. J. Nanomedicine* **7**, 1525–1541 (2012).
 144. Smyth, T. J., Redzic, J. S., Graner, M. W. & Anchordoquy, T. J. Examination of the specificity of tumor cell derived exosomes with tumor cells in vitro. *Biochim. Biophys. Acta* **1838**, 2954–2965 (2014).
 145. Matsuo, H. Role of LBPA and Alix in Multivesicular Liposome Formation and Endosome Organization. *Science (80-.)*. **303**, 531–534 (2004).
 146. Trajkovic, K. *et al.* Ceramide triggers budding of exosome vesicles into multivesicular endosomes. *Science* **319**, 1244–1247 (2008).
 147. Babst, M. MVB Vesicle Formation: ESCRT-dependent, ESCRT-Independent and everything in between. *Cell* **127**, 452–457 (2011).
 148. Vanlandingham, P. A. & Ceresa, B. P. Rab7 regulates late endocytic trafficking downstream of multivesicular body biogenesis and cargo sequestration. *J. Biol. Chem.* **284**, 12110–12124 (2009).
 149. Zerial, M. & McBride, H. Rab Proteins As Membrane Organizers. *Nat. Rev. Mol. Cell Biol.* **2**, 107–117 (2001).
 150. Savina, A., Fader, C. M., Damiani, M. T. & Colombo, M. I. Rab11 promotes docking and fusion of multivesicular bodies in a calcium-dependent manner. *Traffic* **6**, 131–143 (2005).
 151. Simons, M. & Raposo, G. Exosomes--vesicular carriers for intercellular communication. *Curr. Opin. Cell Biol.* **21**, 575–581 (2009).
 152. Lee, S. C., Jeong, H. J., Lee, S. K. & Kim, S.-J. Lipopolysaccharide preconditioning of adipose-derived stem cells improves liver-regenerating activity of the secretome. *Stem Cell Res. Ther.* **6**, 75 (2015).
 153. Lespagnol, A. *et al.* Exosome secretion, including the DNA damage-induced p53-dependent secretory pathway, is severely compromised in TSAP6/Steap3-null mice. *Cell Death Differ* **15**, 1723–1733 (2008).
 154. Feng, Z. p53 Regulation of the IGF-1 / AKT / mTOR Pathways and the Endosomal Compartment p53 Regulation of the IGF-1 / AKT / mTOR Pathways and the Endosomal

- Compartment. *Cold Spring Harb. Perspect. Biol.* 1–10 (2010). doi:10.1101/cshperspect.a001057
155. Yu, X., Harris, S. L. & Levine, A. J. The regulation of exosome secretion: A novel function of the p53 protein. *Cancer Res.* **66**, 4795–4801 (2006).
 156. D'Souza-Schorey, C. & Chavrier, P. ARF proteins: roles in membrane traffic and beyond. *Nat. Rev. Mol. Cell Biol.* **7**, 347–358 (2006).
 157. Muralidharan-Chari, Vandhana; Clancy, James; Plou, Carolyn; Romao, Maryse; Chavrier, Philippe; Raposo, Graca; D'Souza-Schorey, C. ARF6-regulated shedding of tumor-cell derived plasma membrane microvesicles. *Curr Biol.* **19**, 1875–1885 (2009).
 158. Nguyen, D. H. D. *et al.* Myosin light chain kinase functions downstream of Ras/ERK to promote migration of urokinase-type plasminogen activator-stimulated cells in an integrin-selective manner. *J. Cell Biol.* **146**, 149–164 (1999).
 159. Muralidharan-Chari, V., Clancy, J. W., Sedgwick, A. & D'Souza-Schorey, C. Microvesicles: mediators of extracellular communication during cancer progression. *J. Cell Sci.* **123**, 1603–1611 (2010).
 160. Feng, D. *et al.* Cellular internalization of exosomes occurs through phagocytosis. *Traffic* **11**, 675–687 (2010).
 161. Fabbri, M. *et al.* MicroRNAs bind to Toll-like receptors to induce prometastatic inflammatory response. *Pnas* **109**, (2012).
 162. Ehrlich, M. *et al.* Endocytosis by random initiation and stabilization of clathrin-coated pits. *Cell* **118**, 591–605 (2004).
 163. Taylor, M. J., Lampe, M. & Merrifield, C. J. A feedback loop between dynamin and actin recruitment during clathrin-mediated endocytosis. *PLoS Biol.* **10**, (2012).
 164. Kirchhausen, T. Clathrin. *Blood* 699–727 (2000).
 165. Nanbo, A., Kawanishi, E., Yoshida, R. & Yoshiyama, H. Exosomes derived from Epstein-Barr virus-infected cells are internalized via caveola-dependent endocytosis and promote phenotypic modulation in target cells. *J. Virol.* **87**, 10334–47 (2013).
 166. Barrès, C. *et al.* Galectin-5 is bound onto the surface of rat reticulocyte exosomes and modulates vesicle uptake by macrophages. *Blood* **115**, 696–705 (2010).
 167. Menck, K. *et al.* Induction and transport of Wnt 5a during macrophage-induced malignant invasion is mediated by two types of extracellular vesicles. *Oncotarget* **4**, 2057–66 (2013).
 168. Doherty, G. J. & McMahon, H. T. Mechanisms of endocytosis. *Annu. Rev. Biochem.* **78**, 857–902 (2009).
 169. Swanson, J. A. Shaping cups into phagosomes and macropinosomes. *Mol. Cell* **9**, (2010).
 170. Nabi, I. R. & Le, P. U. Caveolae/raft-dependent endocytosis. *J. Cell Biol.* **161**, 673–677 (2003).
 171. Parolini, I. *et al.* Microenvironmental pH is a key factor for exosome traffic in tumor cells. *J. Biol. Chem.* **284**, 34211–34222 (2009).
 172. Lotvall, J. & Valadi, H. Cell to cell signalling via exosomes through esRNA. *Cell Adh. Migr.* **1**, 156–158 (2007).
 173. Jahn, R. & Südhof, T. C. Membrane Fusion and Exocytosis. *Annu. Rev. Biochem.* **68**, 863–911 (1999).
 174. Svensson, K. J. *et al.* Exosome uptake depends on ERK1/2-heat shock protein 27 signaling and lipid raft-mediated endocytosis negatively regulated by caveolin-1. *J. Biol. Chem.* **288**, 17713–17724 (2013).
 175. Zech, D., Rana, S., Büchler, M. W. & Zöller, M. Tumor-exosomes and leukocyte activation: an ambivalent crosstalk. *Cell Commun. Signal.* **10**, 37 (2012).
 176. Kalimuthu, S., Gangadaran, P., Li, X. J., Oh, J. M. & Lee, H. W. In Vivo therapeutic potential of mesenchymal stem cell-derived extracellular vesicles with optical imaging reporter in tumor mice model. *Nat. Publ. Gr.* 1–11 (2016). doi:10.1038/srep30418
 177. Kharmate, G., Hosseini-Beheshti, E., Caradec, J., Chin, M. Y. & Tomlinson Guns, E. S. Epidermal Growth Factor

- Receptor in Prostate Cancer Derived Exosomes. *PLoS One* **11**, e0154967 (2016).
178. Taverna, S. *et al.* Exosomes isolation and characterization in serum is feasible in non-small cell lung cancer patients: critical analysis of evidence and potential role in clinical practice. *Oncotarget Advance Pu*, 1–13 (2016).
179. Lai, R. C. *et al.* Exosome secreted by MSC reduces myocardial ischemia/reperfusion injury. *Stem Cell Res.* **4**, 214–222 (2010).
180. Kanazawa, H. *et al.* Bone marrow-derived mesenchymal stem cells ameliorate hepatic ischemia reperfusion injury in a rat model. *PLoS One* **6**, 2–9 (2011).
181. Zhu, Y., Feng, X., Abbott, J., Fang, X. & Hao, Q. Human Mesenchymal Stem Cell Microvesicles for Treatment of Escherichia coli Endotoxin-Induced Acute Lung Injury in Mice. *Stem ...* 116–125 (2014).
182. Zhang, J. *et al.* Exosomes released from human induced pluripotent stem cells-derived MSCs facilitate cutaneous wound healing by promoting collagen synthesis and angiogenesis. *J. Transl. Med.* **13**, 49 (2015).
183. Yuyama, K. *et al.* Decreased amyloid-?? pathologies by intracerebral loading of glycosphingolipid-enriched exosomes in Alzheimer model mice. *J. Biol. Chem.* **289**, 24488–24498 (2014).
184. Urbanelli, L. *et al.* Exosome-based strategies for diagnosis and therapy. *Recent Pat. CNS Drug Discov.* 10–27 (2015). at <<http://www.ncbi.nlm.nih.gov/pubmed/26133463>>
185. Smith-Vikos, T. & Slack, F. J. MicroRNAs and their roles in aging. *J. Cell Sci.* **125**, 7–17 (2012).
186. Pourrajab, F., Vakili Zarch, A., Hekmatimoghaddam, S. & Zare-Khormizi, M. R. The master switchers in the aging of cardiovascular system, reverse senescence by microRNA signatures; as highly conserved molecules. *Prog. Biophys. Mol. Biol.* **119**, 111–128 (2015).
187. van Schooneveld, E. *et al.* Dysregulation of microRNAs in breast cancer and their potential role as prognostic and predictive biomarkers in patient management. *Breast Cancer Res.* **17**, 21 (2015).
188. Jung, H. J. & Suh, Y. MicroRNA in Aging: From Discovery to Biology. *Curr. Genomics* **13**, 548–57 (2012).
189. Cha, D. J. *et al.* KRAS-dependent sorting of miRNA to exosomes. *Elife* **4**, 1–22 (2015).
190. McKenzie, A. J. *et al.* KRAS-MEK Signaling Controls Ago2 Sorting into Exosomes. *Cell Rep.* **15**, 978–987 (2016).
191. Kuo, Y.-C. *et al.* Human Mesenchymal Stem Cells Suppress the Stretch-Induced Inflammatory miR-155 and Cytokines in Bronchial Epithelial Cells. *PLoS One* **8**, e71342 (2013).
192. Laine, S. K., Alm, J. J., Virtanen, S. P., Aro, H. T. & Laitala-Leinonen, T. K. MicroRNAs miR-96, miR-124, and miR-199a regulate gene expression in human bone marrow-derived mesenchymal stem cells. *J. Cell. Biochem.* **113**, 2687–2695 (2012).
193. Ceppi, M. *et al.* MicroRNA-155 modulates the interleukin-1 signaling pathway in activated human monocyte-derived dendritic cells. *Proc. Natl. Acad. Sci. U. S. A.* **106**, 2735–2740 (2009).
194. Tili, E. *et al.* Modulation of miR-155 and miR-125b levels following lipopolysaccharide/TNF- α stimulation and their possible roles in regulating the response to endotoxin shock. *J. Immunol.* **179**, 5082–9 (2007).
195. Cheung, K. S. C. *et al.* MicroRNA-146a regulates human foetal femur derived skeletal stem cell differentiation by down-regulating SMAD2 and SMAD3. *PLoS One* **9**, 1–16 (2014).
196. Lagos, D. *et al.* miR-132 regulates antiviral innate immunity through suppression of the p300 transcriptional co-activator. *Nat. Cell Biol.* **12**, 513–9 (2010).
197. Aalaei-Andabili, S. H. & Rezaei, N. MicroRNAs (MiRs) Precisely Regulate Immune System Development and Function in Immunosenescence Process. *Int. Rev. Immunol.* **185**, 1–10 (2015).

8. REFERENCES

198. Cătană, C. S., Calin, G. A. & Berindan-Neagoe, I. Inflammation-miRs in Aging and Breast Cancer: Are They Reliable Players? *Front. Med.* **2**, 85 (2015).
199. Ell, B. & Kang, Y. MicroRNAs as regulators of bone homeostasis and bone metastasis. *Bonekey Rep.* **3**, 549 (2014).
200. Sangiao-Alvarellos, S. *et al.* Testicular expression of the Lin28/let-7 system: Hormonal regulation and changes during postnatal maturation and after manipulations of puberty. *Sci. Rep.* **5**, 15683 (2015).
201. Dimmeler, S. & Nicotera, P. MicroRNAs in age-related diseases. *EMBO Mol. Med.* **5**, 180–190 (2013).
202. Seeger, T. *et al.* Immunosenescence-associated microRNAs in age and heart failure. *Eur. J. Heart Fail.* **15**, 385–393 (2013).
203. Eglon, M., Mcgrath, B. & Brien, T. O. Advanced Protocols in Oxidative Stress II. *Business* **594**, 395–408 (2010).
204. Mukhopadhyay, P. *et al.* Simultaneous detection of apoptosis and mitochondrial superoxide production in live cells by flow cytometry and confocal microscopy. *Nat. Protoc.* **2**, 2295–301 (2007).
205. Rasola, A. & Geuna, M. A flow cytometry assay simultaneously detects independent apoptotic parameters. *Cytometry* **45**, 151–157 (2001).
206. Livak, K. J. & Schmittgen, T. D. Analysis of relative gene expression data using real-time quantitative PCR and. *Methods* **25**, 402–408 (2001).
207. Rabilloud, T., Brodard, V., Peltre, G., Righetti, P. G. & Ettori, C. Modified silver staining for immobilized pH gradients. *Electrophoresis* **13**, 264–266 (1992).
208. Rappsilber, J., Mann, M. & Ishihama, Y. Protocol for micro-purification, enrichment, pre-fractionation and storage of peptides for proteomics using StageTips. *Nat. Protoc.* **2**, 1896–1906 (2007).
209. Lopes, L. R. *et al.* Genetic complexity in hypertrophic cardiomyopathy revealed by high-throughput sequencing. *J Med Genet* **50**, 228–239 (2013).
210. Szklarczyk, D. *et al.* The STRING database in 2011: Functional interaction networks of proteins, globally integrated and scored. *Nucleic Acids Res.* **39**, 561–568 (2011).
211. Schröder, M. S., Gusenleitner, D., Quackenbush, J., Culhane, A. C. & Haibe-Kains, B. RamiGO: An R/Bioconductor package providing an AmiGO Visualize interface. *Bioinformatics* **29**, 666–668 (2013).
212. Betel, D., Wilson, M., Gabow, A., Marks, D. S. & Sander, C. The microRNA.org resource: Targets and expression. *Nucleic Acids Res.* **36**, 149–153 (2008).
213. Lewis, B. P., Burge, C. B. & Bartel, D. P. Conserved seed pairing, often flanked by adenosines, indicates that thousands of human genes are microRNA targets. *Cell* **120**, 15–20 (2005).
214. Mantovani, C. *et al.* Morphological, molecular and functional differences of adult bone marrow- and adipose-derived stem cells isolated from rats of different ages. *Exp. Cell Res.* **318**, 2034–2048 (2012).
215. Bajek, a *et al.* Aging bone marrow mesenchymal stromal cells have altered membrane glycerophospholipid composition and functionality. *PLoS One* **4**, 44 (2014).
216. Yoon, B. H. *et al.* The Laboratory Rat: Relating Its Age With Human 's. *Am. J. Obstet. Gynecol.* **4**, 624–630 (2014).
217. Harting, M. T., Jimenez, F., Pati, S., Baumgartner, J. & Cox, C. S. Immunophenotype characterization of rat mesenchymal stromal cells. *Cytotherapy* **10**, 243–253 (2008).
218. Thomas Scholzen, J. G. The Ki-67 protein: From the known and the unknown. *J. Cell. Physiol.* **322**, 311–322 (2000).
219. Mateos, J., Pernas, P., Labora, J., Blanco, F. & Arufe, M. Proteomic Applications in the Study of Human Mesenchymal Stem Cells. *Proteomes* **2**, 53–71 (2014).
220. Jadaliha, M. *et al.* Quantitative Proteomic Analysis of Human Embryonic Stem Cell Differentiation by 8-Plex iTRAQ Labelling. *PLoS One* **7**, e38532 (2012).

8. REFERENCES

221. Maulik, N. & Das, D. K. Emerging potential of thioredoxin and thioredoxin interacting proteins in various disease conditions. *Biochim. Biophys. Acta - Gen. Subj.* **1780**, 1368–1382 (2008).
222. Toma-Jonik, A. *et al.* Active heat shock transcription factor 1 supports migration of the melanoma cells via vinculin down-regulation. *Cell. Signal.* **27**, 394–401 (2015).
223. Piltti, J., Varjosalo, M., Qu, C., Häyrynen, J. & Lammi, M. J. Rho-kinase inhibitor Y-27632 increases cellular proliferation and migration in human foreskin fibroblast cells. *Proteomics* **15**, 2953–2965 (2015).
224. Holle, A. W. *et al.* In situ mechanotransduction via vinculin regulates stem cell differentiation. *Stem Cells* **31**, 2467–2477 (2013).
225. Ahmed, A. *et al.* A switch in hepatic cortisol metabolism across the spectrum of non alcoholic fatty liver disease. *PLoS One* **7**, (2012).
226. Wu, J. *et al.* TGF- β 1 induces senescence of bone marrow mesenchymal stem cells via increase of mitochondrial ROS production. *BMC Dev. Biol.* **14**, 21 (2014).
227. Zhang, F., Ren, T. & Wu, J. TGF- β 1 induces apoptosis of bone marrow-derived mesenchymal stem cells via regulation of mitochondrial reactive oxygen species production. 1224–1228 (2015). doi:10.3892/etm.2015.2590
228. Terme, J. M. *et al.* Histone H1 variants are differentially expressed and incorporated into chromatin during differentiation and reprogramming to pluripotency. *J. Biol. Chem.* **286**, 35347–35357 (2011).
229. Horne, G. A. *et al.* Nanog Requires BRD4 to Maintain Murine Embryonic Stem Cell Pluripotency and Is Suppressed by Bromodomain Inhibitor JQ1 Together with Lefty1. *Stem Cells Dev.* **24**, 879–91 (2015).
230. Bermeo, S., Vidal, C., Zhou, H. & Duque, G. Lamin A/C Acts as an Essential Factor in Mesenchymal Stem Cell Differentiation Through the Regulation of the Dynamics of the Wnt/ β -Catenin Pathway. *J. Cell. Biochem.* **116**, 2344–2353 (2015).
231. Mateos, J. *et al.* Lamin A deregulation in human mesenchymal stem cells promotes an impairment in their chondrogenic potential and imbalance in their response to oxidative stress. *Stem Cell Res.* **11**, 1137–1148 (2013).
232. Stolzing, A. & Scutt, A. Age-related impairment of mesenchymal progenitor cell function. *Aging Cell* **5**, 213–224 (2006).
233. Easley, C. a *et al.* mTOR-Mediated Activation of p70 S6K Induces Differentiation of Pluripotent Human Embryonic Stem Cells. *Cell. Reprogramming (Formerly 'Cloning Stem Cells')* **12**, 263–273 (2010).
234. Harris, H. E. & Andersson, U. The nuclear protein HMGB1 as a proinflammatory mediator. *Eur. J. Immunol.* **34**, 1503–1512 (2004).
235. Pattappa, G., Heywood, H. K., de Bruijn, J. D. & Lee, D. A. The metabolism of human mesenchymal stem cells during proliferation and differentiation. *J. Cell. Physiol.* **226**, 2562–2570 (2011).
236. Sabers, C. J. *et al.* Isolation of a protein target of the FKBP12-rapamycin complex in mammalian cells. *J. Biol. Chem.* **270**, 815–822 (1995).
237. Han, J. *et al.* Nanog reverses the effects of organismal aging on mesenchymal stem cell proliferation and myogenic differentiation potential. **2**, 2–4 (2013).
238. Martins, I., Galluzzi, L. & Kroemer, G. Hormesis, cell death and aging. *Aging (Albany, NY)*. **3**, 821–828 (2011).
239. Luo, Y. *et al.* Rapamycin inhibits mSin1 phosphorylation independently of mTORC1 and mTORC2. *Oncotarget* **6**, 4286–4298 (2015).
240. Dillenburg, C. S., Martins, M. D., Meurer, L., Castilho, R. M. & Squarize, C. H. Keratoacanthoma of the Lip: Activation of the mTOR Pathway, Tumor Suppressor Proteins, and Tumor Senescence. *Medicine (Baltimore)*. **94**, e1552 (2015).
241. Yang, A. *et al.* Differential Responses of Hematopoietic Stem and Progenitor Cells to mTOR Inhibition. *Stem Cells Int.* **2015**, 1–9 (2015).
242. Mearadji, A. *et al.* Decrease of CD117 expression as possible prognostic marker

- for recurrence in the resected specimen after imatinib treatment in patients with initially unresectable gastrointestinal stromal tumors: a clinicopathological analysis. *Anticancer Drugs* **19**, 607–612 (2008).
243. Zhang, N. *et al.* Biodegradable polymeric micelles encapsulated JK184 suppress tumor growth through inhibiting Hedgehog signaling pathway. *Nanoscale* **7**, 2609–2624 (2015).
244. Lee, H. J. *et al.* Novel pathway for hypoxia-Induced proliferation and migration in human mesenchymal stem cells: Involvement of HIF-1 α , FASN, and mTORC1. *Stem Cells* 2182–2195 (2015). doi:10.1002/stem.2020
245. Zeng, Z. *et al.* apoptosis in AML cells under conditions mimicking the bone marrow microenvironment Targeting of mTORC1 / 2 by the mTOR kinase inhibitor PP242 induces apoptosis in AML cells under conditions mimicking the bone marrow microenvironment. *Blood* **120**, 2679–2689 (2012).
246. Jiang, S. *et al.* Synergistic effects between mTOR complex 1/2 and glycolysis inhibitors in non-small-cell lung carcinoma cells. *PLoS One* **10**, 1–19 (2015).
247. Lesovaya, E. A. *et al.* Rapatar, a nanoformulation of rapamycin, decreases chemically-induced benign prostate hyperplasia in rats. *Oncotarget* **6**, 9718–9727 (2015).
248. Blagosklonny, M. V. Rejuvenating immunity: ‘anti-aging drug today’ eight years later. *Oncotarget* **6**, (2015).
249. Yang, I. S. & Kim, S. Analysis of Whole Transcriptome Sequencing Data: Workflow and Software. *Genomics Inform.* **13**, 119–25 (2015).
250. Fafián-Labora, J. *et al.* Influence of age on rat bone-marrow mesenchymal stem cells potential. *Sci. Rep.* **5**, 16765 (2015).
251. Del Fattore, A. *et al.* Differential effects of extracellular vesicles secreted by mesenchymal stem cells from different sources on glioblastoma cells. *Expert Opin. Biol. Ther.* **15**, 1–10 (2014).
252. Dragovic, R. A. *et al.* Sizing and phenotyping of cellular vesicles using Nanoparticle Tracking Analysis. *Nanomedicine Nanotechnology, Biol. Med.* **7**, 780–788 (2011).
253. Gercel-Taylor, C., Atay, S., Tullis, R. H., Kesimer, M. & Taylor, D. D. Nanoparticle analysis of circulating cell-derived vesicles in ovarian cancer patients. *Anal. Biochem.* **428**, 44–53 (2012).
254. Nawaz, M. *et al.* Extracellular Vesicles: Evolving Factors in Stem Cell Biology. *Stem Cells Int.* **2016**, (2016).
255. Pietilä, M. *et al.* CD200 positive human mesenchymal stem cells suppress TNF- α secretion from CD200 receptor positive macrophage-like cells. *PLoS One* **7**, 1–12 (2012).
256. Kawai, T. & Akira, S. TLR signaling. *Semin. Immunol.* **19**, 24–32 (2007).
257. Waterman, R. S., Tomchuck, S. L., Henkle, S. L. & Betancourt, A. M. A new mesenchymal stem cell (MSC) paradigm: Polarization into a pro-inflammatory MSC1 or an immunosuppressive MSC2 phenotype. *PLoS One* **5**, (2010).
258. Chen, X. *et al.* The E-F Hand Calcium-Binding Protein S100A4 Regulates the Proliferation, Survival and Differentiation Potential of Human Osteosarcoma Cells. *Cell Physiol Biochem* **32**, 1083–1096 (2013).
259. Donato, R. *et al.* Functions of S100 proteins. *Curr. Mol. Med.* **13**, 24–57 (2013).
260. Park, J. S. *et al.* Involvement of toll-like receptors 2 and 4 in cellular activation by high mobility group box 1 protein. *J Biol Chem* **279**, 7370–7377 (2004).
261. Pistoia, V. & Raffaghello, L. Damage-associated molecular patterns (DAMPs) and mesenchymal stem cells: A matter of attraction and excitement. *Eur. J. Immunol.* **41**, 1828–1831 (2011).
262. Xu, C. *et al.* MiR-155 regulates immune modulatory properties of mesenchymal stem cells by targeting TAK1-binding protein 2. *J. Biol. Chem.* **288**, 11074–11079 (2013).
263. Tomé, M. *et al.* miR-335 orchestrates cell proliferation, migration and differentiation in human mesenchymal stem cells. *Cell Death Differ.* **18**, 985–995 (2011).

8. REFERENCES

264. Tomé, M. *et al.* MiR-335 correlates with senescence/aging in human mesenchymal stem cells and inhibits their therapeutic actions through inhibition of AP-1 activity. *Stem Cells* **32**, 2229–2244 (2014).
265. Feng, J. *et al.* miR-21 attenuates lipopolysaccharide-induced lipid accumulation and inflammatory response: potential role in cerebrovascular disease. *Lipids Health Dis.* **13**, 27 (2014).
266. He, X. *et al.* TLR4 activation promotes bone marrow MSC proliferation and osteogenic differentiation via wnt3a and wnt5a signaling. *PLoS One* **11**, 1–20 (2016).
267. Zhang, L. *et al.* The role of Toll-like receptor 3 and 4 in regulating the function of mesenchymal stem cells isolated from umbilical cord. *Int. J. Mol. Med.* 1003–1010 (2015). doi:10.3892/ijmm.2015.2106
268. Gharibi, B., Farzadi, S., Ghuman, M. & Hughes, F. J. Inhibition of Akt/mTOR attenuates age-related changes in mesenchymal stem cells. *Stem Cells* **32**, 2256–2266 (2014).
269. Rauner, M. *et al.* WNT5A is induced by inflammatory mediators in bone marrow stromal cells and regulates cytokine and chemokine production. *J. Bone Miner. Res.* **27**, 575–585 (2012).
270. He, W. *et al.* Lipopolysaccharide enhances Wnt5a expression through toll-like receptor 4, myeloid differentiating factor 88, phosphatidylinositol 3-OH kinase/AKT and nuclear factor kappa B pathways in human dental pulp stem cells. *J. Endod.* **40**, 69–75 (2014).
271. Tian, T. *et al.* Exosome uptake through clathrin-mediated endocytosis and macropinocytosis and mediating miR-21 delivery. *J. Biol. Chem.* **289**, 22258–22267 (2014).
272. Koumangoye, R. B., Sakwe, A. M., Goodwin, J. S., Patel, T. & Ochieng, J. Detachment of breast tumor cells induces rapid secretion of exosomes which subsequently mediate cellular adhesion and spreading. *PLoS One* **6**, (2011).
273. Montecalvo, A. *et al.* Mechanism of transfer of functional microRNAs between mouse dendritic cells via exosomes. *Blood* **119**, 756–766 (2012).
274. Morelli, A. E. *et al.* Endocytosis, intracellular sorting, and processing of exosomes by dendritic cells. *Blood* **104**, 3257–3266 (2004).
275. Kallas, A., Pook, M., Trei, A. & Maimets, T. SOX2 is regulated differently from NANOG and OCT4 in human embryonic stem cells during early differentiation initiated with sodium butyrate. *Stem Cells Int.* **2014**, (2014).
276. Descalzo, S. M., Ru??, P., Garcia-Ojalvo, J. & Arias, A. M. Correlations between the levels of Oct4 and Nanog as a signature for na??ve pluripotency in mouse embryonic stem cells. *Stem Cells* **30**, 2683–2691 (2012).
277. Parsons, X. H. The Dynamics of Global Chromatin Remodeling are Pivotal for Tracking the Normal Pluripotency of Human Embryonic Stem Cells. *Anat Physiol* (2013).
278. Goldmann, W. H., Auernheimer, V., Thievensen, I. & Fabry, B. Vinculin, cell mechanics and tumour cell invasion. *Cell Biol. Int.* **37**, 397–405 (2013).
279. Ahlqvist, K. J., Suomalainen, A. & Hämäläinen, R. H. Stem cells, mitochondria and aging. *Biochim. Biophys. Acta - Bioenerg.* **1847**, 1380–1386 (2015).
280. Malda, J., Boere, J., van de Lest, C., van Weeren, P. R. & Wauben, M. H. Extracellular vesicles - new tool for joint repair and regeneration - IN PRESS. *Nat. Rev. Rheumatol.* **12**, 243–249 (2016).

8. SUPPLEMENTS

Antibody	Reference	Dilution	Company, City, Country
Alexa Fluor 647 hamster anti-rat CD29	RU0-562153	1:1000	BD Pharmigen™, Haryana, India
PE mouse anti-human CD34	RUO-5558222	1:1000	BD Pharmigen™, Haryana, India
FITC mouse anti-rat CD45RA	RUO-561886	1:1000	BD Pharmigen™, Haryana, India
PE mouse anti-rat CD90	RUO-551401	1:1000	BD Pharmigen™, Haryana, India
APC anti-human CD117	117A-10T	1:1000	Immunostep, Salamanca, Spain
FITC anti-rat CD200	1399990143	1:1000	Immunostep, Salamanca, Spain
FITC mouse anti-Ki67	RUO-556026	1:1000	BD Pharmigen™, Haryana, India
Alexa Fluor 647 mouse IgG1 k isotype control	RUO-557783	1:1000	BD Pharmigen™, Haryana, India
Rabbit anti-goat IgG-FITC	sc-2777	1:1000	St.Cruz Biotechnology, St.Cruz, United States
Rabbit anti-goat IgG-PE	sc-3755	1:1000	St.Cruz Biotechnology, St.Cruz, United States

Table 8.1. List of antibodies to flow cytometry.

Primary Antibodies	Reference	Dilution	Company, City, Country
Mouse monoclonal to Lamin-A/C (LMNA)- purified	BM6000P	1:1000	Acris, Schillerstr, Germany
Rabbit polyclonal to p70S6K	ab47511	1:1000	Abcam, Cambridge, United Kingdom
Rabbit monoclonal to mTOR (7C10)	#2983	1:1000	Cell Signaling, Barcelona, Spain
Rabbit monoclonal to Raptor (24C12)	#2280	1:1000	Cell Signaling, Barcelona, Spain
Rabbit monoclonal to Rictor (53A2)	#2114	1:1000	Cell Signaling, Barcelona, Spain
Rabbit monoclonal to Gβ1 (86b8)	#3274	1:1000	Cell Signaling, Barcelona, Spain
Rabbit monoclonal to Phospho-mTOR (Ser2448)	#5536	1:1000	Cell Signaling, Barcelona, Spain
Mouse anti-rat TLR4-purified	1399990142	1:1000	Immunostep, Salamanca, Spain
Rabbit monoclonal to AMPKα (23A3)	#2603	1:1000	Cell Signaling, Barcelona, Spain
Mouse monoclonal to Wnt5a	ab86720	1:1000	Abcam, Cambridge, United Kingdom
Rabbit monoclonal to Akt	#9272	1:500	Cell Signaling, Barcelona, Spain
Rabbit monoclonal to phospho-Akt (Ser473)	#9271	1:500	Cell Signaling, Barcelona, Spain
Mouse monoclonal to Vimentin	ab8069	1:1000	Abcam, Cambridge, United Kingdom
Mouse monoclonal to manganese superoxide dismutase (SOD-2)	611580	1:1000	BD Pharmigen™, Haryana, India
Rabbit polyclonal to HMGB1	ab18256	1:1000	Abcam, Cambridge, United Kingdom
Rabbit monoclonal to α-tubulin (11H10)	#2125	1:5000	Cell Signaling, Barcelona, Spain
Mouse monoclonal to β-actin	A5441	1:5000	Sigma-Aldrich,
Anti-rabbit immunoglobulins, HRP-linked antibody	#7074	1:1000	Cell Signaling, Barcelona, Spain
Anti-mouse immunoglobulins, HRP-linked antibody	11689	1:1000	Dako, Glostrup, Denmark

Table 8.2. List of antibodies to western-blot.

Gene	Number acces	Forward primer (5'-3')	Reverse primer (5'-3')	T /°C
Nanog	NM_005103.4	atgcctcacacggagactgt	aagtgggtgtttgcctttg	61
Oct4	NM_00510	ctcctggagggccaggaatc	atatacacaggccgatgtgg	61
Rex1	NM_005106.4	gtgcatcacacctcagactgt	cgttggtgaaggccaactg	61
Sox2	NM_001109181.1	ctccgggacatgatcagc	ggtagtgctgggacatgtgaa	61
Vinculin	NM_012583.2	aggagacctgcgaagacagg	gcggttgccactgtttag	61
S100A4	NM_012618.1	agctactgaccaggagctg	ctggaatgcagcttcgtct	59
S100A6	NM_053485.2	tgatccagaaggagctcacc	agatcatccatcagccttgc	60
HMGB1	NM_012963.2	ccggatgcttctgtcaactt	ttgattttggcggttactc	60
HPRT	NM_012583.2	agccgaccggttctgtcat	agccgaccggttctgtca	61

Table 8.3. Specific primers of different rat genes for qRT-PCR.

Target	Number acces	Sequence (5'-3')
hsa-miR-16	MIMAT0000069	tagcagcacgtaaattggcg
rno-miR-21-5p	MIMAT0000790	tagcttatcagactgatgtga
hsa-miR-132-5p	MIMAT0004594	accgtggcttctgattgttact
hsa-miR-146a	MIMAT0000449	tgagaactgaattccatgggtt
rno-miR-155-5p	MIMAT0030409	ttaatgctaattgtgataggggt
rno-miR-335	MIMAT0000575	tcaagagcaataacgaaaaatgt

Table 8.4. Specific primers of miRNAs for qRT-PCR.

Buffer	Composition	Company, City, Country
Fixative	10% (v/v) acetic acid 40% (v/v) ethanol	All from PANREAC, Barcelona, Spain
Sensitizer	0.02 % (w/v) sodium thiosulfate	All from Sigma-Aldrich, St.Louis, United States
Silver	0.075% (v/v) formaldehyde 0.2% (w/v) silver nitrate	All from Sigma-Aldrich, St.Louis, United States
Revealing	0.025% (v/v) formaldehyde 3% (w/v) sodium carbonate 12.5 mg/l sodium thiosulfate	All from Sigma-Aldrich, St.Louis, United States
Stop	10% (v/v) acetic acid 3% (w/v) Tris-base	All from Sigma-Aldrich, St.Louis, United States

Table 8.5. List of buffer to silver-staining.

7. SUPPLEMENTS

Energy metabolism

Accession	Name	Peptides (95%)	I/N	PVal I/N	Y/I	PVal Y/I	PP/Y	PVal PP/Y	P/PP	PVal P/PP	A/P	PVal A/P
Q6P783	6-phosphofructokinase	5	0.7228	0.1496	1.0497	0.7085	1.1027	0.3079	1.4117	0.0388	1.2082	0.2192
Q7TP11	6-phosphogluconate dehydrogenase. decarboxylating	5	0.8664	0.0404	0.9404	0.345	1.1936	0.1035	1.2877	0.0026	0.6857	0.0099
P06761	78 kDa glucose-regulated protein	35	0.9172	0.0089	0.9677	0.334	1.1997	0	0.8295	0.002	1.4611	0
M0RDC5	Acyl-CoA-binding protein (Fragment)	1	0.9923	0.9393	1.0172	0.8471	1.0129	0.8865	1.1744	0.4947	1.408	0.0299
F1LN88	Aldehyde dehydrogenase. mitochondrial	9	0.915	0.2981	0.9521	0.605	1.0255	0.8092	0.8105	0.1287	1.249	0.0303
P07943	Aldose reductase	9	1.0984	0.3717	0.8893	0.186	0.9549	0.5728	0.9715	0.7164	1.2055	0.0389
Q91W30	Aldose reductase-like protein	10	1.6948	0.0054	0.5021	0.0183	1.2079	0.2492	1.0106	0.9424	1.2476	0.0229
D3ZUM4	Beta-galactosidase	5	1.0315	0.7835	1.3171	0.0441	1.0942	0.385	1.1471	0.1506	0.9005	0.1892
O35567	Bifunctional purine biosynthesis protein PURH	13	0.9914	0.9389	0.8798	0.2663	1.1514	0.3918	0.8194	0.0166	1.1312	0.0362
Q99JD5	Branched-chain-amino-acid aminotransferase	5	1.0463	0.7187	0.842	0.0756	1.3485	0.0127	0.9146	0.4169	0.9297	0.5047
P15791	Calcium/calmodulin-dependent protein kinase type II subunit delta	5	0.9646	0.825	0.9676	0.8106	1.3814	0.0071	0.7966	0.044	1.0233	0.8049
G3V9E3	Caldesmon 1. isoform CRA_b	18	1.0648	0.1599	0.9241	0.1919	1.4728	0	0.7388	0.0002	1.6353	0
Q08290	Calponin-1	9	0.8714	0.0531	1.3003	0.0464	0.8214	0.2876	0.723	0.0013	1.2572	0.0412
P37397	Calponin-3	10	1.3337	0.0378	0.8281	0.0224	1.0857	0.2275	0.7288	0.0035	1.1632	0.1397
P18418	Calreticulin	12	1.1514	0.0446	0.8607	0.0394	1.3403	0.0004	0.7119	0.0002	1.4109	0.0004
G3V6S3	Calumenin	5	1.0591	0.4369	1.0768	0.3271	0.9833	0.8456	0.7673	0.2524	1.5598	0.0141
Q6P6T6	Cathepsin D	7	0.8801	0.1287	1.0622	0.3991	1.5419	0.0105	0.9111	0.1808	1.3326	0.0234

Table 8.6. List of modulated proteins ($P < 0.05$) in rBM-MSCs at different ages classified according to their principal biological process using iTRAQ-8plex. I/N= infant vs newborn; Y/I=young vs infant; PP/Y= pre-pubertal vs young; P/PP= pubertal vs pre-pubertal; A/P= adult vs pubertal.

7. SUPPLEMENTS

Accession	Name	Peptides (95%)	I/N	PVal I/N	Y/I	PVal Y/I	PP/Y	PVal PP/Y	P/PP	PVal P/PP	A/P	PVal A/P
P97601	Chaperonin 10	3	1.0204	0.7796	1.0011	0.9902	0.9415	0.5177	0.939	0.4419	1.4235	0.0087
G3V936	Citrate synthase	3	0.7934	0.0267	1.167	0.0848	0.7904	0.0267	1.1452	0.2405	0.857	0.2318
F1M779	Clathrin heavy chain	9	1.2157	0.0137	1	0.9994	0.9612	0.7295	1.1343	0.2338	0.8853	0.3235
Q6TUH9	Corticosteroid dehydrogenase isozyme 1	3	0.7341	0.2686	1.3756	0.2277	1.6421	0.0328	1.9857	0.0672	0.7338	0.0642
P47875	Cysteine and glycine-rich protein 1	7	1.0015	0.9815	1.0448	0.5131	1.2576	0.0488	0.6896	0.0389	1.2501	0.0705
O08651	D-3-phosphoglycerate dehydrogenase	3	0.8786	0.1902	0.7465	0.0308	1.1981	0.1105	1.1565	0.1448	1.0565	0.5069
Q5BJ93	Enolase 1. (Alpha)	23	1.0226	0.655	1.026	0.5722	1.054	0.2406	0.7412	0	1.2752	0.0123
Q8R4A1	ERO1-like protein alpha	5	0.8236	0.0936	1.0042	0.9607	1.1541	0.1632	1.0604	0.6296	1.4685	0.0439
P05065	Fructose-bisphosphate aldolase A	7	0.7852	0.0001	0.9961	0.9275	1.1519	0.0055	1.17	0.0228	1.1494	0.0589
P11762	Galectin-1	13	0.8947	0.1869	1.0817	0.3224	0.9378	0.4491	0.738	0.0127	1.2891	0.0226
Q8CJG5	Gene	3	0.9562	0.7992	0.6552	0.233	1.5338	0.0488	1.0942	0.6762	0.9227	0.7939
P05370	Glucose-6-phosphate dehydrogenase	16	1.0157	0.847	1.0285	0.7414	0.9947	0.9314	1.0827	0.1708	1.2136	0.0003
Q6P6V0	Glucose-6-phosphate isomerase	13	0.859	0.1021	0.9669	0.5321	1.1179	0.0929	1.1489	0.1394	1.2446	0.0072
P04797	Glyceraldehyde-3-phosphate dehydrogenase	28	1.0559	0.3012	1.2268	0.0077	0.8176	0.0404	1.0972	0.4988	0.8495	0.1048
P56574	Isocitrate dehydrogenase [NADP]. mitochondrial	3	1.0223	0.8926	1.0131	0.8828	0.8721	0.3389	1.3609	0.025	0.8545	0.1231
B5DEN4	L-lactate dehydrogenase	14	0.7058	0.0001	1.146	0.00197	1.1828	0.0191	1.2617	0	1.416	0
Q6P7A9	Lysosomal alpha-glucosidase	4	0.9754	0.7869	1.0694	0.6226	1.4268	0.048	0.8687	0.254	1	1
Q6AYC4	Macrophage-capping protein	2	1.1578	0.3404	1.3646	0.0086	0.8334	0.049	0.7546	0.0948	1.3655	0.0617
F1LP60	Moesin (Fragment)	40	1.0168	0.6741	0.8227	0.0003	1.4257	0	0.9895	0.8299	0.9461	0.1782
P20070	NADH-cytochrome b5 reductase 3	2	0.7339	0.0716	1.4911	0.0447	0.9088	0.5256	0.9743	0.903	0.8315	0.169
Q6XD99	Non-erythroid spectrin beta	2	1.3375	0.0053	1.0624	0.4554	1.1109	0.3101	0.7568	0.0122	1.5134	0.0041
P16617	Phosphoglycerate kinase 1	29	0.775	0	1.0397	0.3579	1.0241	0.6829	1.1179	0.0446	1.3076	0

Table 8.6. List of modulated proteins ($P < 0.05$) in rBM-MSCs at different ages classified according to their principal biological process using iTRAQ-8plex. I/N= infant vs newborn; Y/I=young vs infant; PP/Y= pre-pubertal vs young; P/PP= pubertal vs pre-pubertal; A/P= adult vs pubertal.

7. SUPPLEMENTS

Accession	Name	Peptides (95%)	I/N	PVal I/N	Y/I	PVal Y/I	PP/Y	PVal PP/Y	P/PP	PVal P/PP	A/P	PVal A/P
P25113	Phosphoglycerate mutase 1	9	0.7559	0.0052	1.1081	0.1211	1.1188	0.142	1.105	0.1848	1.3205	0.0024
P54001	Prolyl 4-hydroxylase subunit alpha-1	15	0.9432	0.3007	0.923	0.1417	1.26	0.0005	0.779	0.0002	0.9234	0.2253
M0R9D5	Protein Ahnak	60	1.4134	0	0.9734	0.2788	1.2761	0	0.8082	0	2.1551	0
D3ZIE9	Protein Aldh18a1	5	1.2134	0.1403	1.038	0.7002	0.5751	0.0236	0.8643	0.2248	0.7301	0.0622
M0R3X6	Protein LOC100912203	6	0.8645	0.163	1.0325	0.6321	1.1276	0.2248	0.9918	0.9068	1.2992	0.0104
D4A5L9	Protein LOC679794	4	0.6761	0.0039	1.6157	0.0178	0.7517	0.0082	0.9865	0.8661	1.0755	0.375
Q6P9U0	Protein Serpinb6	8	0.9886	0.8679	1.0239	0.6691	1.3013	0.0066	0.8823	0.2774	1.1196	0.16
D3ZF39	Protein Uap1	10	1.0277	0.7709	1.0072	0.947	1.6544	0.0038	0.9744	0.7756	1.6238	0.0005
B0BMT0	RCG47746, isoform CRA_a	90	1.0669	0.6161	0.7141	0.0061	1.4858	0.0047	0.5813	0.0012	0.7691	0.1418
Q6IRL3	Reticulon	7	1.0111	0.8671	0.8818	0.3109	1.3224	0.0677	0.7406	0.0052	0.9133	0.4439
B2GVB1	S100 calcium binding protein A6	3	1.0605	0.5609	1.2045	0.2186	1.7118	0.0122	0.3918	0.0244	1.665	0.037
Q5U3Z7	Serine hydroxymethyltransferase	3	0.7739	0.0051	0.9472	0.5152	1.0085	0.9511	1.1442	0.2328	1.0402	0.831
F1M953	Stress-70 protein, mitochondrial	12	0.9377	0.2437	0.7924	0.0057	1.174	0.0025	0.8961	0.1199	1.5666	0
P48500	Triosephosphate isomerase	16	0.6753	0.0004	1.174	0.0315	1.0854	0.3958	1.2639	0.1091	1.4017	0.0001
Q9Z1A6	Vigilin	3	1.1784	0.0874	0.8426	0.0918	1.0244	0.862	0.9978	0.9727	1.2104	0.0345
P81155	Voltage-dependent anion-selective channel protein 2	6	1.0012	0.9931	1.0633	0.4458	1.2708	0.0343	0.8377	0.1616	0.992	0.9444
<i>Pluripotency</i>												
P63102	14-3-3 protein zeta/delta	24	0.9971	0.9573	0.9743	0.6297	1.0748	0.2065	0.8947	0.1104	1.1562	0.0250
Q7TP91	Ab1-205	3	0.9802	0.8434	1.2607	0.1387	0.9026	0.3795	1.0629	0.7975	0.6232	0.0302
Q64640	Adenosine kinase	2	0.9609	0.8197	1.1207	0.3134	1.1155	0.346	1.0828	0.4536	0.6855	0.0454
P39069	Adenylate kinase isoenzyme 1	4	0.7781	0.0775	1.2606	0.053	1.0747	0.7679	0.9795	0.8759	1.6777	0.029

Table 8.6. List of modulated proteins ($P < 0.05$) in rBM-MSCs at different ages classified according to their principal biological process using iTRAQ-8plex. I/N= infant vs newborn; Y/I=young vs infant; PP/Y= pre-pubertal vs young; P/PP= pubertal vs pre-pubertal; A/P= adult vs pubertal.

7. SUPPLEMENTS

Accession	Name	Peptides (95%)	I/N	PVal I/N	Y/I	PVal Y/I	PP/Y	PVal PP/Y	P/PP	PVal P/PP	A/P	PVal A/P
P23928	Alpha-crystallin B chain	5	1.207	0.0573	1.8689	0.0119	2.2257	0.0003	0.2931	0.0035	1.5629	0.0723
Q6IMZ3	Annexin A6	24	1.2484	0.0001	1.1079	0.0199	0.9791	0.5623	1.0031	0.9354	1.0187	0.5863
Q07936	Annexin A2	22	1.2928	0	1.0234	0.6825	1.368	0.0001	0.8172	0.003	1.072	0.1567
Q05175	Brain acid soluble protein 1	3	0.9481	0.8617	1.209	0.454	1.3727	0.148	0.4584	0.0445	1.6462	0.1009
Q6T487	Brain-specific alpha actinin 1 isoform	48	0.7786	0.0007	1.1584	0.0465	1.0249	0.6506	0.8259	0.0018	1.1052	0.2188
Q8R4A2	Caveolin 1 (Fragment)	4	0.9676	0.8582	1.8465	0.0328	1.0661	0.7396	0.7326	0.1573	1.0726	0.6061
P02454	Collagen alpha-1(I) chain	21	1.9314	0.0008	0.4642	0	1.3783	0	1.1251	0.0342	1.123	0.1023
F1LS40	Collagen alpha-2(I) chain	19	1.486	0.0008	0.6971	0	1.1467	0.0083	0.9555	0.2908	1.3211	0.0003
F1LMA7	C-type mannose receptor 2	5	1.1259	0.191	0.8731	0.3184	0.8322	0.3836	0.8408	0.3689	1.7697	0.0009
P47875	Cysteine and glycine-rich protein 1	5	1.0995	0.2349	0.9264	0.4028	1.275	0.0227	0.7329	0.0396	1.2025	0.1773
Q6AY11	DEAD (Asp-Glu-Ala-Asp) box polypeptide 5	9	0.9335	0.2865	0.9937	0.9257	0.8965	0.0659	1.2504	0.0032	0.9596	0.434
Q62952	Dihydropyrimidinase-related protein 3	8	1.2443	0.0364	1.5656	0.0028	0.858	0.2853	0.8247	0.0165	1.0088	0.9184
Q4V8H8	EH domain-containing protein 2	0	0.9656	0.7399	1.3396	0.2041	0.8004	0.248	1.6703	0.0471	0.7495	0.491
Q68FR6	Elongation factor 1-gamma	9	1.0087	0.8562	0.9072	0.4157	1.2134	0.0011	0.9535	0.5667	0.8485	0.0109
C0JPT7	Filamin alpha	100	1.2134	0	1.3022	0	0.8202	0	0.9147	0.0068	1.386	0
D4A8D5	Filamin. beta (Predicted)	19	1.0951	0.0867	1.2541	0.0012	0.8193	0.0061	0.7937	0.0124	1.329	0.0009
B6DYQ7	Glutathione S-transferase pi	4	1.0946	0.3206	1.1008	0.6055	1.5111	0.0241	3.1507	0.0004	0.3406	0.0033
G3V913	Heat shock 27kDa protein 1	5	1.6407	0.0562	0.9647	0.8462	1.5674	0.0118	0.636	0.038	1.3145	0.0077

Table 8.6. List of modulated proteins ($P < 0.05$) in rBM-MSCs at different ages classified according to their principal biological process using iTRAQ-8plex. I/N= infant vs newborn; Y/I=young vs infant; PP/Y= pre-pubertal vs young; P/PP= pubertal vs pre-pubertal; A/P= adult vs pubertal.

7. SUPPLEMENTS

Accession	Name	Peptides (95%)	I/N	PVal I/N	Y/I	PVal Y/I	PP/Y	PVal PP/Y	P/PP	PVal P/PP	A/P	PVal A/P
P63018	Heat shock cognate 71 kDa protein	30	0.9815	0.6625	1.2334	0.0221	0.8841	0.0143	1.0164	0.8526	1.1903	0.0184
F1M3D3	Heterogeneous ribonucleoprotein M nuclear	3	0.6983	0.0017	1.0334	0.5966	0.9158	0.4502	1.1725	0.1239	1.0388	0.7714
Q6IMY8	Heterogeneous ribonucleoprotein U nuclear	8	0.7965	0.0032	1.0228	0.7409	0.9994	0.9956	1.1924	0.0262	0.8534	0.1414
P15865	Histone H1.4	8	0.7411	0.0048	2.4013	0.0005	1.0711	0.2301	0.5016	0.0007	0.6377	0.007
D3ZBN0	Histone H1.5	4	1.911	0.0166	0.4907	0.0135	0.9905	0.9189	1.4031	0.0552	0.8838	0.2767
G3V9C7	Histone H2B	20	1.2535	0.0051	0.9957	0.9764	0.8311	0.1792	1.4957	0.0005	0.7706	0.0027
M0RBX6	Histone H3	6	1.1323	0.058	1.4413	0.0125	1.201	0.0272	0.5991	0.0004	0.494	0.0002
P62804	Histone H4	13	1.4819	0.0057	0.5999	0.0004	1.1515	0.0641	1.7155	0.0008	0.6785	0.002
Q6P6G9	Hnrpa1 protein	8	0.6091	0.0304	0.9626	0.6587	0.943	0.663	1.1142	0.7189	0.969	0.7865
P50503	Hsc70-interacting protein	4	0.9785	0.7614	1.0509	0.7519	1.1426	0.4415	0.8392	0.2581	1.5699	0.0074
P49134	Integrin beta-1	6	1.5471	0.0002	0.9023	0.1179	1.5398	0.0098	0.7217	0.0064	1.311	0.0037
G3V7Q7	IQ motif containing GTPase activating protein 1 (Predicted). isoform CRA_b	29	0.9058	0.0331	0.8665	0.0016	1.2223	0	1.0398	0.2744	0.8961	0.0032
G3V8L3	Lamin A. isoform CRA_b	26	0.9048	0.0029	0.968	0.4478	1.1812	0.0001	1.0126	0.746	1.2067	0
Q6TXE9	LRRGT00050	4	0.8206	0.0425	0.8878	0.4999	1.0972	0.6832	1.5	0.0036	0.8044	0.129
Q6TUD1	LRRGT00113	2	0.7362	0.0289	1.0159	0.9238	1.0387	0.7991	1.0836	0.5779	0.9606	0.8364
Q5M7W5	Microtubule-associated protein 4	2	1.6111	0.1601	0.845	0.5023	1.0907	0.433	0.6693	0.1236	1.6243	0.0414
B2GV99	Myl6 protein	11	1.0049	0.9535	1.1269	0.1948	1.0655	0.29	0.9193	0.1676	1.3394	0.0011

Table 8.6. List of modulated proteins ($P < 0.05$) in rBM-MSCs at different ages classified according to their principal biological process using iTRAQ-8plex. I/N= infant vs newborn; Y/I=young vs infant; PP/Y= pre-pubertal vs young; P/PP= pubertal vs pre-pubertal; A/P= adult vs pubertal.

7. SUPPLEMENTS

Accession	Name	Peptides (95%)	I/N	PVal I/N	Y/I	PVal Y/I	PP/Y	PVal PP/Y	P/PP	PVal P/PP	A/P	PVal A/P
G3V9Y1	Myosin, heavy polypeptide 10, non-muscle, isoform CRA_b	51	0.9356	0.0771	1.0793	0.1827	0.8786	0.0186	0.8988	0.0205	0.792	0.0018
G3V6P7	Myosin, heavy polypeptide 9, non-muscle	98	0.9405	0.0071	1.1877	0	1.0117	0.6464	0.957	0.2338	1.3299	0
P05982	NAD(P)H dehydrogenase [quinone] 1	8	1.3454	0.0036	0.7746	0.0108	1.2457	0.0611	0.817	0.2198	1.7303	0.0017
G3V8R1	Nucleobindin 2, isoform CRA_b	3	0.7234	0.0259	2.0743	0.0023	0.5945	0.0061	0.8133	0.1039	1.5101	0.0176
F1M4W3	Palladin (Fragment)	6	1.0033	0.9633	0.8726	0.1096	1.0418	0.6509	0.6823	0.0117	1.0929	0.2707
P52944	PDZ and LIM domain protein 1	8	1.0741	0.3026	1.0802	0.1599	1.3743	0.0005	0.9648	0.7456	1.2349	0.03
Q62920	PDZ and LIM domain protein 5	17	0.9467	0.5156	0.6947	0.0022	1.4784	0.0057	0.6885	0.0358	0.8014	0.071
Q6AYQ9	Peptidyl-prolyl cis-trans isomerase	6	0.9218	0.2069	0.9782	0.6989	1.2033	0.0649	0.7408	0.0209	0.837	0.0475
Q62658	Peptidyl-prolyl cis-trans isomerase FKBP1A	2	1.254	0.0638	1.1087	0.2151	1.0291	0.6981	0.8516	0.0786	1.38	0.0149
D3ZAF5	Periostin, osteoblast specific factor (Predicted), isoform CRA_a	4	0.5315	0.1266	1.4489	0.0583	0.7663	0.0352	1.3251	0.0507	0.8907	0.4068
Q63716	Peroxiredoxin-1	13	0.8935	0.0404	1.0622	0.5224	1.083	0.5586	0.884	0.3841	1.2919	0.0335
P35704	Peroxiredoxin-2	5	0.9438	0.6729	1.3399	0.0331	0.9268	0.3898	0.8375	0.2252	1.1003	0.4352
Q9R063	Peroxiredoxin-5, mitochondrial	5	1.0571	0.6808	0.7826	0.0577	1.2214	0.0908	0.8798	0.195	1.4277	0.0498
F1LPK7	Phospholipid scramblase 3	5	1.3539	0.015	0.7564	0.0206	1.2564	0.0285	0.9783	0.8008	1.0061	0.9704
G3V8L9	Polymerase I and transcript release factor	10	1.0181	0.7755	1.5741	0.0001	1.2442	0.0026	0.6574	0.0001	1.2032	0.1746

Table 8.6. List of modulated proteins ($P < 0.05$) in rBM-MSCs at different ages classified according to their principal biological process using iTRAQ-8plex. I/N= infant vs newborn; Y/I=young vs infant; PP/Y= pre-pubertal vs young; P/PP= pubertal vs pre-pubertal; A/P= adult vs pubertal.

7. SUPPLEMENTS

Accession	Name	Peptides (95%)	I/N	PVal I/N	Y/I	PVal Y/I	PP/Y	PVal PP/Y	P/PP	PVal P/PP	A/P	PVal A/P
G3V9I0	Procollagen-lysine,2-oxoglutarate 5-dioxygenase 2	15	0.6772	0.0001	1.3393	0.0139	0.8435	0.0459	1.1106	0.2824	1.033	0.765
D3ZRX9	Protein Cnn2	9	0.9803	0.7232	0.9782	0.6955	1.1542	0.0382	0.7727	0.0037	1.1053	0.1116
G3V6T7	Protein disulfide isomerase associated 4	4	1.094	0.3778	1.5291	0.0042	0.7583	0.087	0.8527	0.0368	1.1596	0.0466
P04785	Protein disulfide-isomerase	18	0.9524	0.2161	0.9019	0.0205	1.1449	0.002	0.91	0.0672	1.3562	0
P11598	Protein disulfide-isomerase A3	23	1.0044	0.9331	1.1813	0.0003	1.0096	0.899	0.888	0.1863	1.151	0.1114
Q63081	Protein disulfide-isomerase A6	9	0.7832	0.0043	1.1044	0.262	1.2788	0.0234	0.9335	0.4195	1.0394	0.5727
D3ZHA0	Protein Flnc	28	0.9537	0.2739	1.6131	0	0.8375	0.0128	0.9354	0.1802	1.1796	0.0125
E2RUH2	Protein LOC100360501	3	0.8715	0.4837	1.2547	0.0379	0.7763	0.024	1.2418	0.1487	0.7978	0.0359
M0R7B4	Protein LOC684828	6	1.9171	0.003	0.4959	0.0035	1.0813	0.3542	1.3227	0.0305	0.8447	0.1021
F1MA29	Protein LOC685520	5	0.7506	0.0026	1.15	0.0892	0.9181	0.414	1.0561	0.438	1.066	0.4416
D3ZUB0	Protein Rcn1	2	1.0185	0.8167	0.8941	0.2217	1.1262	0.2053	0.8607	0.297	1.3273	0.0313
I6L9G5	Protein Rcn3	2	1.0873	0.4834	0.5646	0.023	1.147	0.2936	0.9716	0.7715	1.3833	0.2381
D4A1P2	Protein Rpl10l	7	1.0101	0.8587	0.8912	0.0814	0.8855	0.0554	1.4153	0.0002	0.6894	0.0001
F1M853	Protein Rrbp1	12	0.9865	0.8266	0.9487	0.2254	1.4058	0.0002	0.6416	0.0002	1.4396	0
P05942	Protein S100-A4	8	1.3344	0.0883	0.8596	0.3432	2.371	0.0005	0.6816	0.0449	1.6256	0.0034
B0BMT9	Protein Sqrcl	5	0.8772	0.1123	0.8745	0.2138	1.3482	0.0318	0.672	0.0272	1.1637	0.2917
P50399	Rab GDP dissociation inhibitor beta	5	0.6527	0	1.1226	0.1842	0.8087	0.0191	1.2167	0.0909	0.8327	0.0497
Q5FVG5	Similar to tropomyosin 1, embryonic fibroblast-rat, isoform CRA_c	21	0.8189	0.0635	0.8236	0.0664	1.5332	0.0055	0.4284	0.0029	0.9622	0.622

Table 8.6. List of modulated proteins ($P < 0.05$) in rBM-MSCs at different ages classified according to their principal biological process using iTRAQ-8plex. I/N= infant vs newborn; Y/I=young vs infant; PP/Y= pre-pubertal vs young; P/PP= pubertal vs pre-pubertal; A/P= adult vs pubertal.

7. SUPPLEMENTS

Accession	Name	Peptides (95%)	I/N	PVal I/N	Y/I	PVal Y/I	PP/Y	PVal PP/Y	P/PP	PVal P/PP	A/P	PVal A/P
Q6IRH6	Slc25a3 protein	5	0.6221	0.0046	1.2418	0.0813	0.9018	0.3869	1.2937	0.0271	0.7334	0.0095
P06685	Sodium/potassium-transporting ATPase subunit alpha-1	6	1.0612	0.5229	0.847	0.0206	0.9521	0.6531	1.1204	0.4092	0.8973	0.1495
P16975	SPARC	5	1.2574	0.0585	0.8963	0.1879	1.0501	0.5303	0.9358	0.5629	1.2361	0.0437
Q63413	Spliceosome RNA helicase Ddx39b	4	0.7567	0.0206	1.0276	0.7991	0.904	0.431	1.3219	0.0189	0.679	0.0523
Q6IRK8	Spna2 protein	9	1.3867	0	1.211	0.003	1.0232	0.7136	0.7877	0.0016	1.7205	0
D4A8Y5	Staphylococcal nuclease domain- containing protein 1	3	0.919	0.451	1.2908	0.0445	0.8256	0.0815	1.2376	0.0644	0.7802	0.1202
Q71SA3	Thrombospondin 1	7	0.8058	0.0398	0.7166	0.0007	1.3192	0.0007	0.9713	0.6767	1.4974	0.0023
P31232	Transgelin	39	1.2096	0.0003	1.2967	0.0743	1.133	0.0136	0.5637	0.0001	1.7372	0
Q5XFX0	Transgelin-2	17	0.9888	0.8414	1.0039	0.955	1.3666	0.0009	0.9786	0.7678	1.1396	0.048
Q6AYT3	tRNA-splicing ligase RtcB homolog	4	0.6896	0.019	0.9867	0.8815	0.8815	0.1894	1.1372	0.1808	0.8525	0.4565
Q63610	Tropomyosin alpha-3 chain	9	0.9843	0.838	1.4987	0.0199	1.2255	0.0709	0.6776	0.0538	1.8819	0.0153
P09495	Tropomyosin alpha-4 chain	12	0.9739	0.7802	1.356	0.0682	1.0117	0.925	0.8335	0.1905	1.5771	0.0401
G3V6C4	UDP-glucose 6-dehydrogenase	8	1.0597	0.478	0.9444	0.6809	1.256	0.011	1.0009	0.9911	1.4008	0.0135
Q63355	Unconventional myosin-Ic	10	1.2333	0.0007	0.8095	0.0071	1.2252	0.0431	1.0652	0.3451	0.8854	0.0253
P31000	Vimentin	110	1.0703	0.0545	1.0991	0.0394	1.1756	0.0018	0.76	0	0.9955	0.9047
<i>Proliferation</i>												
P62268	40S ribosomal protein S23	3	1.0729	0.3955	0.7949	0.0312	1.0116	0.8769	0.9447	0.6609	1.0981	0.4568

Table 8.6. List of modulated proteins ($P < 0.05$) in rBM-MSCs at different ages classified according to their principal biological process using iTRAQ-8plex. I/N= infant vs newborn; Y/I=young vs infant; PP/Y= pre-pubertal vs young; P/PP= pubertal vs pre-pubertal; A/P= adult vs pubertal.

7. SUPPLEMENTS

Accession	Name	Peptides (95%)	I/N	PVal I/N	Y/I	PVal Y/I	PP/Y	PVal PP/Y	P/PP	PVal P/PP	A/P	PVal A/P
M0RD75	40S ribosomal protein S6 (Fragment)	5	1.213	0.0348	0.7478	0.0343	1.0648	0.6105	0.8839	0.3222	1.2172	0.0637
B2RYR8	40S ribosomal protein S8	5	1.156	0.0743	0.7651	0.0113	0.9563	0.6408	1.1034	0.3318	1.0474	0.6037
P29314	40S ribosomal protein S9	10	1.2232	0.0078	0.7297	0.0002	1.1604	0.014	1.0442	0.4378	1.0231	0.6427
P38983	40S ribosomal protein SA	7	1.0045	0.948	0.8267	0.0864	1.0707	0.3666	1.3083	0.0159	0.8177	0.0379
P63039	60 kDa heat shock protein. mitochondrial	14	1.0284	0.7397	1.0424	0.6331	1.0209	0.827	0.7502	0.0126	1.1048	0.3793
Q6PDV7	60S ribosomal protein L10	8	1.2944	0.0232	0.7476	0.0503	1.0811	0.4911	0.9186	0.3735	1.079	0.2893
P41123	60S ribosomal protein L13	4	1.2788	0.1225	0.8351	0.0607	1.0613	0.7175	1.269	0.0179	0.8472	0.0781
P61314	60S ribosomal protein L15	2	1.0608	0.6431	0.9332	0.5211	0.8939	0.228	1.6856	0.0065	0.7429	0.0338
Q0QEW8	60S ribosomal protein L18 (Fragment)	3	0.8899	0.3903	1.0505	0.6391	0.9184	0.5621	1.4963	0.0365	0.7225	0.0735
P62718	60S ribosomal protein L18a	4	1.0118	0.8521	0.8707	0.2832	1.0157	0.9288	1.3147	0.032	0.8694	0.1711
P62832	60S ribosomal protein L23	6	1.2256	0.0212	0.838	0.0334	0.9969	0.9615	0.9723	0.8064	1.1553	0.1309
P83732	60S ribosomal protein L24	7	1.5524	0.0024	0.5064	0.0004	1.2108	0.0391	0.8698	0.2155	1.2834	0.0175
P25886	60S ribosomal protein L29	3	1.5331	0.0443	0.9651	0.7362	1.0984	0.4167	0.8404	0.5923	0.7419	0.2733
P21531	60S ribosomal protein L3	5	1.0552	0.6436	0.8494	0.0879	0.932	0.5476	1.463	0.0213	0.7223	0.0148
Q6P3V9	60S ribosomal protein L4	9	1.419	0.0021	0.627	0.0002	1.0227	0.7849	0.9688	0.6057	1.139	0.0543
P09895	60S ribosomal protein L5	6	0.9424	0.3628	0.9732	0.6933	0.9466	0.5073	1.2345	0.0225	0.8597	0.1305
H7C5Y5	60S ribosomal protein L6	7	1.3496	0.0261	0.6716	0.0068	1.0461	0.66	1.0542	0.451	1.0501	0.6358
Q6P790	60S ribosomal protein L6 (Fragment)	7	1.2191	0.0025	1.0302	0.7281	1.0286	0.6572	0.8965	0.2512	0.987	0.8763

Table 8.6. List of modulated proteins ($P < 0.05$) in rBM-MSCs at different ages classified according to their principal biological process using iTRAQ-8plex. I/N= infant vs newborn; Y/I=young vs infant; PP/Y= pre-pubertal vs young; P/PP= pubertal vs pre-pubertal; A/P= adult vs pubertal.

7. SUPPLEMENTS

Accession	Name	Peptides (95%)	I/N	PVal I/N	Y/I	PVal Y/I	PP/Y	PVal PP/Y	P/PP	PVal P/PP	A/P	PVal A/P
P05426	60S ribosomal protein L7	5	1.3498	0.0462	0.6788	0.065	1.1405	0.3092	0.9309	0.3885	1.0532	0.5387
P85970	Actin-related protein 2/3 complex subunit 2	11	0.9564	0.6557	0.9226	0.2715	1.3327	0.0061	1.0044	0.938	1.0774	0.3839
Q9Z1P2	Alpha-actinin-1	77	0.8727	0.0028	0.8694	0.0002	1.3424	0.0013	0.8164	0.0001	0.9543	0.1358
Q9QXQ0	Alpha-actinin-4	50	1.2074	0.0004	1.1204	0.037	1.0349	0.3567	0.9069	0.2105	1.1419	0.036
Q66HH8	Annexin 5	9	0.9925	0.8998	1.0383	0.7603	0.9707	0.811	0.9909	0.8915	1.4149	0.0034
P45592	Cofilin-1	12	1.2442	0.0041	1.0603	0.5475	1.0804	0.2025	0.9203	0.5481	1.2685	0.011
D3ZH41	Cytoskeleton-associated protein 4 (Predicted)	12	0.7853	0.0004	1.107	0.0513	0.9476	0.3458	0.7919	0.0005	1.2344	0.0033
Q6AYH5	Dynactin subunit 2	3	1.151	0.2739	0.8845	0.3112	1.1661	0.2508	0.8114	0.3778	1.3787	0.0248
P52555	Endoplasmic reticulum resident protein 29	2	1.0186	0.8459	1.3064	0.1141	1.2519	0.2488	0.8626	0.2226	1.5742	0.0319
Q6P3V8	Eukaryotic translation initiation factor 4A1	13	1.0465	0.4461	0.8673	0.0328	1.055	0.416	1.0269	0.6429	0.7893	0.0001
P04937	Fibronectin	17	1.1267	0.3104	0.7887	0.0119	1.2538	0.0001	0.6481	0.0907	2.4985	0.0056
Q6P792	Four and a half LIM domains 1	6	0.7431	0.0006	1.7903	0.0001	1.1108	0.096	0.7768	0.0085	0.8731	0.0375
P11762	Galectin-1 OS=Rattus norvegicus	14	0.7674	0.0204	0.7313	0.053	1.2804	0.0564	0.8213	0.4313	1.1116	0.227
B6DYQ2	Glutathione S-transferase mu 2	5	1.1023	0.4484	1.0507	0.6202	0.8053	0.0678	0.8616	0.3082	1.2838	0.0235
P63245	Guanine nucleotide-binding protein subunit beta-2-like 1	6	1.0188	0.7481	0.8543	0.044	1.0255	0.6962	1.0046	0.963	0.9843	0.8938
Q6P7Q4	Lactoylglutathione lyase	6	0.8942	0.2376	0.9113	0.2336	1.2099	0.0449	0.9186	0.2639	1.0132	0.8509
Q99MZ8	LIM and SH3 domain protein 1	5	1.4773	0.0032	1.0103	0.9316	1.1251	0.1144	0.7622	0.0071	1.3922	0.0031

Table 8.6. List of modulated proteins ($P < 0.05$) in rBM-MSCs at different ages classified according to their principal biological process using iTRAQ-8plex. I/N= infant vs newborn; Y/I=young vs infant; PP/Y= pre-pubertal vs young; P/PP= pubertal vs pre-pubertal; A/P= adult vs pubertal.

7. SUPPLEMENTS

Accession	Name	Peptides (95%)	I/N	PVal I/N	Y/I	PVal Y/I	PP/Y	PVal PP/Y	P/PP	PVal P/PP	A/P	PVal A/P
O08557	N(G).N(G)-dimethylarginine dimethylaminohydrolase 1	4	0.8682	0.4556	2.2145	0.0173	0.5358	0.0395	0.7504	0.1763	1.2909	0.0453
Q6S3A0	Plectin 6	28	1.0437	0.2665	0.9378	0.1139	1.1564	0.0026	0.996	0.9259	1.2269	0.0027
D4A4Z9	Protein Ktn1	7	0.9773	0.8388	0.901	0.2289	1.3423	0.0487	0.7373	0.0131	1.0952	0.3487
D3ZPL5	Protein LOC100361311	10	1.2843	0.0356	0.683	0.017	1.0148	0.8697	0.9663	0.7274	1.1144	0.0623
M0RCY2	Protein LOC683961	6	0.9886	0.9133	0.9596	0.6555	0.761	0.0353	1.4335	0.0202	0.591	0.0003
D3ZN21	Protein RGD1309586	6	0.951	0.6075	0.9746	0.7735	0.957	0.6381	1.2502	0.0226	0.8539	0.0205
D4A6W6	Protein RGD1561333	6	1.7423	0.0038	0.5049	0.0038	1.2265	0.2464	0.8945	0.5405	1.1717	0.2285
D4A6W6	Protein RGD1561333	5	1.1352	0.1387	1.0601	0.5478	0.9173	0.2914	1.5332	0.0034	0.6202	0.0124
F1LT35	Protein RGD1564606 (Fragment)	6	1.1172	0.1379	1.1037	0.4799	1.0681	0.4407	0.772	0.0124	1.2544	0.0157
G3V852	Protein Tln1	38	1.2686	0	1.2229	0	0.8272	0	0.9642	0.3307	1.3768	0
Q4QQV0	Protein Tubb6	22	1.0776	0.4062	0.8668	0.3417	1.2995	0.0298	0.946	0.6332	1.0638	0.6569
Q6P3E1	Rps16 protein (Fragment)	7	1.6881	0.0047	0.5471	0.0061	1.508	0.0481	0.8378	0.1083	1.2384	0.0629
Q9QZR6	Septin-9	6	1.0595	0.4348	0.9334	0.3019	1.2185	0.0277	0.8772	0.1483	1.017	0.8438
Q6LDS4	Superoxide dismutase [Cu-Zn]	6	1.1464	0.0737	1.169	0.0483	0.8679	0.0643	1.0068	0.9549	1.3603	0.0094
P07895	Superoxide dismutase [Mn], mitochondrial	10	0.76	0.2573	0.9976	0.9829	2.2825	0.02	1.074	0.2946	1.3438	0.0046
P28480	T-complex protein 1 subunit alpha	6	0.7782	0.0579	1.5251	0.0086	0.9731	0.7177	1.2381	0.2501	0.9675	0.8659
Q68FQ0	T-complex protein 1 subunit epsilon	4	0.8933	0.2273	1.0047	0.9576	0.9601	0.7021	1.1826	0.1497	0.8175	0.0229
Q6P502	T-complex protein 1 subunit gamma	5	1.0456	0.4189	0.8549	0.0333	1.0502	0.74	1.0936	0.3134	0.9009	0.3475

Table 8.6. List of modulated proteins ($P < 0.05$) in rBM-MSCs at different ages classified according to their principal biological process using iTRAQ-8plex. I/N= infant vs newborn; Y/I=young vs infant; PP/Y= pre-pubertal vs young; P/PP= pubertal vs pre-pubertal; A/P= adult vs pubertal.

7. SUPPLEMENTS

Accession	Name	Peptides (95%)	I/N	PVal I/N	Y/I	PVal Y/I	PP/Y	PVal PP/Y	P/PP	PVal P/PP	A/P	PVal A/P
P11232	Thioredoxin	9	0.9519	0.7004	0.9806	0.8828	1.1098	0.4942	0.9058	0.4438	1.2619	0.0373
Q99PD6	Transforming growth factor beta-1-induced transcript 1 protein	6	1.0858	0.7029	0.7535	0.8138	1.2703	0.2603	0.635	0.0115	0.8607	0.8969
P68370	Tubulin alpha-1A chain OS=Rattus norvegicus GN=Tuba1a PE=1 SV=1	19	1.1996	0.0477	1.1154	0.0721	0.7776	0.0946	0.9411	0.7092	0.7696	0.0004
R9PXU6	Vinculin	57	1.1908	0	0.9981	0.9534	1.4169	0	0.8383	0.0001	1.1453	0

Table 8.6. List of modulated proteins ($P < 0.05$) in rBM-MSCs at different ages classified according to their principal biological process using iTRAQ-8plex. I/N= infant vs newborn; Y/I=young vs infant; PP/Y= pre-pubertal vs young; P/PP= pubertal vs pre-pubertal; A/P= adult vs pubertal.

9. PUBLICATIONS

Review

Proteomic Applications in the Study of Human Mesenchymal Stem Cells

Jesús Mateos¹, Pablo Fernández Pernas^{2,3}, Juan Fafián Labora^{2,3}, Francisco Blanco^{1,2,4} and María del Carmen Arufe^{2,3,*}

¹ Rheumatology Division, ProteoRed/ISCIII, INIBIC-Hospital Universitario A Coruña, A Coruña 15006, Spain; E-Mail: jesus.mateos.martin@sergas.es (J.M.); fblagar@sergas.es (F.B.)

² CIBER-BBN, INIBIC-Hospital Universitario A Coruña, A Coruña 15006, Spain; E-Mail: pablofpernas@gmail.com (P.F.P.); juanlaru_15@hotmail.com (J.F.L.)

³ Department of Medicine, University of A Coruña, A Coruña 15006, Spain

⁴ Department of Medicine, University of Santiago de Compostela, Santiago de Compostela 15782, Spain

* Author to whom correspondence should be addressed; E-Mail: maria.arufe@udc.es.

Received: 4 December 2013; in revised form: 15 January 2014 / Accepted: 26 January 2014 /

Published: 7 February 2014

Abstract: Mesenchymal stem cells (MSCs) are undifferentiated cells with an unlimited capacity for self-renewal and able to differentiate towards specific lineages under appropriate conditions. MSCs are, *a priori*, a good target for cell therapy and clinical trials as an alternative to embryonic stem cells, avoiding ethical problems and the chance for malignant transformation in the host. However, regarding MSCs, several biological implications must be solved before their application in cell therapy, such as safe *ex vivo* expansion and manipulation to obtain an extensive cell quantity amplification number for use in the host without risk accumulation of genetic and epigenetic abnormalities. Cell surface markers for direct characterization of MSCs remain unknown, and the precise molecular mechanisms whereby growth factors stimulate their differentiation are still missing. In the last decade, quantitative proteomics has emerged as a promising set of techniques to address these questions, the answers to which will determine whether MSCs retain their potential for use in cell therapy. Proteomics provides tools to globally analyze cellular activity at the protein level. This proteomic profiling allows the elucidation of connections between broad cellular pathways and molecules that were previously impossible to determine using only traditional biochemical analysis. However; thus far, the results obtained must be orthogonally validated with other approaches. This review will

focus on how these techniques have been applied in the evaluation of MSCs for their future applications in safe therapies.

Keywords: mesenchymal stem cell; proteomic analysis; characterization; differentiation

Abbreviations:

DIGE	difference in-gel electrophoresis
2D-PAGE	two-dimensional polyacrylamide gel electrophoresis
ESI	electrospray ionization
GELFREE	gel-eluted liquid fraction entrapment electrophoresis
IEF	iso-electric focusing
IMAC	immobilized metal ion affinity chromatography
iTRAQ	isobaric tags for relative and absolute quantification
LC	liquid chromatography
LCM	laser capture micro-dissection
MALDI-MSI	matrix-assisted laser desorption ionization mass spectrometry imaging
MSCs	mesenchymal stem cells
¹⁸ O	(18)O-labeling of reactive carbonyl modifications
PCR	polymerase chain reaction
PMF	peptide mass fingerprinting
SELDI-TOF-MS	surface enhanced laser desorption/ionization-time of flight-mass spectrometry
SCX	strong cation exchange
SDS-PAGE	sodium dodecyl sulfate polyacrylamide gel electrophoresis
SID	stable isotope dilution
SILAC	stable isotope labeling by/with amino acids in cell culture
Ti ²⁰	tolerable intake 20

1. Introduction

Mesenchymal stem cells (MSCs) are multipotent cells with an important potential in human regenerative medicine because of their ability to migrate to sites of injury [1], their capability of suppressing the immune response [2] and their accessibility in large numbers from the patient's own bone marrow or fat tissue. It has been increasingly observed that the transplanted MSCs do not necessarily engraft and differentiate at the site of injury, but might exert their therapeutic effects through secreted trophic signals [3]. MSCs secrete a variety of autocrine/paracrine factors that make up the secretome, which supports regenerative processes in the damaged tissue, induces angiogenesis, protects cells from apoptotic cell death and modulates the immune system. The MSC secretome has become a subject of intensive proteomic profiling in the search for and identification of released factors and microvesicles that might be applicable in regenerative medicine. Jointly with the methods for MSC isolation, expansion and differentiation, proteomic secretome analysis of MSC has been increased in use, mainly due to the extensive development of protein separation techniques and mass spectrometry, recently reviewed by Skalnikova *et al.* [4]. This review will focus on the study of the intracellular proteome.

The term proteomics encompasses all research methodologies aimed at qualitative and quantitative study of the proteins, or proteome, present in a cell type, tissue or organism at a given stage of development [5]. In the last decade, there has been an exponential increase in the use of these techniques in translational research, due in large part to the progress in state-of-the-art mass spectrometry. With this technique, developed in the middle of the last century [6], it is possible to calculate, with remarkable accuracy, the mass/charge ratio of any compound that can ionize, as well as the mass/charge ratio of the fragments originated by the collision of the compound with an inert gas. The accuracy in the measurement is so high that it is actually possible to identify the compound. In the case of proteomics, mass spectrometers are designed to identify and quantify peptides and proteins in a very sensitive and high-throughput manner. It has been widely accepted that proteomics can never replace, but complements, genomic information [7,8]. First, unlike what happens in genomics, proteomics studies lack a technique, such as polymerase chain reaction (PCR), to amplify these very low abundance molecules for study. This greatly complicates the study of very scarce proteins, such as growth factors or cytokines [9]. Unfortunately, the wide dynamic range of protein concentration causes the most abundant signal to mask the signal of low-abundance molecules. Finally, post-translational modifications, such as phosphorylation, glycosylation, *etc.*, can completely change the function of a protein, but the total amount thereof does not vary. Due, at least in part, to these limitations, it is now required that the data obtained in individual samples be tested using proteomic techniques, including Western blot or enzyme-linked immuno sorbent assay (ELISA) or even genomic techniques, such as real-time PCR (RT-PCR).

The protein expression profile of MSCs may reveal potential hazards associated with senescence and tumoral transformation that may occur during culture. Proteomic is a valuable tool for human MSC characterization following physiological modifications of the phenotypes of MSCs and identification of possible changes occurring during expansion. Mass spectrometry-based comparative membrane proteomics can enable the identification of novel cancer biomarkers by distinguishing proteins that change membrane localization between normal and malignant tissues and cells. The combination of analyzers and other types of available components has led in recent years to a long list of devices designed specifically for each type of molecule. Specifically, the range of platforms designed for the analysis of peptides and proteins has been adapted specifically to different qualitative and quantitative techniques (Table 1). This review describes proteomic techniques currently applied or prospectively applicable to MSC studies.

Table 1. Studies of mesenchymal stem cells (MSCs) using quantitative proteomic techniques.

Proteomic Technique	MSC Source	Biological significance	Instrument	Ref.
2D-LC-MS/MS	Bone marrow	Characterization	Q-TOF	[10]
2DE-MALDI-TOF/TOF MS	Umbilical cord blood	Characterization	MALDI-TOF/TOF	[11]
2DE-MALDI-TOF-MS	Amniotic fluid	Characterization	MALDI-TOF	[12]
2D-LC-MALDI-MS	Bone marrow	Characterization	MALDI-TOF	[13]
2DE and combined MS and MS/MS	Bone marrow	Characterization	MALDI-TOF/TOF	[14]
2DE and combined MS and MS/MS	Umbilical cord	Characterization	MALDI-TOF/TOF	[14]
2DE and combined MS and MS/MS	Placenta	Characterization	MALDI-TOF/TOF	[14]

Table 1. Cont.

Proteomic Technique	MSC Source	Biological significance	Instrument	Ref.
DIGE-MALDI-TOF/TOF	Bone marrow	Characterization	MALDI-TOF/TOF	[15]
2DE-PMF	Bone marrow	Characterization	MALDI-TOF/TOF	[16]
2DE-PMF	Bone marrow	Characterization	MALDI-TOF/TOF	[17]
GELFREE-LC-MALDI-TOF/TOF	Bone marrow	Characterization	MALDI-TOF/TOF	[18]
2DE-MALDI-TOF-MS	Bone marrow	Extension culture	MALDI-TOF	[19]
2DE-MALDI-TOF-MS	Bone marrow	Extension culture	MALDI-TOF	[20]
2DE-MALDI-TOF-MS/MS	Bone marrow	Extension culture	MALDI-TOF	[21]
2DE-MALDI-TOF-MS/MS	Bone marrow	Extension culture	MALDI-TOF	[22]
SELDI-TOF-MS	Adipose tissue	Extension culture	SELDI-TOF	[23]
2DE coupled MS	Bone marrow	Extension culture	Q-TOF	[24]
2DE-MALDI-MS	Bone marrow	Senescence	MALDI-TOF	[25]
2DE-ESI-Q-TOF-MS/MS	Bone marrow	Senescence	Q-TOF	[26]
DIGE-MALDI-TOF-MS	Bone marrow	Extension culture	MALDI-TOF	[27]
2DE-ESI-MS/MS	Bone marrow	Differentiation	Q-TOF	[28]
LC-MS/MS	Bone marrow	Differentiation	Q-TOF	[29]
DIGE-MALDI-TOF-MS	Bone marrow	Differentiation	MALDI-TOF	[30]
2DE-MALDI-TOF-MS	Bone marrow	Differentiation	MALDI-TOF	[31]
2DE-ESI-Q-TOF-MS/MS	Umbilical cord blood	Differentiation	Q-TOF	[32]
DIGE-MALDI-TOF/TOF-MS/MS	Adipose tissue	Differentiation	MALDI-TOF/TOF	[33]
2DE-MALDI-TOF/MS	Umbilical cord blood	Differentiation	MALDI-TOF	[34]
LC-coupled MS/MS	Intervertebral disc	Differentiation	LTQ	[35]
LC-coupled MS/MS	Bone marrow	Differentiation	LTQ-Orbitrap	[36]
DIGE-MALDI-TOF/TOF-MS/MS	Umbilical cord stroma	Differentiation	MALDI-TOF	[37]
SILAC-LC-MALDI-TOF/TOF-MS/MS	Bone marrow	Differentiation	MALDI-TOF/TOF	[38]
DIGE-MALDI-TOF-MS	Bone marrow	Differentiation	MALDI-TOF	[39]
SILAC-LC-MS/MS	Bone marrow	Differentiation	LTQ-Orbitrap	[40]
DIGE-IEF-MALDI-MS/MS	Bone marrow	Cell Therapy	MALDI-TOF/TOF	[41]
2DE-MALDI-TOF-MS	Bone marrow	Cell Therapy	MALDI-TOF	[42]
DIGE-MALDI-TOF/TOF-MS/MS	Bone marrow	Cell Therapy	MALDI-TOF/TOF	[43]
SDS-PAGE-LC coupled MS/MS	Bone marrow	Cell Therapy	LTQ	[44]
LC-coupled MS/MS	Bone marrow	Cell Therapy	LTQ-Orbitrap	[36]
DIGE-MALDI-TOF-MS	Bone marrow	Cell Therapy	MALDI-TOF	[45]

2DE, two-dimensional electrophoresis; MALDI, matrix-assisted laser desorption ionization; TOF, time of flight; PMF, peptide mass fingerprinting; DIGE, difference in-gel electrophoresis; SELDI, surface enhanced laser desorption/ionization; ESI, electrospray ionization; SILAC, stable isotope labeling by/with amino acids in cell culture; IEF, iso-electric focusing; SDS-PAGE, sodium dodecyl sulfate polyacrylamide gel electrophoresis; LTQ, linear trap quadrupole.

2. Proteomic Techniques

Proteins extracts coming from cultured cells are highly complex protein samples that present a wide dynamic range of concentrations [46]. Fractionation of the sample is therefore necessary to reduce its complexity. Protein quantification performed by colorimetric or fluorometric assays is one of the

weaknesses of the entire proteome flow, because there is currently no universal method to quantify any sample with high accuracy and reproducibility. After fractionation by electrophoretic techniques, isoelectric focusing or chromatographic analysis, subsequent identification and quantification of the peptides allows the identification and quantification of the original proteins using certain algorithms. In some cases, directed digestion is initially performed in solution, followed by peptide fractionation as liquid chromatography (LC), strong cation exchange (SCX) or the off-gel separation of peptides. Alternatively, fractionation of proteins by gel size or isoelectric point is performed first as sodium dodecyl sulfate polyacrylamide gel electrophoresis (SDS-PAGE), two-dimensional polyacrylamide gel electrophoresis (2D-PAGE) or isoelectric focusing (IEF) followed by digestion. Sometimes, the digestion is performed between two successive fractionations, depending on the sample type and complexity. In any case, fractionation of the studied sample clearly decreases the complexity of the resulting fractions, but also lengthens the total time for analysis.

It is currently accepted that a research project based on proteomics should have two phases. In the initial phase of shaping or profiling, the proteome or protein profile of a particular type of sample, such as a cell line or tissue samples at a given stage of development of MSCs, is determined. One way to do this is by two-dimensional electrophoresis (2DE) with subsequent identification of proteins by peptide mass fingerprinting using a matrix-assisted laser desorption ionization-time of flight (MALDI-TOF) platform. In this technique, developed in the early nineteen-nineties by Henzel *et al.* [47], proteins are separated on acrylamide gels in two dimensions, by isoelectric point and by size and can be identified by the pattern of tryptic peptides, *i.e.*, from in-gel digestion with trypsin, which specifically digests protein in lysine and arginine residues. The combination of peptides with a specific ion m/z ratio is unique to each protein and depends only on their amino acid sequence and post-translational modifications of these; so, this is called protein finger printing. The study may simply be qualitative, *i.e.*, determine which peptides and, therefore, proteins are or are not present in the sample, or quantitative, to determine their relative abundance between the conditions under study. Many diseases are not due to the presence or absence of a specific protein or group of proteins, but to changes in the abundance; in this case, it is necessary, as in most cases, to perform a differential metabolic or chemical labeling of the samples. Once differentially labeled, samples are mixed, and thereafter, it becomes a single process in order to reduce experimental variability and bias, assuming, of course, that a precise quantification of the total amount of protein in the different samples has been done previously.

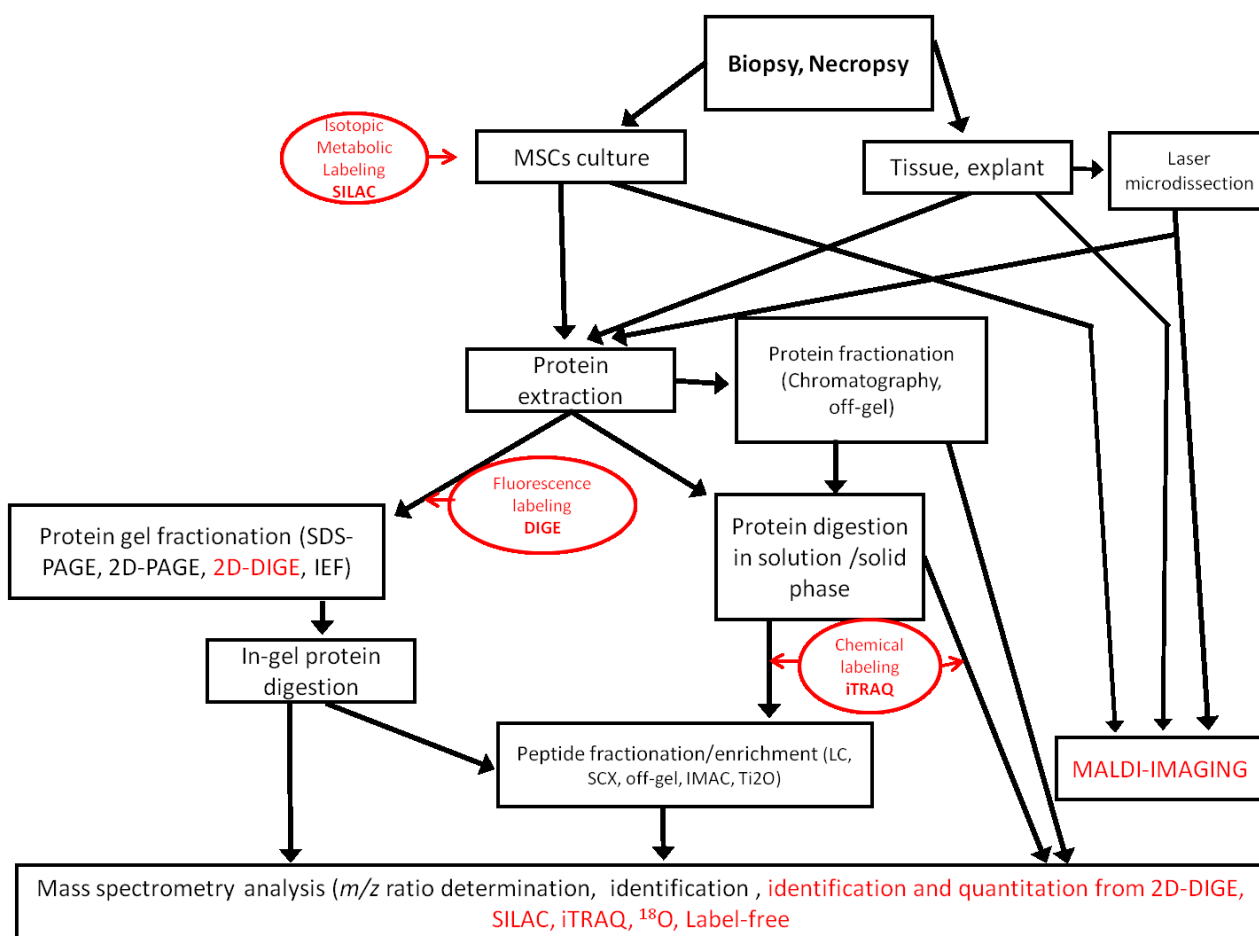
In a second discovery phase, techniques, such as the difference in-gel electrophoresis (DIGE) [48], a variant of the two-dimensional electrophoresis in which the proteins are labeled with a fluorophore, the isobaric tags for relative and absolute quantification (iTRAQ) or stable isotope labeling by/with amino acids in cell culture (SILAC) are used for relative quantification. The analysis is performed on a selected number of samples (in many cases working with sets or pools of samples) and generates a panel of several tens of proteins or peptides modulated between the different conditions under study and, therefore, to be candidates for potential targets, such as a possible drug treatment. Among the most popular platforms used in this phase, we find the linear trap quadrupole (LTQ)-orbitrap and the MALDI-TOF/TOF or LC-MALDI-TOF/TOF when combined with an off-line chromatographic system. At a later stage of verification, the linear trap quadrupole coupled to Fourier transform ion cyclotron resonance (LTQ-FT) or triple quadrupole-ion trap (QqQ-trap) platforms are used, allowing direct absolute quantification of a specific candidate in a large number of individual samples, which is

known as multiple or selected reaction monitoring or assays (MRM and SRM, respectively). This involves the selection of representative peptides of the candidate that must meet certain characteristics and also the synthesis of isotope-labeled versions of that peptides that are spiked in the sample in a known amount, enabling absolute quantification of the protein [49].

In any case, the raw data generated in the analysis of any of the phases are reflected in the mass spectra and fragmentation of peptides, which is a dimensional graphical representation of the different intensities of detected ions against their *m/z* ratio. These data are processed and interpreted by search engines, equipped with powerful software, using complicated algorithms that integrate the raw data with existing protein databases at different sequence repositories (Uniprot, Nextprot, NCBI), allowing the identification and, if appropriate, quantification of the proteins present in the samples analyzed.

The proteomic approach generates informative data on the expression and post-translational modifications of proteins that are useful to assess the true potential of MSCs in regenerative medicine. No matter which technologies are used, proteomic analysis is always a challenge, because the proteome is extremely diverse [50], changes with time and is highly sensitive to pre-analytical conditions (Figure 1).

Figure 1. Workflows used in MSC proteomic analysis. Quantitative methods are indicated in red. SCX, strong cation exchange; IMAC, immobilized metal ion affinity chromatography; iTRAQ, isobaric tags for relative and absolute quantification.



3. Characterization of Mesenchymal Stem Cells

To date, 2DE gel analysis has been the most used proteomic approach for determining cell surface markers of MSCs [51]. The goal is to compare cells from different origins, to follow their differentiation and to ultimately define a specific MSC proteomic signature. One important initial task is the optimization of 2DE protocols, so that they are robust enough to be used in a multisite project. Provansal *et al.* detailed several thorough protocols that can be used for MSCs in culture [50].

Salasznyk *et al.* [10] identified markers for two cell populations, analyzed the expression of human MSC proteins and compared them to those of human osteoblasts using 2D-LC-MS/MS. Among the 755 different proteins identified in both cell populations, two sets of proteins, 247 found only in human MSCs and 158 in human osteoblast cells, were identified. Substantial differences in clusters of proteins responsible for calcium-based signaling and cell adhesion were found between the two cell types.

Feldmann *et al.* [11] achieved protein identification using MALDI-TOF-MS and gel-matching with previously identified databases in their characterization of MSCs from umbilical cord blood after 2DE. Roughly 205 molecules were identified representing 145 different proteins and 60 isoforms or post-translational modifications. The identified proteins could be grouped into several functional categories, including metabolism, folding, cytoskeleton, transcription, signal transduction, protein degradation, detoxification, vesicle/protein transport, cell cycle regulation, apoptosis and calcium homeostasis.

Roubelakis *et al.* [12], using 2DE and the MALDI-TOF-MS approach, have generated, for the first time, a protein map of cultured amniotic fluid MSCs by identifying 261 proteins. They directly compared the amniotic fluid MSC protein map with that of cultured MSCs from bone marrow and found that the functional pattern of the identified proteins from both sources was similar. However, cultured MSCs from amniotic fluid displayed a number of unique proteins related to proliferation and a primitive phenotype, which may be attributable to the distinct features of the two MSC types.

Protein profiling of MSC clonal populations was conducted by 2D-LC-MALDI-MS by Mareddy *et al.* [13]. A total of 83 proteins was identified with high confidence, of which 11 showed differential expressions between subpopulations, including cytoskeletal and structural proteins, calcium binding proteins, cytokinetic proteins and members of the intermediate filament family. This study generated a proteome reference map of bone marrow MSCs from the clonal populations, which will be valuable to better understand the underlying mechanism of MSC self-renewal and differentiation.

Li *et al.* [14], using 2DE and combined MS and MS/MS analysis, identified six differentially expressed proteins among MSC samples derived from bone marrow, umbilical cord and placenta, with five of them known to be involved in cell migration as either migration enhancing or inhibiting proteins. Consistent with their migration capacity, the levels of migration enhancing proteins, including cathepsin B, cathepsin D and prohibitin, were significantly lower in MSCs from umbilical cord when compared with those MSCs from bone marrow and MSCs from placenta. A higher expression for migration inhibiting proteins, including plasminogen activator inhibitor-1 (PAI-1) and manganese superoxide dismutase, was found in MSCs from umbilical cord. They also showed that the overexpression of PAI-1 impaired the migration capacity for bone marrow and placenta MSCs, while silencing of PAI-1 enhanced the migration capacity of umbilical cord MSCs. Their study indicated that migration-related proteins are pivotal in the chain of events governing the migration capacity of MSCs.

Jaishankar *et al.* [15] reported a nuclear proteomic analysis of human embryonic and bone marrow-derived MSCs. Their proteomic screen highlighted a five-fold difference in the expression of Reptin52. They showed, using 2D-DIGE, that Reptin52 is more abundantly expressed in human embryonic stem cells than human MSCs. Moreover, they observed differential expression of Pontin52 and beta-catenin-proteins known to interact with Reptin52, known regulators of beta-catenin, further supporting a role for Wnt signaling in stem cell self-renewal and proliferation.

The expression of a specific set of cell surface cluster differentiation (CD) markers, (CD13, CD29, CD44, CD73, CD90, CD105 and CD166) and the absence of hematopoietic stem cell markers (CD34, CD45, CD117 [52], HLA class I and HLA-DR antigens [16,17]) strongly support the characterization of MSCs using 2DE-PMF. In this regard, it is worth noting that different groups reach similar conclusions using different proteomic platforms.

Mindaye *et al.* [18] achieved the proteomic analysis of membrane proteins, which is challenging and notably underrepresented in proteomic studies, due to the difficulty in the extraction and isolation of lipophilic proteins embedded in lipidic layers. They introduced a new approach, including high pressure-assisted membrane protein extraction, protein fractionation by gel-eluted liquid fraction entrapment electrophoresis [18] and the combined use of liquid chromatography MALDI and ESI tandem mass spectrometry. This report presented the first comprehensive proteomic analysis of the membrane proteome of undifferentiated and culture-expanded human MSCs from bone marrow obtained from different human donors. This new workflow approach enabled them to identify at least two-fold more membrane proteins compared to previous published works. A total of 84 cell surface CDs were identified, including 14 newly-identified CDs.

From these works, we can conclude that cellular compartment pre-fractionation drives to a better characterization of the stem cell populations, which may be defined in the near future by their proteomic profile regardless of their origin, age or stage.

4. *Ex Vivo* Cultivation of Mesenchymal Stem Cells

MSCs hold great promise for cell-based therapeutic use, because of their multipotency and the existence of simple methods for *in vitro* expansion. However, during *in vitro* expansion, MSCs will age and lose their multipotency and proliferation capability. Several studies have provided evidence that homogeneous MSCs preparations can be reproducibly isolated under standardized conditions; however, culture conditions exert a major impact on the transcriptome, proteome and cellular organization of MSCs. Sun *et al.* [19] used 2DE-MALDI-TOF-MS to perform an analysis during the serial subculture of human MSCs. The expression of 12 polypeptides was consistently differentially regulated (eight upregulated and four downregulated) during serial subculture until the seventh passage. The profile changes were concentrated on proteins related to cell cycle, cell morphology and cell proliferation. The data indicated that MSCs underwent morphological changes and a decline in proliferation over the course of serial cultivation. Of the differentially regulated proteins, cytoskeletal components, including annexin A1 and A2, were upregulated, whereas metabolic, synthetic and degradation pathway-related proteins, such as T-complex protein 1 alpha and T-complex protein 1 gamma, were downregulated during the serial subculture of the isolated human MSCs. Wagner *et al.* [20] using 2DE, also identified 136 protein spots from MALDI-TOF-MS corresponding to the differential

protein expression of two human bone marrow populations cultured in two different conditions. Proteins involved in metabolism were more highly expressed in low glucose media, whereas proteins involved in development, morphogenesis, extracellular matrix and differentiation were more highly expressed in a commercial medium.

Lazzarotto-Silva *et al.* [21] compared and analyzed MSCs from human bone marrow at different culture passages using 2DE-MALDI-TOF-MS/MS and observed similar results in all cultures at all passages, suggesting a high degree of similarity among them. The same result was found by Binato *et al.* [22] after image analysis demonstrated that MSCs would have similar protein expression patterns at the first passage. These results suggested that the protein profile of human MSC cultures derived from different passages and different donors were equivalent. However, changes in the proteomic profile of different tissue-derived MSCs during passages in culture have been evaluated using surface enhanced laser desorption/ionization-time of flight-mass spectrometry (SELDI-TOF-MS) by Capra *et al.* [23]. This group evaluated the presence of stable molecular markers in adipose tissue-derived MSCs and found changes in the proteomic phenotype following prolonged *in vitro* culture. The protein with the greatest change in expression during cell culture was identified as calcyclin.

Lee *et al.* [24] used 2DE coupled to MS to identify differentially expressed proteins at the cell membrane level in MSCs growing in basic fibroblast growth factor (bFGF) containing medium; a total of 15 differentially expressed proteins were identified, of which nine of them were upregulated and six downregulated. The expression level of three actin-related proteins, F-actin-capping protein subunit alpha-1, actin-related protein 2/3 complex subunit 2 and myosin regulatory light chain 2, was confirmed by complementary analysis. The results indicated that the expression levels of these three actin-related proteins were important to the bFGF-induced morphological change of MSCs.

Madeira *et al.* [25] studied the molecular mechanisms underlying cellular senescence resulting from extended *ex vivo* cultivation of bone marrow MSCs; they used 2DE-MALDI-MS to demonstrate significant evidence of culture-induced senescence. Proteins involved in cellular structure, the structure of the cytoskeleton, folding and stress response were less abundant in cells with advanced senescence, while proteins involved in energy metabolism, cell cycle regulation, aging and apoptosis were more abundant.

Several studies have reported that caloric restriction increases the proliferation of MSCs and decreases apoptosis. Kim *et al.* [26] examined the effect of low glucose on human bone marrow MSC proliferation compared with that under normal glucose conditions to learn if calorie restrictions modify the proteomic profile of MSCs in culture. 2DE was utilized, and the results found that calorie restriction does not have a significant effect on cell proliferation, reactive oxygen species generation, glucose consumption, population doublings and adipogenic differentiation of MSCs. However, they identified three upregulated proteins and seven downregulated proteins. These results indicate that calorie restriction induced differentially expressed proteins, which may provide further information on the aging and differentiation of stem cells.

A study by Kuboki *et al.* [27] focused on the mechanotransduction of MSCs in response to matrix elasticity. Proteomic profiles of MSCs cultured on tissue culture plastic and soft and stiff matrices were determined using DIGE. The results indicated abundance and organization changes in cytoskeletal proteins, as well as differential regulation of important signaling-related proteins, stress-responsive proteins and also proteins involved in collagen synthesis. The expressions of major

cytoskeletal proteins, including actin, tubulin and vimentin, of cells cultured on the gels were remarkably changed. Significant downregulation of α -tubulin and β -actin was observed on gel samples in comparison to the rigid tissue culture plates. The abundance of expression of vimentin appeared to be highest in MSCs cultured on hard gels. These results suggest that the substrate stiffness significantly affects the expression levels of the cytoskeletal proteins of MSCs, with implications for cellular integrity.

The proteomic studies done on cultivated MSCs show the high plasticity of these cells, which are able to regulate the expression of proteins related to the generation of energy, oxidative stress, cell cycle and apoptosis in order to adapt to the factors and conditions of culture. Furthermore, the importance of the support used for the culture should be mentioned, since this affects the expression of, mainly, proteins related to cytoskeleton structure and cell attachment.

5. The Mesenchymal Stem Cell Differentiation Process

Proteomic techniques help to study changes in the human MSC signaling transduction network during early differentiation lineage commitment. Several works have demonstrated the value of proteomic tools for studying stem cell differentiation and elucidating the underlying molecular mechanisms.

Wang *et al.* [28] used ESI-MS/MS to identify proteins in 2DE from human bone marrow MSCs cultured with transforming growth factor- β (TGF- β). They generated a proteome reference map of MSCs, and they identified approximately 30 proteins with an increase or decrease in the expression or phosphorylation in response to TGF- β . The proteins regulated by TGF- β included cytoskeletal proteins, matrix synthesis proteins, membrane proteins, metabolic enzymes and others. TGF- β increased the expression of smooth muscle alpha-actin and decreased the expression of gelsolin. Overexpression of gelsolin inhibited TGF- β -induced assembly of smooth muscle alpha-actin. On the other hand, reduction of gelsolin expression enhanced the assembly of alpha-actin and actin filaments without significantly affecting alpha-actin expression. These results suggest that TGF- β coordinates the increase of alpha-actin and the decrease of gelsolin to promote MSC differentiation.

Foster *et al.* [29] used LC coupled MS/MS to characterize changes in the expression of membrane protein markers before and after short-term induction of osteoblast differentiation in a cell model of human MSCs. They identified 463 unique proteins with extremely high confidence, including all known markers of human MSCs, such as CD71, CD105, CD166 and CD44, among 148 integral membrane or membrane-anchored proteins and 159 membrane-associated proteins. Twenty-nine integrins and cell adhesion molecules, 20 receptors and 18 Ras-related small GTPases were also identified. Upon osteoblast differentiation, the expression levels of 83 proteins increased by at least two-fold, whereas the levels of another 21 proteins decreased by at least two-fold.

DIGE-LC coupled with tandem MS analysis of the plasma membrane-containing fraction from bone marrow MSCs differentiated towards adipocytes allowed Jeong *et al.* [30] to identify 707 proteins, approximately half of which could be identified as membrane-related proteins. Of particular interest was a subset of ectodomain-containing membrane-bound proteins, which encompasses most known surface markers for MSCs, but also contains a multitude of solute carriers and ATPases. Upon adipogenic differentiation, this proteomic profile was amended to include several proteins involved in lipid metabolism and trafficking, at the expense of, most noticeably, ectoenzymes.

Zhang *et al.* [31] analyzed protein expression profiles of undifferentiated, as well as osteogenic-induced MSCs, using 2DE-MALDI-TOF-MS to investigate the early gene expression in osteoblast differentiation. They generated proteome maps of undifferentiated human MSCs and osteogenic-induced human MSCs on day 3 and day 7. One-hundred two spots with at least two-fold changes in expression and 52 differently expressed proteins were successfully identified. These proteins were classified into more than seven functional categories: metabolism, signal transduction, transcription, calcium-binding protein, protein degradation, protein folding, and others.

Kim *et al.* [32] focused on proteins that were differentially expressed during osteogenic differentiation of MSCs from umbilical cord blood. They analyzed the protein expression inherent to osteogenic differentiation with 2DE-ESI-Q-TOF. Eleven differentially expressed spots were observed between the two groups, before and after differentiation; four proteins were found to be involved in the osteogenic process for the first time: PGAM1, VBP1, hsp27 and β -actin. β -actin might also prove useful as a cytosolic biomarker protein for osteogenesis and could be employed in the quality control of osteoblasts for cell-therapy applications.

Proteomic analysis of human MSCs derived from adipose tissue undergoing osteoblast differentiation was realized by Giusta *et al.* [33]. Phenotypic modifications were observed during the *in vitro* osteogenic differentiation process using DIGE-MALDI-TOF/TOF-MS/MS towards osteoblast-like cells. A total of 51 differentially expressed proteins were identified when comparing the three observed conditions; 16 of these proteins were identified, five of which were overexpressed in the early stages of osteogenic differentiation. All five, superoxide dismutase, lamin A, filamin, heat shock protein-27, cathepsin D and fibulin 1, play a very important role in the formation of osteoprogenitor cells. The identification of these proteins opened new ways for their use as biomarkers for the detection of cells undergoing osteogenesis.

Kim *et al.* [34] realized 2DE-MALDI-TOF-MS to study the direct differentiation of MSC from umbilical cord blood towards osteoblasts. They found the 308 spots that were identified during the differentiation process. Sixteen of these proteins were identified with a mean OD (optical density) ratio >30 and were acting in the extracellular region, cytosol or mitochondria, while 20 of these proteins with a mean OD ratio <0.1 had high catalytic activity. These results provide an initial proteomic database for umbilical cord blood MSCs differentiation.

Human MSCs differentiated towards chondrocytic cells with conditioned medium derived from porcine notochordal cells in native tissue or in alginate beads, and compared with chondrogenic (TGF β -3) or basal medium, were studied by Purmessur *et al.* [35]. Dried peptides subjected to LC-coupled MS/MS for detection indicated the highest levels of glycosaminoglycan (GAG), as well as the upregulation of SOX9 and Collagen II gene expression in MSCs differentiated towards chondrocyte cells in medium from porcine notochordal cells.

Protein phosphorylation plays a critical role in the signaling transduction network during early human MSCs osteogenic lineage commitment. Human MSCs cultured in osteogenic induction medium were analyzed using LC-coupled MS/MS by Lo *et al.* [36]. They observed a dramatic loss of the protein phosphorylation level after one day of osteogenic induction. Pathway analysis of the resulting phosphoproteins revealed a high correlation with cell proliferation and protein synthesis pathways. During osteogenic differentiation, differentially expressed phosphoproteins demonstrated the dynamic alterations in cytoskeleton at early stages of differentiation.

De la Fuente *et al.* [37] followed protein profile changes during the chondrogenic differentiation process of MSCs from umbilical cord stroma using DIGE-MALDI-TOF/TOF-MS/MS. A total of 97 spots were modulated during the chondrogenesis process; 54 of these spots were identified as 39 different proteins and 15 isoforms. Of the 39 different proteins identified, 15 were downregulated, 21 were upregulated and three were up- and down-regulated at different phases of the chondrogenic process.

Rocha *et al.* [38] applied the SILAC technique for the quantitative analysis of protein modulation during the chondrogenic differentiation process of human MSCs from bone marrow. They could identify 622 different proteins by LC-MALDI-TOF/TOF-MS/MS analysis and found 65 proteins whose abundance was significantly modulated between day 2 and day 14 of chondrogenesis. Fibronectin, gelsolin, vimentin, alpha-ATPase, mitochondrial superoxide dismutase and cyclophilin A were increased at day 14 compared to day 2 of chondrogenic induction, thus being markers of the enhanced extracellular matrix synthesis, cell adhesion, metabolism and response to stress processes that take place in the early steps of chondrogenesis.

Herencia *et al.* [39] evaluated the role of Wnt/ β -catenin activation during human MSC differentiation into hepatocytes. The differentiation to hepatocytes was achieved using two different conditioned media. Comparison of both differentiation protocols by DIGE revealed the differential expression of 11 proteins with altered expression in hepatocellular carcinoma. In one of these protocols, β -catenin nuclear translocation and the upregulation of genes related to the Wnt/ β -catenin pathway, such as Lrp5 and Fzd3, as well as the oncogenes, c-myc and p53, were observed. In the other protocol, Wnt/ β -catenin was inactivated. Hepatocytes with nuclear translocation of β -catenin also had abnormal cellular proliferation and expressed membrane proteins involved in hepatocellular carcinoma, metastatic behavior and cancer stem cells. Further, these cells had also an increased auto-renewal capability, as shown in a spheroid formation assay. Cathepsin B and D, adenine phosphoribosyltransferase, triosephosphate isomerase, inorganic pyrophosphatase, peptidyl-prolyl *cis*-trans isomerase A or lactate dehydrogenase β -chain were upregulated only with the protocol associated with Wnt signaling activation, while other proteins involved in tumor suppression, such as transgelin or tropomyosin β -chain, were downregulated in this protocol.

Alves *et al.* [40] used SILAC to study the effect of activin A on the osteogenic differentiation of MSCs from bone marrow. They found 104 proteins changed more than 1.5-fold following activin A treatment. More than half of these proteins, 74 proteins, were downregulated by activin A, while only 30 proteins were upregulated. They observed changes in the expression of collagen XII, osteonectin and several cytoskeleton-binding proteins. Moreover, in osteoblasts differentiated from MSCs, matrix vesicle production was deficient, containing a very low expression of annexin proteins.

Proteomics provides, therefore, very valuable information in directed differentiation studies of MSCs. All the works above have generated new knowledge on the metabolic pathways modulated during the differentiation, thus permitting a better understanding of the processes. The precision and accuracy of the techniques allow the detection of very subtle changes in the expression of proteins or in their phosphorylation state. It is also remarkable that proteomics has permitted the detection in cultured MSCs of the activation of oncogenic factors by certain culture conditions, an undesirable process when it comes to the use of these cells in therapeutic treatment.

6. Cellular Therapy with Mesenchymal Stem Cell

MSCs have emerged as a promising tool for treating degenerative or incurable diseases. Proteomic techniques provide a comprehensive basis for understanding the potential effect of MSCs on tissue repair and regeneration. Knowledge of the molecular mechanisms governing the different adult lineages differentiation process is critical to the development of therapeutic applications for human diseases.

Seshi B *et al.* [41] reported a 2D-DIGE protocol in which complex protein samples from normal and leukemic human bone marrow mesenchymal progenitor cells were used as model samples for a combination of liquid-phase IEF with DIGE. Using liquid-phase IEF, the normal and leukemic cells were pre-fractionated into five sub-proteomes after multiplexing, but prior to DIGE. This analysis mapped protein identities to 128 mesenchymal progenitor cell proteins with at least one unique peptide match at >95% confidence. Of these proteins, 72 (56%) were expressed more than 1.25-fold higher or lower in leukemic cells compared with normal cells ($p < 0.05$). These data were used to infer gene ontology biological processes that may be altered in leukemic bone marrow mesenchymal progenitor cells.

The first proteomic analysis of human MSCs after exposure to shear stress was realized by Yi *et al.* [42] using 2DE and MALDI-TOF-MS. Overall, 32 protein spots were identified with high confidence. Thirteen of these proteins were found to be consistently regulated by over two-fold after 3 dyn/cm² shear stress treatment for six hours; 10 were upregulated and three downregulated.

DIGE-MALDI-TOF/TOF was utilized by Zhuang *et al.* [43] to analyze the differential proteome of bone marrow-derived MSCs from adolescent idiopathic scoliosis. A total of 41 significantly altered protein spots were detected, of which 34 were identified, representing 25 distinct gene products. Among these proteins, five related to bone growth and development, including pyruvate kinase M2, annexin A2, heat shock 27 kDa protein, γ -actin, and β -actin, were found to be dysregulated. At the protein level, the results supported the previous hypothesis that the decreased osteogenic differentiation ability of MSCs is one of the mechanisms leading to osteopenia in adolescent idiopathic scoliosis.

Recent studies have shown that microvesicles from MSCs contribute to the recovery of damaged tissues in animal disease models. Kim *et al.* [44] profiled the MSC microvesicles proteome from bone marrow to investigate its therapeutic effects. Seven-hundred thirty proteins were identified by LC coupled MS/MS analysis of MSC microvesicles separated by SDS-PAGE. This proteome included five positive and two variable known markers of MSCs, but no negative markers. In addition, 43 surface receptors and signaling molecules controlling self-renewal and differentiation of MSCs were identified. This analysis showed that cellular processes represented by the MSC microvesicle proteins include cell proliferation, adhesion, migration and morphogenesis. The integration of the self-renewal of MSCs and differentiation-related genes that can be associated with the therapeutic effects of MSC microvesicles includes: surface receptors; signaling molecules (CDC42 and VAV2; cell adhesion); and MSC-associated antigens (CD109, CD151, CD248 and CD276). These proteomes provide a comprehensive basis for understanding their potential effect on MSC microvesicle tissue repair and regeneration.

Dynamic changes in the phosphoproteomic profiles of human MSCs during osteogenic differentiation and revealed potential candidates mediating the osteogenic commitment of human MSCs shown by

liquid chromatography tandem mass spectrometry [36] may shed light on the development of new therapeutic targets for metabolic bone diseases, such as osteoporosis and osteomalacia.

Han S *et al.* [45] studied differential proteins expressed in the MSCs of patients with degenerative scoliosis. They compared MSCs from patients with degenerative scoliosis and patients with lumbar spinal stenosis. The MSC samples were analyzed by DIGE-MALDI-TOF-MS to find the differential proteins. They found 115 spots that were expressed differently in the MSCs of degenerative scoliosis patient; 44 proteins were identified. Of these proteins, PIAS2, NDUFA2 and TRIM 68 were upregulated in degenerative scoliosis. This information from this proteomics analysis will be useful in understanding the pathophysiology of degenerative scoliosis and opens further lines of investigation on the functional pathway, the specificity and the mechanism of action of these proteins.

Proteomic profiling has provided a variety of novel molecular procedures that can form the basis for more in-depth investigations into the effects of shear stress *in vitro* human MSCs proliferation, differentiation and apoptosis; this may, in turn, significantly influence applications in stem cell therapy and tissue regeneration.

7. Outlook and Perspectives

Liquid chromatography-multiple reaction monitoring mass spectrometry of peptides using stable isotope dilution [53] provides a powerful tool for targeted protein quantification. However, the high cost of labeled peptide standards for stable isotope dilution (SID) is an obstacle to multiple reaction monitoring studies. Zhang *et al.* [53] compared SID to a labeled reference peptide (LRP) method, which uses a single labeled peptide as a reference standard for all measured peptides, and a label-free (LF) approach, in which quantification is based on the analysis of un-normalized peak areas for detected MRM transitions. They concluded that the LRP and LF methods provide cost-effective alternatives to SID for many quantitative liquid chromatography-multiple reaction monitoring mass spectrometry applications. These procedures have not yet been applied to study the application of MSCs to cell therapy, but offer this opportunity. Proteomic differential displays could help to increase the cell therapies with MSCs through specific adjustments based on these displays.

Promising techniques need special mention here. Matrix assisted laser desorption ionization mass spectrometry imaging (MALDI-MSI) and laser micro-dissection are currently under expansion and development. The MALDI-MSI combines high resolution power and the ability to monitor a large number of proteins in a single analysis feature of the mass spectrometry and has the advantage of being able to apply histomorphologic techniques, including providing visual information about the spatial distribution of analytes. The approach is as simple as a laser “sweep” with a given spatial resolution, 50 microns or less, of a tissue, cut with histological techniques for mass spectrometry, to determine the intensity at each pixel of a certain range of m/z . In practice, this involves making a two-dimensional map of the distribution of ions (peptides, lipids, sugars) in a histological section. Although, at first, it was successful only in soft tissues (brain, kidney, lung, *etc.*) [54,55], investigators have recently begun to utilize it successfully in tissues, such as cartilage [56]. The laser capture micro-dissection (LCM) technique identifies LCM regions corresponding to individual cells or groups of cells in tissue sections, using a laser coupled to a microscope. The resulting sections are deposited in micro-tubes for analysis, in this case, an extraction of proteins that can be further examined with

differential labeling to, for example, determine the differential proteome of cells or groups of adjacent cells in the same tissue [57]. This technique opens possibilities to study small groups of MSCs undergoing cell division after differentiation.

8. Conclusions

To summarize, applied mass spectrometry proteomics has enabled a breakthrough in resolving the power and speed of analysis. Few techniques have proven valid for detection, analysis and quantification, in a single experiment, of many analytes; mass spectrometry is one of them. Thus far, 2D-based proteomic strategies have been primarily used to characterize MSCs. In the future, it will be essential to use gel-free-based strategies to delve deeper into the characteristic proteomes of different MSC populations. While increasingly specific and sensitive equipment is launched on the market every year, clinical validation by other, even more sensitive techniques, such as RT-PCR and immunoassays, is still needed.

Acknowledgements

This review was supported by Instituto de Salud Carlos III N° Expediente PI11/02799 Fondos Europeos de Desarrollo Regional (FEDER).

Author Contributions

J.M. drafted the manuscript and participated in its design and coordination. P.F.P, J.F.L. and F.B. participated in its design and coordination. M.C.A. conceived the study, participated in its design and coordination and helped to draft the manuscript. She has given final approval of the version to be published.

Conflicts of Interest

The authors declare no conflict of interest.

References

1. Park, D.; Spencer, J.A.; Koh, B.I.; Kobayashi, T.; Fujisaki, J.; Clemens, T.L.; Lin, C.P.; Kronenberg, H.M.; Scadden, D.T. Endogenous bone marrow MSCs are dynamic, fate-restricted participants in bone maintenance and regeneration. *Cell Stem Cell* **2012**, *10*, 259–272.
2. Huang, A.H.; Snyder, B.R.; Cheng, P.H.; Chan, A.W. Putative dental pulp-derived stem/stromal cells promote proliferation and differentiation of endogenous neural cells in the hippocampus of mice. *Stem Cells* **2008**, *26*, 2654–2663.
3. Hayashi, E.; Hosoda, T. Therapeutic application of cardiac stem cells and other cell types. *BioMed Res. Int.* **2013**, *2013*, e736815.
4. Skalnikova, H.K. Proteomic techniques for characterisation of mesenchymal stem cell secretome. *Biochimie* **2013**, *95*, 2196–2211
5. Mann, M.; Højrup, P.; Roepstorff, P. Use of mass spectrometric molecular weight information to identify proteins in sequence databases. *Biol. Mass Spectrom.* **1993**, *22*, 338–345.


6. Nier, A.O. Determination of isotopic masses and abundances by mass spectrometry. *Science* **1955**, *121*, 737–744.
7. Ardekani, A.M.; Akhondi, M.M.; Sadeghi, M.R. Application of genomic and proteomic technologies to early detection of cancer. *Arch. Iran Med.* **2008**, *11*, 427–434.
8. Mittal, V.; Nolan, D.J. Genomics and proteomics approaches in understanding tumor angiogenesis. *Expert Rev. Mol. Diagn.* **2007**, *7*, 133–147.
9. Choi, Y.S. Reaching for the deep proteome: Recent nano liquid chromatography coupled with tandem mass spectrometry-based studies on the deep proteome. *Arch. Pharm. Res.* **2012**, *35*, 1861–1870.
10. Salasznyk, R.M.; Westcott, A.M.; Klees, R.F.; Ward, D.F.; Xiang, Z.; Vandenberg, S.; Bennett, K.; Plopper, G.E. Comparing the protein expression profiles of human mesenchymal stem cells and human osteoblasts using gene ontologies. *Stem Cells Dev.* **2005**, *14*, 354–366.
11. Feldmann, R.E.; Bieback, K.; Maurer, M.H.; Kalenka, A.; Bürgers, H.F.; Gross, B.; Hunzinger, C.; Klüter, H.; Kuschinsky, W.; Eichler, H. Stem cell proteomes: A profile of human mesenchymal stem cells derived from umbilical cord blood. *Electrophoresis* **2005**, *26*, 2749–2758.
12. Roubelakis, M.G.; Pappa, K.I.; Bitsika, V.; Zagoura, D.; Vlahou, A.; Papadaki, H.A.; Antsaklis, A.; Anagnou, N.P. Molecular and proteomic characterization of human mesenchymal stem cells derived from amniotic fluid: Comparison to bone marrow mesenchymal stem cells. *Stem Cells Dev.* **2007**, *16*, 931–952.
13. Mareddy, S.; Broadbent, J.; Crawford, R.; Xiao, Y. Proteomic profiling of distinct clonal populations of bone marrow mesenchymal stem cells. *J. Cell Biochem.* **2009**, *106*, 776–786.
14. Li, G.; Zhang, X.A.; Wang, H.; Wang, X.; Meng, C.L.; Chan, C.Y.; Yew, D.T.; Tsang, K.S.; Li, K.; Tsai, S.N.; *et al.* Comparative proteomic analysis of mesenchymal stem cells derived from human bone marrow, umbilical cord, and placenta: Implication in the migration. *Proteomics* **2009**, *9*, 20–30.
15. Jaishankar, A.; Barthelery, M.; Freeman, W.; Salli, U.; Ritty, T.; Vrana, K. Human embryonic and mesenchymal stem cells express different nuclear proteomes. *Stem Cells Dev.* **2009**, *18*, 793–802.
16. Roche, S.; Delorme, B.; Oostendorp, R.A.; Barbet, R.; Caton, D.; Noel, D.; Boumediene, K.; Papadaki, H.A.; Cousin, B.; Crozet, C.; *et al.* Comparative proteomic analysis of human mesenchymal and embryonic stem cells: towards the definition of a mesenchymal stem cell proteomic signature. *Proteomics* **2009**, *9*, 223–232.
17. Roche, S.; D'Ippolito, G.; Gomez, L.A.; Bouckenooghe, T.; Lehmann, S.; Montero-Menei, C.N.; Schiller, P.C. Comparative analysis of protein expression of three stem cell populations: Models of cytokine delivery system *in vivo*. *Int. J. Pharm.* **2013**, *440*, 72–82.
18. Mindaye, S.T.; Ra, M.; Lo Surdo, J.; Bauer, S.R.; Alterman, M.A. Improved proteomic profiling of the cell surface of culture-expanded human bone marrow multipotent stromal cells. *J. Proteomics* **2013**, *78*, 1–14.
19. Sun, H.J.; Bahk, Y.Y.; Choi, Y.R.; Shim, J.H.; Han, S.H.; Lee, J.W. A proteomic analysis during serial subculture and osteogenic differentiation of human mesenchymal stem cell. *J. Orthop. Res.* **2006**, *24*, 2059–2071.

20. Wagner, W.; Feldmann, R.E.; Seckinger, A.; Maurer, M.H.; Wein, F.; Blake, J.; Krause, U.; Kalenka, A.; Bürgers, H.F.; Saffrich, R.; *et al.* The heterogeneity of human mesenchymal stem cell preparations—Evidence from simultaneous analysis of proteomes and transcriptomes. *Exp. Hematol.* **2006**, *34*, 536–548.
21. Lazzarotto-Silva, C.; Binato, R.; Rocher, B.D.; Costa, J.A.; Pizzatti, L.; Bouzas, L.F.; Abdelhay, E. Similar proteomic profiles of human mesenchymal stromal cells from different donors. *Cytotherapy* **2009**, *11*, 268–277.
22. Binato, R.; de Souza Fernandez, T.; Lazzarotto-Silva, C.; Du Rocher, B.; Mencialha, A.; Pizzatti, L.; Bouzas, L.F.; Abdelhay, E. Stability of human mesenchymal stem cells during *in vitro* culture: Considerations for cell therapy. *Cell Prolif.* **2013**, *46*, 10–22.
23. Capra, E.; Beretta, R.; Parazzi, V.; Viganò, M.; Lazzari, L.; Baldi, A.; Giordano, R. Changes in the proteomic profile of adipose tissue-derived mesenchymal stem cells during passages. *Proteome Sci.* **2012**, *10*, e46.
24. Lee, S.K.; Kim, Y.; Kim, S.S.; Lee, J.H.; Cho, K.; Lee, S.S.; Lee, Z.W.; Kwon, K.H.; Kim, Y.H.; Suh-Kim, H.; *et al.* Differential expression of cell surface proteins in human bone marrow mesenchymal stem cells cultured with or without basic fibroblast growth factor containing medium. *Proteomics* **2009**, *9*, 4389–4405.
25. Madeira, A.; da Silva, C.L.; dos Santos, F.; Camafeita, E.; Cabral, J.M.; Sá-Correia, I. Human mesenchymal stem cell expression program upon extended *ex-vivo* cultivation, as revealed by 2-DE-based quantitative proteomics. *PLoS One* **2012**, *7*, e43523.
26. Kim, H.J.; Ji, B.R.; Kim, J.S.; Lee, H.N.; Ha, D.H.; Kim, C.W. Proteomic analysis of proteins associated with cellular senescence by calorie restriction in mesenchymal stem cells. *In Vitro Cell Dev. Biol. Anim.* **2012**, *48*, 186–195.
27. Kuboki, T.; Kantawong, F.; Burchmore, R.; Dalby, M.J.; Kidoaki, S. 2D-DIGE proteomic analysis of mesenchymal stem cell cultured on the elasticity-tunable hydrogels. *Cell Struct. Funct.* **2012**, *37*, 127–139.
28. Wang, D.; Park, J.S.; Chu, J.S.; Krakowski, A.; Luo, K.; Chen, D.J.; Li, S. Proteomic profiling of bone marrow mesenchymal stem cells upon transforming growth factor beta1 stimulation. *J. Biol. Chem.* **2004**, *279*, 43725–43734.
29. Foster, L.J.; Zeemann, P.A.; Li, C.; Mann, M.; Jensen, O.N.; Kassem, M. Differential expression profiling of membrane proteins by quantitative proteomics in a human mesenchymal stem cell line undergoing osteoblast differentiation. *Stem Cells* **2005**, *23*, 1367–1377.
30. Jeong, J.A.; Ko, K.M.; Park, H.S.; Lee, J.; Jang, C.; Jeon, C.J.; Koh, G.Y.; Kim, H. Membrane proteomic analysis of human mesenchymal stromal cells during adipogenesis. *Proteomics* **2007**, *7*, 4181–4191.
31. Zhang, A.X.; Yu, W.H.; Ma, B.F.; Yu, X.B.; Mao, F.F.; Liu, W.; Zhang, J.Q.; Zhang, X.M.; Li, S.N.; Li, M.T.; *et al.* Proteomic identification of differently expressed proteins responsible for osteoblast differentiation from human mesenchymal stem cells. *Mol. Cell Biochem.* **2007**, *304*, 167–179.
32. Kim, J.S.; Lee, H.K.; Kim, M.R.; Kim, P.K.; Kim, C.W. Differentially expressed proteins of mesenchymal stem cells derived from human cord blood (hUCB) during osteogenic differentiation. *Biosci. Biotechnol. Biochem.* **2008**, *72*, 2309–2317.

33. Giusta, M.S.; Andrade, H.; Santos, A.V.; Castanheira, P.; Lamana, L.; Pimenta, A.M.; Goes, A.M. Proteomic analysis of human mesenchymal stromal cells derived from adipose tissue undergoing osteoblast differentiation. *Cytotherapy* **2010**, *12*, 478–490.
34. Kim, S.; Min, W.K.; Chun, S.; Lee, W.; Chung, H.J.; Choi, S.J.; Yang, S.E.; Yang, Y.S.; Yoo, J.I. Protein expression profiles during osteogenic differentiation of mesenchymal stem cells derived from human umbilical cord blood. *Tohoku J. Exp. Med.* **2010**, *221*, 141–150.
35. Purmessur, D.; Schek, R.M.; Abbott, R.D.; Ballif, B.A.; Godburn, K.E.; Iatridis, J.C. Notochordal conditioned media from tissue increases proteoglycan accumulation and promotes a healthy nucleus pulposus phenotype in human mesenchymal stem cells. *Arthritis Res. Ther.* **2011**, *13*, R81.
36. Lo, T.; Tsai, C.F.; Shih, Y.R.; Wang, Y.T.; Lu, S.C.; Sung, T.Y.; Hsu, W.L.; Chen, Y.J.; Lee, O.K. Phosphoproteomic analysis of human mesenchymal stromal cells during osteogenic differentiation. *J. Proteome Res.* **2012**, *11*, 586–598.
37. De la Fuente, A.; Mateos, J.; Lesende-Rodríguez, I.; Calamia, V.; Fuentes-Boquete, I.; de Toro, F.J.; Arufe, M.C.; Blanco, F.J. Proteome analysis during chondrocyte differentiation in a new chondrogenesis model using human umbilical cord stroma mesenchymal stem cells. *Mol. Cell Proteomics* **2012**, *11*, M111.010496.
38. Rocha, B.; Calamia, V.; Mateos, J.; Fernández-Puente, P.; Blanco, F.J.; Ruiz-Romero, C. Metabolic labeling of human bone marrow mesenchymal stem cells for the quantitative analysis of their chondrogenic differentiation. *J. Proteome Res.* **2012**, *11*, 5350–5361.
39. Herencia, C.; Martínez-Moreno, J.M.; Herrera, C.; Corrales, F.; Santiago-Mora, R.; Espejo, I.; Barco, M.; Almadén, Y.; de la Mata, M.; Rodríguez-Ariza, A.; *et al.* Nuclear translocation of β -catenin during mesenchymal stem cells differentiation into hepatocytes is associated with a tumoral phenotype. *PLoS One* **2012**, *7*, e34656.
40. Alves, R.D.; Eijken, M.; Bezstarosti, K.; Demmers, J.A.; van Leeuwen, J.P. Activin A suppresses osteoblast mineralization capacity by altering extracellular matrix composition and impairing matrix vesicle production. *Mol. Cell Proteomics* **2013**, doi:10.1074/mcp.M112.024927.
41. Seshi, B. Proteomics strategy based on liquid-phase IEF and 2-D DIGE: Application to bone marrow mesenchymal progenitor cells. *Proteomics* **2007**, *7*, 1984–1999.
42. Yi, W.; Sun, Y.; Wei, X.; Gu, C.; Dong, X.; Kang, X.; Guo, S.; Dou, K. Proteomic profiling of human bone marrow mesenchymal stem cells under shear stress. *Mol. Cell Biochem.* **2010**, *341*, 9–16.
43. Zhuang, Q.; Li, J.; Wu, Z.; Zhang, J.; Sun, W.; Li, T.; Yan, Y.; Jiang, Y.; Zhao, R.C.; Qiu, G. Differential proteome analysis of bone marrow mesenchymal stem cells from adolescent idiopathic scoliosis patients. *PLoS One* **2011**, *6*, e18834.
44. Kim, H.S.; Choi, D.Y.; Yun, S.J.; Choi, S.M.; Kang, J.W.; Jung, J.W.; Hwang, D.; Kim, K.P.; Kim, D.W. Proteomic analysis of microvesicles derived from human mesenchymal stem cells. *J. Proteome Res.* **2012**, *11*, 839–849.
45. Han, S.; Zhu, Y.; Wu, Z.; Zhang, J.; Qiu, G. The differently expressed proteins in MSCs of degenerative scoliosis. *J. Orthop. Sci.* **2013**, *18*, 885–892.
46. Ståhlberg, A.; Thomsen, C.; Ruff, D.; Åman, P. Quantitative PCR analysis of DNA, RNAs, and proteins in the same single cell. *Clin. Chem.* **2012**, *58*, 1682–1691.

47. Henzel, W.J.; Billeci, T.M.; Stults, J.T.; Wong, S.C.; Grimley, C.; Watanabe, C. Identifying proteins from two-dimensional gels by molecular mass searching of peptide fragments in protein sequence databases. *Proc. Natl. Acad. Sci. USA* **1993**, *90*, 5011–5015.
48. Knowles, M.R.; Cervino, S.; Skynner, H.A.; Hunt, S.P.; de Felipe, C.; Salim, K.; Meneses-Lorente, G.; McAllister, G.; Guest, P.C. Multiplex proteomic analysis by two-dimensional differential in-gel electrophoresis. *Proteomics* **2003**, *3*, 1162–1171.
49. Percy, A.J.; Parker, C.E.; Borchers, C.H. Pre-analytical and analytical variability in absolute quantitative MRM-based plasma proteomic studies. *Bioanalysis* **2013**, *5*, 2837–2856.
50. Provansal, M.; Jorgensen, C.; Lehmann, S.; Roche, S. Two dimensional gel electrophoresis analysis of mesenchymal stem cells. *Methods Mol. Biol.* **2011**, *698*, 431–442.
51. Maurer, M.H. Proteomic definitions of mesenchymal stem cells. *Stem Cells Int.* **2011**, *2011*, e704256.
52. Huang, P.; Lin, L.M.; Wu, X.Y.; Tang, Q.L.; Feng, X.Y.; Lin, G.Y.; Lin, X.; Wang, H.W.; Huang, T.H.; Ma, L. Differentiation of human umbilical cord Wharton's jelly-derived mesenchymal stem cells into germ-like cells *in vitro*. *J. Cell Biochem.* **2010**, *109*, 747–754.
53. Zhang, H.; Liu, Q.; Zimmerman, L.J.; Ham, A.J.; Slebos, R.J.; Rahman, J.; Kikuchi, T.; Massion, P.P.; Carbone, D.P.; Billheimer, D.; *et al.* Methods for Peptide and protein quantitation by liquid chromatography-multiple reaction monitoring mass spectrometry. *Mol. Cell Proteomics* **2011**, *10*, M110.006593.
54. Louie, K.B.; Bowen, B.P.; McAlhany, S.; Huang, Y.; Price, J.C.; Mao, J.H.; Hellerstein, M.; Northen, T.R. Mass spectrometry imaging for *in situ* kinetic histochemistry. *Sci. Rep.* **2013**, *3*, e1656.
55. Pirman, D.A.; Reich, R.F.; Kiss, A.; Heeren, R.M.; Yost, R.A. Quantitative MALDI tandem mass spectrometric imaging of cocaine from brain tissue with a deuterated internal standard. *Anal. Chem.* **2013**, *85*, 1081–1089.
56. Cillero-Pastor, B.; Eijkel, G.B.; Kiss, A.; Blanco, F.J.; Heeren, R.M. Matrix-assisted laser desorption ionization-imaging mass spectrometry: A new methodology to study human osteoarthritic cartilage. *Arthritis Rheum.* **2013**, *65*, 710–720.
57. Mukherjee, S.; Rodriguez-Canales, J.; Hanson, J.; Emmert-Buck, M.R.; Tangrea, M.A.; Prieto, D.A.; Blonder, J.; Johann, D.J. Proteomic analysis of frozen tissue samples using laser capture microdissection. *Methods Mol. Biol.* **2013**, *1002*, 71–83.

SCIENTIFIC REPORTS



OPEN

Influence of age on rat bone-marrow mesenchymal stem cells potential

Received: 25 August 2015
Accepted: 20 October 2015
Published: 19 November 2015

J. Fafián-Labora¹, P. Fernández-Pernas¹, I. Fuentes¹, J. De Toro¹, N. Oreiro², S. Sangiao-Alvarellos³, J. Mateos¹ & M.C. Arufe¹

Mesenchymal stem cells promising role in cell-based therapies and tissue engineering appears to be limited due to a decline of their regenerative potential with increasing donor age. Six age groups from bone marrow mesenchymal stem cells of Wistar rats were studied (newborn, infant, young, pre-pubertal, pubertal and adult). Quantitative proteomic assay was performed by iTRAQ using an 8-plex iTRAQ labeling and the proteins differentially expressed were grouped in pluripotency, proliferative and metabolism processes. Proliferation makers, CD117 and Ki67 were measured by flow cytometry assay. Real time polymerase chain reaction analysis of pluripotency markers *Rex1*, *Oct4*, *Sox2* and *Nanog* were done. Biological differentiation was realized using specific mediums for 14 days to induce osteogenesis, adipogenesis or chondrogenesis and immunostain analysis of differentiated cells resulting were done. Enzyme immunoassay analysis of several enzymes as L-lactate dehydrogenase and glucose-6-phosphate isomerase were also done to validate iTRAQ data. Taking together these results indicate for the first time that mesenchymal stem cells have significant differences in their proliferative, pluripotency and metabolism profiles and those differences are age depending.

Mesenchymal Stem Cells (MSCs) have self-renewal capacity and multiple differentiation potentials, and *a priori*, could play important roles in regenerative medicine. The promising role of MSCs in cell-based therapies is their trophic, paracrine and immunomodulatory functions that may have the greatest therapeutic impact *in vivo*^{1,2}. Tissue engineering from MSCs are of highly importance for regeneration of mesenchymal tissues such as craniofacial bone³, cartilage⁴ and connective tissues⁵.

Since several years ago, numerous studies have shown that MSCs from different tissues have similar levels of surface antigen expression, immunosuppressive activity, and differentiation ability⁶. The ability of MSC to carry out normal tissue regeneration in the body and their potential for using in clinical applications may be impaired by loss of stem cell number and function with age⁷. There are different rates of cell proliferation and clonality between MSCs depending on source from the cells are obtained⁸ and the chronological age of the donors and also the number of the *in vitro* culture passages⁹. MSCs are missing their characteristics during the chronological or *in vitro* culture of them¹⁰ but not in the same

¹Grupo de Terapia Celular y Medicina Regenerativa (TCMR-CHUAC). CIBER-BBN/ISCIII. Servicio de Reumatología. Instituto de Investigación Biomédica de A Coruña (INIBIC). Complejo Hospitalario Universitario de A Coruña (CHUAC). SERGAS. Departamento de Medicina. Facultad de Oza. Universidade de A Coruña (UDC). As Xubias, 15006. A Coruña, Spain. ²Grupo de Proteómica-PBR2-ProteoRed/ISCIII-Servicio de Reumatología. Instituto de Investigación Biomédica de A Coruña (INIBIC), Complejo Hospitalario Universitario de A Coruña (CHUAC), Sergas. Universidade da Coruña (UDC). As Xubias, 15006. A Coruña, España. ³Grupo Fisiopatología Endocrina, Nutricional y Médica (FENM-CHUAC). Instituto de Investigación Biomédica de A Coruña (INIBIC). Complejo Hospitalario Universitario de A Coruña (CHUAC). SERGAS. Departamento de Medicina. Facultad de Oza. Universidade de A Coruña (UDC). As Xubias, 15006. A Coruña, Spain. Correspondence and requests for materials should be addressed to J.M. (email: jesusmateosmartin@gmail.com) or M.C.A. (email: maria.arufe@udc.es)

way. Various attempts have been made to address challenges associated with aging of MSC including culture in hypoxic conditions¹¹ and ectopic expression of pluripotency-associated factors¹². This study applied the 8-plex iTRAQ system to analyze MSCs from six different aging groups, as this quantitative proteomic technology has the capability to compare several time points in a single experiment.

The major contributor to the development of the senescent cellular phenotype is hyper activation of nutrient sensor and growth pathways, in particular mTOR and its derivative complexes mTORC1 and mTORC2^{13,14}. mTOR family regulates senescence and autophagy during reprogramming of somatic cells to pluripotency indicating the important role of energy metabolism to stem cell renewal and aging¹⁵. We studied the relationship between mTOR and the proliferation markers CD117 and Ki67 using imatinib mesylate, the inhibitor of tyrosine kinase receptor for CD117¹⁶ and JK184 which reduce expression of Ki67¹⁷. We establish a framework for future comparative and functional studies; we have analyzed the phenotypic, genotypic features and biological-related changes in MSCs of rat bone marrow from animals of different ages.

Material and Methods

Isolation and culture of cells. For isolation of MSCs, the animals were anesthetized with Fluorane (Izasa, A Coruña, SP) and sacrificed by cervical dislocation method. Femurs were dissected from male Wistar rat (Animal Service, CHUAC) at different ages: neonate (0 days old), infant (7 days old), young (14 days old), pre-pubertal (35–38 days old), pubertal (45 days old) and adult (2 months old). All the methods were carried out in “accordance” with the approved guidelines of Spanish law (32/2007). All experimental protocols were approved by Animal Ethical Committee of Galicia. The protocol used by Karaoz *et al.*¹⁸ was followed in this work. Briefly, the ends of the bones were cut away and a 21-gauge needle that was inserted into shaft of the bone marrow was extruded by flushing with 5 ml D-Hank's solution supplemented with 100 IU/ml penicillin–100 mg/ml streptomycin (all from Life Technologies, Madrid, Spain). Marrow plug suspension was dispersed by pipetting, successively filtered through 70- μ m mesh nylon filter (BD Biosciences, Bedford, MA, USA), and centrifuged at 20000 g for 10 min. Supernatant containing thrombocytes and erythrocytes was discarded, and the cell pellet was resuspended in the medium. The cells from four rats were seeded onto 100 cm² dish plate (TM Nunclon) and incubated at 37 °C with 5% humidified CO₂. The MSCs were isolated on the basis of their ability to adhere to the culture plates. On the third day, red blood cells and other non-adherent cells were removed and fresh medium was added to allow further growth. The adherent cells grown to 70% confluence were defined as passage zero (P0) cells. After 5 min of centrifugation, 1×10^6 MSCs were seeded on two dish plates 100 cm² (TM Nunclon) in RPMI supplemented with 10% fetal bovine serum (FBS), 100 U/ml penicillin and 100 mg/ml streptomycin (all from Sigma-Aldrich, St. Louis, MO, USA). The medium was added and replaced every 3 or 4 days for 2 weeks. Before being used in inducing mesoderm differentiation, the MSCs had been expanded for 2 passages and characterized. Afterwards MSCs from adult group were incubated during 12 hours previously to protein extraction with imatinib mesylate or JK184 (all from Sigma-Aldrich).

Flow Cytometry. To characterize the different populations of MSCs from chronological different animals, their MSCs were washed twice in PBS (Sigma-Aldrich, St. Louis, MO, USA), then pre-blocked with 2% rat serum in PBS. The following direct antibodies were used: PE-conjugated mouse anti-human CD34 (1:20 from DakoCytomation, Barcelona, SP); FITC-conjugated mouse anti-rat CD45 (1:20 BD Pharmingen, New Jersey, USA); PE-Cy5.5-conjugated mouse anti-rat CD90 (1:20 Immunostep, Salamanca, SP) and APC-conjugated mouse anti-rat CD29 (1:20 Immunostep, Salamanca, SP). The cells were washed with PBS after one hour of incubation with the corresponding antibody at room temperature. To check proliferation profile of the different populations of MSCs from chronological different animals, their MSCs were incubated with APC conjugated mouse anti-rat CD117 (1:20 Immunostep, Salamanca, SP), mouse anti-BRDU (sigma-Aldrich) and FITC conjugated mouse anti-human Ki67 (1:20 Immunostep, Salamanca, SP). The secondary FITC-conjugated rabbit anti-mouse antibody was used to link cells incubated with anti-BRDU. The stained cells were then washed twice with PBS and 2×10^5 cells were analyzed with a FACSAria flow cytometer (BD Science, Madrid, SP). FACS data was generated by DIVA software (BD Science). Negative control staining was performed using FITC-conjugated mouse IgG1K isotype, PE- conjugated mouse IgG1K isotype, PE-Cy5.5- conjugated mouse IgG1K isotype and APC- conjugated mouse IgG1K isotype (all from BD Pharmingen). For the intracellular ROS accumulation was used H₂DCFDA. Upon oxidation by ROS, the non-fluorescent H₂DCFDA is converted to the highly fluorescent 2',7'-dichlorofluorescein. MitoSOX™ Red Reagent was used to determine mitochondrial ROS including superoxide dismutase activity. Tetramethylrhodamine, methyl ester (TMRM) (from Thermo Fisher Scientific, Life Technologies, SP), the permanent dye that accumulates in active mitochondria with intact potentials, was used to detect functional mitochondria in the MSCs at different ages following functional mitochondrial staining protocol from commercial.

Proliferation assay. Different numbers of cells (0, 1000, 2000, 4000, 8000 and 16000 cells), were plated in triplicate in 96-well plates and allowed to adhere for 8 hours, were used to calculate the proliferation curve. The number of cells was then calculated using CellTiter 96® Aqueous Non-Radioactive Cell Proliferation Assay (Promega, Madison, WI, USA) following manufacturer instructions. For the assay,

Gene Name	Fw primer	Rv primer	mRNA ID	A.T. (°C)
<i>Rex1</i>	gtgcatcacacctcagactgt	cgttggttgaagccaactg	NM_005106.4	61
<i>Oct4</i>	ctcctggaggccaggaatc	atatacacagccgatgtgg	NM_00510	61
<i>Sox2</i>	ctccgggacatgatcagc	ggtagtctgggacatgtgaa	NM_001109181.1	61
<i>Nanog</i>	atgctcacacggagactgt	aagtgggttgttgccttg	NM_005103.4	61
<i>Vinculin</i>	aggagaccttccgaagacagg	gcggttgccactgttttag	NM_001107248	61
<i>HPRT</i>	agccgaccggttctgcat	agccgaccggttctgca	NM_012583.2	61

Table 1. Specific primers for real-time reverse transcriptase-polymerase chain reaction (RT-PCR) amplification, listed with their annealing temperature (A.T.). Fw = forward; Rv = reverse.

4000 cells were plated for each cell line in triplicate in 96-well plates, and the total number of cells was calculated at different time points (0, 1, 2, 5 and 6 days).

The cytotoxicity assay was realized using Cell Counting Kit-8 (Dojindo Molecular Technologies, Inc. MD 20850, USA). Briefly 100 all of cell suspension (5000 cells/well) in a 96-well plate were incubated for 24 hours at 37 °C, 5% CO₂. After that medium with imatinib mesylate or JK184 was added to the wells 48 hours later, 10 µl of CCK-8 solution was added to each well of the plate. After four hours incubation the absorbance was measured at 450 nm using a microplate reader.

Histological and immunohistochemical analysis. MSCs following differentiation into chondrocyte-like or adipocyte-like cells were frozen in OCT embedding matrix (BDH Chemicals, Poole, UK). The cells were fixed in 4% (w/v) paraformaldehyde (Sigma-Aldrich) in PBS at pH 7.6. Some cells were stained with Safranin O, Modified Masson's (Sigma-Aldrich) to evaluate the distribution of proteoglycan in the extracellular matrix generated by the cells differentiated towards chondrocyte-like cells. Other cells were stained with Alizarin red (Sigma-Aldrich) to check alkaline deposits in cells differentiated towards osteocyte-like cells. Other cells were stained with Oil red (Sigma-Aldrich) to check oil drops in cells differentiated towards adipocyte-like cells.

Densitometry analysis. AnalySIS Image Processing (Soft Imaging system GmbH V. 5.0, Olympus, Münster, Germany) was used to do a densitometry quantification of the staining obtained by immunohistochemistry analysis shown in the plots. Three fields 200 mm² in size from each immunostain- safranin O, oil red, modified Masson's and alizarin red - and time studied were quantified using arbitrary units for immunohistochemistry values provided by the computer program. Values expressed as percentage of positive stain for each marker studied were used for immunohistochemistry analysis. All values were referenced with respect to values obtained from cells cultured in the control medium (RPMI 5% knockout serum, 1% penicillin and 1% streptomycin).

Real time quantitative polymerase chain reaction (qRT-PCR) analysis. Primers for amplification of rat *Rex1*, *Oct4*, *Sox2* and *Nanog* genes were used to determine the expression of those markers for pluripotency in the different populations of MSCs from chronological different animals. Details are shown in Table 1. The amplification program consisted of initial denaturation at 92 °C for 2 minutes followed by 40 cycles from 92 °C for 15 seconds, annealing at 55–62 °C, depending on the gene, for 30 seconds and extension at 72 °C for 15 seconds. PCR analyses were done in triplicate, with each set of assays repeated three times. To minimize the effects of unequal quantities of starting RNA and to eliminate potential sources of inconsistency, relative expression levels of each gene was normalized to ribosomal protein (*HPRT*) using the 2- $\Delta\Delta$ Ct method¹⁹. Control experiments utilized no reverse transcriptase.

Protein isolation and immunoblot analysis. Immunoblot analysis was performed on 40 µg of total protein extracted from MSCs, as previously described²⁰. The blots were probed with antibodies, made into rabbit, directed against mTOR, raptor (Cell Signaling, Izasa, Madrid, ES), vimentin, superoxide dismutase (SOD-2), lamin A/C and tubulin (all from Sigma-Aldrich) was used for housekeeping. A secondary anti-goat antibody (Cell Signaling) was used to visualize proteins using an AmershamTM ECLTM Western Blotting Analysis System (GE Healthcare, Amersham Biotechnology, Manchester, UK). Ideal concentrations for each antibody were determined empirically. Working concentrations were 1:1000 of the recommended stock solutions.

iTRAQ labelling. Equal amounts of proteins from each group of different age cells (100 µg) were denatured with 2% sodium dodecyl sulfate (SDS) in 1 M triethylammonium bicarbonate (TEAB) (ABSciex, Foster City, CA). The samples were then reduced for 1 h at 60 °C using 50 mM tris-(2-carboxyethyl) phosphine (TCEP) (ABSciex), and cysteine-blocked with 84 mM iodoacetamide (Sigma-Aldrich) at room temperature in the dark for 30 min. The proteins were digested with spectrometry grade trypsin (Gold Mass, Promega, Madison, WI) at a concentration of 1:50 trypsin/protein for 16 h at 37 °C. Each peptide

solution was labeled for 1.5 h at room temperature using the iTRAQ reagents previously reconstituted in 70 μ L of ethanol, following the manufacture Protocol (ABSciex). The samples were labeled with iTRAQ reagents as follows: newborn: 119 and 121 as a control infant: 114; young: 116; pre-pubertal: 118; pubertal: 115; adult: 117. The reaction was stopped by adding deionized water, and the labeled samples were combined. The mixture was desalted using home-made stage-tips.

iTRAQ relative quantification by 2D-LC-MALDI-TOF/TOF analysis. In a first step, the desalted peptides were fractionated by basic reversed phase extraction in a 1400 HPLC system (Agilent). The fractions were collected along a 110 minutes gradient and subjected to further acidic reversed phase extraction in a nanoHPLC system (Tempo, ABSciex) into a C18 silica-based column (New Objective, Woburn, MA) with an internal diameter of 300 \AA . The injection volume was 5 μ L, and peptides were eluted during a ninety minutes gradient at a constant flow rate of 0.35 μ L/min. Eluting peptides were automatically mixed with alpha-cyano at 4 mg/mL in 70% AcN, TFA 0.1% and deposited on a MALDI LC-plate using a SunCollect (SunChrom) spotter. The chromatograms, composed by 350 spots, each one comprising a 15 sec deposition, were then analyzed in a 4800 MALDI-TOF/TOF platform (ABSciex). 4000 series Explorer v.4.2 software was used to generate the spectra and peak list. After manual deposition of mass calibrates, plate model and default calibration of the MALDI plate was done with a laser voltage of 3200 kV and 1000 shots/spectrum. Samples were automatically analyzed in MS mode with a laser voltage of 3400 kV and 1500 shots/spectrum. Automated precursor selection was done using a Job-wide interpretation method (up to 12 precursors/fraction, Signal to Noise lower threshold = 50) excluding trypsin autolytic peptides and other background ions, with a laser voltage of 4200 and 2000 shots/spectrum. CID collision energy range: medium. LC-MALDI-TOF/TOF data were analyzed using ProteinPilot 4.0 software (ABSciex). Protein Pilot Search parameters were as follows: Sample type: iTRAQ 8-plex; Cys-alkylation: iodoacetamide; Digestion: trypsin; ID focus: Biological modifications; Database: last SwissProt release; Species filtering: none; Search effort: Thorough ID and Detection Protein Threshold Unused ProtScore (Conf) > 1.3 (95.0%). Scoring model was defined by the Paragon algorithm. In the case of the high complexity samples, False Discovery Rate -FDR- was estimated in less than 1% by doing the searching in parallel against a decoy database using "PSPEP on" mode -data not shown-.

Bioinformatics. Biological functional analysis of different modulated proteins detected by iTRAQ quantification, were categorized according to their function, biological process and cellular component, using the String 9.0 software²¹. Proteins with statistically significant changes were identified by filtering according to these criteria: 1) they had to be present in two biological replicates; 2) changes between groups had to be statistically significant ($P < 0.05$); and 3) fold change had to be greater than 1.2 and lower than 0.8 (date do not shown) This approach allowed us to select 201 differentially expressed proteins for further analysis.

Enzymatic Analysis. 5×10^5 cells from each group of different age were used for the assessment of enzyme activities. The cells were homogenized in 200 μ L of 250 mM sucrose (Sigma-Aldrich, St.Louis, MO), 50 mM HEPES (Sigma-Aldrich), 0,5 mM EDTA (Sigma Aldrich) and one tablet protease inhibitor cocktail (Roche, Mannheim, Germany). Enzymes activities were determined using a SUNRISE spectrophotometer (TECAN, Mannedorf, Switzerland). Reaction rates of enzymes were determined by the increase or decrease in absorbance of NAD(P)H (Sigma-Aldrich, St.Louis, MO) at 340 nm at 37 °C. Lactate dehydrogenase (EC 1.1.1.27) was determined in BM-MSCs using 50 mM Trizma base (pH 7,4), 0,15 mM NADH and 5 mM sodium pyruvate (omitted for control) (all Sigma Aldrich, St.Louis, MO). Glucose-6-phosphate 1-dehydrogenase (EC 1.1.1.49) and 6-phosphogluconate dehydrogenase, decarboxylating (EC 1.1.1.343) was determined in BM-MSCs using 78 mM Trizma base, 5 mM MgCl₂(pH 7,4), 0,1 mM NADP, 0,5 mM D-Glucose 6-phosphate disodium salt hydrate and 6-Phosphogluconic acid trisodium salt (omitted for control) (all Sigma-Aldrich, St.Louis, MO).

Statistics. All experiments were performed in triplicate and one representative is shown. Non-parametric statistical analyses were performed by Mann-Whitney-U and Kruskal-Wallis tests using GraphPad Prism6 (GraphPad Software, La Jolla, CA). Each group was compared with previous group. A p value less than 0.05 or 0.01 were considered statistically significant. All the the data are presented as standard error of the mean.

Results

Characterization of populations of MSCs from different ageing group by flow cytometry revealed that no statistical significant differences exist between group respects levels of mesenchymal and hematopoietic markers used for that (Fig. 1A). Positive cells for CD45 and CD34 were less than 1%, positive cells for CD29 were $30 \pm 5\%$ and positive cells for CD90 were $75 \pm 5\%$ in all groups studied.

Proliferation Assays results indicated that MSCs from groups of newborn ($17 \times 10^3 \pm 100$), young ($21 \times 10^3 \pm 200$), pubertal ($15 \times 10^3 \pm 300$) and adult ($16 \times 10^3 \pm 100$) animals had a statistically significant higher ($p < 0.01$) number the cells compared to infant ($9 \times 10^3 \pm 500$), and pre-pubertal ($10 \times 10^3 \pm 500$) (Fig. 1B).

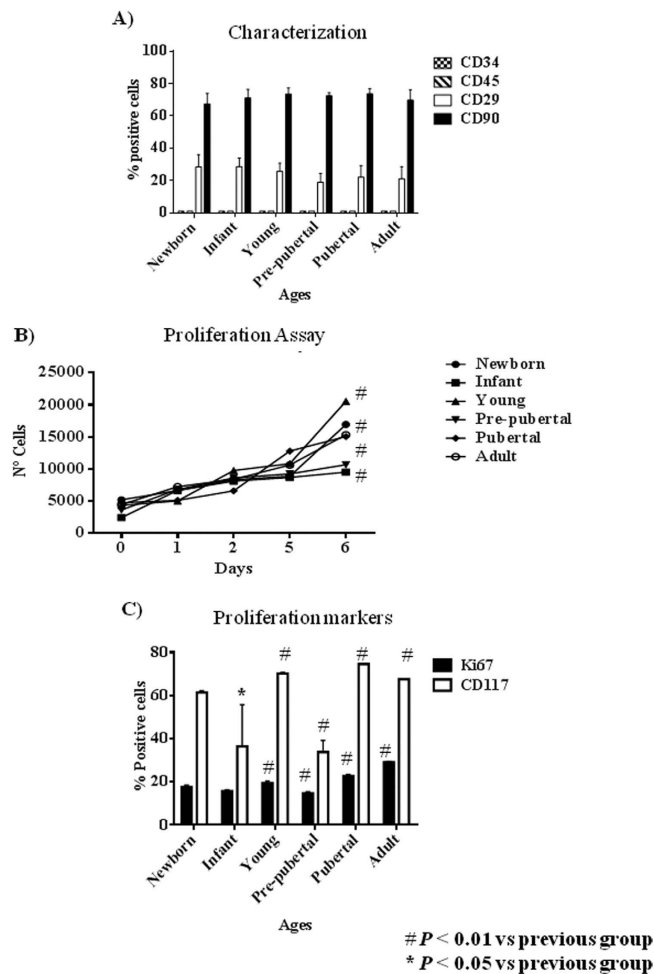


Figure 1. Proliferation profile from rat mesenchymal stem cells at different age. (A) Characterization by flow cytometry assay of percentage of positives mesenchymal stem cells markers (CD29 and CD73) and negative hematopoietic markers (CD34 and CD45). (B) Proliferation assay of studied aging groups for 6 days. (C) Percentage of proliferation markers, DC117 and Ki67, from studied aging groups by flow cytometry assay. One representative experiment is shown. # p value less than 0.05 compared with previous group and * p value less than 0.01 compared with previous group, were considered statistically significant using Mann-Whitney-U tests.

Flow cytometry assays to detect CD117 and Ki67 positive cells indicated that MSCs from pubertal and young groups had the statistical significant ($p < 0.01$ and $p < 0.05$ respectively) higher CD117 positive cells percentage of MSCs (74.65 ± 0.07 and 71.95 ± 3.10 respectively) than the rest of the groups studied, newborn: 61.53 ± 0.37 ; infant: 60.50 ± 1.58 ; adult: 61.12 ± 6.35 and pre-pubertal: 35.25 ± 2.14 . On the other hand, infant and pre-pubertal groups had the statistical significant ($p < 0.05$) lower Ki67 positive cells percentage (15.63 ± 0.24 and 14.65 ± 0.41 respectively) than the rest of the groups studied, newborn: 18 ± 0.55 ; young: 19.33 ± 0.43 ; pubertal 22.68 ± 0.40 and adult: 29.02 ± 0.16 (Fig. 1C)

Differentiation capacity of the groups studied was tested through direct mesoderm induction using specific culture medium. It was observed that pre-pubertal group presented statistically significant ($p < 0.05$) highest stain for safranin O, modified Masson's and oil red by histological analysis followed by pubertal with respect to the other groups. Young group presented the highest staining, statistically significant ($p < 0.05$) for alizarin red with respect to others groups and the adult group presented the lowest statistically significant ($p < 0.05$) differentiation potential with respect to other groups (Fig. 2A,B). Nanog, Oct4, Sox2 and Rex1 gene expression were tested by qRT-PCR analysis to check the pluripotency potential of the studied groups. The results shown the statistically significant ($p < 0.05$) highest expression of Nanog in young group with respect to the others groups in opposition of statistically significant ($p < 0.01$) decrease expression of this same gene, Nanog, in the pre-pubertal group respect to the others (Fig. 2C).

All proteins from MSCs of rat bone marrow at different ages studied were compared between them. Summary each group was composed of a pool from 6 animals and two different iTRAQ experiments were performed. The results obtained in the iTRAQ study indicated that 1.072 proteins were identified, 201 of

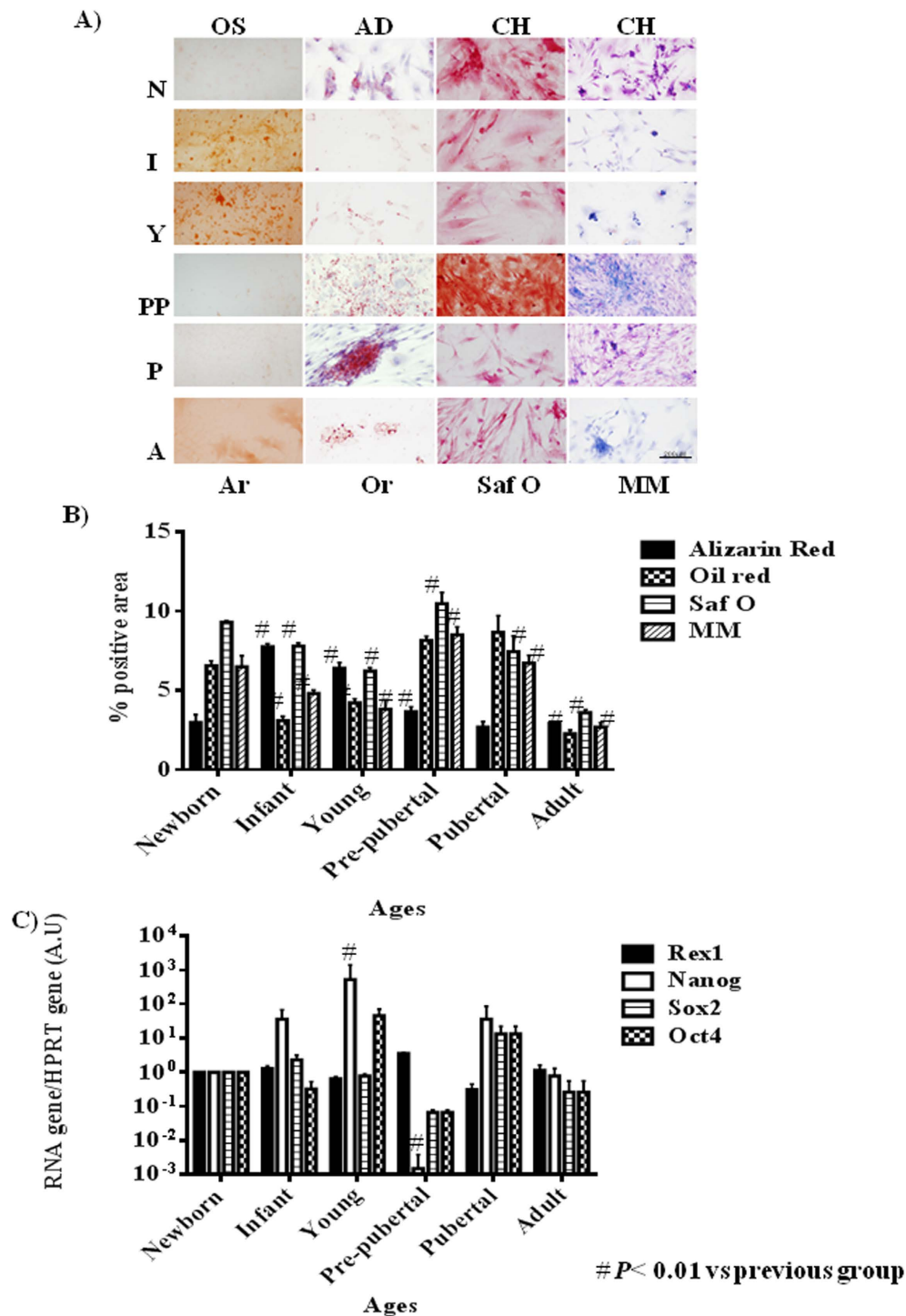


Figure 2. Pluripotency profile from rats mesenchymal stem cells at different age. (A) Representative pictures of mesenchymal stem cell from bone marrow of studied age group after 14 days with specific differentiation medium. On the top specific medium is indicated; OS=osteogenic medium; AD = adipogenic medium; CH= chondrogenic medium. Differentiation medium are indicated in Material and methods. On the bottom stain is indicated; Ar= alizarin red; Or= oil red; Saf O= safranin O and MM= Modified Masson's stain. Straight size is 200 μ M. (B) Densitometry study of mesenchymal stem cell from bone marrow of studied aging group after 14 days with specific differentiation medium after immunostaining assay. AnalySIS Image Processing computer was used to quantify the signal of different stain obtained. # p value less than 0.01 was considered statistically significant using Mann-Whitney-U tests. (C) Histogram represents gene expression of pluripotency markers, Rex1, Nanog, Sox2 and Oct4. Real-time reverse transcriptase PCR (qRT-PCR) analysis normalized by expression of HPRT gene used as housekeeping. # p value less than 0.01 compared with previous group was considered statistically significant using Mann-Whitney-U tests. Three replicates were made.

them statistically significant modulated between groups (Table 2). These proteins have been grouped by three processes attending String 9.0 software; those groups were proliferation (60 proteins), pluripotency (86 proteins) and energy metabolism (55 proteins) (Table 2). Significant activates pathways obtained by comparing modulated proteins obtained by iTRAQ analysis employing functional annotations according to the String 9.0 software and classified in three biological process for better comprehension were shown in Fig. 3. A. Several proteins found in our analysis associated with proliferation were 60S ribosomal proteins with different sedimentation speed like 60S RP L10, 60S RP L9, 60S RP L23, 60S RP L24, 60S RP L4, 60S RP L6 and 60S RP L7; also Vinculin which gene expression was validated by qRT-PCR analysis (Fig. 3D), all of them were statistically significant ($p < 0.05$) higher in newborn and adults with respect to the others groups. Superoxide dismutase-2 (SOD2) and Lamin A were increasing through the increasing age group like occurred in the iTRAQ analysis; all of them were validated by western blot (Fig. 3B). Mitosox and total ROS were studied by flow cytometry to explain SOD2 results in our iTRAQ study, ROS and mitosox were statistically significant ($p < 0.05$) lower in infant and pre-pubertal groups with respect to the others groups respectively (Fig. 4A,B). A fluorescence-based assay to detect functional mitochondria indicated that adult group had their functional mitochondria statistically significant decreased with respect to others groups of study (Fig. 5B). Proteins found in our iTRAQ analysis were associated with pluripotency like histones H1.5; H2B; H4 and protein disulfide-isomerase A1 (PDIA1) which were statistically significant ($p < 0.05$) high-regulated in infant and pubertal groups with respect to the others (Table 2). Several proteins found in our iTRAQ analysis associated with energy metabolism were lactate dehydrogenase (LDH), glucose 6 phosphate dehydrogenase (G6PDH) and 6-phosphogluconate dehydrogenase (6PGDH), which were validated through analysis of their activity by enzyme immunoassay (EIA). Lactate dehydrogenase (LDH) activity was increased in young group in front to infant and newborn group, decreased in pre-pubertal group in a statistically significant way ($p < 0.01$) and come back to increase its activity in pubertal and adult groups (Fig. 4C), glucose 6 phosphate dehydrogenase (G6PDH) and 6-phosphogluconate dehydrogenase (6PGDH) were statistically significant increased ($p < 0.01$) in pubertal and adult groups in front to others (Fig. 4D).

Immunoblot analysis indicated that mTOR and Raptor were statistically significant ($p < 0.05$) lower in pre-pubertal and pubertal groups with respect to the other groups studied. Adult group presented the statistically significant ($p < 0.05$) most increased level of mTOR and Raptor (Fig. 5A), the permanent dye TMRM analysis indicated a decrease in functional mitochondria which was statistically significant ($p < 0.01$) in infant and adult groups with respect to newborn and pubertal groups respectively (Fig. 5B). Viability assay using two physiological concentrations of Imatinib mesylate or JK184 did not affect the cells in culture (Fig. 5C). JK184 decreased statistically significant ($p < 0.01$) the expression of KI67 at 1mg/ml dose in culture (Fig. 5D). mTOR decreased dramatically in adult group when the cells were incubated with Imatinib mesylate or JK184 (Fig. 5E).

Discussion

It is good known that long-term *in vitro* culture, but not chronological aging, alters their morphology, susceptibility to senescence and mitochondrial function. Thus, independent from donor animal age, *in vitro* aging of MSCs seems to result in complete loss of their progenitor characteristics⁹. Accordingly, functional analysis demonstrated altered mitochondrial morphology, decreased antioxidant capacities and elevated ROS levels in long-term cultivated independently the aged of the donor. Our present study is limited to the usage of rat MSCs instead can be able to apply on human MSCs; it provides direct comparison between chronological aged MSC not only at the cellular but also at the molecular level.

MSCs populations from different ageing groups were characterized by flow cytometry to check percentage of positive cells for mesenchymal markers, CD29 and CD90, and to check that were negative for hematopoietic markers (CD34, CD45) (Fig. 1A). We did not observe statistical significant differences between the mesenchymal markers into the different MSCs aging group studied (Fig. 2C). These were coincident with results published by Jin *et al.*⁶ indicating that MSCs have similar levels of surface antigen expression included MSCs from different tissues. Although the mesenchymal markers were not as abundant as published by Harting *et al.*²² these cells were able to adhere to the plastic plate and this is an intrinsic characteristic of mesenchymal stem cells and all of the groups were able to differentiate towards several mesoderm lineages (Fig. 2A,B). iTRAQ analysis is an adequate technique to study complex samples like we have used in this work²³. Our results by iTRAQ analysis allowed the identification of 1,072 proteins. 201 of them were statistically significant modulated between groups (Table 2). Our study represents a step further from a previous iTRAQ-based study²⁴ where 156 differentially expressed proteins were detected. Furthermore we compared six chronologically different groups, giving more strength to our study. To generate the quantitative proteome using iTRAQ labeling, it was first determined the labeling efficiency, which exceeded 99% (data not shown). Next, the cut-off for significant fold-change was determined based on the 2 biological replicates of two iTRAQ experiments which were chosen based on the following criteria: it contained more than 3 unique peptides (>95%) and p value < 0.05 for the 114/119 reporter ions. Accordingly, 90% of the commonly observed in the biological replicates fell within 25% of the respective experimental variation (Data not shown). The fold-change thresholds of >1.20 or <0.80 was set to identify true differences between expression of reporter ions.

One of the aims of our study was to establish the differences into proliferation process relating them to chronological donor age. Our results indicated that chronological age is directly influencing the

Accession	Name	Peptides (95%)	I/N	PVal I/N	Y/I	PVal Y/I	PP/Y	Pval PP/Y	P/PP	PVal P/PP	A/P	PVal A/P
Metabolism												
Q6P783	6-phosphofructokinase	5	0,7228	0,1496	1,0497	0,7085	1,1027	0,3079	1,4117	0,0388	1,2082	0,2192
Q7TP11	6-phosphogluconate dehydrogenase, decarboxylating	5	0,8664	0,0404	0,9404	0,345	1,1936	0,1035	1,2877	0,0026	0,6857	0,0099
P06761	78 kDa glucose-regulated protein	35	0,9172	0,0089	0,9677	0,334	1,1997	0	0,8295	0,002	1,4611	0
M0RDC5	Acyl-CoA-binding protein (Fragment)	1	0,9923	0,9393	1,0172	0,8471	1,0129	0,8865	1,1744	0,4947	1,408	0,0299
F1LN88	Aldehyde dehydrogenase, mitochondrial	9	0,915	0,2981	0,9521	0,605	1,0255	0,8092	0,8105	0,1287	1,249	0,0303
P07943	Aldose reductase	9	1,0984	0,3717	0,8893	0,186	0,9549	0,5728	0,9715	0,7164	1,2055	0,0389
Q91W30	Aldose reductase-like protein	10	1,6948	0,0054	0,5021	0,0183	1,2079	0,2492	1,0106	0,9424	1,2476	0,0229
D3ZUM4	Beta-galactosidase	5	1,0315	0,7835	1,3171	0,0441	1,0942	0,385	1,1471	0,1506	0,9005	0,1892
O35567	Bifunctional purine biosynthesis protein PURH	13	0,9914	0,9389	0,8798	0,2663	1,1514	0,3918	0,8194	0,0166	1,1312	0,0362
Q99JD5	Branched-chain-amino-acid aminotransferase	5	1,0463	0,7187	0,842	0,0756	1,3485	0,0127	0,9146	0,4169	0,9297	0,5047
P15791	Calcium/calmodulin-dependent protein kinase type II subunit delta	5	0,9646	0,825	0,9676	0,8106	1,3814	0,0071	0,7966	0,044	1,0233	0,8049
G3V9E3	Caldesmon 1, isoform CRA_b	18	1,0648	0,1599	0,9241	0,1919	1,4728	0	0,7388	0,0002	1,6353	0
Q08290	Calponin-1	9	0,8714	0,0531	1,3003	0,0464	0,8214	0,2876	0,723	0,0013	1,2572	0,0412
P37397	Calponin-3	10	1,3337	0,0378	0,8281	0,0224	1,0857	0,2275	0,7288	0,0035	1,1632	0,1397
P18418	Calreticulin	12	1,1514	0,0446	0,8607	0,0394	1,3403	0,0004	0,7119	0,0002	1,4109	0,0004
G3V6S3	Calumenin	5	1,0591	0,4369	1,0768	0,3271	0,9833	0,8456	0,7673	0,2524	1,5598	0,0141
Q6P6T6	Cathepsin D	7	0,8801	0,1287	1,0622	0,3991	1,5419	0,0105	0,9111	0,1808	1,3326	0,0234
P97601	Chaperonin 10	3	1,0204	0,7796	1,0011	0,9902	0,9415	0,5177	0,939	0,4419	1,4235	0,0087
G3V936	Citrate synthase	3	0,7934	0,0267	1,167	0,0848	0,7904	0,0267	1,1452	0,2405	0,857	0,2318
F1M779	Clathrin heavy chain	9	1,2157	0,0137	1	0,9994	0,9612	0,7295	1,1343	0,2338	0,8853	0,3235
Q6TUH9	Corticosteroid 11-beta-dehydrogenase isozyme 1	3	0,7341	0,2686	1,3756	0,2277	1,6421	0,0328	1,9857	0,0672	0,7338	0,0642
P47875	Cysteine and glycine-rich protein 1	7	1,0015	0,9815	1,0448	0,5131	1,2576	0,0488	0,6896	0,0389	1,2501	0,0705
O08651	D-3-phosphoglycerate dehydrogenase	3	0,8786	0,1902	0,7465	0,0308	1,1981	0,1105	1,1565	0,1448	1,0565	0,5069
Q5BJ93	Enolase 1, (Alpha)	23	1,0226	0,655	1,026	0,5722	1,054	0,2406	0,7412	0	1,2752	0,0123
Q8R4A1	ERO1-like protein alpha	5	0,8236	0,0936	1,0042	0,9607	1,1541	0,1632	1,0604	0,6296	1,4685	0,0439
P05065	Fructose-bisphosphate aldolase A	7	0,7852	0,0001	0,9961	0,9275	1,1519	0,0055	1,17	0,0228	1,1494	0,0589
Continued												

Accession	Name	Peptides (95%)	I/N	PVal I/N	Y/I	PVal Y/I	PP/Y	Pval PP/Y	P/PP	PVal P/PP	A/P	PVal A/P
P11762	Galectin-1	13	0,8947	0,1869	1,0817	0,3224	0,9378	0,4491	0,738	0,0127	1,2891	0,0226
Q8CJG5	Gene	3	0,9562	0,7992	0,6552	0,233	1,5338	0,0488	1,0942	0,6762	0,9227	0,7939
P05370	Glu- cose-6-phos- phate 1-dehy- drogenase	16	1,0157	0,847	1,0285	0,7414	0,9947	0,9314	1,0827	0,1708	1,2136	0,0003
Q6P6V0	Glu- cose-6-phos- phate isomerase	13	0,859	0,1021	0,9669	0,5321	1,1179	0,0929	1,1489	0,1394	1,2446	0,0072
P04797	Glyceralde- hyde-3-phos- phate dehydro- genase	28	1,0559	0,3012	1,2268	0,0077	0,8176	0,0404	1,0972	0,4988	0,8495	0,1048
P56574	Isocitrate dehydrogenase [NADP], mito- chondrial	3	1,0223	0,8926	1,0131	0,8828	0,8721	0,3389	1,3609	0,025	0,8545	0,1231
B5DEN4	L-lactate dehy- drogenase	14	0,7058	0,0001	1.146	0,00197	1.1828	0,0191	1.2617	0	1.416	0
Q6P7A9	Lysosomal alpha-gluco- sidase	4	0,9754	0,7869	1,0694	0,6226	1,4268	0,048	0,8687	0,254	1	1
Q6AYC4	Mac- rophage-cap- ping protein	2	1,1578	0,3404	1,3646	0,0086	0,8334	0,049	0,7546	0,0948	1,3655	0,0617
F1LP60	Moesin (Frag- ment)	40	1,0168	0,6741	0,8227	0,0003	1,4257	0	0,9895	0,8299	0,9461	0,1782
P20070	NADH-cy- tochrome b5 reductase 3	2	0,7339	0,0716	1,4911	0,0447	0,9088	0,5256	0,9743	0,903	0,8315	0,169
Q6XD99	Non-erythroid spectrin beta	2	1,3375	0,0053	1,0624	0,4554	1,1109	0,3101	0,7568	0,0122	1,5134	0,0041
P16617	Phosphoglycer- ate kinase 1	29	0,775	0	1,0397	0,3579	1,0241	0,6829	1,1179	0,0446	1,3076	0
P25113	Phosphoglycer- ate mutase 1	9	0,7559	0,0052	1,1081	0,1211	1,1188	0,142	1,105	0,1848	1,3205	0,0024
P54001	Prolyl 4-hy- droxylase sub- unit alpha-1	15	0,9432	0,3007	0,923	0,1417	1,26	0,0005	0,779	0,0002	0,9234	0,2253
M0R9D5	Protein Ahnak	60	1,4134	0	0,9734	0,2788	1,2761	0	0,8082	0	2,1551	0
D3ZIE9	Protein Ald- h18a1	5	1,2134	0,1403	1,038	0,7002	0,5751	0,0236	0,8643	0,2248	0,7301	0,0622
M0R3 × 6	Protein LOC100912203	6	0,8645	0,163	1,0325	0,6321	1,1276	0,2248	0,9918	0,9068	1,2992	0,0104
D4A5L9	Protein LOC679794	4	0,6761	0,0039	1,6157	0,0178	0,7517	0,0082	0,9865	0,8661	1,0755	0,375
Q6P9U0	Protein Ser- pin6	8	0,9886	0,8679	1,0239	0,6691	1,3013	0,0066	0,8823	0,2774	1,1196	0,16
D3ZF39	Protein Uap1	10	1,0277	0,7709	1,0072	0,947	1,6544	0,0038	0,9744	0,7756	1,6238	0,0005
B0BMT0	RCG47746, iso- form CRA_a	90	1,0669	0,6161	0,7141	0,0061	1,4858	0,0047	0,5813	0,0012	0,7691	0,1418
Q6IRL3	Reticulon	7	1,0111	0,8671	0,8818	0,3109	1,3224	0,0677	0,7406	0,0052	0,9133	0,4439
B2GVB1	S100 calcium binding protein A6	3	1,0605	0,5609	1,2045	0,2186	1,7118	0,0122	0,3918	0,0244	1,665	0,037
Q5U3Z7	Serine hydrox- ymethyltrans- ferase	3	0,7739	0,0051	0,9472	0,5152	1,0085	0,9511	1,1442	0,2328	1,0402	0,831
F1M953	Stress-70 protein, mito- chondrial	12	0,9377	0,2437	0,7924	0,0057	1,174	0,0025	0,8961	0,1199	1,5666	0
P48500	Triosephos- phate isomerase	16	0,6753	0,0004	1,174	0,0315	1,0854	0,3958	1,2639	0,1091	1,4017	0,0001
Q9Z1A6	Vigilin	3	1,1784	0,0874	0,8426	0,0918	1,0244	0,862	0,9978	0,9727	1,2104	0,0345

Continued

Accession	Name	Peptides (95%)	I/N	PVal I/N	Y/I	PVal Y/I	PP/Y	Pval PP/Y	P/PP	PVal P/PP	A/P	PVal A/P
P81155	Voltage-dependent anion-selective channel protein 2	6	1,0012	0,9931	1,0633	0,4458	1,2708	0,0343	0,8377	0,1616	0,992	0,9444
Pluripotency												
P63102	14-3-3 protein zeta/delta	24	0,9971	0,9573	0,9743	0,6297	1,0748	0,2065	0,8947	0,1104	1,1562	0,0250
Q7TP91	Ab1-205	3	0,9802	0,8434	1,2607	0,1387	0,9026	0,3795	1,0629	0,7975	0,6232	0,0302
Q64640	Adenosine kinase	2	0,9609	0,8197	1,1207	0,3134	1,1155	0,346	1,0828	0,4536	0,6855	0,0454
P39069	Adenylate kinase isoenzyme 1	4	0,7781	0,0775	1,2606	0,053	1,0747	0,7679	0,9795	0,8759	1,6777	0,029
P23928	Alpha-crystallin B chain	5	1,207	0,0573	1,8689	0,0119	2,2257	0,0003	0,2931	0,0035	1,5629	0,0723
Q6IMZ3	Annexin A6	24	1,2484	0,0001	1,1079	0,0199	0,9791	0,5623	1,0031	0,9354	1,0187	0,5863
Q07936	Annexin A2	22	1,2928	0	1,0234	0,6825	1,368	0,0001	0,8172	0,003	1,072	0,1567
Q05175	Brain acid soluble protein 1	3	0,9481	0,8617	1,209	0,454	1,3727	0,148	0,4584	0,0445	1,6462	0,1009
Q6T487	Brain-specific alpha actinin 1 isoform	48	0,7786	0,0007	1,1584	0,0465	1,0249	0,6506	0,8259	0,0018	1,1052	0,2188
Q8R4A2	Caveolin 1 (Fragment)	4	0,9676	0,8582	1,8465	0,0328	1,0661	0,7396	0,7326	0,1573	1,0726	0,6061
P02454	Collagen alpha-1(I) chain	21	1,9314	0,0008	0,4642	0	1,3783	0	1,1251	0,0342	1,123	0,1023
F1LS40	Collagen alpha-2(I) chain	19	1,486	0,0008	0,6971	0	1,1467	0,0083	0,9555	0,2908	1,3211	0,0003
P07335	Creatine kinase B-type	3	0,7036	0,0109	1,1785	0,2497	1,4259	0,0546	0,8379	0,2386	1,2443	0,3604
F1LMA7	C-type mannose receptor 2	5	1,1259	0,191	0,8731	0,3184	0,8322	0,3836	0,8408	0,3689	1,7697	0,0009
P47875	Cysteine and glycine-rich protein 1	5	1,0995	0,2349	0,9264	0,4028	1,275	0,0227	0,7329	0,0396	1,2025	0,1773
Q6AYI1	DEAD (Asp-Glu-Ala-Asp) box polypeptide 5	9	0,9335	0,2865	0,9937	0,9257	0,8965	0,0659	1,2504	0,0032	0,9596	0,434
Q62952	Dihydropyrimidinase-related protein 3	8	1,2443	0,0364	1,5656	0,0028	0,858	0,2853	0,8247	0,0165	1,0088	0,9184
Q4V8H8	EH domain-containing protein 2	0	0,9656	0,7399	1,3396	0,2041	0,8004	0,248	1,6703	0,0471	0,7495	0,491
Q68FR6	Elongation factor 1-gamma	9	1,0087	0,8562	0,9072	0,4157	1,2134	0,0011	0,9535	0,5667	0,8485	0,0109
C0JPT7	Filamin alpha	100	1,2134	0	1,3022	0	0,8202	0	0,9147	0,0068	1,386	0
D4A8D5	Filamin, beta (Predicted)	19	1,0951	0,0867	1,2541	0,0012	0,8193	0,0061	0,7937	0,0124	1,329	0,0009
B6DYQ7	Glutathione S-transferase pi	4	1,0946	0,3206	1,1008	0,6055	1,5111	0,0241	3,1507	0,0004	0,3406	0,0033
G3V913	Heat shock 27kDa protein 1	5	1,6407	0,0562	0,9647	0,8462	1,5674	0,0118	0,636	0,038	1,3145	0,0077
P63018	Heat shock cognate 71 kDa protein	30	0,9815	0,6625	1,2334	0,0221	0,8841	0,0143	1,0164	0,8526	1,1903	0,0184
F1M3D3	Heterogeneous nuclear ribonucleoprotein M	3	0,6983	0,0017	1,0334	0,5966	0,9158	0,4502	1,1725	0,1239	1,0388	0,7714
Continued												

Accession	Name	Peptides (95%)	I/N	PVal I/N	Y/I	PVal Y/I	PP/Y	Pval PP/Y	P/PP	PVal P/PP	A/P	PVal A/P
Q61MY8	Heterogeneous nuclear ribonucleoprotein U	8	0,7965	0,0032	1,0228	0,7409	0,9994	0,9956	1,1924	0,0262	0,8534	0,1414
P15865	Histone H1.4	8	0,7411	0,0048	2,4013	0,0005	1,0711	0,2301	0,5016	0,0007	0,6377	0,007
D3ZBN0	Histone H1.5	4	1,911	0,0166	0,4907	0,0135	0,9905	0,9189	1,4031	0,0552	0,8838	0,2767
G3V9C7	Histone H2B	20	1,2535	0,0051	0,9957	0,9764	0,8311	0,1792	1,4957	0,0005	0,7706	0,0027
M0RBX6	Histone H3	6	1,1323	0,058	1,4413	0,0125	1,201	0,0272	0,5991	0,0004	0,494	0,0002
P62804	Histone H4	13	1,4819	0,0057	0,5999	0,0004	1,1515	0,0641	1,7155	0,0008	0,6785	0,002
Q6P6G9	Hnrpa1 protein	8	0,6091	0,0304	0,9626	0,6587	0,943	0,663	1,1142	0,7189	0,969	0,7865
P50503	Hsc70-interacting protein	4	0,9785	0,7614	1,0509	0,7519	1,1426	0,4415	0,8392	0,2581	1,5699	0,0074
P49134	Integrin beta-1	6	1,5471	0,0002	0,9023	0,1179	1,5398	0,0098	0,7217	0,0064	1,311	0,0037
G3V7Q7	IQ motif containing GTPase activating protein 1 (Predicted), isoform CRA_b	29	0,9058	0,0331	0,8665	0,0016	1,2223	0	1,0398	0,2744	0,8961	0,0032
Q6TXE9	LRRGT00050	4	0,8206	0,0425	0,8878	0,4999	1,0972	0,6832	1,5	0,0036	0,8044	0,129
Q6TUD1	LRRGT00113	2	0,7362	0,0289	1,0159	0,9238	1,0387	0,7991	1,0836	0,5779	0,9606	0,8364
Q5M7W5	Microtubule-associated protein 4	2	1,6111	0,1601	0,845	0,5023	1,0907	0,433	0,6693	0,1236	1,6243	0,0414
B2GV99	Myl6 protein	11	1,0049	0,9535	1,1269	0,1948	1,0655	0,29	0,9193	0,1676	1,3394	0,0011
G3V9Y1	Myosin, heavy polypeptide 10, non-muscle, isoform CRA_b	51	0,9356	0,0771	1,0793	0,1827	0,8786	0,0186	0,8988	0,0205	0,792	0,0018
G3V6P7	Myosin, heavy polypeptide 9, non-muscle	98	0,9405	0,0071	1,1877	0	1,0117	0,6464	0,957	0,2338	1,3299	0
P05982	NAD(P)H dehydrogenase [quinone] 1	8	1,3454	0,0036	0,7746	0,0108	1,2457	0,0611	0,817	0,2198	1,7303	0,0017
G3V8R1	Nucleobindin 2, isoform CRA_b	3	0,7234	0,0259	2,0743	0,0023	0,5945	0,0061	0,8133	0,1039	1,5101	0,0176
F1M4W3	Palladin (Fragment)	6	1,0033	0,9633	0,8726	0,1096	1,0418	0,6509	0,6823	0,0117	1,0929	0,2707
P52944	PDZ and LIM domain protein 1	8	1,0741	0,3026	1,0802	0,1599	1,3743	0,0005	0,9648	0,7456	1,2349	0,03
Q62920	PDZ and LIM domain protein 5	17	0,9467	0,5156	0,6947	0,0022	1,4784	0,0057	0,6885	0,0358	0,8014	0,071
Q6AYQ9	Peptidyl-prolyl cis-trans isomerase	6	0,9218	0,2069	0,9782	0,6989	1,2033	0,0649	0,7408	0,0209	0,837	0,0475
Q62658	Peptidyl-prolyl cis-trans isomerase FKBP1A	2	1,254	0,0638	1,1087	0,2151	1,0291	0,6981	0,8516	0,0786	1,38	0,0149
D3ZAF5	Periostin, osteoblast specific factor (Predicted), isoform CRA_a	4	0,5315	0,1266	1,4489	0,0583	0,7663	0,0352	1,3251	0,0507	0,8907	0,4068
Q63716	Peroxiredoxin-1	13	0,8935	0,0404	1,0622	0,5224	1,083	0,5586	0,884	0,3841	1,2919	0,0335
P35704	Peroxiredoxin-2	5	0,9438	0,6729	1,3399	0,0331	0,9268	0,3898	0,8375	0,2252	1,1003	0,4352
Q9R063	Peroxiredoxin-5, mitochondrial	5	1,0571	0,6808	0,7826	0,0577	1,2214	0,0908	0,8798	0,195	1,4277	0,0498
F1LPK7	Phospholipid scramblase 3	5	1,3539	0,015	0,7564	0,0206	1,2564	0,0285	0,9783	0,8008	1,0061	0,9704

Continued

Accession	Name	Peptides (95%)	I/N	PVal I/N	Y/I	PVal Y/I	PP/Y	Pval PP/Y	P/PP	PVal P/PP	A/P	PVal A/P
G3V8L9	Polymerase I and transcript release factor	10	1,0181	0,7755	1,5741	0,0001	1,2442	0,0026	0,6574	0,0001	1,2032	0,1746
G3V9I0	Procollagen-ly-sine,2-ox-oglutamate 5-dioxygenase 2	15	0,6772	0,0001	1,3393	0,0139	0,8435	0,0459	1,1106	0,2824	1,033	0,765
D3ZRX9	Protein Cnn2	9	0,9803	0,7232	0,9782	0,6955	1,1542	0,0382	0,7727	0,0037	1,1053	0,1116
G3V6T7	Protein disulfide isomerase associated 4	4	1,094	0,3778	1,5291	0,0042	0,7583	0,087	0,8527	0,0368	1,1596	0,0466
P04785	Protein di-sulfide-isomerase	18	0,9524	0,2161	0,9019	0,0205	1,1449	0,002	0,91	0,0672	1,3562	0
P11598	Protein di-sulfide-isomerase A3	23	1,0044	0,9331	1,1813	0,0003	1,0096	0,899	0,888	0,1863	1,151	0,1114
Q63081	Protein di-sulfide-isomerase A6	9	0,7832	0,0043	1,1044	0,262	1,2788	0,0234	0,9335	0,4195	1,0394	0,5727
D3ZHA0	Protein Flnc	28	0,9537	0,2739	1,6131	0	0,8375	0,0128	0,9354	0,1802	1,1796	0,0125
E2RUH2	Protein LOC100360501	3	0,8715	0,4837	1,2547	0,0379	0,7763	0,024	1,2418	0,1487	0,7978	0,0359
M0R7B4	Protein LOC684828	6	1,9171	0,003	0,4959	0,0035	1,0813	0,3542	1,3227	0,0305	0,8447	0,1021
F1MA29	Protein LOC685520	5	0,7506	0,0026	1,15	0,0892	0,9181	0,414	1,0561	0,438	1,066	0,4416
D3ZUB0	Protein Rcn1	2	1,0185	0,8167	0,8941	0,2217	1,1262	0,2053	0,8607	0,297	1,3273	0,0313
I6L9G5	Protein Rcn3	2	1,0873	0,4834	0,5646	0,023	1,147	0,2936	0,9716	0,7715	1,3833	0,2381
D4A1P2	Protein Rp110l	7	1,0101	0,8587	0,8912	0,0814	0,8855	0,0554	1,4153	0,0002	0,6894	0,0001
F1M853	Protein Rrbp1	12	0,9865	0,8266	0,9487	0,2254	1,4058	0,0002	0,6416	0,0002	1,4396	0
P05942	Protein S100-A4	8	1,3344	0,0883	0,8596	0,3432	2,371	0,0005	0,6816	0,0449	1,6256	0,0034
B0BMT9	Protein Sqrld	5	0,8772	0,1123	0,8745	0,2138	1,3482	0,0318	0,672	0,0272	1,1637	0,2917
P50399	Rab GDP dissociation inhibitor beta	5	0,6527	0	1,1226	0,1842	0,8087	0,0191	1,2167	0,0909	0,8327	0,0497
Q5FVG5	Similar to tropomyosin 1, embryonic fibroblast-rat, isoform CRA_c	21	0,8189	0,0635	0,8236	0,0664	1,5332	0,0055	0,4284	0,0029	0,9622	0,622
Q6IRH6	Slc25a3 protein	5	0,6221	0,0046	1,2418	0,0813	0,9018	0,3869	1,2937	0,0271	0,7334	0,0095
P06685	Sodium/potassium-transporting ATPase subunit alpha-1	6	1,0612	0,5229	0,847	0,0206	0,9521	0,6531	1,1204	0,4092	0,8973	0,1495
P16975	SPARC	5	1,2574	0,0585	0,8963	0,1879	1,0501	0,5303	0,9358	0,5629	1,2361	0,0437
Q63413	Spliceosome RNA helicase Ddx39b	4	0,7567	0,0206	1,0276	0,7991	0,904	0,431	1,3219	0,0189	0,679	0,0523
Q6IRK8	Spna2 protein	9	1,3867	0	1,211	0,003	1,0232	0,7136	0,7877	0,0016	1,7205	0
D4A8Y5	Staphylococcal nuclease domain-containing protein 1	3	0,919	0,451	1,2908	0,0445	0,8256	0,0815	1,2376	0,0644	0,7802	0,1202
Q71SA3	Thrombospondin 1	7	0,8058	0,0398	0,7166	0,0007	1,3192	0,0007	0,9713	0,6767	1,4974	0,0023
P31232	Transgelin	39	1,2096	0,0003	1,2967	0,0743	1,133	0,0136	0,5637	0,0001	1,7372	0
Q5XF0	Transgelin-2	17	0,9888	0,8414	1,0039	0,955	1,3666	0,0009	0,9786	0,7678	1,1396	0,048
Q6AYT3	tRNA-splicing ligase RtcB homolog	4	0,6896	0,019	0,9867	0,8815	0,8815	0,1894	1,1372	0,1808	0,8525	0,4565

Continued

Accession	Name	Peptides (95%)	I/N	PVal I/N	Y/I	PVal Y/I	PP/Y	Pval PP/Y	P/PP	PVal P/PP	A/P	PVal A/P
Q63610	Tropomyosin alpha-3 chain	9	0,9843	0,838	1,4987	0,0199	1,2255	0,0709	0,6776	0,0538	1,8819	0,0153
P09495	Tropomyosin alpha-4 chain	12	0,9739	0,7802	1,356	0,0682	1,0117	0,925	0,8335	0,1905	1,5771	0,0401
G3V6C4	UDP-glucose 6-dehydrogenase	8	1,0597	0,478	0,9444	0,6809	1,256	0,011	1,0009	0,9911	1,4008	0,0135
Q63355	Unconventional myosin-Ic	10	1,2333	0,0007	0,8095	0,0071	1,2252	0,0431	1,0652	0,3451	0,8854	0,0253
P31000	Vimentin	110	1,0703	0,0545	1,0991	0,0394	1,1756	0,0018	0,76	0	0,9955	0,9047
Proliferation												
P62268	40S ribosomal protein S23	3	1,0729	0,3955	0,7949	0,0312	1,0116	0,8769	0,9447	0,6609	1,0981	0,4568
M0RD75	40S ribosomal protein S6 (Fragment)	5	1,213	0,0348	0,7478	0,0343	1,0648	0,6105	0,8839	0,3222	1,2172	0,0637
B2RYR8	40S ribosomal protein S8	5	1,156	0,0743	0,7651	0,0113	0,9563	0,6408	1,1034	0,3318	1,0474	0,6037
P29314	40S ribosomal protein S9	10	1,2232	0,0078	0,7297	0,0002	1,1604	0,014	1,0442	0,4378	1,0231	0,6427
P38983	40S ribosomal protein SA	7	1,0045	0,948	0,8267	0,0864	1,0707	0,3666	1,3083	0,0159	0,8177	0,0379
P63039	60 kDa heat shock protein, mitochondrial	14	1,0284	0,7397	1,0424	0,6331	1,0209	0,827	0,7502	0,0126	1,1048	0,3793
Q6PDV7	60S ribosomal protein L10	8	1,2944	0,0232	0,7476	0,0503	1,0811	0,4911	0,9186	0,3735	1,079	0,2893
P41123	60S ribosomal protein L13	4	1,2788	0,1225	0,8351	0,0607	1,0613	0,7175	1,269	0,0179	0,8472	0,0781
P61314	60S ribosomal protein L15	2	1,0608	0,6431	0,9332	0,5211	0,8939	0,228	1,6856	0,0065	0,7429	0,0338
Q0QEW8	60S ribosomal protein L18 (Fragment)	3	0,8899	0,3903	1,0505	0,6391	0,9184	0,5621	1,4963	0,0365	0,7225	0,0735
P62718	60S ribosomal protein L18a	4	1,0118	0,8521	0,8707	0,2832	1,0157	0,9288	1,3147	0,032	0,8694	0,1711
P62832	60S ribosomal protein L23	6	1,2256	0,0212	0,838	0,0334	0,9969	0,9615	0,9723	0,8064	1,1553	0,1309
P83732	60S ribosomal protein L24	7	1,5524	0,0024	0,5064	0,0004	1,2108	0,0391	0,8698	0,2155	1,2834	0,0175
P25886	60S ribosomal protein L29	3	1,5331	0,0443	0,9651	0,7362	1,0984	0,4167	0,8404	0,5923	0,7419	0,2733
P21531	60S ribosomal protein L3	5	1,0552	0,6436	0,8494	0,0879	0,932	0,5476	1,463	0,0213	0,7223	0,0148
Q6P3V9	60S ribosomal protein L4	9	1,419	0,0021	0,627	0,0002	1,0227	0,7849	0,9688	0,6057	1,139	0,0543
P09895	60S ribosomal protein L5	6	0,9424	0,3628	0,9732	0,6933	0,9466	0,5073	1,2345	0,0225	0,8597	0,1305
H7C5Y5	60S ribosomal protein L6	7	1,3496	0,0261	0,6716	0,0068	1,0461	0,66	1,0542	0,451	1,0501	0,6358
Q6P790	60S ribosomal protein L6 (Fragment)	7	1,2191	0,0025	1,0302	0,7281	1,0286	0,6572	0,8965	0,2512	0,987	0,8763
P05426	60S ribosomal protein L7	5	1,3498	0,0462	0,6788	0,065	1,1405	0,3092	0,9309	0,3885	1,0532	0,5387
P85970	Actin-related protein 2/3 complex sub-unit 2	11	0,9564	0,6557	0,9226	0,2715	1,3327	0,0061	1,0044	0,938	1,0774	0,3839
Q9Z1P2	Alpha-actinin-1	77	0,8727	0,0028	0,8694	0,0002	1,3424	0,0013	0,8164	0,0001	0,9543	0,1358
Q9QXQ0	Alpha-actinin-4	50	1,2074	0,0004	1,1204	0,037	1,0349	0,3567	0,9069	0,2105	1,1419	0,036
Q66HH8	Annexin 5	9	0,9925	0,8998	1,0383	0,7603	0,9707	0,811	0,9909	0,8915	1,4149	0,0034
Continued												

Accession	Name	Peptides (95%)	I/N	PVal I/N	Y/I	PVal Y/I	PP/Y	Pval PP/Y	P/PP	PVal P/PP	A/P	PVal A/P
P45592	Cofilin-1	12	1,2442	0,0041	1,0603	0,5475	1,0804	0,2025	0,9203	0,5481	1,2685	0,011
D3ZH41	Cytoskeleton-associated protein 4 (Predicted)	12	0,7853	0,0004	1,107	0,0513	0,9476	0,3458	0,7919	0,0005	1,2344	0,0033
Q6AYH5	Dynactin subunit 2	3	1,151	0,2739	0,8845	0,3112	1,1661	0,2508	0,8114	0,3778	1,3787	0,0248
P52555	Endoplasmic reticulum resident protein 29	2	1,0186	0,8459	1,3064	0,1141	1,2519	0,2488	0,8626	0,2226	1,5742	0,0319
Q6P3V8	Eukaryotic translation initiation factor 4A1	13	1,0465	0,4461	0,8673	0,0328	1,055	0,416	1,0269	0,6429	0,7893	0,0001
P04937	Fibronectin	17	1,1267	0,3104	0,7887	0,0119	1,2538	0,0001	0,6481	0,0907	2,4985	0,0056
Q6P792	Four and a half LIM domains 1	6	0,7431	0,0006	1,7903	0,0001	1,1108	0,096	0,7768	0,0085	0,8731	0,0375
P11762	Galectin-1 OS=Rattus norvegicus	14	0,7674	0,0204	0,7313	0,053	1,2804	0,0564	0,8213	0,4313	1,1116	0,227
B6DYQ2	Glutathione S-transferase mu 2	5	1,1023	0,4484	1,0507	0,6202	0,8053	0,0678	0,8616	0,3082	1,2838	0,0235
P63245	Guanine nucleotide-binding protein subunit beta-2-like 1	6	1,0188	0,7481	0,8543	0,044	1,0255	0,6962	1,0046	0,963	0,9843	0,8938
Q6P7Q4	Lactoylglutathione lyase	6	0,8942	0,2376	0,9113	0,2336	1,2099	0,0449	0,9186	0,2639	1,0132	0,8509
G3V8L3	Lamin A, isoform CRA_b	26	0,9048	0,0029	0,968	0,4478	1,1812	0,0001	1,0126	0,746	1,2067	0
Q99MZ8	LIM and SH3 domain protein 1	5	1,4773	0,0032	1,0103	0,9316	1,1251	0,1144	0,7622	0,0071	1,3922	0,0031
O08557	N(G), N(G)-dimethylarginine dimethylamino-hydrolase 1	4	0,8682	0,4556	2,2145	0,0173	0,5358	0,0395	0,7504	0,1763	1,2909	0,0453
Q6S3A0	Plectin 6	28	1,0437	0,2665	0,9378	0,1139	1,1564	0,0026	0,996	0,9259	1,2269	0,0027
D4A4Z9	Protein Ktn1	7	0,9773	0,8388	0,901	0,2289	1,3423	0,0487	0,7373	0,0131	1,0952	0,3487
D3ZPL5	Protein LOC100361311	10	1,2843	0,0356	0,683	0,017	1,0148	0,8697	0,9663	0,7274	1,1144	0,0623
M0RCY2	Protein LOC683961	6	0,9886	0,9133	0,9596	0,6555	0,761	0,0353	1,4335	0,0202	0,591	0,0003
D3ZN21	Protein RGD1309586	6	0,951	0,6075	0,9746	0,7735	0,957	0,6381	1,2502	0,0226	0,8539	0,0205
D4A6W6	Protein RGD1561333	6	1,7423	0,0038	0,5049	0,0038	1,2265	0,2464	0,8945	0,5405	1,1717	0,2285
D4A6W6	Protein RGD1561333	5	1,1352	0,1387	1,0601	0,5478	0,9173	0,2914	1,5332	0,0034	0,6202	0,0124
F1LT35	Protein RGD1564606 (Fragment)	6	1,1172	0,1379	1,1037	0,4799	1,0681	0,4407	0,772	0,0124	1,2544	0,0157
G3V852	Protein Tln1	38	1,2686	0	1,2229	0	0,8272	0	0,9642	0,3307	1,3768	0
Q4QQV0	Protein Tubb6	22	1,0776	0,4062	0,8668	0,3417	1,2995	0,0298	0,946	0,6332	1,0638	0,6569
Q6P3E1	Rps16 protein (Fragment)	7	1,6881	0,0047	0,5471	0,0061	1,508	0,0481	0,8378	0,1083	1,2384	0,0629
Q9QZR6	Septin-9	6	1,0595	0,4348	0,9334	0,3019	1,2185	0,0277	0,8772	0,1483	1,017	0,8438
Q6LDS4	Superoxide dismutase [Cu-Zn]	6	1,1464	0,0737	1,169	0,0483	0,8679	0,0643	1,0068	0,9549	1,3603	0,0094

Continued

Accession	Name	Peptides (95%)	I/N	PVal I/N	Y/I	PVal Y/I	PP/Y	Pval PP/Y	P/PP	PVal P/PP	A/P	PVal A/P
P07895	Superoxide dismutase [Mn], mitochondrial	10	0,76	0,2573	0,9976	0,9829	2,2825	0,02	1,074	0,2946	1,3438	0,0046
P28480	T-complex protein 1 subunit alpha	6	0,7782	0,0579	1,5251	0,0086	0,9731	0,7177	1,2381	0,2501	0,9675	0,8659
Q68FQ0	T-complex protein 1 subunit epsilon	4	0,8933	0,2273	1,0047	0,9576	0,9601	0,7021	1,1826	0,1497	0,8175	0,0229
Q6P502	T-complex protein 1 subunit gamma	5	1,0456	0,4189	0,8549	0,0333	1,0502	0,74	1,0936	0,3134	0,9009	0,3475
P11232	Thioredoxin	9	0,9519	0,7004	0,9806	0,8828	1,1098	0,4942	0,9058	0,4438	1,2619	0,0373
Q99PD6	Transforming growth factor beta-1-induced transcript 1 protein	6	1,0858	0,7029	0,7535	0,8138	1,2703	0,2603	0,635	0,0115	0,8607	0,8969
P68370	Tubulin alpha-1A chain OS=Rattus norvegicus GN= Tuba1a PE=1 SV=1	19	1,1996	0,0477	1,1154	0,0721	0,7776	0,0946	0,9411	0,7092	0,7696	0,0004
R9PXU6	Vinculin	57	1,1908	0	0,9981	0,9534	1,4169	0	0,8383	0,0001	1,1453	0

Table 2. List of modulated proteins in mesenchymal stem cells at different ages classified according to their principal biological process using iTRAQ analysis.

expression of proliferation marker Ki67²⁵ because of the lowest levels of Ki67 corresponded with less cells number in proliferation assays in infant and pre-pubertal groups. On the other way high levels of CD117, a self-renewal marker in MSCs as indicated Blazquez-Martinez *et al.*²⁶ were corresponding to higher cells number in proliferation assay of pubertal and adult groups of animal respect to the rest groups (Fig. 1B,C).

60 modulated proteins found in our iTRAQ analysis were involved in proliferation as 60S ribosomal proteins with different sedimentation speed like 60S RP L10, 60S RP L9, 60S RP L23, 60S RP L24, 60S RP L4, 60S RP L6 and 60S RP L7 were over-expressed in young group respect to the others indicating their increased potential of pluripotency which would be in concordance with its low expression of Nanog gene by RT-PCR analysis (Fig. 2C) in this group as also Das *et al.*²⁷ found over-expressed these proteins in different animal model process. Our results indicated that expression of Vinculin gene (Fig. 3C) was very low in newborn and young which were the most proliferative groups (Fig. 1B) on the opposite way pre-pubertal and adult presented high Vinculin gene expression coincidentally with less proliferative potential. Toma-Jonik *et al.*²⁸ published very recently that Vinculin, which is a protein involved in cell motility and adherence, was down-regulated in cells with great mobilization and proliferation potential like melanoma cells and at the same time Piltti *et al.*²⁹ published that Rho kinase inhibitor (ROCKi) treatment increased the cellular proliferation up, in human foreskin fibroblast cells and, significantly less Vinculin-associated focal adhesions were present in these ROCKi-treated cells³⁰. 11 β -hydroxysteroid dehydrogenase type 1 (11 β -HSD1), is an enzyme which generates glucocorticoids in intact cells, was found in our iTRAQ analysis significant increased in prepubertal group, this fact could explain the decrease proliferation potential and increase adipogenic differentiation in prepubertal group. All this is coincident with Bujalska *et al.*³¹ who published that 11 β -HSD1 activity is uncommitted adipose stromal cells may facilitate proliferation rather than differentiation. Transforming growth factor β 1 (TGF- β 1) induces senescence in BM-MSCs via increases the mitochondrial reactive oxygen species production and also the ROS intracellular production is associated with decreasing mitochondrial membrane potential, DNA damage and cell senescence^{32,33}, this fact could explain that statistically significant ($p < 0.05$) decreasing of total ROS in pre-pubertal group because TGF- β 1 was found statistically significant ($p < 0.05$) low with respect to other groups in the iTRAQ analysis.

86 modulated proteins found in our iTRAQ analysis were involved in pluripotency process. Terme *et al.*³⁴ showed that pluripotent cells had decreased levels of H1.0 and increased levels of H1.1, H1.3, and H1.5 compared with differentiated cells. Our results also indicated that H4 was statistically significant decrease in adult group which could point towards their less pluripotency with respect to the other groups, differentiation of embryonic stem cells is accompanied by a global reduction of panacetylation of histones H3 and H4 suggesting that histone acetylation plays an important role in maintenance of embryonic stem cells pluripotency³⁵. Results published by Bermeo *et al.*³⁶ indicate that MSCs over-expressing Lamin A had higher oestrogenic and lower radiogenic differentiation

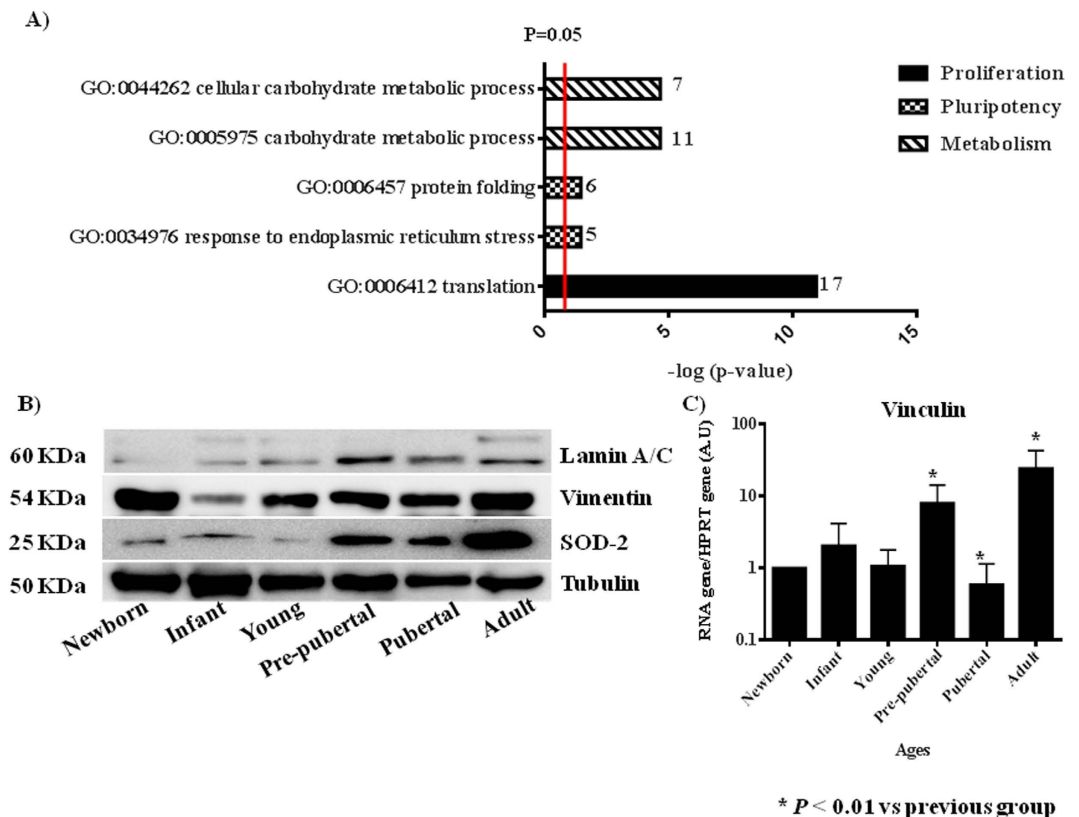


Figure 3. Validation of iTRAQ analysis. (A) Significant activates pathways obtained by comparing modulated proteins obtained by iTRAQ analysis employing functional annotations according to the String 9.0 software. Small numbers on the right of each bar are the modulated protein involved in each process. (B) Western blot analysis of Lamin A/C, Vimentin and Superoxide dismutase 2 (SOD-2). Tubulin was used as housekeeping. On the left molecular weight of each protein is shown. On the bottom the group's source of mesenchymal stem cells used. The gels have been run under the same experimental conditions. (C) Vinculin gene expression using real-time reverse transcriptase PCR (qRT-PCR) analysis normalized by expression of HPRT gene used as housekeeping.

potential. Their studies demonstrated that lamin A/C played a significant role in the differentiation towards both osteoblast and adipocyte lines by regulating some of the elements of Wnt/ β -catenin signaling during early MSCs differentiation, indicating that MSC over expressing Lamina A have higher osteogenic and lower adipogenic differentiation potential. Our results were coincident with Bermeo's results, because of we found high levels of Lamina A/C by western in MSCs from adult group which we could link to lowest adipogenic potential with the statistically significant ($p < 0.05$) lowest levels of oil red staining during its directed differentiation (Fig. 2A,B). Also we consider the role of Lamina A like a senescence marker and its relationship with increase of ROS³⁷ together with increase of Thioredoxin found in our iTRAQ study in adult group could indicate the loss of functionality with age, it might be due to the accumulation of oxidative damage also induce because decrease of SOD2 in this adult group. Stolzing *et al.*³⁸ demonstrated that age influences impairment of mesenchymal progenitor cells function.

55 modulated proteins found were involved in energetic metabolism process. The decision to exit pluripotency and undergo differentiation is of singular importance for pluripotent cells, including MSCs. The molecular mechanisms for these decisions to differentiate, as well as reversing those decisions during induced pluripotency have focused largely on transcriptomic controls. Easley *et al.*³⁹ explored the role of translational control for the maintenance of pluripotency and the decisions to differentiate. ATP-citrate synthase is deep linked to pentose phosphate route and its inhibition has been recently linked to a decrease in proliferation rate⁴⁰. Also it has been reported by Pattapa *et cols.*⁴¹ that MSCs resided under hypoxic conditions which were associated with the inherent metabolism of the cells. However MSCs under normoxia growth conditions derived a significant proportion of ATP from oxidative phosphorylation in addition to glycolysis. The observed increase of LDH in MSCs from adult group (Fig. 4C) could be explained because this group also had the glycolysis increased, on the other way glycolysis decreased in pre-pubertal group. All these results have been supported with our results through pentose phosphate

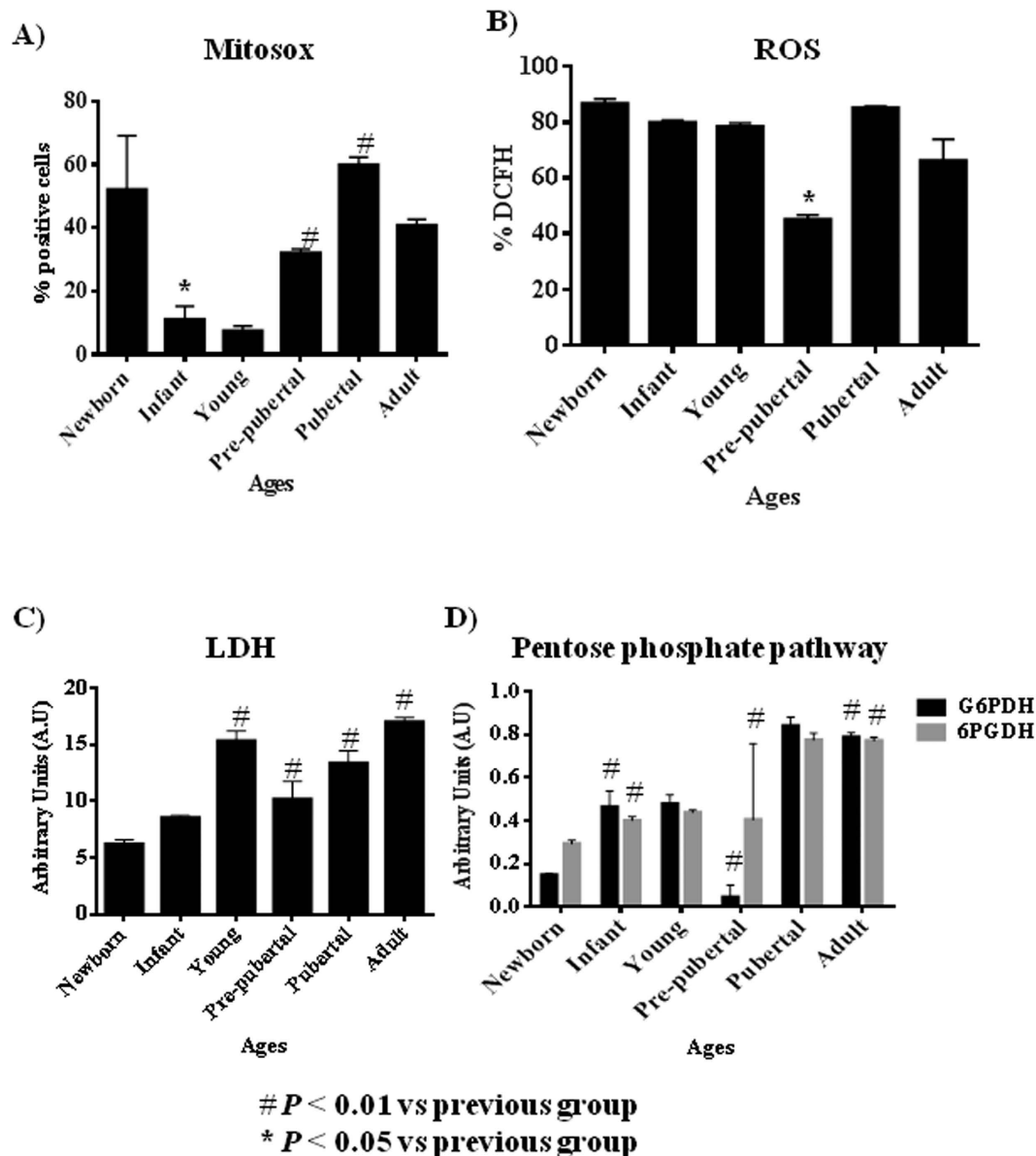


Figure 4. Metabolism profile from rats mesenchymal stem cells at different age. (A) 2',7'-dichlorofluorescein signal measured by flow cytometry to check ROS intracellular (B) Mitoxox signal measured by flow cytometry to check ROS mitochondrial. (C) Lactate-dehydrogenase (LDH) activity measured by spectrophotometer analysis. (D) Pentose phosphate pathway activity measured by spectrometer analysis. G6PDH = Glucose-6-phosphate 1-dehydrogenase; 6PGDH = 6-phosphogluconate-dehydrogenase. * p value less than 0.01 compared with previous group and # p value less than 0.05 compared with previous group, were considered statistically significant using Mann-Whitney-U tests.

pathway activity because of were significantly decreased G6PDH in pre-pubertal group and significantly increased in adult group (Fig. 4D).

Global protein translation is significantly reduced in hESCs compared to their differentiated progeny. mTOR is a Ser/Thr protein kinase that functions as an ATP and amino acid sensor to balance nutrient availability and cell growth⁴². mTOR regulates cellular senescence and drives bioenergetic infrastructure¹². mTOR restrains proliferation potential of stem cells mediating their self-renewal loss, which is an effect that can be suppressed by mTOR-inhibitors, such as rapamycin, antagonizing senescence⁴³. mTOR plays an important role in the regulation of hematopoietic stem cell self-renewal *in vitro* and inhibition of mTOR hyperactivation with rapamycin may represent a novel approach to promote *ex vivo* expansion and their long-term hematopoietic reconstitution of hematopoietic stem cells⁴⁴. Our results of mTOR family by western blot analysis indicated that mTOR (Fig. 5A,B) was statistically significant increased in adult group versus the other groups studied it could mean that MSCs from adult group were more

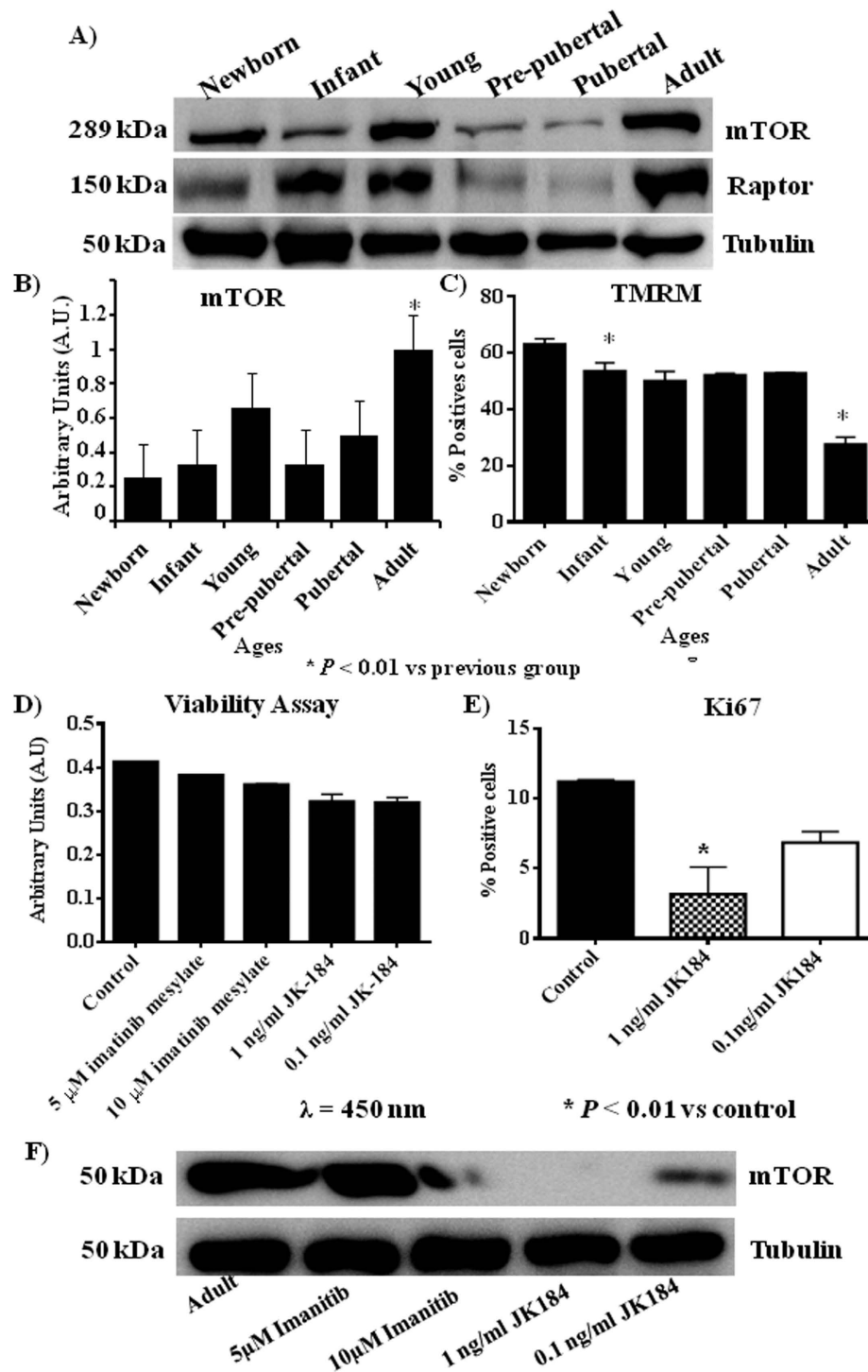


Figure 5. mTOR pathway profile from rat mesenchymal stem cells at different age (A) Western blot of mTOR pathway, mTOR and raptor, Tubulin was used as housekeeping. (B) Densitometry analysis of westerns of mTOR normalized with respect to Tubulin. **p* value less than 0.01 compared with previous group. (C) Tetramethylrhodamine, methyl ester (TMRM) dye accumulated in active mitochondria with intact potentials, was used to detect functional mitochondria in the MSCs at different ages following functional mitochondrial staining protocol from commercial. (D) Viability assay of mesenchymal stem cells from adult group incubated with 10 μM or 5 μM of imatinib mesylate or 1 ng/ml or 0.1 ng/ml of JK184. (E) Flow cytometry of Ki67 from mesenchymal stem cells of adult group incubated with 1 ng/ml or 0.1 ng/ml of JK184 in the medium. (F) Western blot of mTOR and Tubulin of mesenchymal stem cells from adult group after incubating with 10 μM or 5 μM of imatinib mesylate or 1 ng/ml or 0.1 ng/ml of JK184 in the medium. Control = mesenchymal stem cells incubated with growth medium alone. The gels have been run under the same experimental conditions. **p* value less than 0.01 compared with control group was considered statistically significant using Mann-Whitney-U tests.

senescence than MSCs from younger groups and this result was corroborated by expression of Lamin A/C in adult group in front at no expression of Lamin A in the other groups (Fig. 3B) together with less expression of TMRM (Fig. 5C) in adult group.

We found correlation between inhibition of mTOR and decrease of CD117 and Ki67 which are proliferation markers in the literature^{45,46} and we wonder if this relationship between mTOR pathway and proliferation was present when the proliferation markers were inhibited by specific reagents. Our results using inhibitors of CD117 and Ki67, imatinib mesylate and JK184 respectively, indicated that mTOR pathway can be modified through modification of proliferation markers, because the MSCs from adult group was treated with the Ki67 inhibitor at two physiological dose which do not affected their viability (Fig. 5D) but the expression of mTOR was modified when the proliferation marker Ki67 and CD117 were diminished (Fig. 5F).

Conclusions

The importance of our study lies in the fact that age from the MSCs source directly influences their differentiation, proliferative and metabolism profiles and also it is the first time where is shown the direct influence of proliferative markers CD117 and Ki67 on activation of mTOR pathway. Summary we affirm that young group of rats has the most proliferative and pluripotent MSCs be able to future functional studies.

References

- Murphy, M. B., Moncivais, K. & Caplan, A. I. Mesenchymal stem cells: environmentally responsive therapeutics for regenerative medicine. *Experimental & Molecular Medicine*. **45**, e54 (2013).
- Bach, M., Schimmelpfennig, C. & Stolzing, A. Influence of murine mesenchymal stem cells on proliferation, phenotype, vitality, and cytotoxicity of murine cytokine-induced killer cells in coculture. *PLoS One*. **9**, e88115 (2014).
- Zhang, L. *et al.* The Effects of Mesenchymal Stem Cells in Craniofacial Tissue Engineering. *Current Stem Cell Research & Therapy*. **9**, 280–289 (2014).
- Yeh, H. Y. *et al.* Neocartilage formation from mesenchymal stem cells grown in type II collagen-hyaluronan composite scaffolds. *Differentiation*. **86**, 171–183 (2014).
- Song, J. Q. *et al.* Effect of treadmill exercise timing on repair of full-thickness defects of articular cartilage by bone-derived mesenchymal stem cells: an experimental investigation in rats. *PLoS One*. **9**, e90858 (2014).
- Jin, H. J. *et al.* Comparative analysis of human mesenchymal stem cells from bone marrow, adipose tissue, and umbilical cord blood as sources of cell therapy. *International Journal of Molecular Sciences*. **14**, 17986–18001 (2013).
- Gharibi, B. *et al.* Inhibition of Akt/mTOR attenuates age-related changes in mesenchymal stem cells. *Stem Cells*. **32**, 2256–2266 (2014).
- Tawonsawatruk, T. *et al.* Growth kinetics of rat mesenchymal stem cells from 3 potential sources: bone marrow, periosteum and adipose tissue. *Journal of the Medical Association of Thailand*. **95**, 189–197 (2012).
- Geißler, S. *et al.* Functional comparison of chronological and *in vitro* aging: differential role of the cytoskeleton and mitochondria in mesenchymal stromal cells. *PLoS One*. **7**, e2700 (2012).
- Mantovani, C. *et al.* Morphological, molecular and functional differences of adult bone marrow- and adipose-derived stem cells isolated from rats of different ages. *Experimental Cell Research*. **318**, 2034–2048 (2012).
- Tsai, C. C. *et al.* Hypoxia inhibits senescence and maintains mesenchymal stem cell properties through down-regulation of E2A-p21 by HIF-TWIST. *Blood*. **117**, 459–469 (2011).
- Han, J. *et al.* Nanog reverses the effects of organismal aging on mesenchymal stem cell proliferation and myogenic differentiation potential. *Stem Cells*. **30**, 2746–2759 (2012).
- Hay, N. & Sonenberg, N. Upstream and downstream of mTOR. *Genes & Development*. **18**, 1926–1945 (2004).
- Anisimov, V. N. *et al.* Rapamycin increases lifespan and inhibits spontaneous tumorigenesis in inbred female mice. *Cell Cycle*. **10**, 4230–4236 (2011).
- Menendez, J. A. *et al.* mTOR- regulated senescence and autophagy during reprogramming of somatic cells to pluripotency: a roadmap from energy metabolism to stem cell renewal and aging. *Cell Cycle*. **10**, 3658–3677 (2011).
- Mearadji, A. *et al.* Decrease of CD117 expression as possible prognostic marker for recurrence in the resected specimen after imatinib treatment in patients with initially unresectable gastrointestinal stromal tumors: a clinicopathological analysis. *Anticancer Drugs*. **19**, 607–612 (2008).
- Zhang, N. *et al.* Biodegradable polymeric micelles encapsulated JK184 suppress tumor growth through inhibiting Hedgehog signaling pathway. *Nanoscale*. **7**, 2609–2624 (2015).
- Karaoz, E. *et al.* Characterization of mesenchymal stem cells from rat bone marrow: ultrastructural properties, differentiation potential and immunophenotypic markers. *Histochemistry and Cell Biology*. **132**, 533–546 (2009).
- Livak, K. J. & Schmittgen, T. D. Analysis of relative gene expression data using real-time quantitative PCR and the 2^{(-Delta Delta C (T))} Method. *Methods*. **25**, 402–408 (2001).
- Matsushime, H. *et al.* D-type cyclin-dependent kinase activity in mammalian cells. *Molecular and Cellular Biology*. **14**, 2066–2076 (1994).
- Szklarczyk, D. *et al.* The STRING database in 2011: functional interaction networks of proteins, globally integrated and scored. *Nucleic Acids Research*. **39**, 561–568 (2011).
- Harting M., Jimenez F., Pati S. *et al.* Immunophenotype characterization of rat mesenchymal stromal cells. *Cytotherapy*. **10**, 243–253 (2008).
- Mateos, J. *et al.* Proteomic applications in the study of human mesenchymal stem cells. *Proteomes*. **2**, 53–71 (2008).
- Jadaliha, M. *et al.* Quantitative proteomic analysis of human embryonic stem cell differentiation by 8-plex iTRAQ labelling. *PLoS One*. **7**, e38532 (2012).
- Scholzen, T. & Gerdes, J. The Ki-67 protein: from the known and the unknown. *The Journal of Cellular Physiology*. **182**, 311–322 (2000).
- Blazquez-Martinez, A. *et al.* C-Kit identifies a subpopulation of mesenchymal stem cells in adipose tissue with higher telomerase expression and differentiation potential. *Differentiation*. **3**, 147–160 (2014).
- Das, S. *et al.* Over-expression of 60s ribosomal L23a is associated with cellular proliferation in SAG resistant clinical isolates of *Leishmania donovani*. *PLoS Neglected Tropical Diseases*. **7**, e2527 (2013).

28. Toma-Jonik, A. *et al.* Active heat shock transcription factor 1 supports migration of the melanoma cells via vinculin down-regulation. *Cellular Signaling*. **27**, 394–401 (2015).
29. Piltti, J. *et al.* Rho-kinase inhibitor Y-27632 increases cellular proliferation and migration in human foreskin fibroblast cells. *Proteomics*. **15**, 2953–2965 (2015).
30. Holle, A. W. *et al.* *In situ* Mechanotransduction via Vinculin regulates stem cell differentiation. *Stem Cells*. **31**, 10.1002/stem.1490 (2013).
31. Bujalska, I. J. *et al.* A switch in dehydrogenase to reductase activity of 11 β -hydroxysteroid dehydrogenase type 1 upon differentiation of human omental adipose stromal cells. *Mech Ageing Dev.* **124**, 747–757 (2013).
32. Yoon, Y. S. *et al.* Formation of elongated giant mitochondria in DFO-induced cellular senescence: involvement of enhanced fusion process through modulation of Fis1. *Journal of Cellular Physiology*. **209**, 468–480 (2006).
33. Wu, J. *et al.* TGF- β 1 induces senescence of bone marrow mesenchymal stem cells via increase of mitochondrial ROS production. *BMC Developmental Biology*. **14**, 10.1186/1471-213X-14-21 (2014).
34. Terme, J. M. *et al.* Histone H1 variants are differentially expressed and incorporated into chromatin during differentiation and reprogramming to pluripotency. *The Journal of Biological Chemistry*. **286**, 35347–35357 (2011).
35. Horne, G. A. *et al.* Nanog Requires BRD4 to Maintain Murine Embryonic Stem Cell Pluripotency and Is Suppressed by Bromodomain Inhibitor JQ1 Together with Lefty1. *Stem Cells Development*. **24**, 879–891 (2015).
36. Bermeo, S. *et al.* Lamin A/C Acts as an Essential Factor in Mesenchymal Stem Cell Differentiation through the Regulation of the Dynamics of the Wnt/ β -Catenin Pathway. *Journal Cell Biochemistry*. **4**, 10.1002/jcb.25185. (2015).
37. Mateos J., De la Fuente A., Lesende-Rodriguez I. *et al.* Lamin A deregulation in human mesenchymal stem cells promotes an impairment in their chondrogenic potential and imbalance in their response to oxidative stress. *Stem Cell Res.* **11**, 1137–1148 (2013).
38. Stolzing, A. & Scutt, A. Age-related impairment of mesenchymal progenitor cell function. *Ageing Cell*. **5**, 213–224 (2006).
39. Easley, C. A. *et al.* mTOR- mediated activation of p70 S6K induces differentiation of pluripotent human embryonic stem cells. *Cell Reprogramming*. **12**, 263–273 (2010).
40. Lin, R. *et al.* Acetylation stabilizes ATP-citrate lyase to promote lipid biosynthesis and tumor growth. *Molecular Cell*. **51**, 506–518 (2013).
41. Pttappa, G. *et al.* The metabolism of human stem cells during proliferation and differentiation. *J Cell Physiol*. **226**, 2562–2570 (2011).
42. Sabers, C. J. *et al.* Isolation of a protein target of the FKBP12-rapamycin complex in mammalian cells. *The Journal of Biological Chemistry*. **270**, 815–822 (1995).
43. Martins I., Galluzzi L. & Kroemer G. Hormesis cell death and aging. *Ageing*. **3**, 821–828 (2011).
44. Luo, Y. *et al.* Rapamycin enhances long-term hematopoietic reconstitution of *ex vivo* expanded mouse hematopoietic stem cells by inhibiting senescence. *Transplantation*. **97**, 20–29 (2014).
45. Dillenburg, C. S., Martins, M. D., Meurer, L., Castilho, R. M. & Squarize, C. H. Keratoacanthoma of the Lip: Activation of the mTOR Pathway, Tumor Suppressor Proteins, and Tumor Senescence. *Medicine*. **94**, e1552 (2015).
46. Yang, A. *et al.* Differential Responses of Hematopoietic Stem and Progenitor Cells to mTOR Inhibition. *Stem Cells Int.* **561404**, 10.1155/2015/561404. (2015).

Acknowledgements

The authors wish to thank Mrs. Purificación Filgueira Fernández and Mrs. Noa Goyanes and Mrs. María José Sánchez Dopico for technical assistance. This study was supported by a grant EM2013/011(Xunta de Galicia, Spain, to S.S.-A.) and a grant from Instituto de Salud Carlos III - Ministerio Economía y Competitividad N° Expediente PI11/02799 Unión Europea - Fondo Europeo de Desarrollo Regional (FEDER) “Una manera de hacer Europa”

Author Contributions

J.F.-L. realized validation experiments P.F.-P. carried out the isolation of MSCs. S.S. realized the enzymatic experiments. I.F. and N.O. realized the statistical analysis. J.D.T. realized important suggestions which improving the manuscript. J.M. and M.C.A. conceived the study, participated in its design and coordination, and drafted the manuscript. J.F.-L., P.F.-P., J.D.T., N.O., S.S.-A., J.M. and M.C.A. have given final approval of the version to be published.

Additional Information

Competing financial interests: The authors declare no competing financial interests.

How to cite this article: Fafián-Labora, J. *et al.* Influence of age on rat bone-marrow mesenchymal stem cells potential. *Sci. Rep.* **5**, 16765; doi: 10.1038/srep16765 (2015).



This work is licensed under a Creative Commons Attribution 4.0 International License. The images or other third party material in this article are included in the article's Creative Commons license, unless indicated otherwise in the credit line; if the material is not included under the Creative Commons license, users will need to obtain permission from the license holder to reproduce the material. To view a copy of this license, visit <http://creativecommons.org/licenses/by/4.0/>

Dear Editor,

I am re-submitting this new version of manuscript entitled: **Effect of age on pro-inflammatory miRNAs contained in mesenchymal stem cells-derived extracellular vesicles** by Juan Fafián-Labora et al. We would like this manuscript to be considered for publication in Scientific Reports.

All of authors from this manuscript want to grateful the kindly and positive comments from the reviewer and we hope that he/she stays satisfied with our responses in this new version of the manuscript.

Looking forward to hearing from you soon.

María del Carmen Arufe Gonda, Ph.D.
Medicine Department. University of A Coruña
Rheumatology Division. CIBER-BBN/ISCIII
Cellular Therapy and Regenerative Medicine Group (TCMR-CHUAC)
INIBIC-Hospital Universitario A Coruña
15006 A Coruña- Spain
Phone: 34-981-176399 Fax: 34-981-176398 maria.arufe@udc.es

Effect of age on pro-inflammatory miRNAs contained in mesenchymal stem cells-derived extracellular vesicles

J. Fafián-Labora¹, I. Lesende-Rodríguez¹, P. Fernández-Pernas¹, S. Sangiao-Alvarellos², L. Monserrat³, O. J. Arntz⁴, F. J. Van de Loo⁴, J. Mateos¹,* MC. Arufe¹

¹*Grupo de Terapia Celular y Medicina Regenerativa (TCMR-CHUAC). CIBER-BBN/ISCIII. Servicio de Reumatología. Instituto de Investigación Biomédica de A Coruña (INIBIC). Complejo Hospitalario Universitario de A Coruña (CHUAC). SERGAS. Departamento de Medicina. Facultade de Oza. Universidade de A Coruña (UDC). As Xubias, 15006. A Coruña, Spain.*

²*Grupo Fisiopatología Endocrina, Nutricional y Médica (FENM-CHUAC). Instituto de Investigación Biomédica de A Coruña (INIBIC). Complejo Hospitalario Universitario de A Coruña (CHUAC). SERGAS. Departamento de Medicina. Facultade de Oza. Universidade de A Coruña (UDC). As Xubias, 15006. A Coruña, Spain.*

³*Cardiology Department, Health in Code, As Xubias, 15006. A Coruña, Spain*

⁴*Experimental Rheumatology. Radboudumc University Medical Center. Huispost 272, route 272. Postbus 9101. 6500 HB Nijmegen. The Netherlands.*

* Corresponding author

M. C. Arufe PhD

e-mail: maria.arufe@udc.es

Key Words: Mesenchymal stem cells, pro-inflammatory micro-RNAs, extra-cellular vesicles.

Running head: Ageing on MSC-derived EVs

ABSTRACT (195 words)

Stem cells possess significant age-depending differences in their immune-response profile. To deeply study these differences we have analyzed by Next Generation Sequencing six age groups from bone marrow mesenchymal stem cells. A total of 9628 genes presented differences of expression between age groups and those genes were grouped into metabolic pathways. We focused our research in young, pre-pubertal and adult groups which presented the highest amount of genes differentially expressed related with inflammation mediated by chemokine and cytokine signaling pathway compared with newborn group which was used as a control. Afterwards, extracellular vesicles from those groups were extracted and characterized by nanoparticle tracking and flow cytometry analysis and several micro-RNAs were checked by quantitative real time polymerase chain reaction because of their relationship with the pathway of interest. Since miR21-5p was statistically significant highest in extracellular vesicles from mesenchymal stem cells of pre-pubertal group, we realized a functional experiment inhibiting its expression and investigating the modulation of Toll-Like Receptor 4 and their link to damage-associated molecular patterns. Taking together these results indicate for the first time that mesenchymal stem cells extracellular vesicles-derived have significant differences in their immune profile and those differences are age depending.

INTRODUCTION

The promising role of mesenchymal stem cells (MSCs), whose mechanism of action is predominantly paracrine, in cell-based therapies and tissue engineering appears to be limited due to a decline of their regenerative potential with increasing donor age ¹. Next Generation Sequencing (NGS) is a versatile technology which allows cataloguing cellular constituents at a steady state and functional interactions when combined with system perturbation and differential analysis ² and together with novel methods of pattern recognition and network analyses ³, has revolutionized the field of Systems Biology. NGS from newborn, infant, young, pre-pubertal, pubertal and adult MSCs-bone marrow derived have been studied to evaluate the modified expressed genes during ageing. Recently, it has been reported the role of micro-RNAs in ageing and immunosenescence and their relevance on extracellular vesicles from MSCs affecting their therapeutic potential. Extracellular vesicles (EVs), such as exosomes or micro-vesicles are released by cells into environment as sub-micrometer particles enclosed by a phospholipid bilayer ⁴. EVs have been found to mediate interaction between cells, mediate non-classical protein secretion, facilitating processes such as antigen presentation, in trans signalling to neighbouring cells and transfer of RNAs and proteins ⁵. The detection of low copy numbers of mRNA and small RNAs, including micro-RNAs (miRNA), in EVs from mouse and human mast cell lines (MC/9 and HMC-1, respectively) has added much research interest impetus to the field ⁶. While mRNA and miRNA in EVs are inactive, they have the potential to be active when EVs are transfected into nearby cells. Studies indicate that EV miRNA expression profile may be of diagnostic/therapeutic potential ⁷. The Toll-like receptors (TLRs), an important component of innate and adaptive immune responses ⁸, are expressed in MSCs and their derived EVs during ageing. Damage-associated molecular patterns (DAMPs) are molecules that have a physiological role inside but acquire additional functions when exposed to the extracellular environment and they can be secreted or displayed by living cells undergoing a life-threatening stress ⁹. Thus, we studied the changes in activation of Toll-Like receptor 4 (TLR4) together with expression changes in the DAMP; S-100A4, S100A6 and HMGB1 and its relationship with miRNA21-5p in pre-pubertal MSCs.

MATERIAL AND METHODS

Isolation and culture of cells

For isolation of MSCs, the animals were anesthetized with Fluorane (Izasa, A Coruña, SP) and euthanized by cervical dislocation method. Femurs from male Wistar rat were dissected (Animal Service, CHUAC) at different ages: neonate (0 days old), infant (7 days old), young (14 days old), pre-pubertal (35-38 days old), pubertal (45 days old) and adult (more than 3 months old). All the methods were carried out in "accordance" with the approved guidelines of Spanish law (32/2007). All experimental protocols were approved by Animal Ethical Committee of Galicia. The protocol used by Karaoz *et al.*¹⁸ was followed in this work. Briefly, the ends of the bones were cut away and a 21-gauge needle that was inserted into shaft of the bone marrow was extruded by flushing with 5 ml D-Hank's solution supplemented with 100 IU/ml penicillin–100 mg/ml streptomycin (all from Life Technologies, Madrid, Spain). Marrow plug suspension was dispersed by pipetting it up and down, successively filtered through 70- μ m mesh nylon filter (BD Biosciences, Bedford, MA, USA), and centrifuged at 20000 g for 10 min. Supernatant containing platelets and erythrocytes was discarded, and the cell pellet was resuspended in the medium. The cells from four animals were seeded into 100 cm² dish plate (TM Nunclon) and incubated at 37 °C with 5% humidified CO₂. The MSCs were isolated on the basis of their ability to adhere to the culture plates. On the third day, red blood cells and other non-adherent cells were removed by pre-plating technique and fresh medium was added to allow further growth. The adherent cells grown to 70% confluence were defined as passage zero (P0) cells. After 5 min of centrifugation, 1x 10⁶ MSCs were seeded on two dish plates 100 cm² (TM Nunclon) in RPMI supplemented with 10% fetal bovine serum (FBS), 100 U/ml penicillin and 100 mg/ml streptomycin (all from Life Technologies, Madrid, SP). The medium was added and replaced every 3 or 4 days. The MSCs were expanded for 2 passages and characterized by flow cytometry.

RNA-Seq protocol

The study was designed to screen the complete transcriptome sequence per age group of Wistar rat. Sample preparation was carried out as recommended by Agilent SureSelect Strand-Specific RNA Library Prep for Illumina multiplexed sequencing method¹⁰. 1 μ g of total RNA per sample was performed. The Sequencing data was generated on Hiseq 1500 on a rapid mode flow cell from Illumina. Sample prep and sequencing was prepared in duplicate.

Real time quantitative polymerase chain reaction (qRT-PCR) analysis

RNA isolation was done using the TRIzol® extraction method. The quality of 1µL of each RNA samples was checked using as Agilent Bioanalyzer 2100 to determine the RIN (RNA Integrity) score using the Agilent 6000 Nanochip and reagents (Agilent, St. Clara, USA). Samples with a RIN score >7 were retained and converted to cDNA by SureSelet Strand Specific RNA library (Agilent, St. Clara, USA).

For miRNA detection, cDNA was generated from DNaseI-treated RNA, using a QuantiMir RT Kit (System Biosciences, CA, USA) according to the manufacturer's instructions. PCR products were amplified using specific primers for miRNAs: rno-miR-335 (MIMAT0000575; 5'-TCAAGAGCAATAACGAAAAATGT); rno-miR-155-5p (MIMAT0030409; 5'-TTAATGCTAATTGTGATAGGGGT); hsa-miR-132-5p (MIMAT0004594, 5'-ACCGTGGCTTTCGATTGTTACT); hsa-miR-146a (MIMAT0000449, 5'-TGAGAACTGAATCCATGGGTT); rno-miR-21-5p (MIMAT0000790, 5'-TAGCTTATCAGACTGATGTTGA) and hsa-miR-16 (MIMAT0000069, 5'-TAGCAGCACGTAAATATTGGCG). The amplification program consisted of initial denaturation at 50 °C for 2 minutes followed from 95 °C for 10 minutes and 50 cycles annealing at 95°C, depending on the gene, for 15 seconds and extension at 60°C for 1 minute. Primers for amplification of rat genes are described in detail in Table I. The amplification program consisted of initial denaturation at 92°C for 2 minutes followed by 40 cycles from 92°C for 15 seconds, annealing at 55-62°C, depending on the gene, for 30 seconds and extension at 72°C for 15 seconds. PCR analysis were done in triplicate, with each set of assays repeated three times. To minimize the effects of unequal quantities of starting RNA and to eliminate potential sources of inconsistency, relative expression levels of each gene was normalized to ribosomal protein (HPRT) or miR-16 using the 2^{-ΔΔ} Ct method ¹¹. Control experiments utilized no reverse transcriptase.

Isolation extracellular vesicles

Bone marrow mesenchymal stem cells from newborn (0 days), young (14 days), pre-pubertal (35-38 days) and adult (3 months) were cultured in RPMI 1640 Medium with GlutaMAX™ supplement and 10 % FBS-free exosomes (all Thermo Fisher Scientific, Massachusetts, USA), 100 U/ml penicillin and 100 mg/ml streptomycin (Sigma-Aldrich, St.Louis, USA). Cells were cultured with 80% confluence and supernatants

were collected after 48 hours. We isolated MSC-derived EVs using ultra centrifugation following the protocol published by Del Fattore *et al.*¹². In detail, supernatants were centrifugated at 1500 rpm for 10 min at 4 C and filtered using 0,22 µm filter sterilized (GE Healthcare Life Sciences, Maidstone, UK) to eliminate debris. Supernatants were transferred to ultracentrifugation tubes and centrifuged at 100000 x g for 2 hours at 4 C in Optimal-90K with 60 Ti rotor (Beckman Coulter, Mississauga, Canada). Supernatant containing exosomes-free media were removed and pellets were resuspended at 200 µl PBS.

Nanoparticle Tracking Analysis

EVs size distribution was estimated by the Brownian motion of the particles in a NanoSight LM12 using Nanoparticle Tracking Analysis 2.3 software (Nanosight Ltd, Amesbury, UK). EVs were diluted in PBS until a suitable concentration for analysis was reached. Particle concentration was evaluated for particles range between 30–150nm in diameter.

Electronic microscopy

EVs were concentrated using Vivaspin concentrators (Sartorius, Gottingen, Germany). EVs were taken up in small volumes of deionized water, which were placed on nickel grids and allowed to dry for 45 minutes at 37 C. The grids with EVs were then washed by transferring them onto several drops of deionized water. Negative contrast staining was performed by incubating the grids on top of drops of 6% uranyl acetate. Excess fluid was removed and the grids were allowed to dry before examination on a Jeol JEM1400 Transmission Electron Microscope (Jeol, Tokyo, Japan).

Flow Cytometry

To characterize the different populations of MSCs from chronological different animals, their MSCs were washed twice in PBS, then pre-blocked with 2% rat serum in PBS. The following direct antibodies were used: PE-conjugated mouse anti-rat CD34 (1:20 from DakoCytomation, Barcelona, SP); FITC-conjugated mouse anti-rat CD45 (1:20 BD Pharmingen, New Jersey, USA); PE-Cy5.5-conjugated mouse anti-rat CD90 (1:20 Immunostep, Salamanca, SP) and APC-conjugated mouse anti-rat CD29 (1:20 Immunostep, Salamanca, SP). The cells were washed with PBS after one hour of incubation with the corresponding antibody at room temperature. The stained cells were

then washed twice with PBS and 2×10^5 cells were analyzed with a FACS Aria flow cytometer (BD Science, Madrid, SP). FACS data was generated by DIVA software (BD Science). Negative control staining was performed using FITC-conjugated mouse IgG1K isotype, PE- conjugated mouse IgG1K isotype, PE-Cy5.5- conjugated mouse IgG1K isotype and APC- conjugated mouse IgG1K isotype (all from BD Pharmingen).

miRNA transitory transfections

MSCs were incubated with 40 nM hsa-miR-21-5p miRVana™ miRNA inhibitor or 40nM control negative miRVana™ using the expression system following manufacturer indications. Validation by RT-PCR was done using Taqman®MicroRNA Assay following commercial instructions (all from Ambion, Applied Biosystem, Madrid, SP)

Protein isolation and immunoblot analysis

The protein content into EVs was measured with a Micro-BCA kit (Thermo Scientific, Pierce, Rockford, USA) following manufacturer instructions. Immunoblot analysis was performed on 40 µg of total protein extracted from MSCs, as previously described¹³. The blots were probed with antibodies directed against: LMNA/C (Acrix); Wnt5a (Acrix); TLR4 (Immunostep); mTOR (Cell Signaling); HMGB1 (Abcam); pAKT; AKT and tubulin (all from Cell Signaling) or B-actin (Sigma-Aldrich) were used for housekeeping. A secondary anti-rabbit (Cell Signalling) or anti-mouse (DAKO) antibodies was used to visualize proteins using an Amersham ECL Western Blotting Analysis System (GE Healthcare, Amersham Biotechnology, Manchester, UK). Ideal concentrations for each antibody were determined empirically. Working concentrations were 1:1000 of the recommended stock solutions.

Bioinformatic analysis

An average of 25 million paired-end 100bp reads was obtained per sample. The raw RNA-seq reads for each sample were aligned to the reference rat genome browser (rn6 assembly) using Bowtie2 (bowtie-bio.sourceforge.net/index.shtml/) and Tophat2 (<http://tophat.cbcb.umd.edu/>). After alignment, raw sequence read depths was converted to estimate transcript abundance measures as fragments per kilo base of exons per million (FPKM) values Cufflinks (<http://cufflinks.cbcb.umd.edu/>) differentially expressed genes and transcripts were calculate with Cuffdidd. Each group was compared with previous age group. The fold-change thresholds had to be greater than

1.2 and lower than 0.8. Identified genes with statistically significant changes were categorized according to their function, biological process and cellular component, using the R/Bioconductor package RamiGO (<http://bioconductor.org/packages/release/bioc/html/RamiGO.html>)¹⁴.

MicroRNA.org (<http://www.microrna.org>) was a resource of microRNA target predictions and expression profiles used in this work. Target predictions were based on a development of the miRanda algorithm¹⁵ and TargetScan¹⁶.

Statistical analysis

All experiments were realized in triplicate and one representative is shown. Statistical non-parametric analysis (Mann-Whitney U and Kruskal-Wallis tests) was performed using GraphPad Prism6 (GraphPad Software, La Jolla, CA). Each group was compared with previous group. A *p* value less than 0.05 or 0.01 was considered statistically significant. All the the data are presented as standard error of the mean.

RESULTS

Characterization of populations of MSCs from different age groups by flow cytometry indicated these populations presented less than 1% of positive cells for CD45 and CD34 hematopoietic markers and more than 60±5% positive cells for CD29 and more than 85±5% positive cells for CD90 (Fig. 1A).

NGS analysis indicated that a total of 9628 genes presented differences of expression between age groups as is shown in figure 1B. Modulated genes are indicated as up-regulated in red and down-regulated in blue, comparing age groups chronologically continuous. The results indicated that the expression pattern of 4741 genes change between newborn and infant groups; 4939 genes change their expression pattern between infant and young groups; 6339 genes change their expression pattern between young and pre-pubertal groups; 6568 genes change their expression pattern between pre-pubertal and pubertal groups and 6849 genes change their expression pattern between pubertal and adult groups. Figure 1C shows the hierarchical clustering of genes involved into five pathways common between the six age groups studied, using the R/Bioconductor package RamiGO with a signification >1.5-fold. Genes modulated between newborn and infant groups were grouped into eight metabolism pathways, while genes modulated from infant until adult groups were grouped into up to 15 metabolism pathways. The number of modulated genes involved into hormonal changes

as gonadotropin-releasing hormone pathway (PO6664) increased from infant age group until adult age group (76, 89, 116, 112 and 121 genes respectively). Genes involved into programmed death as apoptosis signaling pathway (PO00006) were observed modulated between young, pre-pubertal and adult groups (46, 57, 66 respectively). Genes involved into inflammation mediated by chemokine and cytokine signaling pathway (PO00031) was modulated in infant, young and pubertal groups (78, 82 and 103 genes respectively) (Fig. 2). NTA revealed out that the ratio protein/particle and the production of MSC-derived EVs decreased with increasing donor age ($40\pm 2\%$) (Fig. 3A), however MSC-derived-EVs production was increased with donor age ($26\pm 1\%$) (Fig. 3B). The size of the extracellular vesicles was 160 ± 18 nm and there were not significant differences among groups (Fig. 3C). MSC-derived EVs were visualized by electron microscopy as small vesicles, typically 40-80 nm in diameter (Figure 3D). Flow cytometry analysis of EVs attached to anti-CD63 beads revealed that they were at least $32\%\pm 3$ positive for CD63, an exosome marker membrane protein, at $10\mu\text{M}$ of concentration (Fig. 3E).

qRT-PCR analysis of miRNAs associated with TLR4: miR-146a; miR-155; miR-132; miR-21 and miR-335, which are involved also in immunosenescence process, found out that miR-146a, miR-155 and miR-132 decreased their expression until $93\pm 3\%$ with increase age donor. However, adult group presented the statistically significant highest expression of miR-335 ($P<0.01$) and pre-pubertal group presented the statistically significant highest expression of miR-21 ($P<0.01$) with respect the others (Figure 4 A-D). TLR4 protein concentration by western was checked after 4 hours of 10 ng/mL lipopolysaccharides (LPS) treatment (Fig. 4 F, G) and it was observed a high increase in the response against LPS in pre-pubertal group. To explain these results MSCs from pre-pubertal group was transitory transfected with miRVana miR-21-5p and its expression was checked by qRT-PCR (Fig. 5 A). The transfected cells expressed statistically significant lower ($P<0.05$) levels of miR-21 than the same cells transfected with a mimic miRNA used as control. qRT-PCR analysis of DAMPS associated with TLR4 indicated that miR-21 inhibition promotes a statistically significant decrease of S100A4, S100A6 and HMGB1 with respect to MSCs control (Fig. 5 C, D, E). Nanog gene expression was checked by qRT-PCR and it was statistically significant higher ($P<0.05$) than control (Fig. 5B).

Western analysis of proteins involved into immune response in miR-21 inhibited pre-pubertal MSCs revealed out that LMNA/C, TLR4, mTOR, pAKT were statistically significant down-regulated ($P<0.05$) with respect to control cells (Fig.6 A-C), HMGB1

was also down-regulated in the inhibited cells. On the other way Wnt5a and AKT were up-regulated statistically significant ($P<0.05$) with respect to control cells (Fig. 6A, C). miR-21 inhibition did not affect the immune response in front of LPS treatment since TLR4 through pAKT/AKT were statistically significant ($P<0.05$) up-regulated (Fig. 6D).

DISCUSSION

The use of MSCs has been adopted in cell-based therapy due to their multiple differentiation ability, the low expression of co-stimulatory molecules and immunosuppressive properties¹⁷. Although EVs have long been considered cellular artefacts or dust, recent progress in this area indicates that EVs are intercellular information, that is, extracellular organelles that have multifaceted physiological and pathological functions in intercellular communication as well as inter-species and inter-kingdom communication¹⁸. Martins *et al.*¹⁹ reported that EVs derived from human bone marrow MSCs had a regenerative potential that had been increasingly recognized. MSCs populations from different ageing groups were characterized by flow cytometry to check percentage of positive cells for MSCs markers, CD29 and CD90, and were negative for hematopoietic markers (CD34, CD45) (Fig. 1A). We did not observe statistically significant differences between the MSCs markers into the different MSCs aging group studied (data do not shown). These results were coincident with the results published by Jin *et al.*²⁰⁻²² indicating that MSCs have similar levels of surface antigen expression included MSCs from different tissues. Even the MSCs markers were as abundant as published by Harting *et al.*²³.

RNA-Seq analysis is an adequate technique to study gene expression modulation in complex systems^{24,25}. Our results by RNA-Seq analysis allowed the identification of 9628 genes statistically significant modulated between groups (Fig.1B). Our study represents a step further from a previous iTRAQ-based study²¹ where 210 differentially expressed proteins were detected. We used the R/Bioconductor package RamiGO which is an R interface to AmiGO that enables visualization of Gene Ontology (GO) trees¹⁴. RamiGO provides easy customization of annotation, highlighting of specific GO terms, using of terms by P-value. We showed RamiGO functionalities in a genome-wide gene set analysis of genes differentially expressed comparing six chronologically different groups from bone marrow derived MSCs (Fig. 1C). We were interested in genes involved into inflammation mediated by chemokine and cytokine signaling pathway

(PO00031) which were modulated in infant, young and pubertal groups (Fig. 2). Focusing in this pathway, 55 exosome markers were found using the bioinformatics platform ExoCarta²⁶. In concordance with our previous iTRAQ results based on quantitative proteomics²¹, miRNAs involved into exosomes and their relationship with inflammation mediated by chemokine and cytokine signaling pathway were obtained out by open-source software for target predictions miRanda and TargetScan. We focused then on the functional study of miRNAs expression involved in inflammation mediated by chemokine and cytokine signaling pathway into these groups and their EVs. EVs size was determined by NTA, which calculates the size from total concentration of the vesicles in solution. Also we followed the technique used by Gercel-Taylor *et al.*²⁷ who have reported their optimized method to measure the size distribution of cell-derived vesicles comparable to other analysis instrumentation. We found an increase in the production of MSC-derived EVs from adult group with respect to the others (Figure 3A). A rationale explanation for this fact is that calcium levels play a role in plasma membrane fusion events involved in adipose accumulation in bone marrow stromal cells with age²⁸. We previously found out levels of calcium/calmodulin-dependent protein kinase type II, caldesmon, calponin-1, calponin-3 and calreticulin statistically significant increased in the adult group with respect to the others by quantitative proteomics (iTRAQ) analysis²¹. In our present study, MSC-derived EVs have a size in the range of diameter published by Vallabhaneni *et al.*²⁹ (Figure 3A-C) with no significant differences between age groups. These data were validated by electronic microscopy (Figure 3D) and characterized by flow cytometry and they were more than 32% positives for CD63, a tetraspanin mainly associated with membranes of intracellular vesicles that it is considered as an exosome marker by the International Society for Extracellular Vesicles (ISEV)^{30,31} (Figure 3E). The acquired immune system shows a functional decline in ability to respond to new pathogens during ageing, whereas serum levels of inflammatory cytokines are increased with age³². Inflammaging is a new term coined by Olivieri *et al.*³³ to name those processes associated with age and their relationship with a loss of expression of TLR family, a process which could contribute to such inflammation imbalance. There is controversy on the role of TLR4 in pro-inflammatory and differentiation capacities from MSCs³⁴ and further research thereby will provide helpful tools for regenerative medicine. We checked the following miRNAs associated with TLR4 contained in MSC-derived EVs.

miR-146a because is one of key TLR-induced miRNAs, inhibiting the TLR-signalling pathway by targeting IRAK1 kinase and TRAF6 ligase. miR-132 because is a target of IL1R associated kinase IRAK 4, a regulator of production inflammatory cytokine ³⁵. miR-155 because is induced via TLR in macrophages and exerts profound effect on the activity of immune cells ^{36,37}. In our model we found decreased all these miRNAs contained in EVs with increasing age donor (Fig. 4A-C) suggesting an association among the decrease of immunologically active exosomes and the loss of capacity of activating immune system through the induction of anti-inflammatory cytokines and T cells. MSC-derived EVs from adult group contained the highest level of miR-335 (Fig. 4D). This could be associated with cell senescence and loss the therapeutic capacity and linked to the reduced capacity to activate protein kinase D1 (PRKD1), which in turn reduces the activity of AP-1 transcription factor ^{38,39}. miR-21 regulates negatively LPS-induced lipid accumulation and inflammatory response in macrophages by the TLR4-NF-kB pathway ⁴⁰ which is involved in human MSCs during differentiation by regulating SPRY229. We found the highest level of miR-21 in MSC-derived exosomes from pre-pubertal group and the lowest level in adult group (Fig. 4E) hence TLR4 could be a target to understand role of miR-21 in differentiation of pro-inflammatory capacity depending of donor age. BM-MSCs from adult group have less therapeutic capacity due to TLR4-mediated regulation of bone marrow MSCs proliferation and osteogenic differentiation through Wnt3a and Wnt5a signalling ⁴¹. Conversely, TLR4 activation in MSCs from umbilical cord increased this differentiation to a certain extent ⁴². Our results indicated that TLR4 trend to increase with age and that the treatment with LPS did not affect to their immunological response, at short incubation times such us 4 hours (Fig. 4G). Wnt5a expression augments through TLR4 in response to inflammatory mediators, as LPS, in several stem cells types and regulated cytokine and chemokine production ^{43,44}. Our results indicate that the inhibition of miR-21 produced an over-expression of Wnt5a accompanied by a decrease of LMNA/C, a senescence marker (Fig. 6 A), suggesting a role in self-renewal and pluripotent capacities of the MSCs. The increase of Nanog detected by RT-PCR (Fig. 5D) strongly supports this supposition. The inhibition of miR-21 disrupts TLR4 through AKT/mTOR pathway since mTOR and pAKT were down-regulated (Fig. 6 B, C). Similar results were observed by Gharibi *et al.* ⁴⁵. These authors proposed that inhibition of AKT/mTOR pathway was affecting TLR4. The immunological response of pre-pubertal MSCs group statistically significant

increased when miR-21 was inhibited (Fig. 6D) with respect to normal one (Fig. 4F). In the other side, TLR4 and pAKT/AKT increased their expressions in miR-21 inhibited pre-pubertal MSCs group after treatment with LPS. This result indicate that miR-21 affect to DAMPS and TLR4 levels but no to the immunological response of the MSCs to outside agents as LPS (Fig. 6D) pointing that miR-21 could be a regulator of TLR4 signalling⁴⁶.

CONCLUSION

Our results provide an insight into the mechanism involved in MSC aging and suggest possible interventions into miRNAs to maintain quiescence and function of MSCs and their derived extracellular vesicles prior to *in vivo* transplantation or as pharmacological agents in disease.

ACKNOWLEDGEMENTS

This study was supported by a grant from Instituto de Salud Carlos III - Ministerio Economía y Competitividad N° Expediente PI11/02799 Unión Europea - Fondo Europeo de Desarrollo Regional (FEDER) “Una manera de hacer Europa”. J.F-L was supported by European Molecular Biology Organization (EMBO) during a short-term fellowship in Van de Loo’s group. S.S-A. was supported by a grant EM2013/011 (Xunta de Galicia, Spain)

AUTHOR’S CONTRIBUTIONS

J. F-L. and I.L-R. carried out all experiments P. F-P. carried out the isolation and cultured bone-marrow MSCs. S. S. realized micro-RNA experiments. I. L-R and L. M. and J.M. realized the RNAseq analysis. MC. A. conceived the study, participated in its design and coordination, and drafted the manuscript. J. F-L, I. L-R, P. F-P, L. M, S. S-A, O. A, F. J. vd L, J.M. and M.C.A. have given final approval of the version to be published.

COMPETING FINANCIAL INTEREST

All authors declare not having any competing financial interests in relation to the work described in this manuscript.

REFERENCES

- 1 Efimenko, A. Y., Kochegura, T. N., Akopyan, Z. A. & Parfyonova, Y. V. Autologous Stem Cell Therapy: How Aging and Chronic Diseases Affect Stem and Progenitor Cells. *Biores Open Access* **4**, 26-38, doi:10.1089/biores.2014.0042 (2015).
- 2 Yang, H. J., Ratnapriya, R., Cogliati, T., Kim, J. W. & Swaroop, A. Vision from next generation sequencing: Multi-dimensional genome-wide analysis for producing gene regulatory networks underlying retinal development, aging and disease. *Prog Retin Eye Res*, doi:10.1016/j.preteyeres.2015.01.005 (2015).
- 3 Szklarczyk, D. *et al.* The STRING database in 2011: functional interaction networks of proteins, globally integrated and scored. *Nucleic Acids Res* **39**, D561-568, doi:10.1093/nar/gkq973 (2011).
- 4 Conde-Vancells, J. *et al.* Characterization and comprehensive proteome profiling of exosomes secreted by hepatocytes. *J Proteome Res* **7**, 5157-5166 (2008).
- 5 Simpson, R. J., Jensen, S. S. & Lim, J. W. Proteomic profiling of exosomes: current perspectives. *Proteomics* **8**, 4083-4099, doi:10.1002/pmic.200800109 (2008).
- 6 Valadi, H. *et al.* Exosome-mediated transfer of mRNAs and microRNAs is a novel mechanism of genetic exchange between cells. *Nat Cell Biol* **9**, 654-659, doi:10.1038/ncb1596 (2007).
- 7 Hunter, M. P. *et al.* Detection of microRNA expression in human peripheral blood microvesicles. *PLoS One* **3**, e3694, doi:10.1371/journal.pone.0003694 (2008).
- 8 Ma, Y. U., Zhang, L. I. & Li, Q. Expression levels of cytokines and chemokines increase in human peripheral blood mononuclear cells stimulated by activation of the Toll-like receptor 5 pathway. *Exp Ther Med* **11**, 588-592, doi:10.3892/etm.2015.2914 (2016).
- 9 Vénéreau, E., Ceriotti, C. & Bianchi, M. E. DAMPs from Cell Death to New Life. *Front Immunol* **6**, 422, doi:10.3389/fimmu.2015.00422 (2015).
- 10 Lopes, L. R. *et al.* Genetic complexity in hypertrophic cardiomyopathy revealed by high-throughput sequencing. *J Med Genet* **50**, 228-239, doi:10.1136/jmedgenet-2012-101270 (2013).
- 11 Livak, K. J. & Schmittgen, T. D. Analysis of relative gene expression data using real-time quantitative PCR and the 2(-Delta Delta C(T)) Method. *Methods* **25**, 402-408, doi:S1046-2023(01)91262-9 [pii] 10.1006/meth.2001.1262 (2001).
- 12 Del Fattore, A. *et al.* Differential effects of extracellular vesicles secreted by mesenchymal stem cells from different sources on glioblastoma cells. *Expert Opin Biol Ther* **15**, 495-504, doi:10.1517/14712598.2015.997706 (2015).
- 13 Matsushime, H. *et al.* D-type cyclin-dependent kinase activity in mammalian cells. *Mol Cell Biol* **14**, 2066-2076 (1994).
- 14 Schröder, M. S., Gusenleitner, D., Quackenbush, J., Culhane, A. C. & Haibe-Kains, B. RamiGO: an R/Bioconductor package providing an AmiGO visualize interface. *Bioinformatics* **29**, 666-668, doi:10.1093/bioinformatics/bts708 (2013).
- 15 Betel, D., Wilson, M., Gabow, A., Marks, D. S. & Sander, C. The microRNA.org resource: targets and expression. *Nucleic Acids Res* **36**, D149-153, doi:10.1093/nar/gkm995 (2008).
- 16 Lewis, B. P., Burge, C. B. & Bartel, D. P. Conserved seed pairing, often flanked by adenosines, indicates that thousands of human genes are microRNA targets. *Cell* **120**, 15-20, doi:10.1016/j.cell.2004.12.035 (2005).
- 17 Zhang, J. *et al.* The challenges and promises of allogeneic mesenchymal stem cells for use as a cell-based therapy. *Stem Cell Res Ther* **6**, 234, doi:10.1186/s13287-015-0240-9 (2015).
- 18 Choi, D. S., Kim, D. K., Kim, Y. K. & Gho, Y. S. Proteomics, transcriptomics and lipidomics of exosomes and ectosomes. *Proteomics* **13**, 1554-1571, doi:10.1002/pmic.201200329 (2013).

- 19 Martins, M., Ribeiro, D., Martins, A., Reis, R. L. & Neves, N. M. Extracellular Vesicles Derived from Osteogenically Induced Human Bone Marrow Mesenchymal Stem Cells Can Modulate Lineage Commitment. *Stem Cell Reports* **6**, 284-291, doi:10.1016/j.stemcr.2016.01.001 (2016).
- 20 Jin, H. J. *et al.* Comparative analysis of human mesenchymal stem cells from bone marrow, adipose tissue, and umbilical cord blood as sources of cell therapy. *Int J Mol Sci* **14**, 17986-18001, doi:10.3390/ijms140917986 (2013).
- 21 Fafián-Labora, J. *et al.* Influence of age on rat bone-marrow mesenchymal stem cells potential. *Sci Rep* **5**, 16765, doi:10.1038/srep16765 (2015).
- 22 Han, J. *et al.* Nanog reverses the effects of organismal aging on mesenchymal stem cell proliferation and myogenic differentiation potential. *Stem Cells* **30**, 2746-2759, doi:10.1002/stem.1223 (2012).
- 23 Harting, M., Jimenez, F., Pati, S., Baumgartner, J. & Cox, C. Immunophenotype characterization of rat mesenchymal stromal cells. *Cytotherapy* **10**, 243-253, doi:10.1080/14653240801950000 (2008).
- 24 Wu, Z. & Wu, H. Experimental Design and Power Calculation for RNA-seq Experiments. *Methods Mol Biol* **1418**, 379-390, doi:10.1007/978-1-4939-3578-9_18 (2016).
- 25 Yang, I. S. & Kim, S. Analysis of Whole Transcriptome Sequencing Data: Workflow and Software. *Genomics Inform* **13**, 119-125, doi:10.5808/GI.2015.13.4.119 (2015).
- 26 Simpson, R. J., Kalra, H. & Mathivanan, S. ExoCarta as a resource for exosomal research. *J Extracell Vesicles* **1**, doi:10.3402/jev.v1i0.18374 (2012).
- 27 Gercel-Taylor, C., Atay, S., Tullis, R. H., Kesimer, M. & Taylor, D. D. Nanoparticle analysis of circulating cell-derived vesicles in ovarian cancer patients. *Anal Biochem* **428**, 44-53, doi:10.1016/j.ab.2012.06.004 (2012).
- 28 Hashimoto, R. *et al.* Increased extracellular and intracellular Ca²⁺ lead to adipocyte accumulation in bone marrow stromal cells by different mechanisms. *Biochem Biophys Res Commun* **457**, 647-652, doi:10.1016/j.bbrc.2015.01.042 (2015).
- 29 Vallabhaneni, K. C. *et al.* Extracellular vesicles from bone marrow mesenchymal stem/stromal cells transport tumor regulatory microRNA, proteins, and metabolites. *Oncotarget* **6**, 4953-4967, doi:10.18632/oncotarget.3211 (2015).
- 30 Théry, C., Zitvogel, L. & Amigorena, S. Exosomes: composition, biogenesis and function. *Nat Rev Immunol* **2**, 569-579, doi:10.1038/nri855 (2002).
- 31 Gould, S. J. & Raposo, G. As we wait: coping with an imperfect nomenclature for extracellular vesicles. *J Extracell Vesicles* **2**, doi:10.3402/jev.v2i0.20389 (2013).
- 32 López-Otín, C., Blasco, M. A., Partridge, L., Serrano, M. & Kroemer, G. The hallmarks of aging. *Cell* **153**, 1194-1217, doi:10.1016/j.cell.2013.05.039 (2013).
- 33 Olivieri, F. *et al.* Toll like receptor signaling in "inflammaging": microRNA as new players. *Immun Ageing* **10**, 11, doi:10.1186/1742-4933-10-11 (2013).
- 34 Zeuner, M., Bieback, K. & Widera, D. Controversial Role of Toll-like Receptor 4 in Adult Stem Cells. *Stem Cell Rev* **11**, 621-634, doi:10.1007/s12015-015-9589-5 (2015).
- 35 He, X., Jing, Z. & Cheng, G. MicroRNAs: new regulators of Toll-like receptor signalling pathways. *Biomed Res Int* **2014**, 945169, doi:10.1155/2014/945169 (2014).
- 36 Ceppi, M. *et al.* MicroRNA-155 modulates the interleukin-1 signaling pathway in activated human monocyte-derived dendritic cells. *Proc Natl Acad Sci U S A* **106**, 2735-2740, doi:10.1073/pnas.0811073106 (2009).
- 37 O'Connell, R. M., Chaudhuri, A. A., Rao, D. S. & Baltimore, D. Inositol phosphatase SHIP1 is a primary target of miR-155. *Proc Natl Acad Sci U S A* **106**, 7113-7118, doi:10.1073/pnas.0902636106 (2009).
- 38 Tomé, M. *et al.* miR-335 correlates with senescence/aging in human mesenchymal stem cells and inhibits their therapeutic actions through inhibition of AP-1 activity. *Stem Cells* **32**, 2229-2244, doi:10.1002/stem.1699 (2014).

- 39 Tomé, M. *et al.* miR-335 orchestrates cell proliferation, migration and differentiation in human mesenchymal stem cells. *Cell Death Differ* **18**, 985-995, doi:10.1038/cdd.2010.167 (2011).
- 40 Feng, J. *et al.* miR-21 attenuates lipopolysaccharide-induced lipid accumulation and inflammatory response: potential role in cerebrovascular disease. *Lipids Health Dis* **13**, 27, doi:10.1186/1476-511X-13-27 (2014).
- 41 He, X. *et al.* TLR4 Activation Promotes Bone Marrow MSC Proliferation and Osteogenic Differentiation via Wnt3a and Wnt5a Signaling. *PLoS One* **11**, e0149876, doi:10.1371/journal.pone.0149876 (2016).
- 42 Zhang, L. *et al.* The role of Toll-like receptor 3 and 4 in regulating the function of mesenchymal stem cells isolated from umbilical cord. *Int J Mol Med*, doi:10.3892/ijmm.2015.2106 (2015).
- 43 Rauner, M. *et al.* WNT5A is induced by inflammatory mediators in bone marrow stromal cells and regulates cytokine and chemokine production. *J Bone Miner Res* **27**, 575-585, doi:10.1002/jbmr.1488 (2012).
- 44 He, W. *et al.* Lipopolysaccharide enhances Wnt5a expression through toll-like receptor 4, myeloid differentiating factor 88, phosphatidylinositol 3-OH kinase/AKT and nuclear factor kappa B pathways in human dental pulp stem cells. *J Endod* **40**, 69-75, doi:10.1016/j.joen.2013.09.011 (2014).
- 45 Gharibi, B., Farzadi, S., Ghuman, M. & Hughes, F. J. Inhibition of Akt/mTOR attenuates age-related changes in mesenchymal stem cells. *Stem Cells*, doi:10.1002/stem.1709 (2014).
- 46 Seit-Nebi, A., Cheng, W., Xu, H. & Han, J. MLK4 has negative effect on TLR4 signaling. *Cell Mol Immunol* **9**, 27-33, doi:10.1038/cmi.2011.15 (2012).

Figure 1.

Characterization of mesenchymal stem cells A) Mesenchymal stem cells markers (CD29, CD90) and haematopoietic markers (CD34, CD45) signals measured by flow cytometry. B) Modified expression genes between age groups obtained in the RNA-seq analysis. C) Hierarchical clustering of genes from MSCs age groups grouped into metabolic pathways common in all of them.

Figure 2.

NGS study. Metabolic pathways with statistically significant changes between newborn, infant, young, pubertal and pre-pubertal age groups categorized according to their function, biological process and cellular component. Age groups were shown because of increasing of differential genes involved into inflammation mediated by chemokine and cytokine signalling pathway. No genes involved in this pathway were found between young and pre-pubertal age groups and between pubertal and adult age groups. Small numbers on the right of each bar are the modulated genes involved in each process.

Figure 3.

Characterization of extracellular vesicles MSCs-derived. A) Number of particles by cell at different age groups by NTA assay. B) Concentration of protein by cell at different age groups by NTA assay. C) Mean size of particles expressed in nm at different age groups by NTA assay. D) Extracellular vesicles isolated from MSCs of pre-pubertal group by microscopy electronic (bar= 100nm). E) APC-CD63 antibody signal measured by flow cytometry at different amounts (1, 5 and 10 μ M) from Pre-pubertal extracellular vesicles MSCs-derived using beads.

Figure 4.

Pro-inflammatory study from micro-RNA contained in mesenchymal stem cells-derived extra-vesicles with age. A) miR-146a, B) miR-155, C) miR-132, D) miR-335 and E) miR-21 expression using real-time reverse transcriptase PCR (qRT-PCR)

analysis normalized by expression of miR-16 used as housekeeping. F) Western blot analysis of TLR4 at different age of MSCs groups treated with LPS. B-actin was used as housekeeping. G) Densitometry analysis of western of TLR4 normalized with respect to b-actin. N=newborn; Y=young; PP=pre-pubertal and A=adult.

Figure 5.

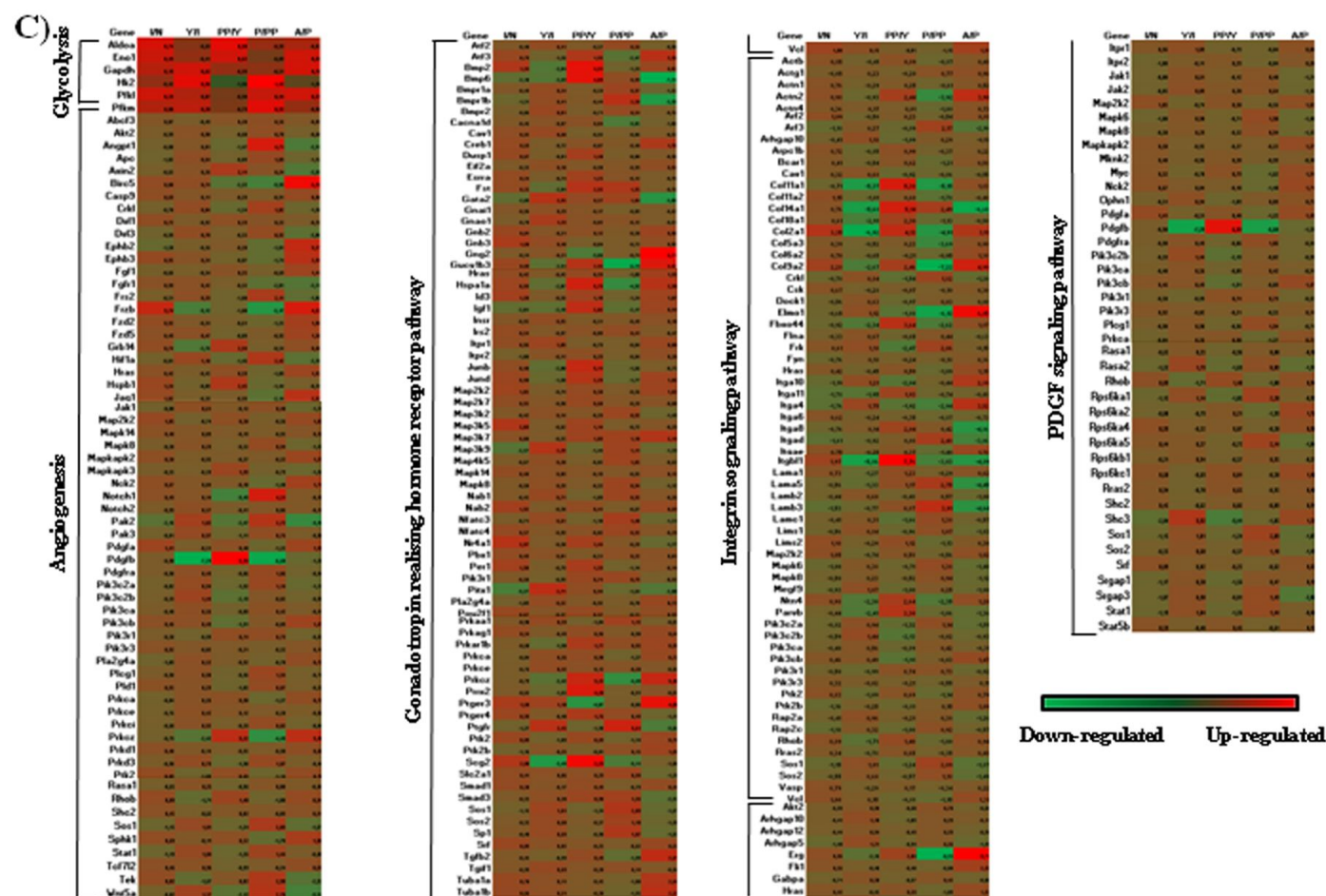
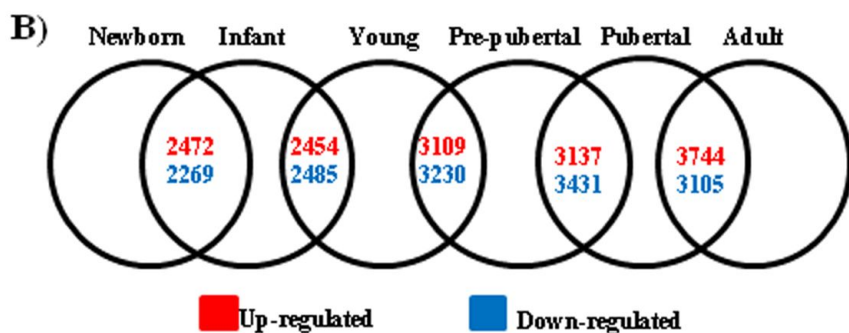
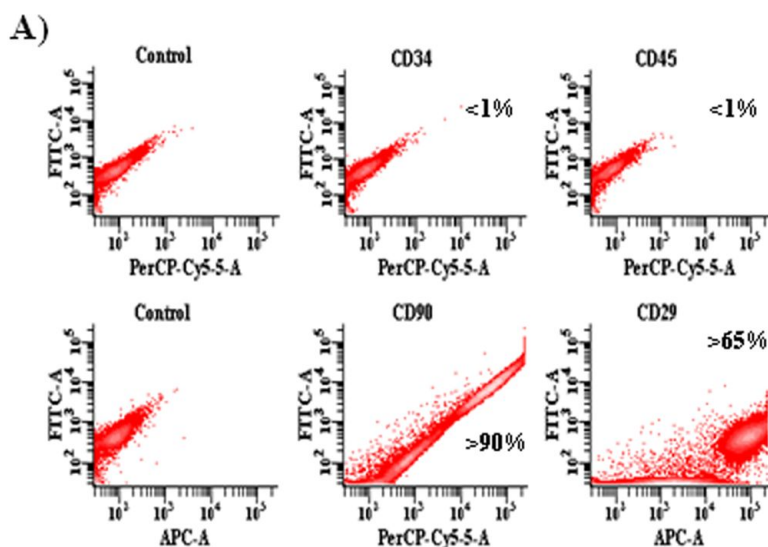
Effect of miR-21-5p on DAMPS in mesenchymal stem cells from pre-pubertal group. A) miR-21-5p expression B) Nanog gene expression C) HMGB1gene expression D) S100A4 gene expression and E) S100A6 gene using real-time reverse transcriptase PCR (qRT-PCR) analysis normalized by expression of miR-16 and HPRT.

Figure 6.

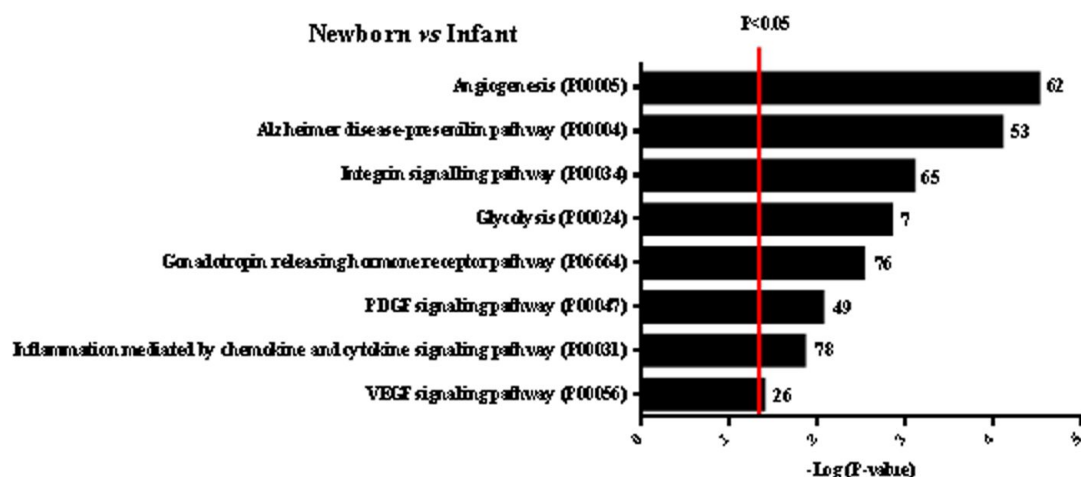
Effect of miR-21-5p on senescence and immune response in mesenchymal stem cells from pre-pubertal group. A) Western blot analysis of LMNA/C and Wnt5a in pre-pubertal MSCs group with or without inhibition of miR-21 and their densitometry analysis normalized with respect to tubulin. B) Western blot analysis of TLR4, mTOR and HMGB1 in pre-pubertal MSCs group with or without inhibition of miR-21 and their densitometry analysis normalized with respect to tubulin. C) Western blot analysis of AKT pathway in pre-pubertal MSCs group with or without inhibition of miR-21 and their densitometry analysis normalized with respect to tubulin. D) Western blot analysis of AKT pathway and TLR4 in pre-pubertal MSCs group miR-21-5p inhibited with or without LPS treatment and their densitometry analysis normalized with respect to tubulin and B-actin.

Table I. Specific primers for real-time reverse transcriptase-polymerase chain reaction (qRT-PCR) amplification.

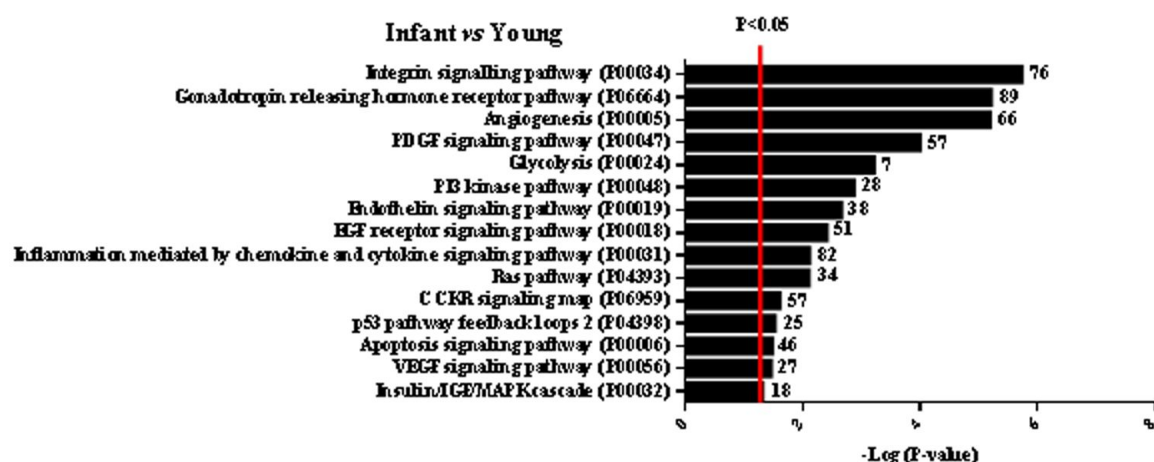
Target	mRNA ID	Forward (5'-3')	Reverse (5'-3')
HMGB1	<u>NM_012963.2</u>	CCGATGCTTCTGTCAACTT	TTGATTTTGGGCGGTACTC
S100A4	<u>NM_012618.2</u>	AGCTACTGACCAGGGAGCTG	CTGGAATGCAGCTTCGTCT
S100A6	<u>NM_053485.2</u>	TGATCCAGAAGGAGCTCACC	AGATCATCCATCAGCCTTGC
NANOG	NM_005103.4	ATGCCTCACACGGAGACTGT	AAGTGGGTTGTTTGCCTTTG
TLR4	NM_019178.1	GCAGAAAATGCCAGGATGATG	AAGTACCTCTATGCAGGGATTAG



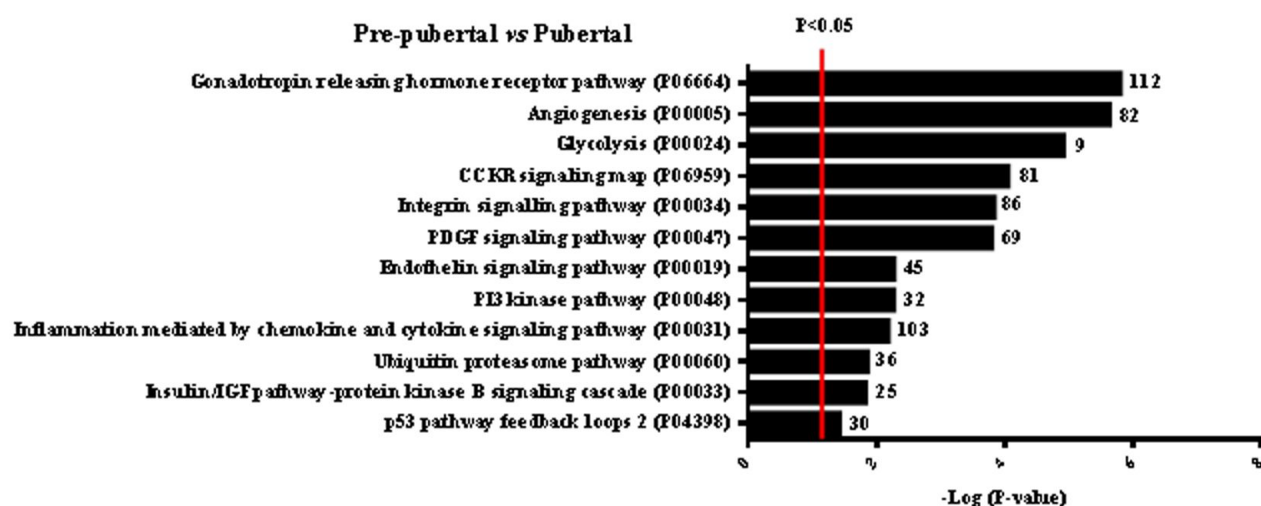
Newborn vs Infant



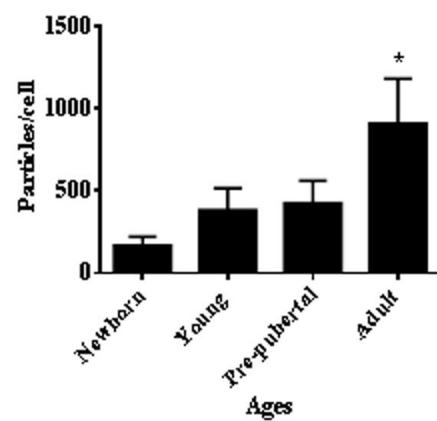
Infant vs Young



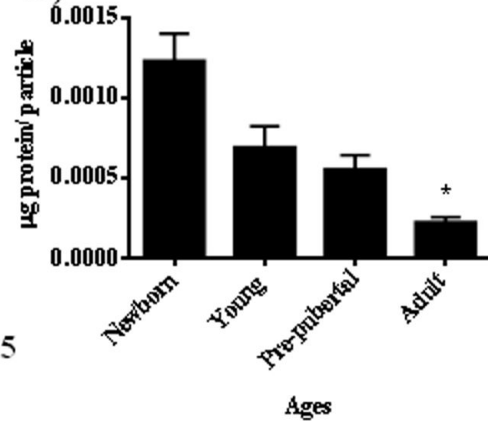
Pre-pubertal vs Pubertal



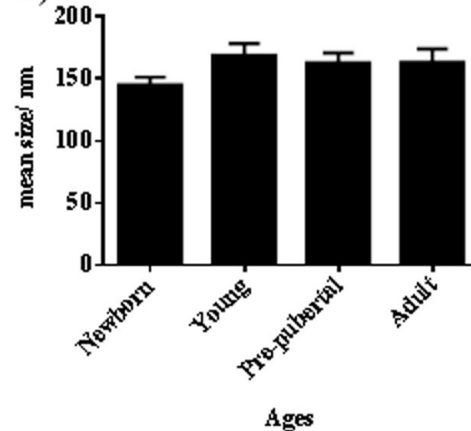
A)

* $P < 0.05$

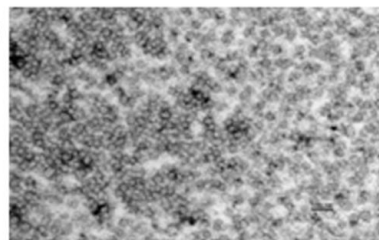
B)



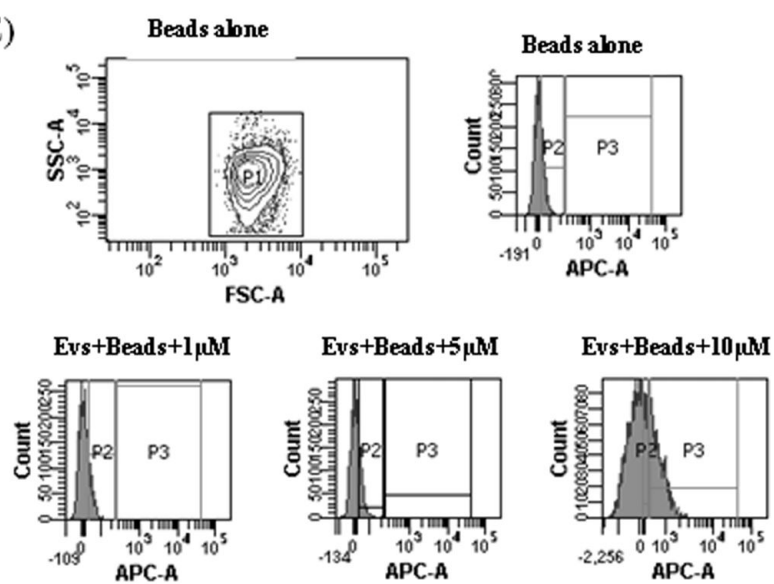
C)

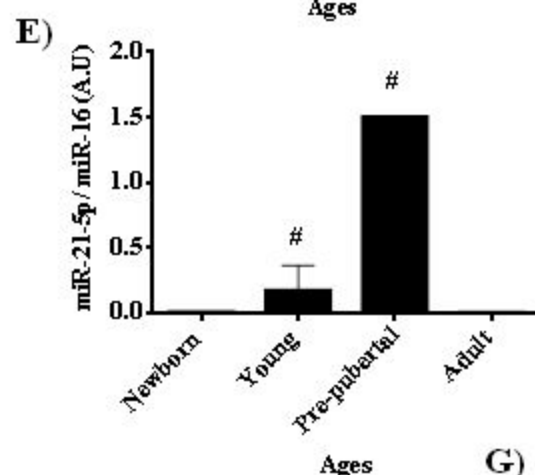
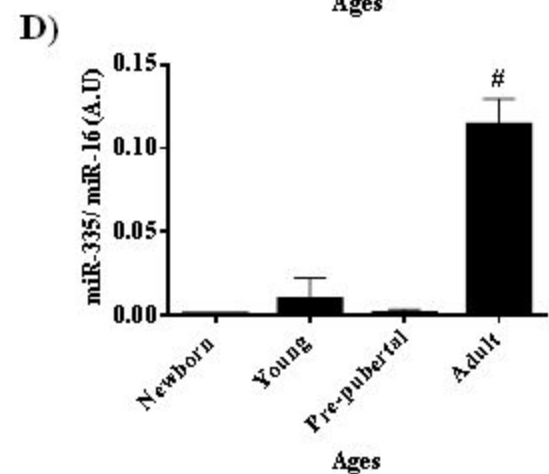
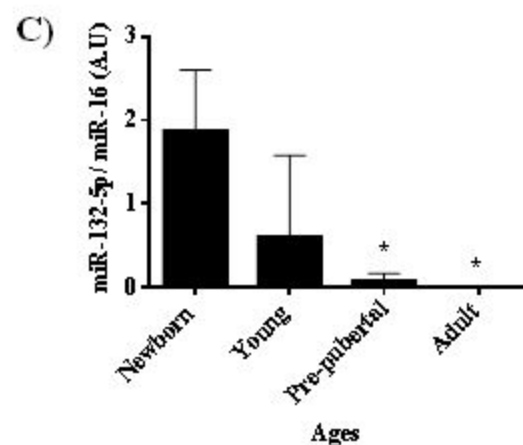
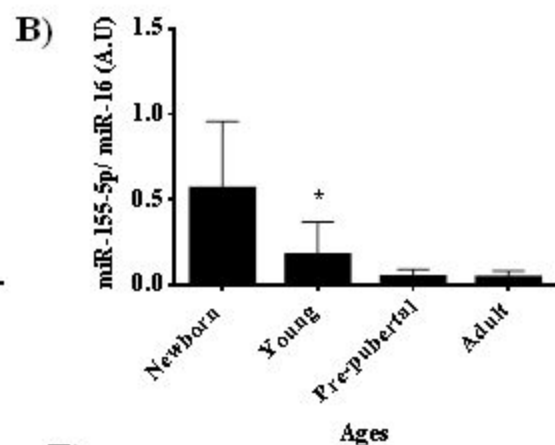
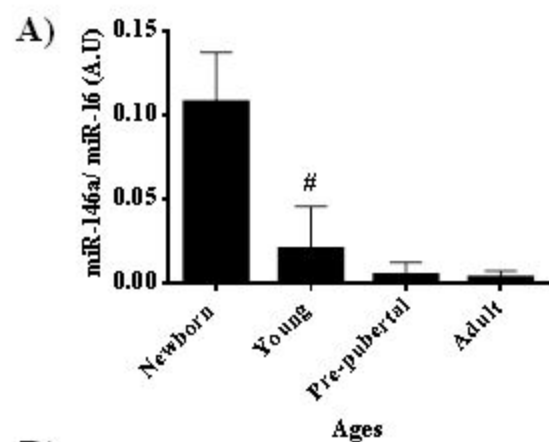


D)

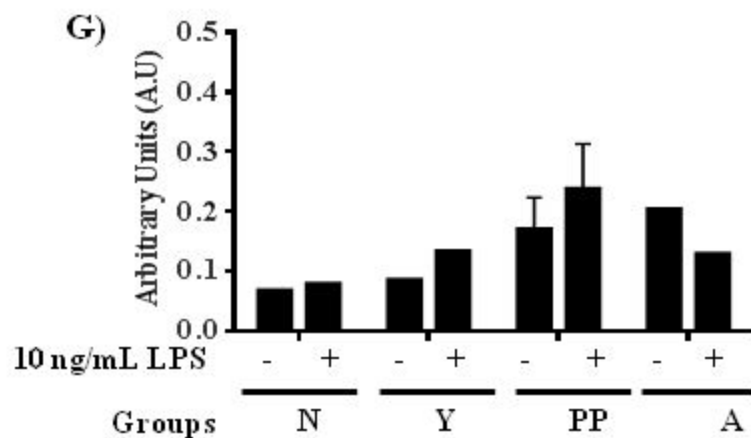
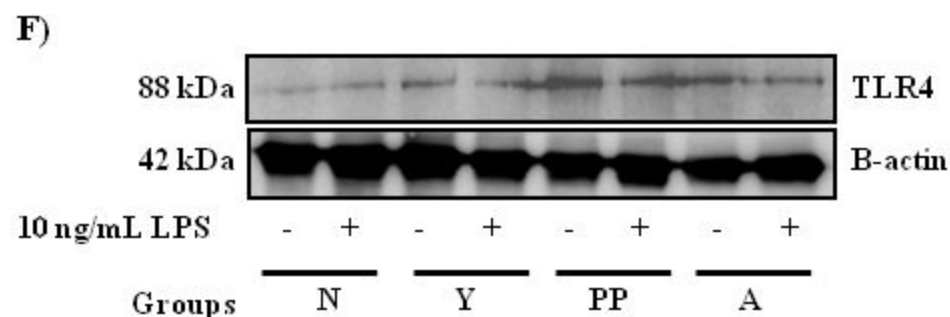


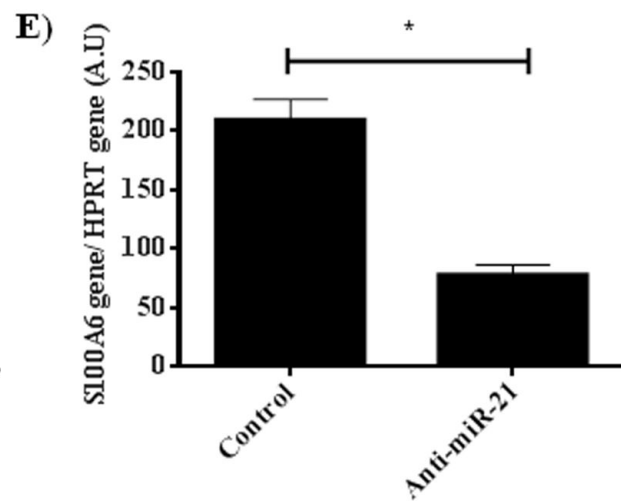
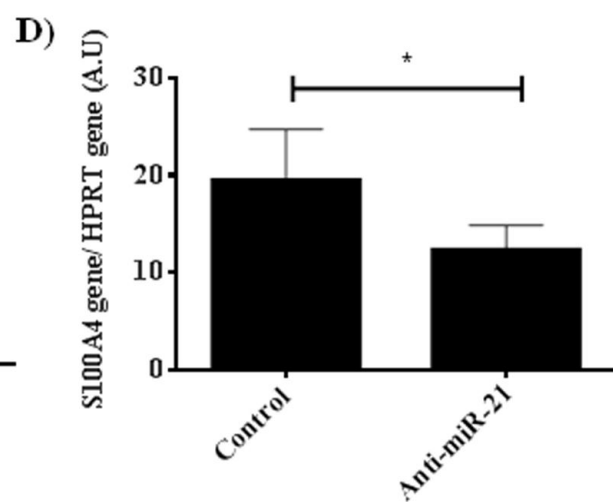
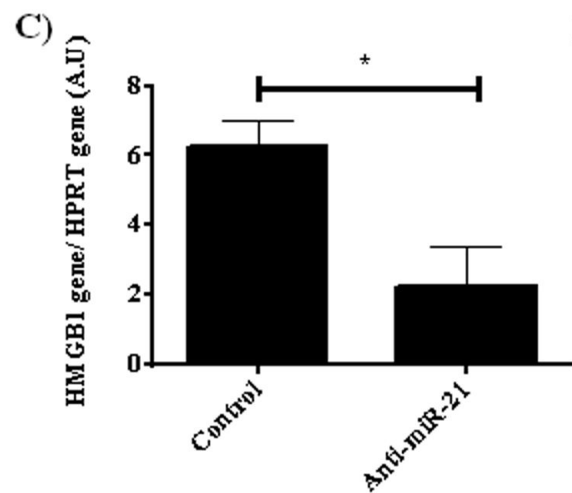
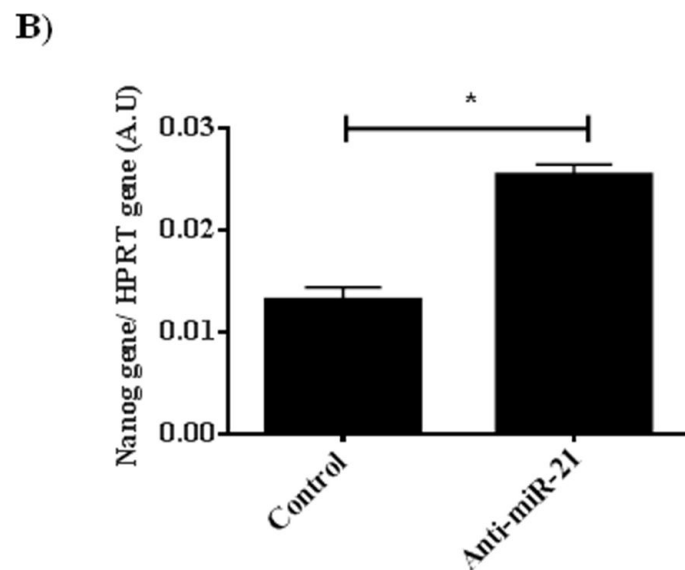
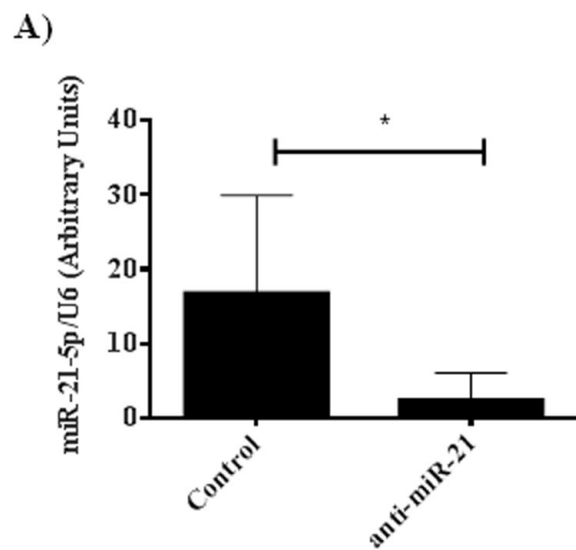
E)



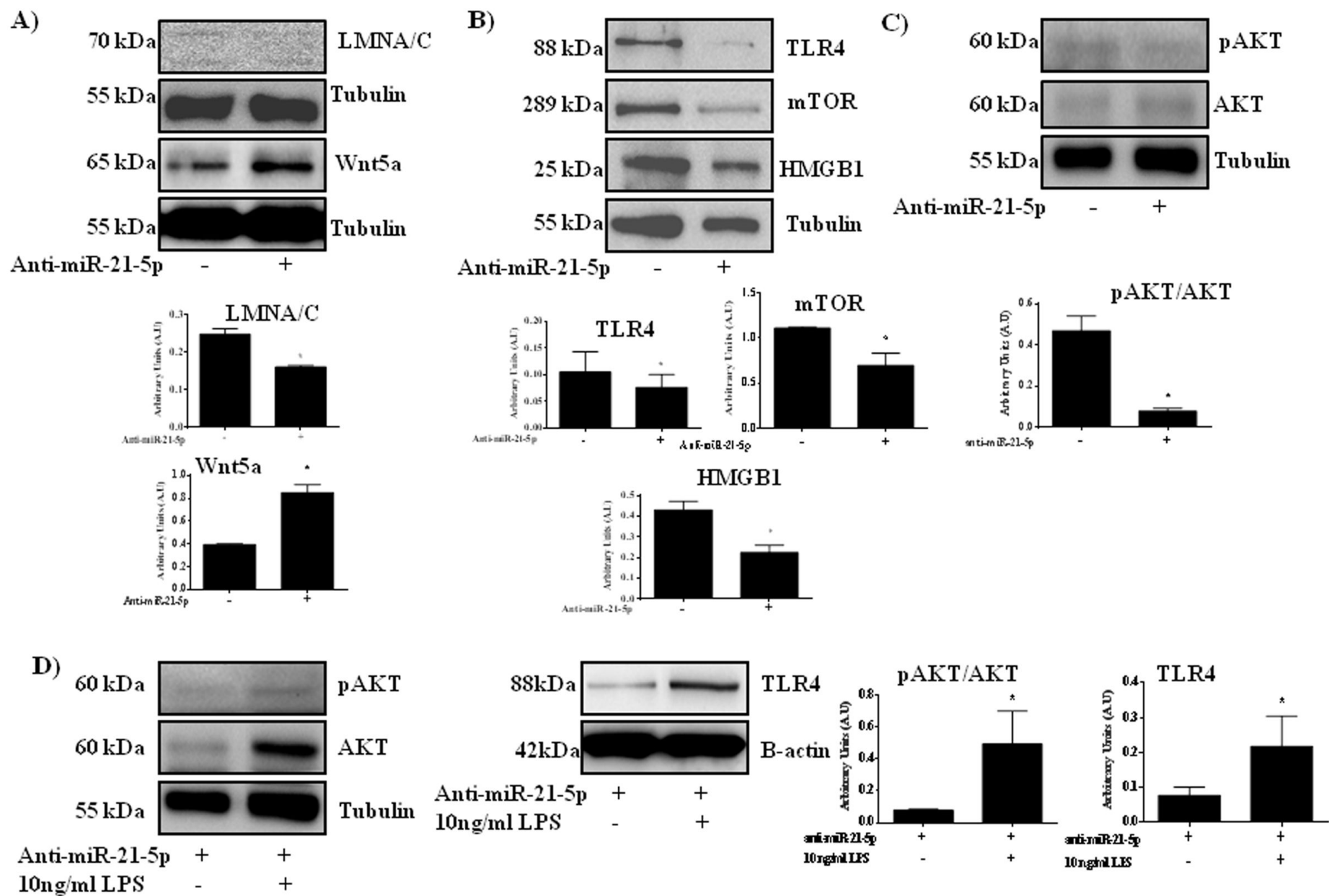


$P < 0.01$ vs previous group
* $P < 0.05$ vs previous group





* $P < 0.05$ vs control



* $P < 0.05$ vs -

Final Decision made for SREP-16-23651

scientificreports@nature.com

Enviado:miércoles, 20 de julio de 2016 10:54

Para: Fafian Labora, Juan Antonio

Dear Mr Fafián-Labora:

We are writing to inform you that a decision letter has been sent to the Corresponding Author of manuscript "Effect of age on pro-inflammatory miRNAs contained in mesenchymal stem cells-derived extracellular vesicles" by Juan Fafián-Labora, Iván Rodríguez-Lesende, Pablo Fernández-Pernas, Susana Sangiao, Lorenzo Monserrat, Onno Arntz, Fons Van de Loo, Jesús Mateos, and María Arufe [Paper #SREP-16-23651], for which you were a Contributing Author.

You can now use a single sign-on for all your accounts, view the status of all your manuscript submissions and reviews, access usage statistics for your published articles and download a record of your refereeing activity for the Nature journals.

In addition, NPG encourages all authors and reviewers to associate an Open Researcher and Contributor Identifier (ORCID) to their account. ORCID is a community-based initiative that provides an open, non-proprietary and transparent registry of unique identifiers to help disambiguate research contributions.

Sincerely,

Manuscript Administration
Scientific Reports
The Macmillan Building
Crinan Street
London N1 9XW

This email has been sent through the NPG Manuscript Tracking System NY-610A-NPG&MTS

Confidentiality Statement:

This e-mail is confidential and subject to copyright. Any unauthorised use or disclosure of its contents is prohibited. If you have received this email in error please notify our Manuscript Tracking System Helpdesk team at <http://platformsupport.nature.com>.

Details of the confidentiality and pre-publicity policy may be found here <http://www.nature.com/authors/policies/confidentiality.html>

[Privacy Policy](#) | [Update Profile](#)

10. CURRICULUM VITAE

CURRICULUM VITAE

Name: Juan Antonio Fafián Labora

Birthdate: June, 6th 1989

Birthplace: A Coruña-SPAIN.

Citizenship: SPANISH

Passport: Spanish 47387789S

e-mail: jfaflab@gmail.com

Office Address:

Juan Antonio Fafián Labora, Ph.D Student.

Medicine Department. University of A Coruña

Rheumatology Division. CIBER-BBN/ISCII

Cellular Therapy and Regenerative Medicine Group (TCMR-CHUAC)

INIBIC-Hospital Universitario A Coruña

15006 A Coruña- Spain

Phone: 34-981-176399 Fax: 34-981-176398

Juan.Antonio Fafián Labora



DATE: 19/09/2016

SIGNATURE:



CURRENT POSITION:

PhD Student

EDUCATION

Graduate in Chemistry: University of Santiago of Compostela-SPAIN. Graduate in 2012

Master Degree in Molecular, Cellular Biology and Genetic. University of A Coruña-SPAIN.

Graduate in 2013

Research fellow:

University Rabdoud in Nijmegen in The Netherlands for 3 months (from 24th September 2015 to 24th December 2015) in Experimental Rheumatology Group

COMMUNICATIONS

Oral presentations

Proteomic study of mesenchymal stem cells during ageing by iTRAQ by Juan Antonio Fafián Labora; Pablo Fernández Pernas; Susana Sangiao Alvarellos, Jesús Mateos Martín and María del Carmen Arufe Gonda in APRS Symposium and Late Summer Meeting 2015 celebrated from 26th to 28th de August, 2015 in Wien, Austrian

Influence of ageing on pro-inflammatory micro-RNAs contained in MSC-derived extracellular vesicles by Juan Fafián-Labora, Onno J. Arntz, Pablo Fernández Pernas, Miranda Bennink, Fons A.J Van de Loo and María del Carmen Arufe Gonda in Biointegrasaúde 2016 celebrated the 12th May, 2016 in Santiago de Compostela, Spain

Posters

Study of the long term stability of an industrial polyamide from a contemporary artwork por Juan Antonio Fafian Labora; Thais López; Massimo Lazzari en The International Congress on Science and Technology for the Conservation of Culture Heritage celebrated from 2th to 5th October, 2012 in Santiago de Compostela, Spain

Análisis proteómico cuantitativo de las células madre mesenquimales de rata Wistar a diferentes estadios de edad by Juan Antonio Fafián Labora; Jesús Mateos Martín; Pablo Fernández Pernas; Susana Sangiao; Issac Fuentes Boquete; Francisco Javier De Toro; Francico Blanco and María del Carmen Arufe in Biointegrasaúde 2014 celebrated in Centro Hospitalario Universitario de A Coruña (CHUAC) the 3th June, 2014 in A Coruña, Spain

Quantitative proteomic analysis of rat mesenchymal stem cells at different ages by Juan Antonio Fafián Labora; Jesús Mateos Martín; Pablo Fernández Pernas; Susana Sangiao; Issac Fuentes Boquete; Francisco Javier De Toro; Francico Blanco and María del Carmen Arufe en el 13th Human Proteome Organization World Congress (HUPO) celebrated from 5th to 8th October, 2014 in Madrid, Spain

Influencia del envejecimiento en el proteoma de las células madre mesenquimales by Juan Antonio Fafián Labora; Jesús Mateos Martín; Pablo Fernández Pernas; Susana Sangiao and María del Carmen Arufe en la IV Jornada Bienal de Jóvenes Investigadores en Proteómica celebrated from 8th to 9th June, 2015 in Bilbao, Spain

Estudio del efecto del envejecimiento sobre el proteoma de las células madre mesenquimales mediante iTRAQ por Juan Antonio Fafián Labora; Jesús Mateos Martín; Pablo Fernández Pernas; Susana Sangiao Alvarellos and María del Carmen Arufe Gonda in III Xornadas de Investigación BioIntegraSaúde 2015 celebrated the 16th June, 2015 in Vigo, Spain

Estudio del efecto del envejecimiento sobre el proteoma de las células madre mesenquimales mediante iTRAQ by Juan Antonio Fafián Labora; Jesús Mateos

Martín; Pablo Fernández Pernas; Susana Sangiao Alvarellos and María del Carmen Arufe Gonda in Simposio S10: Química en la frontera con la Biología de la XXXV Reunión Bienal de la Real Sociedad Española de Química celebrated from 19th to 23th July, 2015 in A Coruña, Spain

Role of ageing in mesenchymal stem cells by Juan Antonio Fafián Labora; Pablo Fernández Pernas; Susana Sangiao Alvarellos; Jesús Mateos Martín and María del Carmen Arufe Gonda in World Conference in Regenerative Medicine celebrated from 21th to 23th October, 2015 in Leipzig, Germany

Influence of ageing on pro-inflammatory micro-RNAs contained in MSC-derived extracellular vesicles by Juan Fafián-Labora; Onno J. Arntz; Pablo Fernández Pernas; Miranda Bennink; Fons A.J Van de Loo and María del Carmen Arufe Gonda in VI Reunión de Jóvenes Investigadores en el extranjero celebrated the 29th December, 2015 in A Coruña, Spain

Influence of ageing on pro-inflammatory micro-RNAs contained in MSC-derived extracellular vesicles by Juan Fafián-Labora; Onno J. Arntz; Pablo Fernández Pernas; Miranda Bennink; Fons A.J Van de Loo and María del Carmen Arufe Gonda in International Society for Extracellular Vesicles celebrated from 4th to 7th, May, 2016 in Rotterdam, The Netherlands

Influence of ageing on pro-inflammatory micro-RNAs contained in MSC-derived extracellular vesicles by Juan Fafián-Labora; Onno J. Arntz; Pablo Fernández Pernas; Miranda Bennink; Fons A.J Van de Loo and María del Carmen Arufe Gonda in 10th Annual Congress of the Spanish Federation of Biotechnologists celebrated from 13th to 15th, July 2016 in Gijón, Spain

Quantitative Proteomics and Whole Transcriptomics Sequencing of Progeria-derived cells Point to a Key of IGF Signaling Pathway in Premature Aging by Juan Fafián-Labora; Iván Lesende-Rodríguez; Lorenzo Monserrat; Antonia Ódena; Eliandre de Oliveira; María del Carmen Arufe and Jesús Mateos in 15th Human Proteome Organization World Congress celebrated from 18th to 22th September, 2016 in Taipei

BIBLIOGRAPHY

Internacional Papers:

J. Fafián Labora; M. Lazzari y T. López Morán
Study of the long term stability of an industrial polyamide from a contemporary artwork.
Science and Technology for the Conservation of Culture Heritage-Rogério-Candelera, Lazzari & Cano (eds)
Taylor & Francis Group, London, ISBN 978-1-138-00009-4 (2013)

J. Mateos, P. Fernández Pernas, J. Fafián Labora, F. Blanco, MC Arufe *
Proteomic Applications in the study of Human Mesenchymal Stem Cells
Proteomes
R **2014**, 2(1), 53-71;
ISSN: 2227-7382. Ranking (2013)
doi:[10.3390/proteomes2010053](https://doi.org/10.3390/proteomes2010053)

J. Mateos, A. Landeira-Abia, J. Fafián-Labora, P. Fernández-Pernas, I. Lesende-Rodríguez, P. Fernández-Puente, M. Fernández-Moreno, A. Delmiro, MA. Martín MA, F. Blanco *, MC Arufe*

iTRAQ-based analysis of progerin expression reveals mitochondrial dysfunction, reactive oxygen species accumulation and altered proteostasis.

Stem Cell Res Ther. 2015

Jun 12;6(1):119.

ISSN: 1757-6512

doi:10.1186/s13287-015-0110-5

Impact factor (2013): **4.634**

Ranking (2013): 19/124 en MEDICINE, RESEARCH & EXPERIMENTAL (**Q1**)

J. Fafián-Labora, P. Fernández-Pernas, I. Fuentes, J. De Toro, N. Oreiro, S. Sangiao-Alvarellos, J. Mateos*, M.C. Arufe*.

Influence of age on rat bone marrow mesenchymal stem cells potential.

Scientific Reports 2015

ISSN: 2045-2322

doi:10.1038/srep16765

Impact factor (2014): **5.578**

Ranking (2013): MULTIDISCIPLINARY SCIENCES 5/57 (**Q1-D1**)

P. Fernández-Pernas, J. Fafián-Labora, I. Lesende-Rodríguez, J. Mateos, A. De la Fuente , I. Fuentes, J. De Toro, F. Blanco García F*, Arufe M*

3, 3',5-Triiodo-L-Thyronine Increases In Vitro Chondrogenesis of Mesenchymal Stem Cells from Human Umbilical Cord Stroma Through SRC2

J Cell Biochem. 2016

ISSN:1097-4644

doi: 10.1002/jcb.25515.

Impact factor (2014): **3.263**

Ranking (2014): BIOCHEMISTRY & MOLECULAR BIOLOGY 107/290 (**Q2**)

RESEARCH INTERESTS:

1. Influence aging on pluripotency, proliferation and immunogenic profiles in mesenchymal stem cells from bone marrow
2. Influence aging on mesenchymal stem cell-derived extracellular vesicles

GRANTS:

APRS 2015/Late Summer meeting

EMBO Fellowship Short-term in 2015 ASTF 268-2015

Grant of investigation by Diputación de A Coruña in 2015

INDITEX Fellowship Short term in 2015

SCIENTIFIC SOCIETIES THAT I BELONG:

SEPROT (SPANISH SOCIETY OF PROTEOMIC)

ISEV (INTERNATIONAL SOCIETY FROM EXTRACELLULAR VESICLES)

SETYGYC (SPANISH SOCIETY OF GENETIC AND CELLULAR THERAPY)

SEBBM (SPANISH SOCIETY OF BIOCHEMISTRY AND BIOLOGY MOLECULAR)

REFERENCES:

Dra. María del Carmen Arufe Gonda. e-mail: maria.arufe@udc.es

Dr. Jesús Mateos Martín. e-mail: Jesus.Mateos.Martin@sergas.es

Dr. Massimo Lazzari: massimo.lazzari@usc.es

Dr. Fons Van de Loo. e-mail: Fons.vandelo@radboudumc.nl